INAUGURALDISSERTATION

zur Erlangung der Doktorwürde der
Naturwissenschaftlich-Mathematischen Gesamtfakultät
der Ruprecht-Karls-Universität Heidelberg

Endothelial regulation of liver fibrosis

Vorgelegt von

Sina Wietje Kürschner

Inaugural dissertation

for

obtaining the doctoral degree

of the

Combined Faculty of Mathematics, Engineering and Natural Sciences

of the

Ruprecht - Karls - University

Heidelberg

Presented by

M.Sc. Sina Wietje Kürschner

Born in: Offenbach am Main, Germany

Oral examination: May 3rd, 2022

Endothelial regulation of liver fibrosis

Referees:

Prof. Dr. rer. nat. Viktor Umansky

Prof. Dr. med. Sergij Goerdt

This thesis is dedicated to my parents.

“People think of science as rolling back the mystery of God.
I look at science as slowly creeping toward the mystery of God.”
Allan Hamilton

Parts of this thesis have been published

“Endothelial GATA4 controls liver fibrosis and regeneration by preventing a pathogenic switch in angiocrine signaling”

Winkler M.*, Staniczek T.*, Kürschner S. W.*, Schmid, C. D.*, Schönhaber H., Cordero J., Kessler L., Mathes A., Sticht C., Nessling M., Uvarovskii A., Anders S., Zhang X. J., von Figura G., Hartmann D., Mogler C., Dobreva G., Schledzewski K., Geraud C.*, Koch P. S.*, Goerdt S.*

Journal of Hepatology, 74 (2): 380-393; February 2021

*Equally contributing first and last authors.

Table of content

Table of content

Table of content

Abstract

Liver fibrosis is a scarring process of the liver in response to sustained liver injury and can progress into cirrhosis, hepatocellular carcinoma (HCC) and liver failure as end stage disease. Moreover, liver fibrosis dictates the long-term prognosis and mortality in non-alcoholic steatohepatitis (NASH) patients. Parenchymal liver cells such as hepatocytes and non-parenchymal liver cells such as hepatic stellate cells (HSC) and endothelial cells (EC) are involved in liver fibrogenesis. Liver sinusoidal endothelial cells (LSEC) are a discontinuous endothelium exhibiting fenestrations and lacking a basement membrane and form the capillary bed of the liver. Sinusoidal capillarization leads to the activation of HSC, which in turn produce extracellular matrix (ECM) proteins resulting in liver fibrosis. Therefore, the physiological differentiation of LSEC is crucial for liver homeostasis and identification of molecules crucial for the homeostasis of LSEC is indispensable. Recently, we identified transcription factor GATA4 as a master regulator of LSEC differentiation. LSEC-specific loss of GATA4 leads to sinusoidal capillarization and perisinusoidal liver fibrosis in $Gata4^{LSEC\text{-}KO}$ mouse. We wondered, if endothelial GATA4 plays a regulatory role in the development of liver fibrosis. Therefore, the aim of this study was to establish two different liver fibrosis models and to analyze the role of GATA4 in the development of liver fibrosis. Chronic toxic carbon tetrachloride (CCl_4) model was compared with diet-induced liver fibrosis NASH models. *Gata4* was rather increased in endothelial cells of mice with bridging peri-central liver fibrosis in the CCl_4 model, whereas downregulation of endothelial *Gata4* was seen in the choline-deficient l-amino acid-defined (CDAA) diet-induced NASH model with perisinusoidal liver fibrosis. Downregulation of *Gata4* in LSEC of CDAA fed mice was accompanied with sinusoidal transdifferentiation of mLSEC and downregulation of GATA4 dependent genes. This data indicates that GATA4 in LSEC seems to play an important role in preventing development of diet-induced perisinusoidal liver fibrosis in NASH but not in toxic-induced bridging fibrosis. For maintenance of *Gata4* expression during perisinusoidal liver fibrosis models on the one hand a LSEC-specific Gata4 knockin mouse ($Gata4^{LSEC\text{-}KI}$) was generated and used in CDAA model. On the other hand, LSEC-specific lentivirus expressing *Gata4* was generated for application of Gata4-therapy. However, the $Gata4^{LSEC\text{-}KI}$ mouse was not able to reduce perisinusoidal liver fibrosis in CDAA model as no functional GATA4 overexpression in LSEC was induced. The lentivirus was able to induce functional GATA4 expression in mouse brain cell line bEnd.3, but not in primary LSEC *in vitro*, indicating that the virus generated is not sufficient to overactivate Gata4 in primary LSEC. Taken together, these data indicate that downregulation of GATA4 is an important factor during CDAA-mediated perisinusoidal liver fibrosis.

Zusammenfassung

Leberfibrose ist ein Vernarbungsprozess der Leber als Reaktion auf eine anhaltende Leberschädigung und kann zu Zirrhose, hepatozellulärem Karzinom (HCC) und Leberversagen als Endstadium fortschreiten. Darüber hinaus bestimmt die Leberfibrose die Langzeitprognose und Mortalität bei Patienten mit nichtalkoholischer Steatohepatitis (NASH). Parenchymale Leberzellen, wie Hepatozyten, und nicht-parenchymale Leberzellen, wie hepatische Sternzellen (HSC) und Endothelzellen (EC), sind an der Leberfibrogenese beteiligt. Lebersinus Endothelzellen (LSEC) sind ein diskontinuierliches Endothel mit Fenestrierung, aber ohne Basalmembran und bilden das Kapillarbett der Leber. Die Kapillarisierung der Sinusendothelien führt zur Aktivierung von HSC, die wiederum extrazelluläre Matrixproteine (ECM) produzieren, was zu Leberfibrose führt. Daher ist die physiologische Differenzierung von LSEC entscheidend für die Leberhomöostase und die Identifizierung von Molekülen, die für die Homöostase von LSEC entscheidend sind, unerlässlich. Vor kurzem haben wir den Transkriptionsfaktor GATA4 als Hauptregulator der LSEC-Differenzierung identifiziert. LSEC-spezifischer Verlust von GATA4 führt bei der $Gata4^{LSEC\text{-}KO}$ Maus zu Kapillarisierung und perisinusoidaler Leberfibrose. Wir fragten uns, ob endotheliales GATA4 eine regulatorische Rolle bei der Entwicklung der Leberfibrose spielt. Ziel dieser Studie war es daher, zwei verschiedene murine Leberfibrosemodelle zu etablieren und die Rolle von GATA4 bei der Entstehung der Leberfibrose zu analysieren. Das chronische toxische Tetrachlorkohlenstoff (CCl_4) Modell wurde mit Diät-induziertem NASH-Modellen verglichen. *Gata4* war in Endothelzellen von Mäusen mit überbrückender perizentraler Leberfibrose im CCl_4-Modell erhöht, während eine Herunterregulierung des endothelialen *Gata4* im cholin-defizientienten l-Aminosäure-definierten (CDAA) Diät-induzierten NASH-Modell mit perisinusoidaler Leberfibrose beobachtet wurde. Die Herunterregulierung von *Gata4* in der LSEC von CDAA-gefütterten Mäusen ging mit einer sinusoidalen Transdifferenzierung von mLSEC und einer Herunterregulierung von Gata4-abhängigen Genen einher. Diese Daten zeigen, dass GATA4 in LSEC eine wichtige Rolle bei der Verhinderung der Entwicklung einer Diät-induzierten perisinusoidalen Leberfibrose bei NASH zu spielen scheint, nicht jedoch bei toxisch induzierter Brückenfibrose. Zur Aufrechterhaltung der Gata4-Expression, während perisinusoidaler Leberfibrose-Modelle, wurde einerseits eine LSEC-spezifische Gata4-Knockin-Maus ($Gata4^{LSEC\text{-}KI}$) generiert und im CDAA-Modell verwendet. Auf der anderen Seite wurde ein LSEC-spezifisches Lentivirus, das *Gata4* exprimiert, für die Anwendung einer Gata4-Therapie erzeugt. Die $Gata4^{LSEC\text{-}KI}$ Maus war jedoch nicht in der Lage, die perisinusoidale Leberfibrose im CDAA-Modell zu reduzieren, da keine funktionelle GATA4-Überexpression in LSEC induziert wurde. Das Lentivirus war in der Lage, eine funktionelle GATA4-Expression in der

murinen Gehirnzelllinie bEnd.3 zu induzieren, jedoch nicht in primären LSEC *in vitro*, was darauf hindeutet, dass das erzeugte Virus nicht ausreicht, um Gata4 in primären LSEC zu überaktivieren. Zusammengenommen deuten diese Daten darauf hin, dass die Herunterregulierung von GATA4 ein wichtiger Faktor bei CDAA-vermittelter perisinusoidaler Leberfibrose ist.

1. Introduction

1.1. Liver structure and function

The liver is the biggest internal organ of the body and the central organ for metabolism. In humans the liver weighs about 1.5 kg and is located below the diaphragm in the upper abdomen. The liver is involved in synthesis of glucose, cholesterol, fatty acids and blood proteins like albumin and clotting factors. Moreover, the liver accumulates glucose, lipids and vitamins and is responsible for production of bile, which is essential for lipid catabolism in the intestine. In addition, toxic substances, such as alcohol or drugs and metabolites, such as bilirubin, are reduced and excreted by the liver [1, 2]. The liver has a distinct structure concomitant with the distinct functions, which is described in the following chapters.

1.1.1. Liver anatomy

The liver is grouped into liver lobes. Humans have two and mice have five liver lobes. Claude Couinaud segmented the liver into eight functional segments [3]. Nowadays this segmentation is put into question but is nevertheless used as a standard for segmentation of the liver. The liver has dual blood supply. The hepatic artery (*Arteria interlobularis*) transports oxygenated blood from the heart into the liver. Whereas the portal vein (*Vena interlobularis*) transports oxygen-deficient but nutrient-rich blood from the gastrointestinal tract and the spleen into the liver. Thereby the portal vein accounts for 75 % and the hepatic artery for 25 % of the blood supply into the liver [4, 5]. Portal vein and Hepatic artery enter the liver at the hepatic porta. Together with the bile duct (*Ductus biliferus*), branches of portal vein and hepatic artery form the portal triads [2]. At the portal triad nutrient-rich blood from the portal vein and oxygen-rich blood from the hepatic artery is mixed in the sinusoid, which forms the capillary bed of the liver and is lined by sinusoidal endothelial cells [6, 7]. The originated mixed blood is transported towards the central veins, which drain the hepatic veins. Blood is transported through the hepatic veins to the vena cava inferior, which transports it to the heart. The bile flows contrary to the blood flow in a central-to-portal direction and is transported through the bile duct to the duodenum, where it is involved in the absorption of fat [8]. The gall bladder stores the bile between the food intakes.

There are three different models to classify the liver in structural or functional units. The classic “Kiernan” lobule described by Kiernan, the portal lobule and the acinus model described by Rappaport [9] (Figure 1). The classic lobule is hexagonal-shaped, with liver cells surrounding

a central vein in the middle. In the periphery in every corner of the lobule the portal triads are localized [10]. The portal lobule model describes a triangular-shaped mass of liver cells which consists of portions of three adjacent hepatic lobules with the portal vein as center. In the periphery a central vein is located at each corner [11]. The third model, the acinus model, is the most functional model because it goes along with the afferent flow of the blood. It consists of liver tissue, which is supplied by oxygen- and nutrient-rich blood at the portal triad, which flows through the sinusoids and enter the central vein [12]. In the acinus there is a radial gradient of nutrients, oxygen and hormones in portal-to-central direction originating. This gradient divides the liver cells into three zones, which is called liver zonation [13].

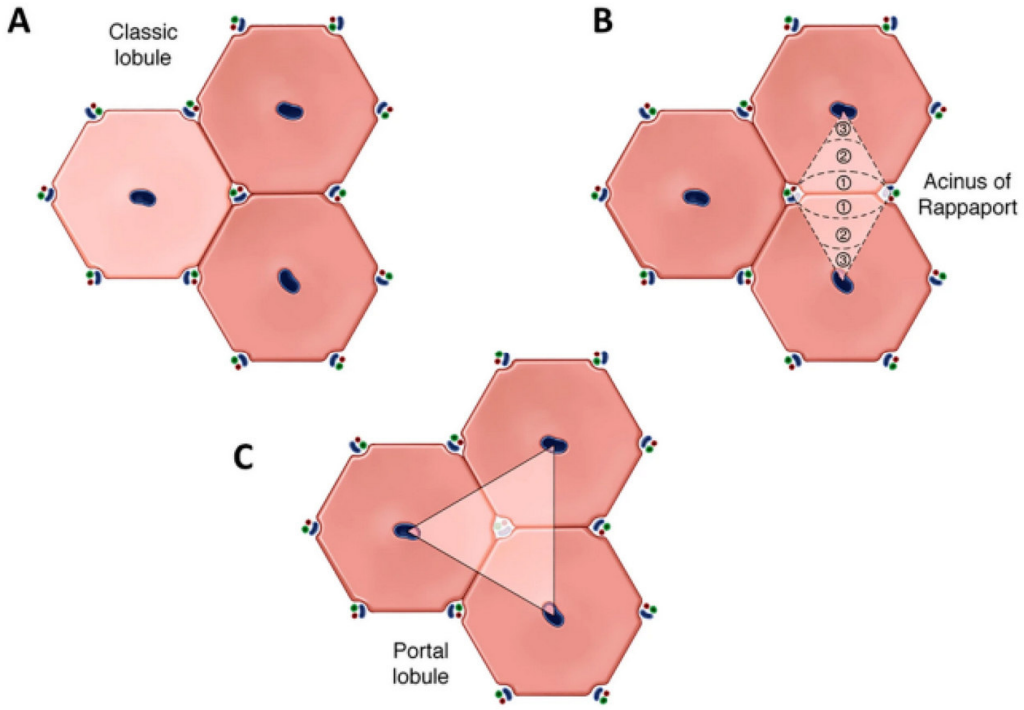

Figure 1. Illustration of three different models to classify the liver in structural or functional units.
(A) Classic "Kiernan" lobule with a hexagonal shape and a central vein in the middle. **(B)** Acinus model described by Rappaport based on terminal portal circulation subdividing the liver cells into three zones (Zone 1-3). **(C)** Portal lobule model with triangular shape and the portal vein in the middle. Figure and labeling are adopted from Lau *et al.* [9]. (CC BY 4.0) https://creativecommons.org/licenses/by/4.0/

1.1.2. Liver histology

The liver consists of parenchymal cells, which are hepatocytes and biliary epithelial cells, and non-parenchymal cells to which Kupffer cells (KC), endothelial cells (EC), and hepatic stellate cells (HSC) belong to [14]. Hepatocytes are the most abundant cell type of the liver and constitute around 60 % of the liver by cell number. From the non-hepatocytes half of the cells are endothelial cells [15].

The functions of hepatocytes are diverse and are dependent on the specific position within the lobule radial axis. This so-called metabolic liver zonation is due to the fact, that there is a blood flow gradient enriched with nutrients and particles from the portal vein to central vein. There are three metabolic zones: Zone 1 consists of periportal hepatocytes, which are involved e.g. in gluconeogenesis, β-oxidation and cholesterol biosynthesis, zone 2 consists of midlobular hepatocytes, which are involved e.g. in iron metabolism and zone 3 consists of pericentral/perivenous hepatocytes, which are involved e.g. in glycolysis, bile acid production and xenobiotic metabolism [15, 16] (Figure 2). On a molecular level, metabolic liver zonation is regulated by a gradient of endothelial-derived Wnt/β-catenin signaling [17-19].

Between the hepatocytes the sinusoids are localized radiating from a central vein towards the portal triad. The sinusoids are lined with discontinuous endothelial cells, called liver sinusoidal endothelial cells (LSEC). In addition, KC which are resident liver macrophages, are localized in the sinusoids. KC are a part of the immune system and clear foreign particles or particles and solutes produced naturally in the body, which enter the liver through the blood of portal vein, by phagocytosis [20]. Oxygen exchange between blood and hepatocytes takes place in the space of Disse, which is the space between LSEC and hepatocytes. Hepatic stellate cells are pericytes, which are located in the space of Disse. There are two different states of HSC, a quiescent and an activated state. Quiescent HSC store vitamin A (retinol) in lipid droplets, which is important for growth, vision and immunity [21]. Upon injury of the liver HSC release large amounts of vitamin A and change into myofibroblast-like cells, which produce extracellular matrix (ECM) proteins, like collagen. A precisely regulated crosstalk and interplay between the different cells of the liver is indispensable for liver function and homeostasis.

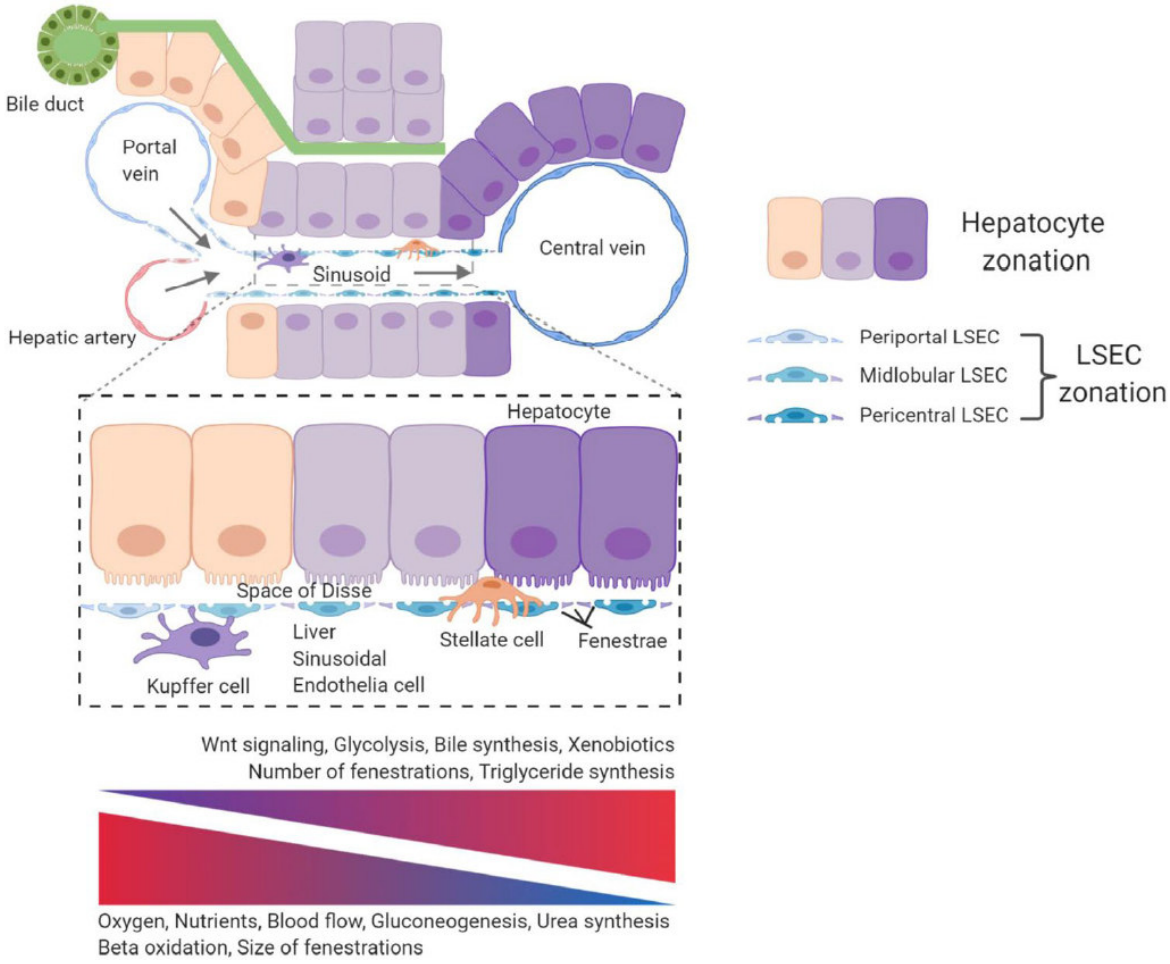

Figure 2. Liver histology and zonation of liver cells.
The liver lobule is comprised of the main four cell types, which are hepatocytes, LSEC, KC and HSC. The vascular bed between hepatocytes is lined by LSEC and named sinusoid. The perisinusoidal space between hepatocytes and LSEC is named “Space of Disse”, in which HSCs reside. KCs are located in the sinusoid. Nutrient-rich blood from the portal vein and oxygen-rich blood from the hepatic artery mix in the sinusoid to exit the liver via the central vein. This blood flow creates a gradient of oxygen and nutrients in portal-to-central direction along the axis of the liver lobule, which lead to the metabolic zonation of liver cells. Functions of hepatocytes is dependent on the location within in liver lobule in portal-to-central direction. Figure and labeling are adopted from Koch *et al. [5]* (CC BY 4.0) https://creativecommons.org/licenses/by/4.0/

1.1.3. Common liver diseases and their epidemiology

The liver plays a central role in metabolism and can affect the whole body in case of altered liver function. The common liver diseases are viral hepatitis, alcoholic liver disease (AFLD) and alcoholic steatohepatitis (ASH), non-alcoholic liver disease (NAFLD) including non-alcoholic steatohepatitis (NASH), liver cirrhosis and liver cancer such as hepatocellular carcinoma (HCC). Hepatitis viruses cause liver inflammation. There are different forms of hepatitis. Hepatitis A virus leads usually to a short-term infection. However, hepatitis B and C virus leads to a chronic infection [22, 23]. In Europe chronic Hepatitis B affects 0.5 - 0.7 % people. Chronic Hepatitis C affects 0.13 – 3.26 % of the European population [24]. AFLD/ASH arises from

alcoholic overconsumption and is characterized by steatosis, hepatitis and fibrosis [25]. In the European population the prevalence is around 6 % [26]. NAFLD/NASH is as well characterized by steatosis, liver inflammation in NASH and development of fibrosis but without alcohol as cause [27]. The prevalence of NAFLD in the European population is around 24 % [26]. Damage of liver tissue leads to tissue repair and subsequent scar tissue formation, called fibrosis. Over a long period of time, liver fibrosis leads to liver cirrhosis, which can ultimately lead to liver dysfunction [28]. Liver cirrhosis causes around 170000 deaths per year in Europe [24]. HCC is the most common liver cancer and arises from hepatocytes. Chronic viral hepatitis, NASH and cirrhosis are risk factors for the development of HCC [29]. In the European population liver cancer is the cause of 47000 deaths per year [24]. If the underlying cause of chronic liver disease is not removed or cured, liver failure can occur. Only in some cases acute liver failure occur, but in most cases liver failure is end stage of many liver diseases and develops over time. When this is the case, liver transplantation is the most promising solution [30]. The liver is a highly regenerative organ therefore living donor liver transplantation is possible as well. In Europe more than 5500 liver transplantations are performed per year [24].

1.2. Liver sinusoidal endothelial cells (LSEC)

1.2.1. Structure and functions of LSEC

1.2.1.1. Structure of LSEC

Unlike most other endothelial cells in different organs and along the vascular tree, liver sinusoidal endothelial cells (LSEC) belong to discontinuous fenestrated endothelial cells which are lining the liver sinusoids. They have highly specialized functions and display a unique morphology. The lack of a basement membrane and the presence of non-diaphragmed fenestrations are unique and make the LSEC the most porous endothelium [31]. Fenestrations are pores arranged in sieve plates with a diameter of 100–175 nm [32, 33] (Figure 3). Fenestrations are a key feature of the specialized functions of LSEC, because they enable the exchange of fluid and non-cellular substrates between the blood and the liver parenchyma. All soluble molecules, small chylomicron remnants, lipoproteins and nanoparticles with a diameter lower than the diameter of fenestrations are able to enter the LSEC fenestrations in a bidirectional manner [34, 35] (Figure 4). Because of the radial gradient of nutrients and oxygen in the lobule the number and diameter of fenestrations differ from periportal to centrilobular (Figure 2). LSEC in centrilobular zone 3 have smaller fenestrations but more fenestrae per

sieve plate compared to the periportal LSEC in zone 1 [36]. The diameter of the LSEC fenestrae is dynamic, which means that it can change upon different conditions and substrates. That includes e.g. aging [37], hormones [38], luminal blood pressure [39], toxins [40], extracellular matrix [41] and diseases [42, 43]. Acetylcholine [44] and increased intrasinusoidal blood pressure [45] lead to increased diameter of LSEC, whereas noradrenaline [38], serotonin [46] and aging [37] lead to a decreased diameter. Not only the diameter but also the number of fenestrae changes. Extracellular matrix proteins, such as laminines and collagen type IV – V, do not change the diameter but lead to a decreased number of fenestrae [41]. Some disease conditions such as fibrosis or cirrhosis can lead to a complete defenestration of LSEC which is termed sinusoidal capillarization [47]. Moreover, LSEC lacks filopodia or lamellopodia and the cells are held together from special intercellular junctions leading to no gaps between cells [48].

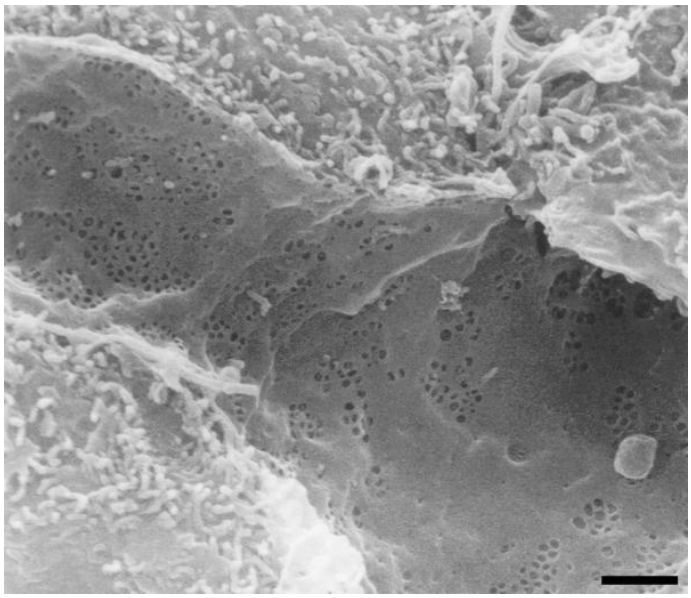

Figure 3. Ultrastructure of LSEC by scanning electron microscopy.
LSEC show fenestrations arranged in sieve plates. Scale bar 1 µm. Figure taken from Breat and Wisse *[42]* © 2002 Braet and Wisse; licensee BioMed Central Ltd. http://www.comparative-hepatology.com/content/1/1/1

1.2.1.2. Scavenging functions of LSEC

Furthermore, LSEC have a high scavenging ability. With aid of endocytotic receptors and clathrin-mediated endocytosis, LSEC are able to clear the blood from waste macromolecules and nanoparticles [49-51] (Figure 4). Scavenger receptors, mannose receptors and Fc-gamma (Fcγ) receptor IIb2 (CD32b) are expressed by LSEC. Stabilin-1 and stabilin-2 are scavenging receptors, which are able to remove for example collagen N-terminal propeptides of types I

and III procollagen [52], hyaluronan [50, 53], AGE-albumin [54] and oxidized low-density lipoproteins [55] from the blood. Ligands of the mannose receptor expressed by LSEC are for example ovalbumin [56], agalacto-orosomucoid [57] and collagen α-chains (types I, II, III, IV, V, and XI) [58, 59]. Fcγ receptor IIb2 is able to bind blood-prone soluble IgG immune complexes [60, 61]. Further receptors involved in clearance expressed on LSEC are LYVE-1, LRP-1, L-SIGN and C-type lectin (CLEC) receptors [62-64].

1.2.1.3. Immunoregulatory functions of LSEC

LSEC are involved in immune response in the liver through pattern recognition, antigen presentation and leukocyte recruitment [65]. Mannose receptor, stabilins and Toll-like receptors (TLR) on LSEC are pattern recognition receptors removing pathogen-associated molecules and damage-associated molecules from the blood and activate the immune system, which is a hallmark of cells with innate immune functions [66, 67] (Figure 4). Binding of ligands like LPS to TLR4 leads to the production of proinflammatory cytokines such as IL-6 and TNF-α via NFκB translocation [68]. Viral particles can get to liver parenchyma through LSEC fenestrations to infect hepatocytes, which then present viral antigens via MHCI. CD8+ T-cells extend their protrusions through fenestrations to recognize the presented viral antigens by hepatocytes to activate immune response [69]. Furthermore, in the presence of PDL1 [70], uptake of antigens by mannose receptor can lead to a tolerogenic CD8+ T-cell response through antigen presentation by MHCI [71] or to regulatory T-cell induction by CD4+ T-cells through antigen presentation by MHCII [72] (Figure 4). LSEC are able to recruit effector T-cells through adhesion molecules VCAM-1, ICAM-1 and VAP-1 [73]. Moreover, recruitment of regulatory T-cells is mediated by Stabilin-1 [74], recruitment of CD4+ T-cells by SCARF1 [75]. Furthermore, recruitment of natural killer cells [76] and natural killer T-cells [77] is mediated through production of CXCL16 by LSEC.

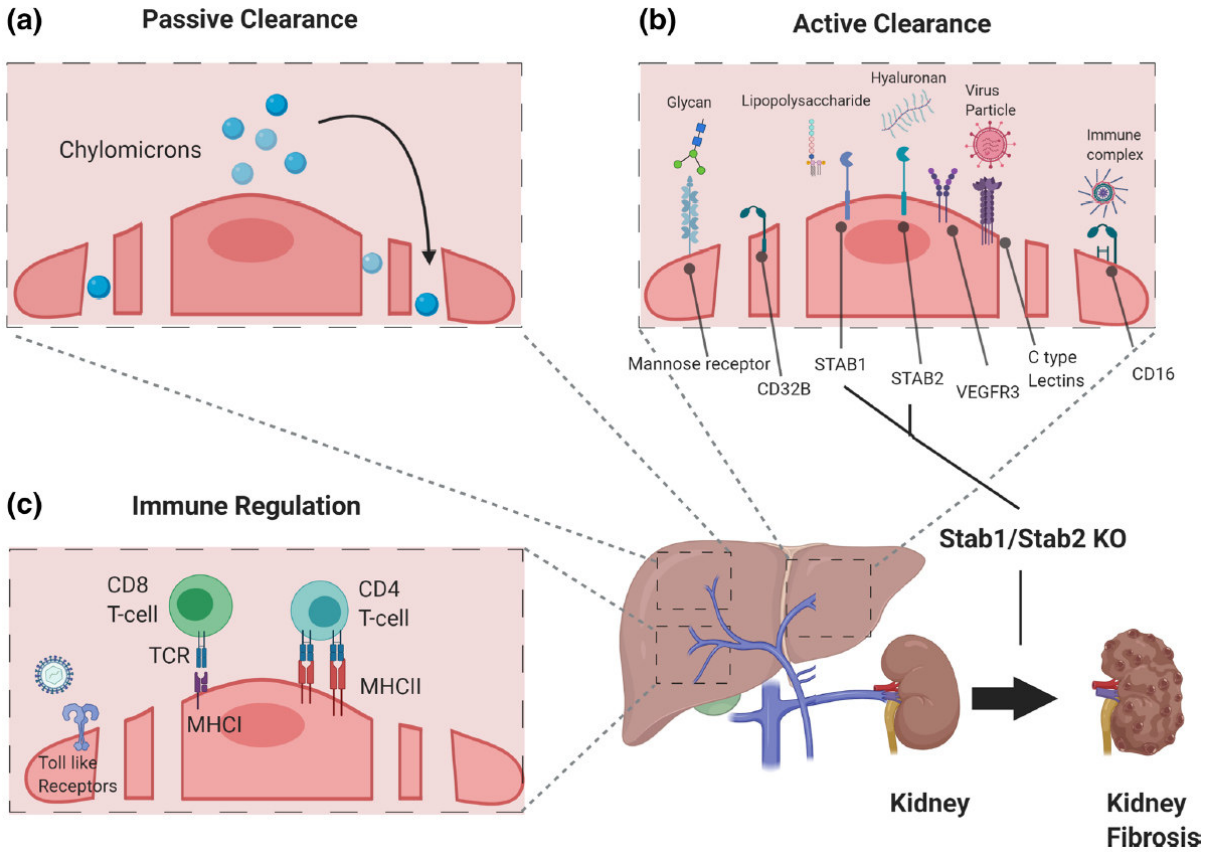

Figure 4. LSEC functions in clearance and immunoregulation.
(a) Fenestrations of LSEC allow passive transfer of nutrients and soluble factors like circulating chylomicrons. **(b)** Active clearance of pathogens, macromolecules, and waste products of LSEC through scavenger receptors like mannose receptor, CD32b, C-type lectins, stabilin-1 and stabilin-2. **(c)** LSEC express TLRs, involved in in innate immunity, MHCI and MHCII receptors, involved in adaptive immunity. Figure and labeling are adopted from Koch *et al. [5]* (CC BY 4.0) https://creativecommons.org/licenses/by/4.0/

1.2.2. LSEC marker

For studying LSEC *in vivo* and *in vitro*, reliable markers to identify LSEC and to distinguish them from all other liver and endothelial cells are essential. The characteristic fenestrae are the best feature to identify LSEC. But fenestrae are only able to be observed via electron microscopy, which makes it not useful for identifying LSEC in light/fluorescence microscopy and for isolation. Some vascular markers used for identification of LSEC in the past, including van Willebrand factor and CD31, are controversial discussed [78]. Van Willebrand factor is expressed in aged livers and in human liver sections but not in young individuals under physiological conditions or cultured human LSEC [79]. CD31 is expressed in the cytoplasm, but not on the cell surface of LSEC. Though, upon capillarization of LSEC, CD31 is expressed on the cell surface in liver fibrosis [80]. Hence, for identification of LSEC, surface receptors of LSEC gained importance. These include Stabilin-2 [81], LYVE-1 [62], FcγRIIb2 (CD32b) [82] and mannose receptor [83]. Another reliable marker is vascular endothelial growth factor

receptor 3 (VEGFR3), which is exclusively expressed in liver endothelial cells but not by another liver cell type [84] (Figure 4). Furthermore, G protein-coupled receptor 182 (GPR182) was shown to be a marker for sinusoidal endothelial differentiation among other things in the liver [85]. In summary, there is no single marker that can exclusively identify LSEC, therefore a combination of markers is the best way to identify them.

1.2.3. Angiocrine functions of LSEC

Angiocrine factors are instructive molecules (such as growth factors, chemokines, cytokines or ECM) produced by endothelial cells which regulate organ homeostasis and regeneration in a paracrine manner [86]. In the liver angiokines were shown to act on hepatocytes to regulate liver zonation and liver regeneration. Angiocrine Wnt signaling controls liver zonation and liver growth. Endothelial specific disruption of Wnt signaling was conducted by EC-specific deletion of Wnt cargo receptor Evi/Wntless (Wls), which is involved in the exocytosis of Wnt ligands, using a *Stab2-Cre* driver mouse. Wls-deficient mice had reduced liver-weight-to-body-weight ratio. Furthermore, deficiency of Wls led to a loss of pericentral β-catenin target genes (Glutamine synthetase, Rh B Glycoprotein, Axin2, cytochrome P450 2E1) and extended the expression of periportal genes such as arginase 1 [5, 87]. Furthermore, endothelial derived Bone Morphogenetic Protein (BMP)-2 and BMP6 regulate iron homeostasis in hepatocytes. Deletion of EC-specific *Bmp2* (*Stab2-Cre*) or *Bmp6* (*Tie2-Cre*) led to reduced hepcidin expression in hepatocytes causing an iron deposition in the liver and serum [88, 89].

The liver has a high regenerative capacity after acute liver injury, wherein LSEC play a crucial role by angiocrine signaling. LSEC regulate the balance between hepatocyte and LSEC proliferation. Liver regeneration is divided in different phases. Hepatocytes proliferate in an early phase at day two after liver injury like partial hepatectomy (PHx), whereas LSEC proliferate in a later phase around day four. In the early inductive phase after PHx, expression of Tie2 receptor antagonist angiopoiteine-2 (ANGPT2) is downregulated in LSEC leading to downregulation of transforming growth factor beta 1 (TGF-β1), which acts as hepatocyte growth inhibitor [90]. Moreover, in the early phase VEGF-A receptor 2 (VEGFR2) signaling leads to upregulation of EC-specific transcription factor inhibitor of DNA binding 1 (ID1) resulting in secretion of Wnt Family Member 2 (WNT2), which is a hepatotropic cytokine, and hepatocyte growth factor (HGF) to boost hepatocyte proliferation [84]. Another signaling pathway inducing upregulation of ID1 and subsequent secretion of WNT2 and HGF is activation of CXCR7 signaling in LSEC [91]. Following injury, activated platelets release stromal-derived factor-1 to induce CXCR7-mediated signaling resulting in hepatocyte proliferation [92]. Loss of liver mass during hepatectomy leads to increased perfusion pressure

in the early phase of liver regeneration. LSEC are able to sense the resulting shear stress and subsequently upregulate expression of integrin β1 and VEGFR3 signaling resulting in production of HGF [93]. During later angiogenic phase, ANGPT2 expression is restored by EC to activate VEGFR2 in an autocrine manner inducing angiogenic EC proliferation in response to hepatocyte-derived VEGF [5, 90].

1.2.4. LSEC capillarization and endothelial dysfunction

1.2.4.1. Capillarization of LSEC

The differentiated sinusoidal, discontinuous phenotype of LSEC, including fenestrations and lack of a basement membrane, is indispensable for liver homeostasis and function (Figure 5). The process of dedifferentiation of LSEC leading to loss of fenestrae and development of basement membrane leading to a capillarized phenotype, is called “sinusoidal capillarization” [94]. This process come along with a switch from sinusoidal (e.g., CD32b, LYVE-1) to continuous EC marker (e.g., CD31, CD34) expression [95]. A phenotypical change of LSEC is also seen during aging which is termed “pseudocapillarization” [96, 97]. Pseudocapillarization is characterized by a reduction of fenestrations in size and number, thickening of the ECs and the formation of an inconsistent basement membrane leading to sinusoidal dysfunction and dyslipidemia [98].

Differentiated LSEC are able to keep HSCs in a quiescent state, whereas capillarization of LSEC lead to activation of HSCs. Activated HSC release stored retinol, gain a proliferative and inflammatory phenotype and begin to produce ECM [99]. Deposition of ECM leads to increasing tissue stiffness, which in turn further stimulates activation of HSCs [100]. HSCs are wrapped around the LSEC and express smooth muscle proteins desmin and α-smooth muscle actin (αSMA) in activated state giving them the ability for constriction of sinusoids [101]. Activation of HSC lead to vasoconstriction which increases vascular resistance, shear stress and can lead to hypoxia. Perpetuated increased vascular resistance can lead to portal hypertension. Finally, activation of HSC is involved in the formation of liver fibrosis. Therefore, LSEC are considered as key regulators of hepatic vascular blood pressure by indirect regulation of blood flow via HSCs [102]. In response to shear stress, triggered by increased blood pressure, LSEC are able to generate vasodilators, which act in a paracrine manner on HSC, keeping them in a quiescent state by inhibiting their vasoconstrictive effects [103]. In summary, capillarization is accompanied by endothelial dysfunction leading to the loss of vasodilatory, anti-inflammatory, anti-angiogenic, pro-regenerative and anti-fibrotic function [104].

1.2.4.2. The role and regulation of nitric oxide bioavailability in LSEC differentiation

Nitric oxide (NO) is a key molecule for LSEC differentiation and subsequent HSC quiescence (Figure 5). LSEC express endothelial nitric oxide synthase (eNOS), which synthesizes NO. Vascular Endothelial Growth Factor (VEGF) produced by neighboring cells, like hepatocytes or HSCs, promotes production of NO in LSEC [105]. Under sustained shear stress Kruppel-like factor 2 (KLF2) is expressed by LSEC inducing NO production, which has a vasodilating effect [106-108]. Furthermore, Endothelin-1, a vasoconstrictive molecule, is downregulated by KLF2 [107]. Notch signaling is also an important pathway for LSEC maintenance and HSC quiescence. Overexpression of endothelial Notch leads to the repression of eNOS signaling followed by less NO production leading to LSEC dedifferentiation and subsequent activation of HSC [109]. Furthermore, overexpression of Notch ligand Delta-like ligand 4 lead to capillarization of LSEC [110]. The inability by LSEC of NO synthesis leads to the activation of HSC and subsequent a switch from vasodilation to vasoconstriction resulting in increased intrahepatic vascular resistance [111].

1.2.4.3. Regulators of LSEC differentiation

In the last years several molecules crucial for LSEC maintenance and homeostasis were identified. Among these ETS-related gene (ERG) regulates TGF-β/BMP-signaling by promoting SMAD1 signaling concurrent repressing SMAD2/3 signaling to prevent endothelial-to-mesenchymal transition (EndMT) subsequent supporting endothelial homeostasis [112]. Furthermore, Hedgehog (Hh) signaling pathway plays a role in LSEC maintenance. Activation of Hh signaling pathway leads to capillarization of LSEC and activation of HSC [113]. Activated HSC in turn produce Hh molecules, which further enhance Hh signaling in LSEC [114]. Liver X receptor α (LXRα) seems to inhibit Hh signaling and thereby restoring LSEC differentiation [115]. Moreover, HSC-derived BMP9 acting on endothelial receptor activin receptor-like kinase 1 (ALK1) is a modulator of LSEC capillarization. Deletion of BMP9 leads to a continuous LSEC phenotype with reduced fenestrae and increased expression of continuous EC marker CD34 resulting in a pro-fibrotic phenotype [116].

1.2.4.3.1. LSEC master regulator GATA4

As described above KLF2, Notch, LXRα, and ERG were suggested to play a role in the regulation of LSEC phenotype and function, but a specific master regulator of LSEC differentiation remained undefined. Recently, our group identified transcription factor GATA4

as a master regulator of LSEC differentiation using LSEC-specific Cre driver mice [117]. Deletion of endothelial *Gata4* in early embryonic development using *Stab2-iCre* driver mouse led to the switch to continuous differentiated EC causing liver fibrosis. Moreover, colonization of hematopoietic progenitor cells into the fetal liver was impaired due to the transdifferentiation of LSEC. Because of that Gata4 deficient mice showed anemia and were embryonic lethal [117]. The use of a new Clec4g-iCre driver mouse with a late embryonic deletion of endothelial *Gata4* allowed the analysis of the role of GATA4 in the adult mouse. Here, LSEC-specific *Gata4* deficiency led to a LSEC-to-continuous EC differentiation of the sinusoids resulting in sinusoidal capillarization with the formation of a basement membrane. These alterations were accompanied with perisinusoidal liver fibrosis and hepatopathy. Analysis of the underlying mechanism revealed that chromatin accessibility was increased for pro-fibrotic genes including *Pdgfb* and the transcription factor *Myc* in *Gata4*-deficient LSEC. Activated MYC was shown to mediate *de novo* expression of the pro-fibrotic angiokine *Pdgfb* [95], which is a known cytokine for activation of HSC.

Transcription factor GATA4 belongs to the GATA family of zinc finger transcription factors. The GATA family includes GATA1 – GATA6, which recognize and bind to the “GATA” consensus sequence 5'-[AT]GATA[AG]-3‘ in promotors of genes regulating their expression [118, 119]. GATA proteins are divided into two subfamilies depending on their expression pattern. GATA1 – GATA3 are expressed in hematopoietic progenitors [120-122]. GATA4 – GATA6 are expressed in mesodermal precursors which give rise to the heart and the endoderm of gut and epithelium [123, 124]. Moreover, expression of GATA4 is seen in the myocardium during embryonic development and in adulthood [124, 125]. The GC-rich gene sequence of Gata4 encodes for a 45 kDa sized protein consisting of 441 amino acids. The function of GATA4 in heart and liver development was studied using Cre/loxP technology with different driver mice. Gata4 homozygous null mice are embryonic lethal between E8.5 and E9.5. The embryos failed in ventral folding morphogenesis resulting in a lack of centralized heart tubes and partial development outside the yolk sac [126]. Rivera-Feliciano *et al.* showed that endothelial Gata4 is necessary for epithelial-to-mesenchymal transition (EMT) and is required for atrioventricular cushion growth and remodeling using a *Tie2-Cre* driver mouse. Moreover, the embryos at E12.5 had liver hypoplasia [127]. Furthermore, conditional deletion of *Gata4* in hepatic mesenchymal cells using *G2-Cre* driver mouse resulted in embryonic lethality around E13.5. The embryos had liver hypoplasia and advanced liver fibrosis [128].

1.2.4.3. Endothelial dysfunction promotes liver disease pathology

Increased shear stress resulting from vasoconstriction and increased vascular resistance can lead to activation of Piezo cation channels facilitated by integrins inducing expression of Notch-dependent transcription factors HES1 and HEY1. Accordingly, LSEC secrete chemokine CXCL1 leading to neutrophil recruitment promoting microthrombus formation and portal hypertension [129]. Moreover, hypoxia, induced during endothelial dysfunction, leads to excessive expression of VEGF promoting HSC activation and angiogenesis [130, 131]. Release of pro-fibrotic angiocrine TGF-β1 by LSEC is linked to HSC activation [132, 133]. Prevention of sinusoidal capillarization and endothelial dysfunction is crucial for liver homeostasis to prevent liver fibrogenesis, which increases the risk for cirrhosis and HCC [65] (Figure 5).

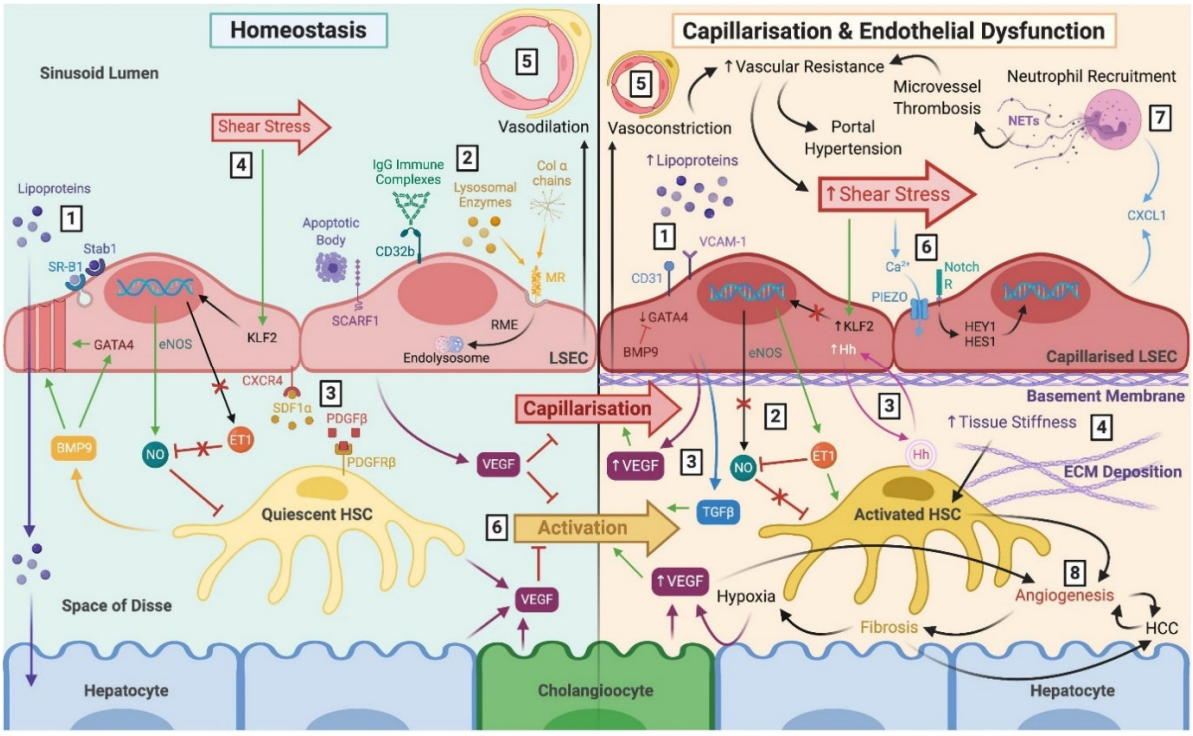

Figure 5. Maintenance of LSEC differentiation through several pathways promoting homeostasis and preventing endothelial dysregulation and disease pathology.
Left: Differentiated phenotype of LSEC maintain liver homeostasis. **1 – 6** Expression of receptors (e.g., MR, CD32b, Stabilin-1, Stabilin-2) and fenestrations facilitate the function of LSEC in clearance. LSEC are in close proximity to HSCs keeping them quiescent in an NO-dependent manner promoting vasodilation of the sinusoids. **Right:** Capillarization of LSEC leading to endothelial dysfunction and promotion of liver diseases like fibrosis. **1 – 8** Loss of fenestrations and basement membrane development occurs during capillarization. LSEC are unable to produce NO leading to activation of HSC. Activation of HSC through several angriocrine molecules (e.g., TGF-β1) and pathways (e.g., Notch signaling) lead to ECM deposition and vasoconstriction. Increased vascular resistance leads to portal hypertension. Figure and labeling are adopted from Wilkinson *et al.* [65] (CC BY 4.0) https://creativecommons.org/licenses/by/4.0/

1.3. Liver fibrosis and cirrhosis

1.3.1. Etiology and epidemiology of liver fibrosis and cirrhosis

Liver fibrosis is excessive ECM (e.g. collagens, fibronectin and laminins) deposition by myofibroblasts upon chronic liver injury during wound healing process leading to scar tissue. Chronic liver injuries can be subdivided into hepatocellular and cholestatic. Injuries to hepatocytes like NASH accounts to hepatocellular, whereas obstruction to bile flow like primary sclerosing cholangitis accounts to cholestatic liver injury. Nevertheless, major causes of liver fibrosis are chronic viral hepatitis infections (Hepatitis B and Hepatitis C), NAFLD/NASH and excessive alcohol consumption leading to AFLD/ASH, which account to chronic hepatocellular liver diseases [134]. Liver fibrosis is a reversible process if the underlying cause of liver injury is diminished [135]. However, if chronic injury is lasting for a longer period of time (approximately 20 years), liver fibrosis can progress to cirrhosis, which is the end stage of chronic fibrotic liver diseases. There are two types of cirrhosis, compensated and decompensated cirrhosis. Compensated cirrhosis causes no major complications for the patients. However decompensated cirrhosis is characterized by the development of portal hypertension and liver failure, resulting in short term survival and the need of liver transplantation [136]. The prevalence and mortality of cirrhosis worldwide is heterogeneous across locations and dependent on age and sex. GBD Cirrhosis Collaborators analyzed the global burden and mortality of cirrhosis. In 2017 cirrhosis caused more than 1.32 million deaths (male: 883000, female: 440000) worldwide which constitute 2.4 % of total deaths. Moreover, the cirrhosis deaths in 2017 in males were mainly caused by hepatitis C (31.7 %) and alcohol-related liver disease (27.3 %). In females the major causes for cirrhosis deaths were hepatitis B (24.0 %) and hepatitis C (26.7 %) [137].

1.3.2. Diagnosis and staging of liver fibrosis and cirrhosis

Liver fibrosis and cirrhosis can be diagnosed by biopsy or noninvasive methods [138]. For specific staging and grading, histological examination of liver biopsies is crucial. There are different semiquantitative staging systems developed, which categorize fibrosis stages. These scoring systems take the extent of fibrosis, location or number of septa and architectural disorganization into account [139]. They have the same concept, that fibrosis begins in the portal tracts, extend to other neighboring portal tracts and in the end to hepatic venules resulting in cirrhosis [118]. Liver biopsy is an invasive procedure with potential side effects i.e. pain, bleeding and/or minor mortality. Because of that, noninvasive methods including routine

laboratory tests and image-based techniques like ultrasonography, computed tomography and magnet resonance imaging are used. The assessment of serum levels for aminotransferases, platelet count, hyaluronic acid and N-terminal propeptide of type III collagen display laboratory options of fibrosis diagnostics [140]. However, staging of fibrosis is not able with these laboratory tests. Whereas liver stiffness can be measured by ultrasonography and correlated with extent of fibrosis [141]. Other image-based techniques can assess fibrosis by changes in the hepatic parenchyma [142].

1.3.3. Types of liver fibrosis

The pattern of fibrosis differs among the different liver disease etiologies. In chronic viral hepatitis B and C, fibrosis starts at the portal tracts, develops to periportal fibrosis leading to bridging septal fibrosis. Fibrosis in alcohol-related disease or NAFLD starts in pericentral lobular region and deposition of ECM in the space of Disse leads to a perisinusoidal (pericellular) fibrosis along the sinusoids around individual hepatocytes. Portal-portal fibrotic septa surrounding liver nodules are seen in fibrosis resulting from biliary tract. Besides the expansion of fibrotic scar area, hepatocellular nodules surrounded by fibrotic septa are formed in cirrhosis [143-145].

1.3.4. Myofibroblasts during fibrogenesis

Hepatic myofibroblasts are the source of excessive ECM in liver fibrosis and therefore play a major role in the development and progression of liver fibrosis. In normal liver myofibroblasts are absent, but upon chronic liver injury they accumulate at sites of injury [146]. They are highly proliferative cells which are characterized by the production of extracellular matrix involving fibrillar collagens and contractility by *de novo* development of stress fibers like αSMA [147]. Myofibroblasts can originate from different cell types through activation or transdifferentiation. Established origins of myofibroblasts are epithelial cells through EMT, fibrocytes, mesenchymal stromal cells, mesothelial cells, portal fibroblasts and HSCs [148]. Nevertheless, portal fibroblasts and HSCs were demonstrated as the major source of myofibroblasts in the liver, HSC in hepatocellular liver injury and portal fibroblasts in cholestatic liver injury, respectively [149].

1.3.5. Endothelial cells and liver fibrosis

Liver fibrosis development and progression is a complex process based on the crosstalk and interplay between different cell types of the liver. Paracrine and autocrine signals and pathways can lead to the activation or transdifferentiation of HSC into myofibroblasts resulting in ECM deposition. Among these are growth factors (e.g., PDGF and TGF-α), chemokines (e.g., CCR5 and CXCL4), adipokines (e.g., leptin and adiponectin) and fibrogenic TGF-β1 signaling pathway as major effectors [144, 150, 151]. LSEC were shown to contribute to liver fibrosis mainly through TGF-β1-mediated synthesis of ECM proteins (laminin, collagen type IV, and entactin) [132] and by regulating hepatic microenvironment induced by secreted pro-fibrotic molecules (Figure 6). Capillarization of LSEC upon liver injury leading to the activation of HSC resulting in ECM production is a critical process during fibrogenesis. In a NAFLD mouse model sinusoidal capillarization was reported early in steatosis phase prior to development of liver fibrosis, hypothesizing LSEC capillarization as relevant event for progression to NASH-associated fibrosis [152]. Moreover, LSEC are involved in the regulation of the balance between regeneration and fibrosis as a response of liver injury. Activation of CXCR7-ID1 pathway in LSEC leads to a pro-regenerative response to acute liver injury. Whereas chronic liver injury leads to the constitutive expression of fibroblast growth factor receptor 1 in LSEC suppressing CXCR7-ID1 pathway by favoring pro-fibrotic CXCR4 pathway [91].

1.3.5.1. Pathways involved in liver fibrosis

Differentiated LSEC are believed to be gatekeepers of fibrosis [153-155]. Pathways involved in the maintenance of LSEC differentiation are important to prevent capillarization and in turn to prevent liver fibrogenesis. Synthesis of NO is a key regulator of LSEC differentiation (Figure **6**). Therefore, VEGF released from hepatocytes and HSCs [105], KLF2 expression in LSEC [156] and suppressed Notch signaling [109] have anti-fibrotic effects. Moreover, transcription factor ERG is crucial for endothelial homeostasis by promoting SAMD1 signaling. Upon loss of ERG, LSEC undergo EndMT resulting in liver fibrosis through activation of SMAD2/3 signaling while repressing SMAD1 signaling [112]. Ding *et al.* showed that activation of endothelial Sphingosine-1-phosphate receptor 1 by its natural ligand or pharmacological agonists have anti-fibrotic affects [157]. Moreover, endothelial loss of LSEC master regulator GATA4 was shown to result in liver fibrogenesis. Deletion of *Gata4* leads to *de novo* expression of HSC activating growth factor PDGFB through a GATA4/MYC/PDGFB axis resulting in perisinusoidal liver fibrosis [95]. Moreover, HSC activation by LSEC can be mediated by release of other pro-fibrotic molecules such as fibronectin, TGF-β, PDGFs and Hh molecules [109, 113, 133, 158, 159]. Furthermore, restoration of LSEC differentiation was sufficient to

promote reversion of activated HSC to quiescent HSC mediated by NO production resulting in regression of fibrosis or prevention of fibrosis progression [103, 160, 161]. Therefore, LSEC could be a potent therapeutic target in liver fibrosis.

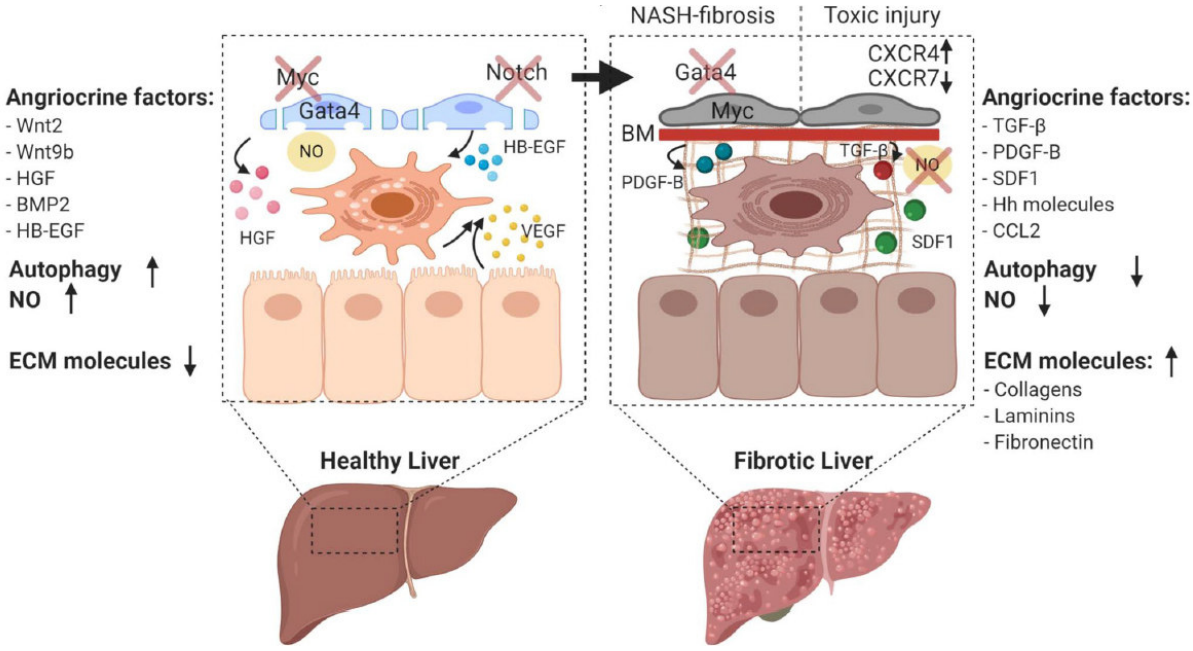

Figure 6. LSEC in different liver fibrosis etiologies.
Left: During liver homeostasis expression of GATA4 maintains the differentiated phenotype of LSEC. Differentiated LSEC synthesize NO, secrete angiocrine factors and the autophagic activity is increased**. Right**: In NASH-induced perisinusoidal liver fibrosis GATA4 is downregulated leading to capillarization of LSEC and secretion of PDGFB. In toxic liver fibrosis the balance shifts from CXCR7 to CXCR4 promoting pro-fibrotic pathways. Secretion of angiocrine factors further stimulates activation of HSC and subsequent ECM deposition in the space of Disse. Synthesis of NO is disrupted and autophagic activity is reduced in activated LSEC. Modified figure and labeling are adopted from Koch *et al.* [5] (CC BY 4.0) https://creativecommons.org/licenses/by/4.0/

1.3.6. Liver fibrosis in NAFLD/NASH

Non-alcoholic liver disease (NAFLD) ranges from simple steatosis (non-alcoholic fatty liver), which is characterized by fat accumulation in ≥ 5 % of hepatocytes without alcohol consumption, to non-alcoholic steatohepatitis (NASH), which is characterized besides steatosis by hepatic inflammation, ballooning of hepatocytes and optional liver fibrosis [27, 162, 163]. In the presence of fibrosis, NASH can progress to cirrhosis and HCC. Obesity is a major risk for developing NAFLD. Furthermore, NAFLD is often associated with features of the metabolic syndrome, like dyslipidemia, insulin resistance and type 2 diabetes, which are risk factors for progression from steatosis to NASH [164, 165]. NAFLD affect around 25 % of the global population, whereas the prevalence of NASH is estimated as 2 % to 5 % of the global population [166]. Although NASH can be present with or without fibrosis, several studies showed that the presence of liver fibrosis dictates the long-term prognosis, and the risk of liver-

related mortality increases exponentially with increase in fibrosis stage in patients with NAFLD [167-170].

In the progression from simple steatosis to NASH a multiple parallel-hit theory emerged. Dietary habits, environmental and genetic factors can lead to insulin resistance, adipocyte proliferation and dysfunction, lipolysis and changes in the intestinal microbiome. Adipocytes produce adipokines and proinflammatory cytokines like IL-6 and TNF-α maintain the insulin resistance state and lead to an increased hepatic free fatty acids (FFA) flux. This processes together with altered gut microbiome lead to synthesis and increased levels of triglycerides, FFAs and free cholesterol inducing oxidative stress and endoplasmic reticulum stress resulting in hepatic inflammation and fibrogenesis [171, 172].

1.3.7. Therapy strategies of liver fibrosis

It was shown in animal and clinical studies that any degree of fibrosis, up to cirrhosis, is potentially reversible [173, 174]. Several experimental studies revealed antifibrotic agents with therapeutic potential for liver fibrosis. However, just few candidates have shown a significant effect in clinical trials and currently there are no antifibrotic therapies licensed for humans [175]. Besides targeting LSEC differentiation maintenance for preventing liver fibrogenesis or stimulate fibrosis regression there are different therapeutic strategies for liver fibrosis.

The removal of etiological factors such as treatment against HBV and HCV infections in chronic hepatitis B and C, abstinence from alcohol abuse in alcohol-related liver disease and lifestyle changes (e.g., weight control and nutrition) in NAFLD is the most effective intervention for liver fibrosis treatment [134, 176-179].

Chronic injury of hepatocytes leads to inflammation and fibrosis progression. Therefore, therapies to reduce liver parenchymal injury and to prevent inflammation are important in inhibiting fibrogenesis. Antioxidants and hepatoprotective agents, like vitamin E, glutathione, N-acetylcysteine, S-adenosyl-methionine, taurine, curcumin and silymarin are able to prevent hepatocyte injury and limit inflammation [180-186]. Besides preventing hepatocyte apoptosis, promoting hepatocyte regeneration was suggested as a useful therapeutic strategy for liver fibrosis. Using ultrasound-targeted microbubble destruction in combination with HGF gene transfer, which stimulates hepatocyte regeneration, had an anti-fibrotic effect in a rat fibrosis model [187].

HSCs are a potential target cell of antifibrotic therapy because of their essential role in liver fibrogenesis. TGF-β and PDGFB are the major cytokines promoting HSC activation and therefore inhibition of TGF-β signaling pathway and PDGFB can lead to inhibition of HSC

activation [188, 189]. Furthermore, induction of HSC apoptosis is associated with cytokines and growth factors like cytokines like insulin-like growth factor-1, IFN-α and inhibitor of IκB kinase [190-192].

Gene therapy and targeted therapy by antisense oligonucleotides or siRNA against genes involved in pathogenesis of liver fibrosis offer potentially effective anti-fibrotic therapeutical strategies. Among these genes TGF-β, PDGFB, CTGF and TIMP have already been used as targets [188, 193-196].

1.4. Mouse models for investigating liver fibrosis

Liver fibrosis mouse models are crucial for analysis of liver fibrosis pathogenesis and treatment. Chemical-based, diet-based, surgery-based, infection-based and genetically modified models are used. Ethanol, carbon tetrachloride (CCl_4) and thioacetamide cause direct injury to hepatocytes leading to hepatic inflammation and pericentral bridging fibrosis [197-199]. The chemical agents can be administered orally, via inhalation or by intraperitoneally (*i.p.*) injection. Liver fibrosis develops faster via *i.p.* injection compared to the other administration options. Chemical-based models have a high reproducibility, simple and fast execution and are close to human liver fibrosis [200].

Diet-based models are used to induce NAFLD and NASH. Methionine and choline-deficient (MCD) diet, high-fat diet (HFD) and choline-deficient l-amino acid-defined diet (CDAA) diet are commonly used diets in these models and lead to perisinusoidal (pericellular) liver fibrosis. The diets have different potential to induce liver fibrosis, which mainly depends on the feeding period. Nevertheless, diet-based models cannot mimic the complete pathology of human NASH in regards of metabolic changes such as obesity and insulin resistance [201, 202].

The most used surgery-based model is common bile duct ligation (BDL), which causes cholestatic injury and periportal biliary fibrosis. It is based on the double ligation of the bile duct leading to increased biliary pressure, inflammation and cytokine secretion resulting in cholestasis and liver damage [203]. BDL is used for short-term studies of liver fibrosis associated with cholestatic injury [204, 205].

Hepatic virus infection is not able to induce liver fibrosis in rodents. To overcome this fact, immunodeficient mice are transfected with a HBV plasmid for analysis of liver fibrosis in hepatic virus infection [206]. Another method of infection-based models is the use of *Schistosoma mansoni* infection. A immunological response based on cytokines against the parasite's egg

evolves leading to the development of granulomas associated with liver fibrosis [207]. However, these infection-based models have a high variability in liver fibrosis development.

The use of genetically modified animals allows the study of individual genes or pathways in the development of liver fibrosis. Moreover, usage of Cre-loxP system allows to modify genes liver-specific or cell type-specific. But mostly the mice need a second stimulus to develop fibrosis. Mice deficient in multidrug resistance-associated protein-2 develop hepatocyte necrosis, portal inflammation and periductal fibrosis, which can lead to biliary fibrosis [208]. Feeding of *Alms1 Fat aussi* mutant mice with HFD lead to lipotoxicity, insulin resistance, diabetes, inflammation, hepatocyte ballooning and pericellular and pericentral fibrosis. This model is close to human NASH and is based on the interaction of genetics and diet, which allows the analysis of the progression from NAFL to NASH [209, 210].

Chronic CCl_4 model and diet (MCD and CDAA diet) induced NASH model were used in this study to analyze liver fibrosis, therefore these two models are described precisely in the following section.

1.4.1. Chronic carbon tetrachloride (CCl_4) model

The chronic CCl_4 model belongs to the chemical-based models of liver fibrosis. Mostly CCl_4 is administered by *i.p.* injection typically of 0.5 to 1 ml/kg body weight CCl_4 (diluted in corn oil) for four to six weeks, two to three times per week [211]. CCl_4 is metabolized by cytochrome P450 2E1 (CYP2E1) enzyme expressed by centrilobular hepatocytes, leading to toxic trichloromethyl radicals resulting in centrilobular liver necrosis, activation of KC and induction of inflammatory response. Moreover, activation of HSC is induced by cytokines leading to pericentral bridging fibrosis [212, 213]. Application of a single CCl_4 dose can be used as model for liver regeneration after toxic injury. The CCl_4 model is a simple and fast model for bridging liver fibrosis with high reproducibility and resembles several properties of human liver fibrosis [200].

1.4.2. Diet induced NASH model

Methionine and choline-deficient (MCD) diet and choline-deficient l-amino acid-defined (CDAA) diet are well-established diet-induced mouse models to analyze NASH [201]. Both nutrients are essential in the hepatic β-oxidation and the production of very low-density lipoprotein (VLDL) [214]. Moreover, they are important for the synthesis of phosphatidylcholine, which is important for the transport of VLDL out of the liver [215]. Deficiency of methionine and choline leads to reduced transport of lipids out of the liver and decreased β-oxidation leading

to lipid deposition in the liver, oxidative stress and changes in cytokines and adipokines [216, 217].

Mice fed a MCD diet develop steatohepatitis and fibrosis after five to eight weeks [218, 219]. However, the metabolic state is different to human NASH, because the mice have no peripheral insulin resistance, no hyperlipidemia and the mice exhibit a high weight loss [214, 220, 221]. Therefore, MCD diet is not appropriate to study NASH pathogenesis and especially the metabolism in NASH. However, it is the fastest model to analyze liver fibrosis associated with NASH [202].

Choline-deficient l-amino acid-defined (CDAA) diet is as also deficient in choline but enriched by a mixture of L-amino acids low in methionine concentration replacing an equivalent and corresponding proteins [222]. CDAA diet leads to increased lipid synthesis, oxidative stress and inflammation resulting in liver fibrosis [214]. Development of NASH and fibrosis takes longer than in MCD diet, but the degree is slightly more severe. But like in MCD diet the metabolic state is not comparable to human NASH [216].

To overcome weight loss and insulin sensitivity of MCD diet and classic CDAA diet, a modified CDAA diet, named CDAA plus, which has a higher fat content and is supplemented with cholesterol. It is worth mentioning, that there are different diet compositions (fat and cholesterol content) of CDAA plus diet. CDAA plus diet with 0.2 % cholesterol was able to induce steatohepatitis after around 10 weeks with liver fibrosis (stage 1-2 fibrosis) with increasing liver fibrosis severity with increasing feeding period and HCC development after around 36 weeks. Moreover, the mice gain a bit weight and there is potential of developing a modest insulin resistance [223-225]. However, it does not mimic the metabolic state in human NASH completely and more metabolic and immunological studies are necessary. Nevertheless, this diet-induced NASH model is suggested as good tool to study NASH-associated liver fibrosis [202].

2. Aims of the thesis

LSEC are discontinuous and fenestrated microvascular endothelial cells of the liver and are gatekeepers of their microenvironment to control organ function in health and disease. Transdifferentiation of LSEC towards a capillary phenotype, namely, sinusoidal capillarization leads to the activation of HSC and deposition of ECM consequently. Liver fibrosis is characterized by excessive ECM deposition leading to scar tissue under persistent liver injury. Therefore, identification of molecular regulators for LSEC differentiation is of great value. Recently, we could identify GATA4 as a master regulator of sinusoidal differentiation in the liver. Hepatic endothelial Gata4-deficiency caused sinusoidal capillarization leading to an angiocrine switch and subsequently to perisinusoidal liver fibrosis in a genetic animal model [95]. Based on this finding, we wondered whether *Gata4* expression is affected by pathological changes in the liver. Therefore, in this study the role of Gata4 in liver fibrosis models should be analyzed. Furthermore, using different strategies to overexpress *Gata4* in LSEC should be applied for evaluating therapeutical use.

Analysis of GATA4 in liver fibrosis models

The first aim of the study was the establishment and analysis of 1) a toxic chronic CCl_4 model leading to bridging liver fibrosis and 2) a diet induced NASH model leading to perisinusoidal liver fibrosis. The liver fibrosis models should be compared for vascular alterations and expression and role of GATA4.

Generation and analysis of LSEC-specific Gata4 knockin mouse

In the second aim, a LSEC-specific knockin mouse overexpressing *Gata4* ($Gata4^{LSEC\text{-}KI}$) should be generated and used in liver fibrosis models. Furthermore, the functionality of $Gata4^{LSEC\text{-}KI}$ mouse should be assessed.

Generation and analysis of LSEC-specific Gata4 overexpressing lentivirus

In the third aim a LSEC-specific lentivirus overexpressing *Gata4* should be generated and analyzed for the application for Gata4-therapy.

3. Material and methods

3.1. Material

3.1.1. Chemicals, solvents and reagents

Chemical/reagent	Manufacturer	Order no.
2-Propanol	Sigma-Aldrich	33539-M
4-(2-hydroxyethyl)-1-piperazineethane-sulfonic acid (HEPES)	Sigma-Aldrich	H3375
4',6-Diamidino-2-phenylindol (DAPI)	Thermo Fisher Scientific	D1306
4 % formaldehyde solution ROTI Histofix	Carl Roth	P087.3
Aceton	Sigma-Aldrich	24201-R
Agarose	Sigma-Aldrich	A9539
Ampicillin	Sigma-Aldrich	A5354
Bovine Serum Albumin (BSA)	VWR	J642-1ML
Carbon tetrachloride (CCl_4)	Sigma-Aldrich	289116
cOmplete Ethylenediaminetetraacetic acid (EDTA) free Protease inhibitor	Sigma-Aldrich	11873580001
CD146 Magnetic-activated cell sorting (MACS) MicroBeads	Miltenyi Biotech	130-092-007
choline-deficient l-amino acid-defined (CDAA) diet	Ssniff	E15666-94
Collagenase A	Sigma-Aldrich	C2674-1G
Corn oil	Sigma-Aldrich	SAFSC8267
Dako 3-amino-9-ethylcarbazole (AEC) substrate chromogen	Agilent Technologies	K346430-2
Dako antibody Diluent	Agilent Technologies	S080983-2
Dako aqueous mounting medium	Agilent Technologies	S302580-2

Chemical/reagent	Manufacturer	Order no.
Dako fluoresecence mounting medium	Agilent Technologies	S302380-2
Dako peroxidase solution	Agilent Technologies	S202386-2
DH5α competent cells	Thermo Fisher Scientific	18265017
Dithiothreitol (DTT),1M	Life Technologies	P2325
Dulbecco's Modified Eagle Medium (DMEM) medium	Life Technologies	61965059
Deoxynucleotide (dNTP) Mix, 10 mM	Invitrogen	18109017
Ethanol	Carl Roth	5054.3
Ethanol denaturated	Carl Roth	K928.4
EDTA	Invitrogen	15575-038
Fc receptor Blocking Reagent, mouse	Miltenyi Biotec	130-092-575
Fetal bovine serum (FBS)	Life Technologies	10270106
Fructose	Sigma-Aldrich	F9048
Gene Ruler deoxyribonucleic acid (DNA) Ladder mix, 100-10000bp	Thermo Fisher Scientific	SM0333
Glucose	Gibco	15023-021
Glycin	Carl Roth	HN07.1
Grey’s balanced salt solution (GBSS)	Sigma-Aldrich	G9779-6X
Heat Induced Epitope Retrieval (HIER) Citrate Buffer pH 6.0, 10 x	Zytomed Systems	ZUC028-500
innuMIX quantitative polymerase chain reaction (qPCR) SyGreen Sensitive	Analytik Jena	845-AS-1310
innuMIX qPCR DSGreen Standard	Analytik Jena	845-AS-1320
Isofluran	WDT	21311
Kanamycin	Sigma-Aldrich	K0254
Laemmli buffer, 2x	Bio-Rad	1610737
Laemmli buffer, 4x	Bio-Rad	1610747

Chemical/reagent	Manufacturer	Order no.
L-Alanine	Carl Roth	3076.1
L-aspartic acid	Carl Roth	1690.1
L-glutamine	Sigma-Aldrich	G8540
L-glutamic acid	Carl Roth	1743.1
L-serine	Carl Roth	1714.1
L-threonine	Carl Roth	1738.1
Loading Dye, 6x	Thermo Fisher Scientific	R0611
Luminata Forte Western horseradish peroxidase (HRP) substrate	Millipore	WBLUF0500
Lysogeny broth (LB) Agar	Thermo Fisher Scientific	2270025
LB Medium	Carl Roth	X964.2
Magnesium chloride ($MgCl_2$)	Carl Roth	KK36.1
Maxima Reverse Transcriptase, 200 U/µL	Thermo Fisher Scientific	EP0741
Mayer's hemalum solution	Merck	109249
Methionine and choline deficient (MCD) diet	Ssniff	E15653-94
Methanol	Carl Roth	CP43.4
Nancy 520	Sigma-Aldrich	01494
Nonident P40 (NP-40) Substitute	Fluka	74385
Normal donkey serum	Dianova	017-000-121
Nycodenz	Axis Shield	102424
Paraformaldehyde (PFA)	Carl Roth	0335.3
Penicillin-Streptomycin, 10.000 U/ml	Thermo Fisher Scientific	15140122
Phosphate-buffered saline (PBS)	Life Technologies	14190169
Potassium chloride (KCl)	Fluka	60128
Precision Protein™ Dual Color Standards	Bio-Rad	1610374
Proteinase K from Tritrachium	Sigma-Aldrich	P6556

Chemical/reagent	**Manufacturer**	**Order no.**
Oligo(dT)18 Primer	Life Technologies	SO132
Restriction enzyme BamHI, 10 U/µL	Thermo Fisher Scientific	ER0051
Restriction enzyme MluI, 10 U/µL	Thermo Fisher Scientific	ER0562
Restriction enzyme NdeI, 10 U/µL	Thermo Fisher Scientific	ER0585
Restriction enzyme XbaI, 10 U/µL	Thermo Fisher Scientific	ER0681
RiboLock RNase Inhibitor	Life Technologies	EO0381
Radioimmunoprecipitation assay (RIPA) buffer	Sigma-Aldrich	R0278
Skim milk powder	Merck	70166
Super Optimal broth with Catabolite repression (S.O.C.) Medium	Invitrogen	15544-034
Sodium bicarbonat ($NaHCO_3$)	Sigma-Aldrich	S5761
Sodium butyrate ($Na(C_3H_7COO)$)	Sigma-Aldrich	B-5887
Sodium phosphate monobasic monohydrate (NaH_2PO_4)	Sigma-Aldrich	59638
Standard (Std) rodent diet	Ssniff	V1534-000
Sucrose	Sigma-Aldrich	16104
T4 DNA Ligase	Thermo Fisher Scientific	EL0011
Tango Buffer, 10 x	Thermo Fisher Scientific	BY5
Tris(hydroxymethyl)aminomethane (Tris)-acetate-EDTA buffer, 50 x	Carl Roth	CL86.2
Tris/Glycine/Sodium Dodecyl Sulfate (SDS), 10 x	Bio-Rad	1610772
Tris-hydrogen chloride (HCl) Ultra Pure, 1M pH8	Life Technologies	15568025
Trypan blue solution	Sigma-Aldrich	T8154
Trypsin-EDTA, 10 x	Sigma-Aldrich	59418C
Tween 20	Sigma-Aldrich	P7949

Chemical/reagent	Manufacturer	Order no.
Ultra Pure Water Dnase/Rnase Free	Life Technologies	10977-049
UltraComp eBeads™ Compensation Beads	Thermo Fisher Scientific	01-2222-42
Xtreme Gene 9 Transfection solution	Sigma-Aldrich	6365787001
Xylene	Carl Roth	9713.5

3.1.2. Buffers and media/recepies

Buffer/medium	composition
4 % PFA pH 7.2	40 g PFA powder 100 mL 10 x PBS 900 mL dH_2O
30 % Sucrose	3 g Sucrose 10 mL 1x PBS
10 x Ca^{2+}-deprived medium (pH 7,4)	0,1 mM L-Asparaginsäure 0,2 mM L-Threonin 0,3mM L-Serin 0,5 mM Glycin 0,6 mM L-Alanin 0,9 mM L-Glutaminsäure 0,9mM L-Glutamin 20 mM D(+) Glucose 120 mM Fructose 197 mM Sucrose 3 mM KCl 0,7 mM NaH_2PO_4-H_2O 0,5 mM $MgCl_2$ 10 mM HEPES 24 mM $NaHCO_3$

Buffer/medium	composition
FACS buffer	1x PBS 5 % FBS
MACS Puffer	1x PBS 1 % FBS 2mM EDTA
35 % Nycodenz	3,5 g Nycodenz up to 10 mL GBSS
Transfer buffer	100 mL 100 % methanol 100 mL 10 x TGS buffer 300 mL dH_2O
bEnd.3 medium	500 mL DMEM medium 10 % FBS 1 % P/S
mLSEC medium	500 mL DMEM medium 10 % FBS 1 % P/S 2 mM L-Glutamine

3.1.3. Kits

Kit	Manufacturer	Order no.
DC Protein Assay	Bio-Rad	5000112
EndoFree Plasmid Maxi Kit	QIAGEN	12362
KAPA HotStart Mouse Genotyping Kit	Sigma-Aldrich	KK7352

Kit	Manufacturer	Order no.
Smart Protein Layers Blue Kit 40W	NH Dyeagnostics	PR925
Triglyceride Quantification Colorimetric Kit	BioVision	K622
innuprep DNA Mini Kit	Analytik Jena	845-KS-10410
innuPREP Gel Extraction Kit	Analytik Jena	845-KS-5030
innuPREP RNA Mini Kit 2.0	Analytik Jena	845-KS-20400
QIAprep Spin Miniprep Kit	QIAGEN	27104
TURBO DNA-free Kit	Thermo Fisher Scientific	AM1907

3.1.4. Unconjugated antibodies

Table 1. Unconjugated antibodies

Specificity	Clone	Manufacturer	Order no.	Applicatio	Dilution
CD31	SZ31	Dianova	DIA-310	IF	1:50
CD31	2H8	Thermo Fisher Scientific	MA3105	IF	1:400
Desmin	polyclonal	Abcam	ab15200	IF	1:200
Endomucin	V.7C7	Life Technologies	14-5851-85	IF	1:100
ERG	EPR3864	Abcam	ab92513	IF	1:1000
GAPDH	14C10	Cell Signaling	2118S	WB	1:2500
GATA4	H-112	Santa Cruz	sc-9053	WB	1:500
GATA4	eBioEvan	Life Technologies	14-9980-82	IF WB	1:50 1:500
Glutamine synthetase	polyclonal	Sigma-Aldrich	G2781	IF	1:2000
LYVE-1	polyclonal	R&D Systems	AF2125	IF	1:100
Podocalyxin	polyclonal	R&D Systems	AF1556	IF	1:100
RFP	polyclonal	Rockland	600-401-379	IF	1:500
V5-tag	E10/V4RR	Life Technologies	MA5-15253	WB	1:500

3.1.5. Conjugated antibodies

Table 2. Conjugated antibodies

Specificity	Conjugate	Clone	Manufacturer	Order no.	Application	Dilution
Armenian hamster IgG	AF488	polyclonal	Dianova	127-545-160	IF	1:400
CD11b	BV510	M1/70	Biolegend	101245	FACS	1:200
CD31	PerCP Cy5.5	MEC13.3	Biolegend	102522	FACS	1:200
Goat IgG	AF488	polyclonal	Dianova	705-545-	IF	1:400
Goat IgG	AF647	polyclonal	Dianova	705-605-	IF	1:400
Goat IgG	Cy3	polyclonal	Dianova	705-165-	IF	1:400
Goat IgG	HRP	polyclonal	Life Technologies	A16005	WB IF	1:5000 1:200
LYVE-1	PE	223322	R&D	FAB21258	FACS	1:200
Live/Dead	APC–Cy7	polyclonal	BD Horizon	565388	FACS	1:500
Mouse IgG	HRP	polyclonal	GE Healthcare	LNXA931	WB	1:5000
Rabbit IgG	AF488	polyclonal	Dianova	711-545-	IF	1:400
Rabbit IgG	AF647	polyclonal	Dianova	711-605-	IF	1:400
Rabbit IgG	Cy3	polyclonal	Dianova	711-165-	IF	1:400
Rabbit IgG	HRP	polyclonal	Sigma-Aldrich	GENA934	WB	1:5000
Rabbit IgG	HRP	polyclonal	Agilent Technologies	K4009	IF	Ready to use
Rat IgG	AF488	polyclonal	Dianova	712-545-	IF	1:400
Rat IgG	AF647	polyclonal	Dianova	712-605-153	IF	1:400
Rat IgG	Cy3	polyclonal	Dianova	712-165-	IF	1:400
Rat IgG	HRP	polyclonal	Dianova	DAB-87238	WB	1:5000
Rat IgG2a	PerCP Cy5.5	RTK2758	Biolegend	400531	FACS	1:200
Rat IgG2b	PE	RTK4530	Biolegend	400607	FACS	1:200

3.1.6. Oligonucleotides

Oligonucleotides were ordered as lyophilized from Metabion international AG.

3.1.6.1. Primers for Genotyping

Table 3. Primes for genotyping

Gene	Sequence 5’ - 3’
Mm Clec4g-iCre_Fw	AAGCTGAACAACAGGAAATGGTTC
Mm Clec4g-iCre_Rv	GGAGATGTCCTTCACTCTGATTCT
Mm Gata4_Fw	CCCAGTAAAGAAGTCAGCACAAGGAAAC
Mm Gata4_Rv	AGACTATTGATCCCGGAGTGAACATT
Mm ROSA26YFP_Common	AAAGTCGCTCTGAGTTGTTAT
Mm ROSA26YFP_Mutant	AAGACCGCGAAGAGTTTGTC
Mm ROSA26YFP_Wildtype	GGAGCGGGAGAAATGGATATG

3.1.6.2. Primers for quantitative reverse transcription (RT)-qPCR

Table 4. Primers for RT-qPCR

Gene	Sequence 5’ - 3’
Mm Acta2_Fw	CAGACATCAGGGAGTAATGGTTG
Mm Acta2_Rv	GGCCACACGAAGCTCGTTAT
Mm Bmp2_Fw	TGCTTCTTAGACGGACTGCG
Mm Bmp2_Rv	CACGGCTTCTTCGTGATGGA
Mm Col1a1_Fw	CAGGCTGGTGTGATGGGATT
Mm Col1a1_Rv	AAACCTCTCTCGCCTCTTGC
Mm Col3a1_Fw	GAGGAATGGGTGGCTATCCG
Mm Col3a1_Rv	GCGTCCATCAAAGCCTCTGT
Mm Des_Fw	GAGGAGAGCAGGATCAACCTT
Mm Des_Rv	CTCTCCATCCCGGGTCTCAA
Mm Gak_Fw	CTGCCCACCAGGCATTTG
Mm Gak_Rv	CCATGTCACATACATATTCAATGTACCT
Mm Gata4 (EJ6/7)_Fw	GCTCCATGTCCCAGACATTC
Mm Gata4 (EJ6/7)_Rv	ATGCATAGCCTTGTGGGGAC
Mm Mrpl46_Fw	GGGAGCAGGCATTCCTACAG

Gene	Sequence 5’ - 3’
Mm Mrpl46_Rv	GGTCCGGTCATTTTTTTTGTCA
Mm Myc_Fw	TACAACACCCGAGCAAGGAC
Mm Myc_Rv	GAGGCTGCTGGTTTTCCACT
Mm Pdgfb_Fw	CTACCTGCGTCTGGTCAGC
Mm Pdgfb_Rv	GCTCAGCCCCATCTTCATCTAC
Mm Pdgfrb_Fw	ATGGGTGGAGATTCGCAGGA
Mm Pdgfrb_Rv	TCATAGCGTGGCTTCTTCTGCC
Mm Srp72_Fw	CACCCAGCAGACAGACAAACTG
Mm Srp72_Rv	GCACTCATCGTAGCGTTCCA
Mm synthGata4_Fw1	GCGGCTTGTACCACAAAATG
Mm synthGata4_Rv1	TTGCAAACTGGTTCGCCTTC
Mm Wnt2_Fw	GCCCTGATGAACCTTCACAAC
Mm Wnt2_Rv	GGAGCCACTCACACCATGAC

3.1.6.3. Primers for sequencing

Table 5. Primers for sequencing

Region	Sequence 5’ - 3’
pCD31Pr_Fw	TGTGGCAGGCAAGAGAATTC
pCD31Pr_Rv	TTTGCGTTGGAGTGTGACA

3.1.7. Plasmids

pSynthMmGata4-V5 (Figure 7) used for pLV-CD31Pr-Gata4-V5-miT-W generation was provided by Integrated DNA Technologies, Inc. (Coralville, USA). Sequence of synthesized murine Gata4 is listed in Table 6. pLV-EF1a-ADR3-IRP-EV (Figure 8) used for expression analysis of synthesized Gata4-V5 is a homemade plasmid. pLV-CD31Pr-KLF2-V5-miT-W (Figure 9) used for lentiviral overexpression in LSEC was kindly provided by Prof. Christian Buchholz (Paul-Ehrlich-Institut, Langen) [226]. For production of lentivirus 3rd generation lentiviral plasmids pMD2.G, pRSV-Rev, pMDLg/pRRE were provided by addgene (Watertown, USA) [227] and pCDNA3.1/p35 was kindly provided by Prof. Martin Leverkus (UMM, Mannheim).

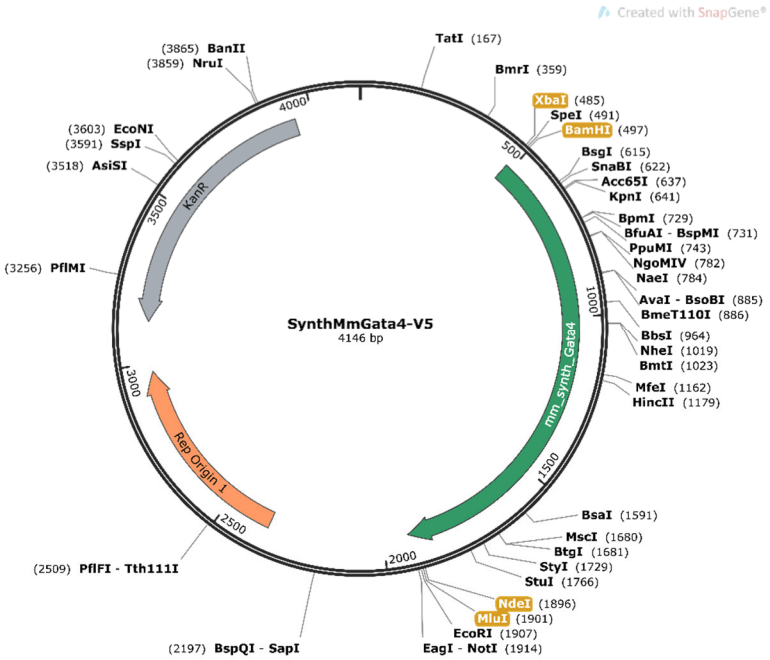

Figure 7. Vector map of SynthMmGata4-V5.
The plasmid contains synthesized murine *Gata4* (*Gata4*, accession numbers: NM_001310610) with a V5-tag and a Kanamycin resistance for selection of bacteria. The restriction enzymes used for cloning are highlighted. Vector map was created using SnapGene.

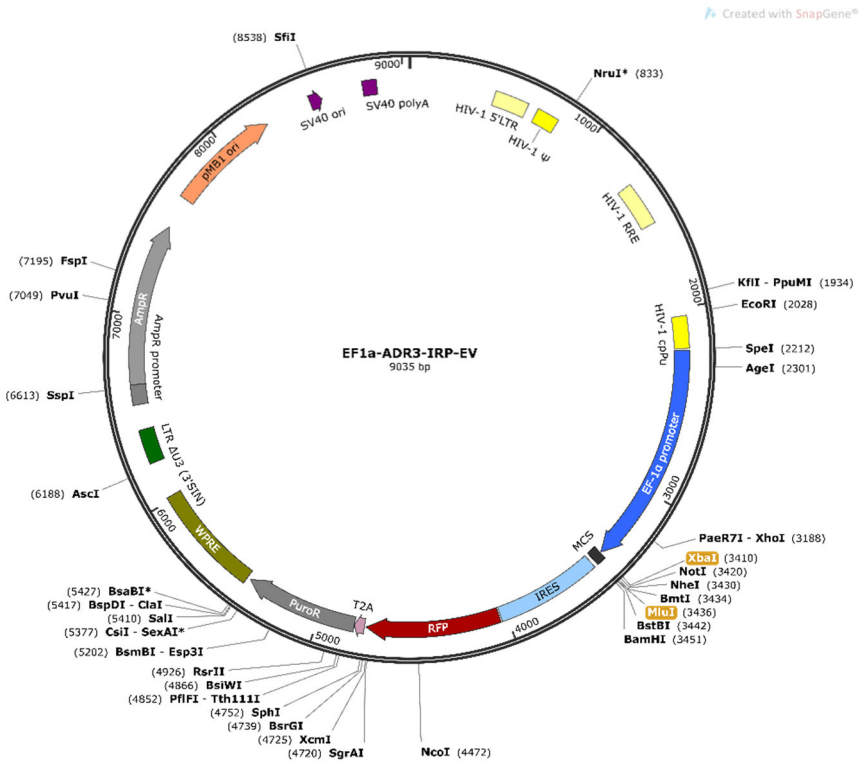

Figure 8. Vector map of pLV-EF1a-ADR3-IRP-EV.
The lentiviral expression plasmid contains a constitutive Elongation factor 1α (EF-1α) promoter for transcription of reporter red fluorescent protein (RFP) and cloned cDNA insert. The plasmid contains Ampicillin and Puromycin resistance for selection of bacteria and mammalian cells. Restriction enzymes used for cloning are highlighted within the multiple cloning site (MCS). Vector map was created using SnapGene.

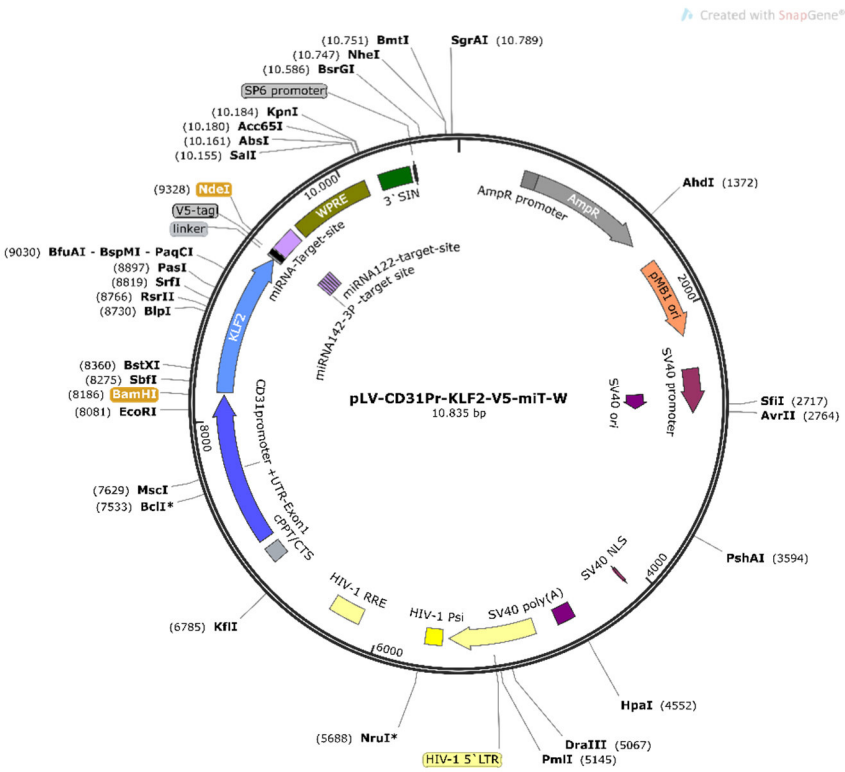

Figure 9. Vector map of pLV-CD31Pr-KLF2-miT-W.
The lentiviral vector contains murine *Klf2* with an V5-tag under CD31 expression promotor. For specific expression in target cells the vector contains miRNA122 and miRNA142-3P target sites. The plasmid contains Ampicillin resistance for selection of bacteria and restriction enzymes used for cloning are highlighted. Vector map was created using SnapGene.

3.1.7.1. Sequence of synthesized murine Gata4-V5

Table 6. Sequence of synthesized murine Gata4-V5.
Binding sites of primers for RT-qPCR of synthesized Gata4 are underlined.

Gene	Sequence
Synthesized murine Gata4-V5	atgtaccagtcccttgcaatggccgcaaatcatggacctccacccggcgcatacgaagcctcaggcccaggcgcctttatgcacagt gcaggagcagcatcatcaccagtctacgtaccaactcccagggtacctagttctgtcctcggtctgtcctatttgcaggggggaggca gcgccgcagcagccggtacaacctctggaggttctagtggggctggtccttctggggcaggtcccggaacacaacagggtagccc aggctggtcccaggccggcgcagaaggcgccgcttacacccctcctcccgtaagcccccgattctcctttccagggaccactggttct cttgccgccgccgccgctgctgctgccgctcgggaagccgccgcttacgggagtggaggcggcgcagccggagccggtcttgcag ggcgagagcagtatggaagaccaggattcgccggttcttatagttctccataccctgcctacatggcagacgtcggggctagctggg ctgcagccgctgcagcctccgctggccccttgacagtccagttttgcacagtctgcctgggcgggccaatccagggcgacatccaa atctggtagacatgtttgacgatttctcagaaggacgagaatgtgtcaattgtggggctatgtcaaccccccttggagacgagacggg accggccactatctgtgcaatgcctgcggcttgtaccacaaaatgaatgggattaaccggccacttattaagcctcagagaaggctgt cagcaagcaggcgcgttggtcttagctgtgccaactgtcaaacaactacaactaccctgtggagacggaatgcagaaggcgaacc agtttgcaacgcttgtggactctatatgaagctgcatggtgtcccaagacctctggctatgcgcaaggagggtatccagacaaggaa gaggaagcccaagaatctcaataaaagtaaaaccccctgccggtcccgccggggagactttgcccccatcttcaggtgcctcctcag ggaactcaagtaatgccacatcctcttcttcatcaagcgaggagatgagacccattaaaacagaacccggtcttagtagccactatg ggcacagtagcagtatgtcccaaacattctccaccgtgagtggccacggtccctccattcatccagtccttagtgcccttaaacttagtc cccaaggctatgcatctcctgttacacaaaccagtcaggcctcctctaagcaagattcttggaactcactggttcttgcagattctcacg gagatataataactgccgccgctgcagctttcgagggcaagcccatccccctgttgggccttgacagcaca

3.1.8. Consumables

Consumable	Manufacturer	Order no.
4 % - 20 % gradient polyacrylamide gels	Bio-Rad	4561094
6-well plate	Greiner Bio-One	657160
6-well plate Collagen IV coated flat	neoLab Migge	354428
15 mL Cellstar Tubes	Greiner Bio-One	18827
50 mL Cellstar Tubes	Greiner Bio-One	2272616
96-well adhesive film	Axon	26979
96-well PCR plate	Analytik Jena	844-70038-0
96-well plate flat	Greiner Bio-One	655101
Affymetrix GeneChip Mouse Gene 2.0 ST Arrays	Thermo Fisher Scientific	902118
Cell culture dish Cellstar, 10 x 2 cm	Greiner Bio-One	664160

Consumable	Manufacturer	Order no.
Cell culture flask, T75	Greiner Bio-One	658175
Cell culture flask, T175	Greiner Bio-One	660175
Cell scraper	CytoOne	CC7600-0220
Cell strainer, 100 µm	neoLab Migge	352360
Compensation Beads	Life Technologies	01-2222-42
Cover slips	VWR	10513234
Cryo tubes, 2 mL	Greiner Bio-One	122263
Cryomold, 15 x 15 x 15 cm	Weckert	4566
Dako Pen	Agilent Technologies	S200230
Disposable scalpel	Carl Roth	T998.1
Erlenmeyer flask	Carl Roth	X749.1
Low Fluorescence Polyvinylidene fluoride (PVDF) membrane	Bio-Rad	1620264
MACS™ LS colums	Miltenyi Biotec	130-042-401
Mesh polyester monol, width 250 µm	neoLab Migge	2-4062
Microscopy slides Super Frost Plus	Langenbrinck	03-0060
Microtome blades, S35	pfm medical	207500000
Mini Cell Buffer Dam	Bio-Rad	1653130
Needle, 26G ½	BD	303800
Needle, 30G ½	BD	304000
Paraffin embedding cassettes	neoLab Migge	60001580
Parafilm® M	Merck	P7793
PCR stripes, 0,2 mL	Sarstedt	72.991.992
Pipette filter tips, 10 µL	Biozym	VT0200
Pipette filter tips, 100 µL	Biozym	VT0230
Pipette filter tips, 200 µL	Biozym	VT0240

Consumable	Manufacturer	Order no.
Pipette filter tips, 12500 µL	Biozym	VT0270
Pipette tips, 10 µL	Biozym	VT0104
Pipette tips, 200 µL	Biozym	VT0144
Pipette tips, 1250 µL	Biozym	VT0174
Polystyrene Round-bottom Tubes, 5 mL	Falcon	352052
Precellys® 2 mL Ceramic kit 1,4/2,8 mm	VWR	431-0170
Reaction Tubes Safe-Lock, 1,5 mL	Eppendorf	30120086
Reaction Tubes Safe-Lock Biopur, 1,5 mL	Eppendorf	30121589
Reaction Tubes Safe-Lock, 2 mL	Eppendorf	30120094
Reaction Tubes Safe-Lock, 5 mL	Eppendorf	30119401
Serological Pipette, 5 mL	Greiner Bio-One	606180
Serological Pipette, 10 mL	Greiner Bio-One	607180
Serological Pipette, 25 mL	Greiner Bio-One	760180
Syringe, 1 mL	B.Braun	9161502
Syringe,20 mL	B.Braun	4606205V
Syringe filters ROTILABO® PVDF, 0.45 µm	Carl Roth	P667.1
Thickblot filter paper	BioRad	1703969
Tissue-Tek® optimum cutting temperature (O.C.T.) Compound	Weckert	600001
Vivaspin 20, 100 000 MWCO	Buddeberg	VS 2042

3.1.9. Technical equipment

Device	Manufacturer
Balance analytical	Sartorius
Balance PT210	Sartorius
Cell culture incubator HERAcell® 150i	Thermo Fisher Scientific

Device	**Manufacturer**
Centrifuge 5417 R	Eppendorf
Centrifuge 5810 R	Eppendorf
Centrifuge 6K15 Refrigerated	Sigma-Aldrich
Cooling plate 4100	pfm medical
Counting chamber Neubauer improoved	Brand
Cryostat CM3050 S	Leica
Eclipse Ni-E motorized upright microscope	Nikon Instruments
DS-Qi2 high-definition monochrome camera	
DS-Ri2 high-definition color camera	
Filterset AHF F36-513 DAPI HC	
Filterset AHF F36-720 Sp. Green HC mFISH	
Filterset AHF F36-740 Sp. Orange HC mFISH	
Filterset Semrock BrightLine Cy5-4040C single-band	
Electrophoresis chamber Mini-PROTEAN Tetra System	Bio-Rad
Flow Cytometer BD FACSCanto II	BD Biosciences
Fridge profiline	Liebherr
Gas anesthesia system XGI-8	Caliper Life Sciences
Gel electrophoresis system Mupid® One	ADVANCE CO., LTD.
Heating block Termo Mixer C	Eppendorf
Heating Immersion Circulator	Julabo
Homogenizer Precellys Evolution	bertin instruments
Imaging System Intas ChemoStar Touch	Intas Science Imaging
Imaging System Intas GelStick IMAGER	Intas Science Imaging
Incubator	Binder
Intensilight Epifluorescence Illuminator	Nikon Instruments
Inverse microscope Axio Vert.A1	Zeiss

Device	Manufacturer
MACS™ Quadro separator	Miltenyi Biotec
MACS™ MultiStand	Miltenyi Biotec
Microplate reader Infinite M 200 Pro	Tecan
Mini-centrifuge Spectrafuge™	neoLab Migge
NanoPhotometer NP80	IMPLEN
Peristaltic pump	Ismatec
Plan Apo λ 4x NA 0.2	Nikon Instruments
Plan Apo λ 10x NA 0.45	Nikon Instruments
Plan Apo λ 20x NA 0.75	Nikon Instruments
Plan Apo λ 40x NA 0.95	Nikon Instruments
PowerPac™ Basic Power Supply	Bio-Rad
Precellys Evolution tissue homogenizer	Bertin Technologies
qTOWER 3 G touch	Analytik Jena
Refrigerator (-20 °C) profiline	Liebherr
Refrigerator (-80 °C)	PHC Europe BV
Rotary microtome 3006EM	pfm medical
Safety cabinet Herasafe KS class II	Thermo Fisher Scientific
Shaker DRS-12	neoLab Migge
Thermal Cycler T100™	Bio-Rad
Thermoblock ThermoMixer C	Eppendorf
Trans-Blot® Turbo™ Transfer System	Bio-Rad
Vortex-Genie™ 2	Scientific Industries
Water bath TW8	Julabo
Water bath pura22	Julabo
Water bath 1000	pfm medical

3.1.10. Software

Software	Version	Manufacturer
Fiji ImageJ	2.0.0	National Institutes of Health
FlowJo	V 10.1	FlowJo, LLC
GraphPad Prism 8	8.4.3	GraphPad Software
Inkscape	1.0.2-2	Inkscape Community
LabImage	4.2.3	Kapelan Bio-Imaging
NIS-Elements Advanced Research (Ar)	5.02	Nikon Instruments
qPCRsoft	4.0.8.0	Analytik Jena
R	3.6.1	R Core Team
SnapGene	5.3.2	GSL Biotech LLC

3.1.11. Mouse strains

Table 7. Mouse strains

Name	Official name	Supplier	Publication
B6N Wildtype	C57BL/6N	Janvier Labs	
Gata4 flox	Gata4$^{tm1.1Sad}$/J	The Jackson Laboratory (JAX: 008194)	[228]
Clec4g-iCre	C57BL/6N-Tg(Clec4g-icre)1.1^{Sgoe}	Our lab	[229]
Gata4$^{LSEC-KO}$	C57BL/6N-Tg(clec4g-icre)tm1.1^{Sgoe} x STOCK-Gata4^{tm1Sad}	Our lab	[95]
ROSA26STOPGata4	C57BL/6N-Gt(ROSA)26Sortm1(tomato-Gata4)^{Sgoe}	Our lab	
Gata4$^{LSEC-KI}$	C57BL/6N-Tg(clec4g-icre)tm1.1^{Sgoe} x C57BL/6N-Gt(ROSA)26Sortm1(tomato-Gata4)^{Sgoe}	Our lab	

3.1.12. Cell lines

Table 8. Cell lines

Name	Species	Description
bEnd.3	mouse	brain, cerebral cortex, endothelial
HEK-293T	human	embryonic kidney
HUVEC	human	umbilical vein/vascular endothelium

3.2. Methods

3.2.1. Animal experiments

3.2.1.1. Animal housing and breeding

Mice were housed under specified pathogen free conditions in a room with a 12 h/12 h light/dark cycle at the animal facility of the Zentrum für Medizinische Forschung (ZMF) in Mannheim. The animals were fed a standard rodent diet *ad libitum* and had free access to water. C57BL/6N mice were purchased from Janvier Labs.
For generation of parents of LSEC-specific conditional Gata4 knockout mouse ($Gata4^{LSEC\text{-}KO}$), homozygous floxed Gata4 mouse ($Gata4^{tm1.1Sad/J}$) on a 129/Sv background were crossed with Clec4g-iCre driver mouse (C57BL/6N-Tg(Clec4g-icre)1.1^{Sgoe}) on C57BL/6N background. The resulting heterozygous Gata4 F1 generation was crossed with homozygous floxed Gata4 mice, generating $Gata4^{LSEC\text{-}KO}$ mice bearing the genotype Clec4g-$iCre^{tg/wt}$ x $Gata4^{fl/fl}$. As control mice, littermates with the genotype Clec4g-$iCre^{wt/wt}$ x $Gata4^{fl/fl}$ or Clec4g-$iCre^{wt/wt}$ x $Gata4^{fl/wt}$ were used.

For generation of LSEC-specific Gata4 overexpressing Gata4 knockin mouse ($Gata4^{LSEC\text{-}KI}$) bearing the genotype Clec4g-$iCre^{tg/wt}$ x $R26STGata4^{fl/wt}$, Clec4g-iCre driver mice were crossed with homozygous floxed ROSA26-STGata4 mice (C57BL/6N-Gt(ROSA)26Sortm1(tomato-Gata4)^{Sgoe}). As control mice, littermates with the genotype Clec4g-$iCre^{wt/wt}$ x $R26STGata4^{fl/wt}$ were used.

The animal welfare commission of the Regierungspräsidium Karlsruhe approved all experiments.

3.2.1.2. Generation of Gata4 Knockin mouse

For generation of LSEC-specific Gata4 knockin mouse ($Gata4^{LSEC\text{-}KI}$), a stop-flox protected expression cassette containing *tdTomato-Gata4* fusion cDNA was cloned into ROSA26 (R26) locus on R26 targeting vector including a neomycin resistance for selection (in cooperation with Division of Cellular Immunology, German Cancer Research Center, Prof. Dr. Hans-Reimer Rodewald). After homologous recombination into embryonic stem (ES) cells and selection of ES cells, the first ROSA26STGata4-neo chimeric mouse generation was generated (Transgenic Service, German Cancer Research Center, Frank van der Hoeven and Interfaculty Biomedical Facility, Biotechnology Lab, Heidelberg University). Chimeric mice were bred with C57BL/6N (Janvier) and two independent ROSA26STGata4-neo sublines (54.2

and 62.1) were established. To delete neomycin cassette, ROSA26STGata4-neo mice were crossed with Flip-deleter mice (B6N.Cg-Tg(ACTFLPe)9205Dym/CjDswJ; JAX Strain #019100) The resulting ROSA26STGata4 x Flip mice were bred with C57BL/6N to remove flip recombinase transgene and afterwards ROSA26STGata4 mice were crossed with Clec4g-iCre driver mice to obtain Gata4$^{LSEC-KI}$ mouse, which express Gata4 LSEC-specific.

3.2.1.3. Mouse liver sinusoidal endothelial cell isolation

For isolation of mouse liver sinusoidal endothelial cells (mLSEC) of Gata4$^{LSEC-KO}$ and Gata4$^{LSEC-KI}$, 12-week-old mice were used and per sample three mice were pooled. Mice were sacrificed by cervical dislocation followed by perfusion of the liver via portal vein with 0.05 % Collagenase in Ca^{2+}-deprived medium at a pump speed of 2 mL/min until blood was flushed out. After dissection and weighing of the liver, the gallbladder was removed and the liver was shredded with the scissor. Until the digestion the livers were kept on ice in pre-cooled GBSS. For digestion of the livers 100 µL collagenase for control livers and 200 µL collagenase for fibrotic livers were added and incubated at 37 °C for 25 min. During the incubation, every 5 min the samples were pipetted up and down and after 10 min of incubation 50 µL collagenase for control livers and 100 µL collagenase for fibrotic livers were added. After filtering the cell suspension through a 250 µm mesh the cells were washed with GBSS at 300 g for 10 min at 4 °C. The supernatant was discarded and the cells were passed through a 100 µm cell strainer. After washing the cells again with GBSS at 300 g for 10 min at 4 °C, the pellet was resuspended in 1 mL GBSS. To separate non-parenchymal cells, a 19.3 % Nycodenz gradient was used. Therefore, the cells were centrifugated at 1400 g for 25 min at RT without brake and after centrifugation the top layer of cells was recovered and resuspended in 4 mL pre-cooled MACS buffer. mLSEC were isolated by Magnetic-activated cell sorting (MACS) using anti-LSEC ($CD146^+$) MicroBeads from Miltenyi Biotec for positive selection according to the manufacturer's instruction. The isolated mLSEC were pelleted at 300 g for 10 min at 4 °C and the supernatant was discarded. For purity check of mLSEC after isolation the cells were analyzed by flow cytometry (3.2.3.5. Flow cytometry). Isolation of mLSEC of CDAA fed mice and controls were jointly done with Theresa Staniczek and Dr. Manuel Winkler. Isolation of mLSEC of Gata4$^{LSEC-KI}$ and controls were jointly done with Stephanie Riester.

3.2.1.4. Dissection of mouse organs, plasma exploitation and tissue sample preparation

Before sacrificing the mice by cervical dislocation, blood samples were taken from the retrobulbar venous plexus under isoflurane anesthesia. The blood was collected in lithium heparin tubes and the plasma was separated by centrifugation at 7000 g for 7 min. The plasma was analyzed in a Cobas c311 analyzer (Roche) according to the manufacturer's protocol by the technicians at the core facility of the ZMF. Following blood parameters were analyzed: alanine transaminase (ALT), glutamate dehydrogenase (GLDH), aspartate transaminase (AST), trigylcerides, glucose, total protein, cholesterol, cholinesterase, creatinine, urea and bilirubin.

For preparation of liver, heart, spleen and kidney, the organs were dissected, weighed and photographed. For histological analysis, sectioned organs (liver, heart, spleen, kidney) were fixed in phosphate-buffered 4 % formaldehyde solution at RT for one to seven days. Formalin fixed tissue was paraffin embedded in embedding cassettes after dehydration of the tissue according to standard protocol.
For molecular biology, biochemical and histological analysis, sectioned organs were snap-frozen in liquid nitrogen in reaction tubes and stored at -80 °C. For histological analysis, inguinal lymph nodes were dissected, incubated in 4 % PFA for 4 h, followed by washing three times with PBS and incubation in 30 % sucrose for at least 2 h or overnight at 4 °C. After washing three times with PBS, the lymph nodes were placed in cryomolds and embedded in green colored optimal cutting temperature compound. Lymph nodes were slowly frozen in the gas phase of liquid nitrogen followed by transfer to liquid nitrogen and storage at -80 °C. Sections of 8 µm of frozen organs were prepared at the cryotome.

3.2.2. Molecular biology methods

3.2.2.1. Genotyping

For genotype analysis of the mouse strains, DNA was extracted from ear tissue and strain-specific identity was visualised by PCR reaction with strain-specific primer combinations using KAPA HotStart Mouse Genotyping Kit according to manufacturer's protocol. The tissue was lysed at 75 °C in 10x KAPA Express Extract Buffer and 1 U/µL KAPA Express Extract Enzyme for 10 min to extract the DNA. For denaturation, the samples were incubated for 5 minutes at 95 °C. The extracted DNA was diluted 10-fold in 10 mM Tris-HCl pH 8 and 1 µL DNA was used for polymerase chain reaction (PCR).

3.2.2.2. Polymerase chain reaction (PCR)

For PCR a PCR mix containing following components was used:

PCR-grade water	3 µL
2x KAPA2g Mix	5 µL
10 µM Forward Primer	0,5 µL
10 µM Reverse Primer	0,5 µL
DNA	1 µL

PCR was performed using a Thermal Cycler with following cycling protocol:

95 °C	3 min	
95 °C	15 sec	⎫
60 °C	15 sec	⎬ 35 x
72 °C	15 sec	⎭
72 °C	1 min	
12 °C	∞	

PCR products were analyzed by agarose gel electrophoresis.

3.2.2.3. Agarose gel electrophoresis

Agarose gel electrophoresis of PCR products or plasmids were performed on a 2 % agarose gel containing 10 % Nancy-520 at 100 V for 30 min. The DNA was visualized with Intas Gel Stick Imager.

3.2.2.4. Cloning of synthetic murine Gata4 in Lentiviral vectors LV-ADR3-EV and LV-CD31-KLF2-V5

For overexpression experiments of Gata4 with a LSEC-targeting lentiviral vector, first a murine synthetic Gata4 with a V5-tag (Gata4-V5) was synthesized (Table 6. **Sequence of synthesized murine Gata4** by Integrated DNA Technologies, Inc. (IDT; Coralville) into a kanamycin resistant plasmid. Lentiviral vector LV-CD31-KLF2-V5-miT122+142 (LV-CD31-KLF2-V5) was kindly provided by Prof. Dr. Christian Buchholz (Paul-Ehrlich-Institut, Langen). The vector contains murine CD31 promotor and two triple miRNA-detargeting sequences targeting miRNA122 and miRNA142-3P, which makes the vector LSEC-specific [226]. Furthermore, it contains an ampicillin selection marker but no reporter gene. Klf2-V5 had to be replaced by Gata4-V5 as described below. To test the functionality of synthetic murine Gata4,

it was cloned into LV-ADR3-IRP-EV (LV-ADR3-EV) which contains a ubiquitous expressed EF1α promotor, puromycin for selection and red fluorescent protein (RFP) as a reporter gene.

For cloning of Gata4-V5 into LV-ADR3-EV, Gata4-V5 and LV-ADR3-EV plasmids were digested with restriction enzymes Xba I and Mlu I (Figure 10).

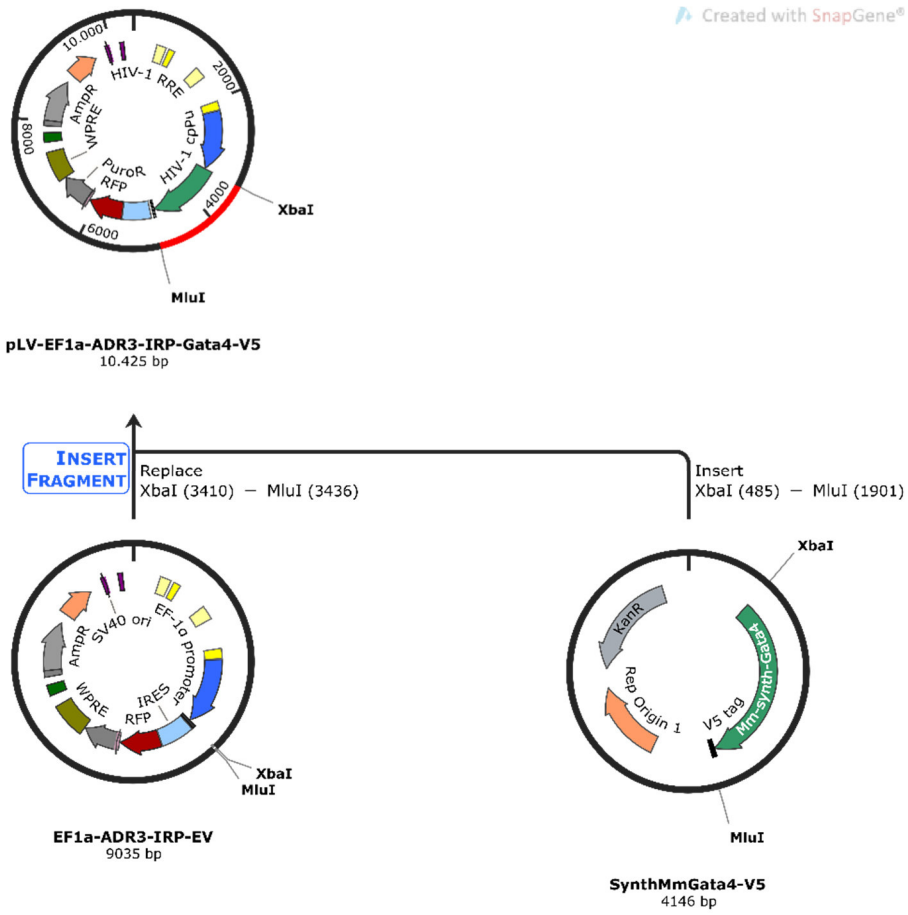

Figure 10. Cloning strategy of cloning synthesized murine Gata4-V5 into pLV-EF1α-ADR3-IRP-EV vector for overexpression experiments of *Gata4*.
Synthesized murine Gata4-V5 was cloned into pLV-EF1a-ADR3-IRP-EV using restriction enzymes XbaI and MluI. Cloning history was created using SnapGene.

To replace Klf2-V5 by Gata4-V5 in LV-CD31-KLF2-V5, both plasmids were digested with restriction enzymes BamH I and Nde I (Figure 11).

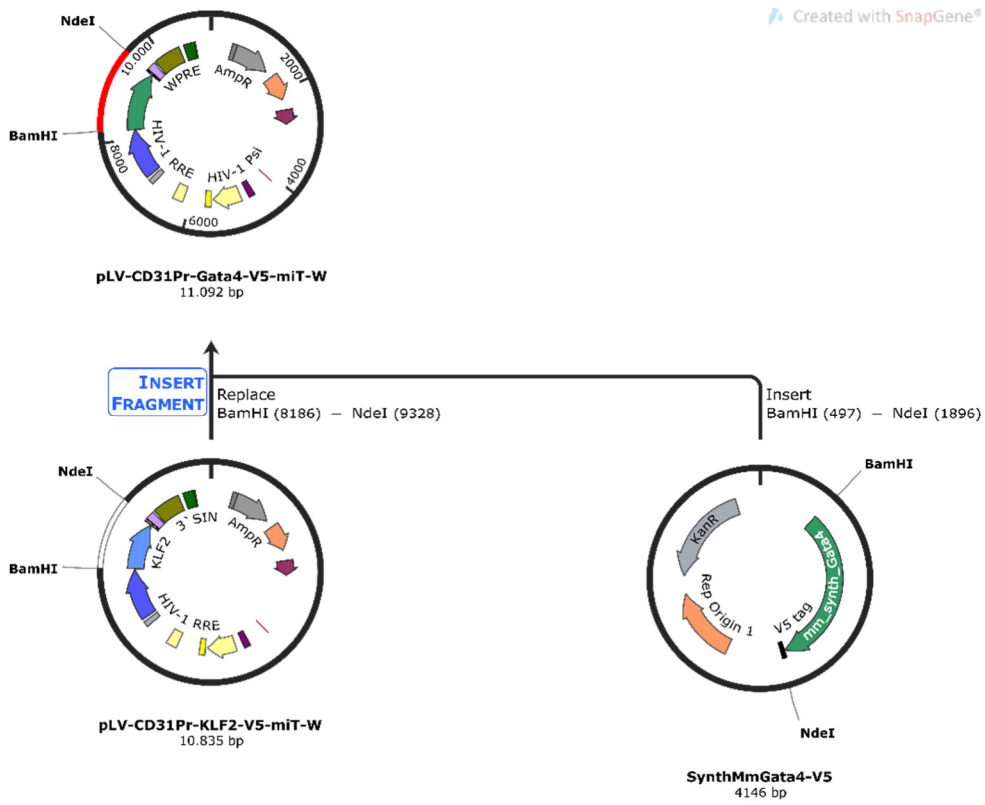

Figure 11. Cloning strategy of replacing murine Klf2-V5 with Gata4-V5 in pLV-CD31Pr-KLF2-V5-miT-W vector for overexpression of *Gata4* in LSEC.
Synthesized murine Gata4-V5 was cloned into pLV-EF1a-ADR3-IRP-EV replacing Klf2-V5 using restriction enzymes BamHI and NdeI. Cloning history was created using SnapGene.

Both restrictions were conducted at 37 °C for 1.5 h in 2x Tango buffer followed by inactivation of the enzymes at 65 °C for 10 min. Restriction enzyme activity was confirmed by agarose gel electrophoresis and Gata4-V5 insert was cut out of the gel. Vector backbones of LV-ADR3-EV and LV-CD31 and Gata4-V5 insert were purified using innuPREP Gel Extraction Kit according to manufacturer's protocol. DNA was eluted in 20 µL Elution buffer. Ligation of the insert with appropriate vector backbone was conducted using T_4 DNA ligase and 10 x T_4 DNA Ligase buffer. After ligation for 1 h at RT, the enzyme was inactivated for 10 min at 65 °C.

For transformation of competent E. coli (DH5α cells), 50 µL of DH5α cells were thawed on ice and 3 µL of ligated vector was added to DH5α cells and incubated for 30 min on ice. Afterwards, heat shock was performed at 42 °C for 45 sec, followed by incubation on ice for 5 min. After addition of 500 µL S.O.C medium, the cells were incubated at 37 °C and 300 rpm for at least 1 h. Thereafter, the cells were seeded on LB agar plates containing 100 µg/mL ampicillin and cultivated at 37 °C overnight for approximately 16 h. In the morning of the following day several colonies were picked and used for inoculation of 3 mL LB medium containing ampicillin for mini culture. The culture was incubated overnight for approximately 16 h at 37 °C and 200 rpm.

In the morning of the following day, one part of the bacteria culture was used for plasmid purification using QIAGEN Plasmid Mini Kit buffers (P1, P2 and P3) and the second part was stored at 4 °C as starter culture for a maxi culture. After centrifugation for 5 min at 5000 rpm and 4 °C, the cell pellet was resuspended in 250 µL P1 buffer and incubated for 5 min at RT. After addition of 250 µL P2 buffer, the reaction tube was inverted six times and incubated for 2 min at RT. Thereafter, 250 µL of P3 buffer was added, the tubes were inverted six times and incubated on ice for 10 min. After centrifugation for 30 min at 14000 rpm and 4 °C, the supernatant was transferred into a new reaction tube. For DNA precipitation, 680 µL isopropanol was added and the samples were centrifuged for 30 min at 14000 rpm and 4 °C. The supernatant was discarded and the pellet was washed two times with 70 % ethanol during centrifugation at 13000 rpm for 5 min at RT. After complete removal of ethanol, the cell pellet was air dried and resuspended in 25 µL sterile dH_2O. The concentrations of DNA were determined using nanophotometer.

For control of prober ligation of insert and vector backbone, the purified plasmids were digested again with restriction enzymes Xba I and Mlu I for LV-ADR3-Gata4-V5 or with BamH I and Nde I for LV-CD31-Gata4-V5 at 37 °C for 1.5 h in 2 x Tango buffer. Agarose gel electrophoresis of restricted plasmids was conducted after inactivation of the enzymes at 65 °C for 10 min.

Bacteria mini cultures containing the proper insertion were used for inoculation of 100 mL LB medium containing ampicillin for maxi culture. After incubation at 37 °C overnight for approximately 16 h at 200 rpm, plasmid DNA was purified using QIAGEN EndoFree Plasmid Maxi Kit according manufacturer's protocol. The concentrations of plasmid DNA were determined using Nanophotometer NP80. Sequencing of plasmids was performed by LGC Genomics GmbH (Berlin) prior use of plasmids for transfection or lentivirus production.

3.2.2.5. RNA isolation

Total RNA isolation was conducted using innuPREP RNA Mini Kit 2.0 according to manufacturer's protocol. For RNA isolation from murine snap frozen liver tissue, a sliced piece of liver was homogenized in tissue homogenizing CKMix Tubes (1.4/2.8 mm) using Precellys Evolution Homogenizer for 20 sec at 5000 rpm and eluted in 30 µL RNase free water. RNA of eukaryotic cells was eluted in 20 µL RNase free water. Using NanoPhotometer NP80 RNA concentration of the samples were measured. RNA was stored at -80 °C or treated with TURBO DNA-free Kit according to manufacturer's protocol to get rid of DNA contamination. After DNA digestion, RNA concentration was measured again using NanoPhotometer NP80 prior reverse transcription.

3.2.2.6. cDNA synthesis

Using Maxima Reverse Transcriptase reverse transcription into complementary DNA (cDNA) was performed according to the manufacturer's protocol:

Oligo dT Primer (100 pmol)	1 µL
dNTP Mix (10 mM)	1 µL
RNA	500 ng or 1 µg
Nuclease-free water	to 14.5 µL

After incubating the premix at 65 °C for 5 min to reduce secondary structures, following components were added:

5x RT Buffer	4 µL
RiboLock RNase Inhibitor	0.5 µL (20 U)
Maxima Reverse Transcriptase	1 µL (200 U)

After incubation at 50 °C for 30 min, Reverse Transcriptase was inactivated by heating the samples at 85 °C for 5 min. cDNA was stored at -80 °C or directly diluted for Quantitative Real-time PCR (RT-qPCR).

3.2.2.7. RT-qPCR

For RT-qPCR, cDNA from 500 ng RNA was diluted 1:25 and cDNA from 1 µg RNA was diluted 1:50 in ultra-pure water. RT-qPCR was performed using innuMIX qPCR SyGreen Sensitive or Standard according to manufacturer's protocol. 2x innuMix Master Mix contains dNTP's, DNA polymerase, buffer and fluorescent dye:

2x innuMix Master Mix	10 µL
Forward Primer (2 µM)	2.5 µL
Reverse Primer (2 µM)	2.5 µL
cDNA (1:25 or 1:50)	5 µL

For each sample a duplet was used. RT-qPCR was conducted in a 96 well RT-qPCR plate on a qTOWER 3 G touch thermal cycler after following protocol:

95 °C	3 min	
95 °C	10 sec	⎫
60 °C	10 sec	⎬ 40x
72 °C	20 sec	⎭

To visualize the PCR products, agarose gel electrophoresis was conducted and PCR products were photographed with Intas Gel Stick Imager.

Data analysis of RT-qPCR was conducted using qPCRsoft. Calculation of normalized expression values was executed using the Pfaffl method. Amplification efficiency values were determined using standard curves. For normalization in murine liver and mLSEC, three reference genes Gak, Mrpl46, and Srp72 were used. For normalization in bEnd.3 cells reference gene β-Actin was used additionally.

3.2.2.8. Microarray transcriptome profiling

RNA was isolated as described (see 3.2.2.5. RNA isolation) of freshly isolated mLSEC of CDAA and control diet fed mice (see 3.2.1.3. Mouse liver sinusoidal endothelial cell isolation). RNA concentration was measured using nanophotometer. At the Affymetrix core facility of the UMM first RNA quality was measured using a 2100 Bioanalyzer followed by transcriptomic profiling using of 1 µg RNA per sample for Affymetrix GeneChipTM Mouse Gene 2.0 ST Array according to manufacturer's protocol. For statistics and bioinformatics, the data was prepared by Dr. Carsten Sticht (ZMF, Mannheim). To annotate the microarrays, a custom chip description Version 22 with ENTREZ based gene definitions was used. By applying quantile normalization, robust multi array analysis background correction and median polish probeset summary the raw fluorescence intensity values were normalized. A false positive rate of $\alpha = 0.05$ with false discovery rate correction was taken as the level of significance. Gene set enrichment analysis (GSEA) was conducted using R 3.6.1 and clusterProfiler 3.12.0 using the molecular signatures database (MSigDB) v6.2 hallmark gene set collection. Overrepresentation analysis was performed by using enrichR package in R 3.6.1. Statistical analysis in R and preparation of graphs of microarray data were done together with Dr. Manuel Winkler.

3.2.2.9. RNA sequencing

After isolation of mLSEC of $Gata4^{LSEC\text{-}KI}$ and control mice (see 3.2.1.3. Mouse liver sinusoidal endothelial cell isolation), RNA was isolated as described (see 3.2.2.5. RNA isolation). RNA concentration measurement was done using nanophotometer followed by RNA quality analysis using a 2100 Bioanalyzer at the Affymetrix core facility of the UMM. 2 µg RNA was sent to BGI (Shenzhen, China) und used for RNA sequencing according manufacturer's protocol. Statistical analysis in R and preparation of graphs of RNA sequencing data were done together with Dr. Manuel Winkler

3.2.3. Proteinbiochemical methods

3.2.3.1. Protein isolation and determination

For protein isolation, RIPA lysis buffer was supplemented with EDTA free protease inhibitor to get RIPA complete buffer. Snap frozen murine liver tissues were homogenized in 200 µL RIPA complete buffer contained in homogenizing CKMix Tubes (1.4/2.8 mm) using Precellys Evolution Homogenizer for 20 sec at 5000 rpm. The lysates were transferred into a new reaction tube.

For preparation of protein lysates of cultivated mLSEC, HUVEC and bEnd.3 cells in culture dish, 100 µL RIPA complete buffer was added after washing the cells twice with PBS. The cells were detached using a cell scraper and transferred into a reaction tube and incubated for 30 min on ice.

To get rid of unlysed tissue or cell debris the samples were centrifugated at 13000 g for 5 min at 4 °C. The supernatant, containing protein, was transferred into a new reaction tube and the protein concentration was measured using colorimetric DC Protein Assay, which is based on Lowry Assay. A bovine serum albumin (BSA) dilution series was prepared by dilution with RIPA lysis buffer to final concentrations of 10 mg/mL, 5 mg/mL, 2.5 mg/mL, 1.25 mg/mL, 0.625 mg/mL, 0.3125 mg/mL and 0.15625 mg/mL. For protein concentration determination, Reagent S was diluted 1:50 in reagent A and 25 µL per well of the mixture was pipetted into a 96-well flat bottom plate. 5 µL of each sample, each BSA standard dilution and blank in duplicates respectively was added into each well containing reagent A/S mixture. To each well 200 µL of reagent B was added and the plate was incubated for 10 min at RT. Absorbance at 655 nm was measured using Tecan Infinite M200 Pro microplate reader. Protein concentration was calculated considering BSA standard curve.

3.2.3.2. SDS-PAGE

Equalized protein concentrations between 15 µg and 50 µg were used for sodium dodecyl sulfate-polyacrylamide gel electrophoresis (SDS-PAGE). For normalization, Smart Protein Layers (SPL) technology [230] was used and samples were prepared using Smart Protein Layers SPL Kit Blue according to manufacturer's protocol. For Labeling of the proteins, equalized protein concentrations were used and mixed with 10 µL RL-mix containing SPL buffer, 60 mM DTT and SMA basic L and finally 1 µL Smart Label working solution was added. After mixing and spinning down, the samples were incubated at 95 °C for 5 min. For SDS-PAGE, samples were loaded on a precast 4 % - 20 % gradient polyacrylamide gel located in

a gel electrophoresis tank containing 1 x TGS running buffer. Electrophoresis was performed at 25 mA per gel for approximately 1 h until the solvent front reached the end of the gel.

3.2.3.3. Western Blot and immunostaining

After SDS-PAGE the solvent front on the gel was removed to avoid interference during the fluorescence imaging. Fluorescence of total protein at 488 nm and SMA basic L at 647 nm were measured on the gel using Intas ChemoStar imaging system including a fluorescence module. For transfer of proteins on PVDF membrane by semi-dry blotting, the membrane was cut to size and activated for 1 min in methanol. The gel was put onto the activated membrane and both were surrounded from each one thick filter paper. Semi-dry blotting was performed using semi-dry Trans Blot Turbo device at 0.45 A (max. 25 V) for 35 min. Subsequently, the membrane was incubated in 5 % skim milk for 1 h at RT to block unspecific binding sites. After blocking, the membrane was incubated with primary antibody diluted in 5 % skim milk for 2 h at RT or overnight at 4 °C. After primary antibody incubation, the membrane was washed three times for 10 min with PBS containing 1 % Tween (PBS-T) and incubated with corresponding horse radish peroxidase (HRP)-labelled secondary antibody in 5 % skim milk for 1 h at RT, shaking. The membrane was washed three times for 10 min in PBS-T followed by incubation with Luminata Forte Western HRP Substrate for 2.5 min. Chemiluminescence of target protein and fluorescences of total protein (488 nm) and SMA basic L (647 nm) were detected using Intas ChemoStar imaging system. Quantification of target signal normalized to total protein was performed using SPL-LabImage software package 4.2.3.

3.2.3.4. Hepatic triglyceride assay

To analyze concentration of hepatic triglycerides in murine liver, Triglyceride Quantification Colorimetric/Fluorometric Kit was used according to manufacturer's protocol. Approximately 100 mg snap frozen liver tissue was homogenized in 1 mL 5 % NP-40 by heating to 80-100 °C for 5 min in a shaking dry incubator followed by a cool down to room temperature and one further heating step. Subsequently, after centrifugation at top speed for 2 min, the supernatant was transferred into a new reaction tube und diluted 10-fold prior the assay. A volume of 10 µL of each sample was used for determining the triglyceride content. Absorbance was measured at 570 nm using Tecan Infinite M200 Pro microplate reader. Triglyceride concentration was calculated considering standard curve.

3.2.3.5. Flow cytometry

For purity check of freshly isolated mLSEC, cells were analyzed by flow cytometry. After isolation of mSLEC the cell pellet was resuspended in 100 µL FACS buffer per 5 x10^5 cells. After putting 100 µL cell suspension per well into a 96-well plate, the cells were centrifugated at 300 g for 5 min at 4 °C. After washing the cells with FACS buffer at 300 g for 5 min at 4 °C, the cells were incubated with Fc block diluted 1:50 in FACS buffer for 10 min at 4 °C in the dark. After washing the cells with FACS buffer, the cells were incubated with fluorochrome conjugated antibodies for extracellular staining for 30 min at 4 °C in the dark. After washing once with FACS buffer, the cell pellet was resuspended in 100 µL FACS buffer for analysis on BD FACSCanto II flow cytometer. FACS data was analyzed by using FlowJo. For gating strategy of isolated mSLEC, first duplicates were excluded, followed by gating on alive cells using a Live/Dead stain. Purity of LSEC was assessed as positivity of cells for CD31 and/or STAB-2. mLSEC isolated from CDAA fed mice had a purity of 88 % and from standard diet fed mice 96 %. mLSEC isolated from Gata4$^{LSEC\text{-}KO}$ mice for *in vitro* analysis of LV-CD31-Gata4-V5 had a purity of 92 %

3.2.4. Histological methods

3.2.4.1. Immunofluorescence staining (IF) of FFPE tissue samples

Paraffin embedded organs were cut in 3 µm thick sections at the microtome and dried at least for 2 h or overnight at 60 °C. For deparaffinization, the sections were rinsed in 100 % xylene three times for 5 min, in 100 % ethanol twice for 3 min and in 90 % ethanol, 80 % ethanol and 70 % ethanol once, each for 3 min. Subsequent, the sections were washed short in dH_2O and in PBS for 3 min. For antigen retrieval, sections were incubated in pre-heated 1 x HIER Citrate Buffer pH 6.0 at 95 °C for 45 min followed by a cool down to RT in Citrate buffer for 20 min. After re-immersion in PBS, a hydrophobic barrier was drawn around the tissue with Dako pen and sections were washed two times for 3 min. The sections were incubated with primary antibody diluted in Dako Antibody Diluent at 4 °C overnight in a humidity chamber. At the following day the sections were washed three times for 5 min in PBS followed by incubation of fluorochrome-labelled secondary antibody diluted in Dako antibody diluent for 45 min at RT in a humidity chamber. After washing three times for 5 min with PBS and rinsing once in dH_2O, the sections were mounted with Dako fluorescent mounting medium. The slides were air dried overnight and stored at 4 °C at the following day. Images of the stainings were captured using Nikon Eclipse NI microscope and the NIS-Elements Advanced Research (Ar) version 5.02. The microscope is equipped with Nikon Intensilight Epifluorescence Illuminator and Nikon CFI

Plan Apochromat Lambda series objectives from four-fold to 100-fold. For microscopy DAPI, SpGreen, SpOrange, Cy5 and FITC filters were used. Images were adjusted and analyzed with Fiji ImageJ 2.0.0 software [231, 232] (see 3.2.4.4. Image adjustment and quantification).

3.2.4.2. Immunofluorescence staining (IF) of cryosections

Cryosections (8 µm) of snap frozen tissue were prepared at the cryotome and air dried for 1 h at RT, subsequently. After drawing a hydrophobic ring around the tissue with Dako pen, the sections were fixed for 10 min in 4 % PFA at RT and rinsed with PBS once. After blocking with 5 % normal donkey serum (NDS) in PBS for 30 min at RT, the sections were incubated with primary antibody diluted in 1 % NDS at 4 °C overnight in a humidity chamber.
Cryosections were washed three times for 5 min in PBS followed by incubation of fluochrome-labelled secondary antibody diluted in Dako antibody diluent for 45 min at RT in a humidity chamber. After washing three times for 5 min with PBS and rinsing once in dH_2O, the sections were mounted with Dako fluorescent mounting medium. The slides were air dried overnight and stored at 4 °C at the following day. Images of the stainings were captured using Nikon Eclipse NI microscope and NIS-Elements Advanced Research (Ar) version 5.02. The microscope is equipped with Nikon Intensilight Epifluorescence Illuminator and Nikon CFI Plan Apochromat Lambda series objectives from four-fold to 100-fold. For microscopy DAPI, SpGreen, SpOrange, Cy5 and FITC filters were used. Images were adjusted and analyzed with Fiji ImageJ software [231, 232] (see 3.2.4.4. Image adjustment and quantification).

3.2.4.3. Histological stainings

Hematoxylin and eosin (H&E) and Picrosirius red (PSR) stainings were conducted on paraffin sections using an automatic stainer according to standard protocols by the technicians at the core facility of the ZMF.

H&E staining		**PSR staining**	
Xylol	3x 2 min	Xylol	3x 2 min
100 % ethanol	1 min	99 % ethanol	1 min
96 % ethanol	1 min	96 % ethanol	1 min
80 % ethanol	1 min	80 % ethanol	1 min
70 % ethanol	1 min	70 % ethanol	1 min
Running tap water	1 min	Tap water	1 min
Hematoxylin	4 min	Aqua dest.	30 sec
Running tap water	10 min	Picro Sirius red	60 min
Eosin	2 min	0,5 % acetic acid	30 sec
Tap water	30 sec	80 % ethanol	30 sec
80 % ethanol	30 sec	96 % ethanol	1 min
96 % ethanol	1 min	99 % ethanol	2x 1 min
100 % ethanol	2x 1 min	Xylol	2x 1 min
Xylol	2x 1 min		

After staining the slides were mounted with Eukitt.

3.2.4.4. Image adjustment and quantification

First, the background of IF stainings was reduced by using rolling ball subtraction tool of NIS-Elements Advanced Research (Ar) software. Thereafter, images were deconvolved and the z-stack images were focused into one focused image. Quantification of images was performed using Fiji ImageJ software. For quantification thresholding was used and the area percentage was measured and is shown in the graphs showing IF quantifications.

For adjustment and quantification of H&E and PSR staining images Fiji ImageJ software was used. First the channels (red, green, blue) were arranged in the right order. After that a composite image was made and stacked to RGB. For quantification of images first a color deconvolution was performed and the image representing the red collagen fibers was used for thresholding for PSR staining. For H&E staining the image representing white areas were used

for thresholding. Area percentage was measured and is shown in the graphs showing quantification of H&E and PSR stainings.

3.2.5. Cell culture methods

3.2.5.1. Cultivation of HUVEC cells

For cultivation of HUVECs, frozen cells were thawed in a water bath at 37 °C and washed in 10 mL PBS at 300 g for 5 min. Cells were resuspended in pre-warmed endothelial cell growth medium mixed 1:2 with Medium 199, supplemented with 10 % FCS, 50 mg/mL gentamycin, 5000 IU/500 µL heparin and 250 µg/mL amphotericin B (HUVEC medium) and cultured at 37 °C and 5 % CO_2.

3.2.5.2. Cultivation of bEnd.3 cells

For cultivation of bEnd.3 cells, frozen cells were thawed in a water bath at 37 °C and washed in 5 mL PBS at 300 g for 5 min. The cell pellet was resuspended in pre-warmed DMEM medium supplemented with 10 % FCS, 1 % Pen/Strep (bEnd.3 medium) and cultured at 37 °C and 5 % CO_2.

3.2.5.3. Cultivation of primary mLSEC

For cultivation of isolated primary mLSEC (see 3.2.1.3. Mouse liver sinusoidal endothelial cell isolation), isolated cells were washed once in PBS and 1.5 x10^6 cells/well were cultured in Collagen IV coated 6-well plate in pre-warmed DMEM medium supplemented with 10 % FBS, 1 % P/S and 2 mM L-Glutamine (mLSEC medium) at 37 °C and 5 % CO_2.

3.2.5.2. Production of lentivirus for transduction of eukaryotic cells

For production of lentiviral particles, HEK293/T17 producer cells were used. 1 x10^6 mycoplasma free HEK293/T17 cells were cultured in DMEM medium supplemented with 10 % FBS, 1 % P/S (DMEM complete) and 100 mM sodium pyruvate in T175 cm^2 flask at 37 °C and 5 % CO_2. After 72 h, the cells were grown to approximately 80 % confluency and transfected with either lentiviral ADR3 vector carrying synthetic murine Gata4 gene (ADR3-Gata4-V5) or with LSEC-targeting CD31-miT122+142-LV carrying synthetic murine Gata4 gene (CD31-Gata4-V5). After renewing HEK293/T17 culture medium, ADR3-Gata4-V5 vector (10 µg) or LV-CD31-Gata4-V5 vector (10 µg) was incubated with 3rd generation packaging plasmids pMD2.G L1 (2.5 µg), pMDLg/pRRE L3 (5 µg), pRSV rev L2 (2.5 µg) and

pCDNA3.1/p35 E 71 (1.5 µg) in DMEM medium and X-treme GENE 9 DNA transfection reagent solution for 15 min at RT and added dropwise to HEK293T/17 cells. In the morning of the following day the culture medium was renewed by DMEM complete medium supplemented with 100 mM sodium butyrate to stimulate release of produced viruses. In the evening, the culture medium was replaced by harvesting medium (DMEM complete + 1 % P/S + 100 mM sodium pyruvate). After 48 h of transfection, the harvesting medium was collected, filtered through a 0.45 µm filter to obtain cell-free medium containing lentiviruses and stored at 4 °C. After 60 h and 72 h of transfection the harvesting step was repeated. Finally, collected harvesting medium containing lentiviral particles was concentrated by centrifugation at 3000 rpm at 4 °C using Vivaspin 20 tubes. Lentivirus solution was aliquoted and stored at -80 °C.

High titer production of LV-CD31-Gata4-V5 lentivirus was executed by the working group of Prof. Dr. Christian Buchholz by co-transfection in HEK293T cells and followed low-speed centrifugation for concentration of the lentivirus [226].

3.2.5.3. Lentiviral transduction of HUVEC, bEnd.3 and primary mLSEC

For lentiviral transduction of HUVECs, 3.5 x10^5 cells were seeded in a 10 cm cell dish in HUVEC medium. For transduction of b.End3 cells, 5 x10^4 cells per well were seeded into a 6-well plate in bEnd.3 medium. For transduction of primary mLSEC, 1.5 x10^6 cells per well were seeded in Collagen IV coated 6-well plate in mLSEC medium. Appropriate medium was renewed complete (HUVEC and bEnd.3) or half (mLSEC) prior transduction. Cells were transduced with concentrated lentivirus by applying several microliters into the culture medium of the cells. HUVECs were transduced after 48 h, bEnd.3 and mLSEC after 24 h cultivation time. HUVECs were incubated with the lentivirus for overall 96 h and bEnd.3 and mLSEC cells for overall 66 h. Medium was renewed of HUVECs after 72 h and of mLSEC after 24 h and 48 h of transduction. After 96 h (HUVECs) or 66 h (bEnd.3 and mLSEC) of transduction the cells were washed twice with PBS. For following RNA isolation, RL lysis buffer was added, the adherent cells were detached using a cell scraper and transferred to a reaction tube. For following protein isolation, RIPA complete was added, the adherent cells were detached using a cell scraper and transferred to a reaction tube.

3.2.6. Liver fibrosis mouse models

3.2.6.1. Chronic carbon tetrachloride (CCl_4) model

For induction of chronic toxic liver fibrosis, the carbon tetrachloride (CCl_4) model was used. Therefore, 10-week-old female C57BL/6N mice were injected intraperitoneally (*i.p.*) with either 100 µL of 20 % CCl_4 dissolved in corn oil or 100 µL corn oil alone twice a week for three weeks. Two days after the last injection blood samples were taken under anesthesia and the mice were sacrificed. The mice were monitored regularly and sacrificed, if reaching one of the termination criteria.

3.2.6.2. Non-alcoholic steatohepatitis (NASH) model

Non-alcoholic steatohepatitis (NASH) model was used to induce dietary induced liver fibrosis. Therefore, 10-week-old female C57BL/6N mice or 10-week-old female $Gata4^{LSEC\text{-}KO}$ mice 10-week-old female $Gata4^{LSEC\text{-}KO}$ mice and control siblings were fed either Methionin and choline-deficient (MCD) diet or choline-deficient, l-amino acid-defined (CDAA) plus diet. MCD diet used in this study has a high sucrose content of 45 % and a moderate fat content of 22 %. CDAA plus diet used in this study has an intermediate fat content of 31 % and is supplemented with 1 % cholesterol and is named only CDAA diet. For establishment of NASH model, C57BL/6N mice were fed either MCD diet for 8 weeks and 10 weeks or CDAA diet for 10 weeks and 20 weeks. For application of NASH model on $Gata4^{LSEC\text{-}KO}$ mice or on $Gata4^{LSEC\text{-}KI}$ mice, the mice were fed CDAA diet for 10 weeks. After the indicated time of feeding, blood samples were taken under anesthesia and the mice were sacrificed. The mice were monitored regularly and sacrificed, if reaching one of the termination criteria.

3.2.7. Statistical analysis

All experiments were performed at least in three replicates. Statistical data analysis was performed using GraphPad Prism and R software [233]. Shapiro-Wilk test was used for assessment of normal distribution and F-test of equality of variances for equal variance of the data. Assuming Gaussian distribution unpaired two-tailed student's t test or Welch's t test was used for statistical analysis of two groups. Mann-Whitney U test was used for not normal distributed data. For statistical comparison of more than two groups with one independent variable, one-way ANOVA (Bonferroni post hoc test) was used and for statistical comparison of more than two groups with two independent variables, two-way ANOVA (Tukey´s post hoc test) was used. Data is shown as means with standard deviation (SD). Asterisks indicate the level of significance $* p \leq 0.05$, $** p < 0.01$, $*** p < 0.001$, $**** p < 0.0001$.

4. Results

4.1. Analysis and comparison of different liver fibrosis mouse models

We were able to show, that deletion of endothelial *Gata4*, using a LSEC-specific Clec4g-iCre driver mouse, leads to the development of perisinusoidal liver fibrosis, which is similar to fibrosis in NASH. An angriocrine switch upon *Gata4* deletion in LSEC of $Gata4^{LSEC\text{-}KO}$ mice leads to *de novo* endothelial expression of hepatic stellate cell-activating cytokine PDGFB, a profibrotic growth factor through the GATA4/MYC/PDGFB axis [95]. We were wondering whether liver fibrosis models lead to a downregulation of *Gata4* and development of a similar fibrosis type seen in $Gata4^{LSEC\text{-}KO}$ mice. Therefore, two different liver fibrosis mouse models with different types of liver fibrosis were analyzed and compared. On the one hand, CCl_4 model, which leads to a toxic liver fibrosis, was used. On the other hand, a NASH model, which leads to diet induced liver fibrosis, was used (Figure 12).

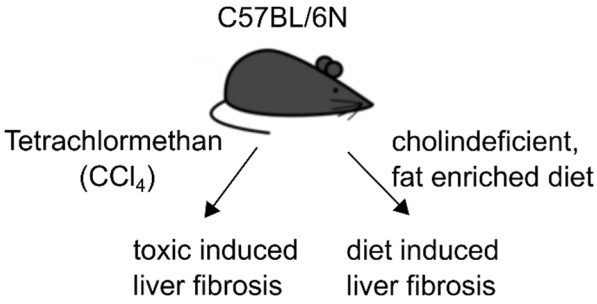

Figure 12. Experimental liver fibrosis mouse models.
Schematic overview of two different liver fibrosis mouse models used in this study.

4.1.1. Analysis of toxic liver fibrosis inducing chronic CCl_4 model

4.1.1.1. Establishment of CCl_4 model

To induce toxic liver fibrosis, a chronic CCl_4 model was used. Therefore, 10-weeks old female wild type C57BL/6N (B6N) mice were injected *i.p.* with 100 µL of 20 % CCl_4 diluted in corn oil for three weeks, two times a week (Figure 13 A). Control mice were injected corn oil alone in the same experimental setting. The livers of CCl_4 treated mice showed an uneven surface (Figure 13 B) and liver-to-body-weight ratio was increased (Figure 13 C).

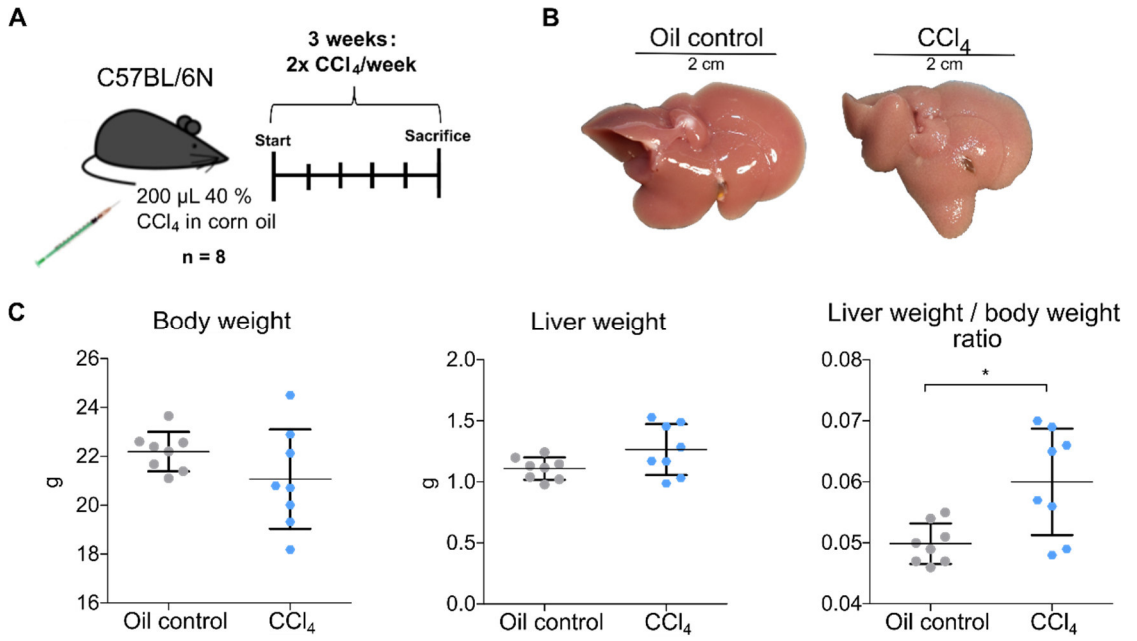

Figure 13. Chronic CCl_4 induced toxic liver fibrosis mouse model.
(A) C57BL/6N female mice were injected *i.p.* with either 20 % CCl_4 diluted in corn oil or corn oil alone for three weeks two times a week to induce toxic liver fibrosis. **(B)** Representative macroscopic picture of livers and **(C)** weight of liver, body and ratio of both in CCl_4 liver fibrosis models. Scale bar 2 cm; n = 8; mean ± SD; * $p < 0.05$.

Liver damage was indicated by higher levels of liver enzymes aspartate aminotransferase (AST), alanine aminotransferase (ALT) and glutamate dehydrogenase (GLDH) in plasma (Figure 14 A) of CCl_4 treated mice compared to oil controls. Furthermore, plasma levels of glucose (Figure 14 B) were decreased, whereas cholesterol (Figure 14 C) and creatinine (Figure 14 D) were increased. All other measured plasma levels were not altered (not shown).

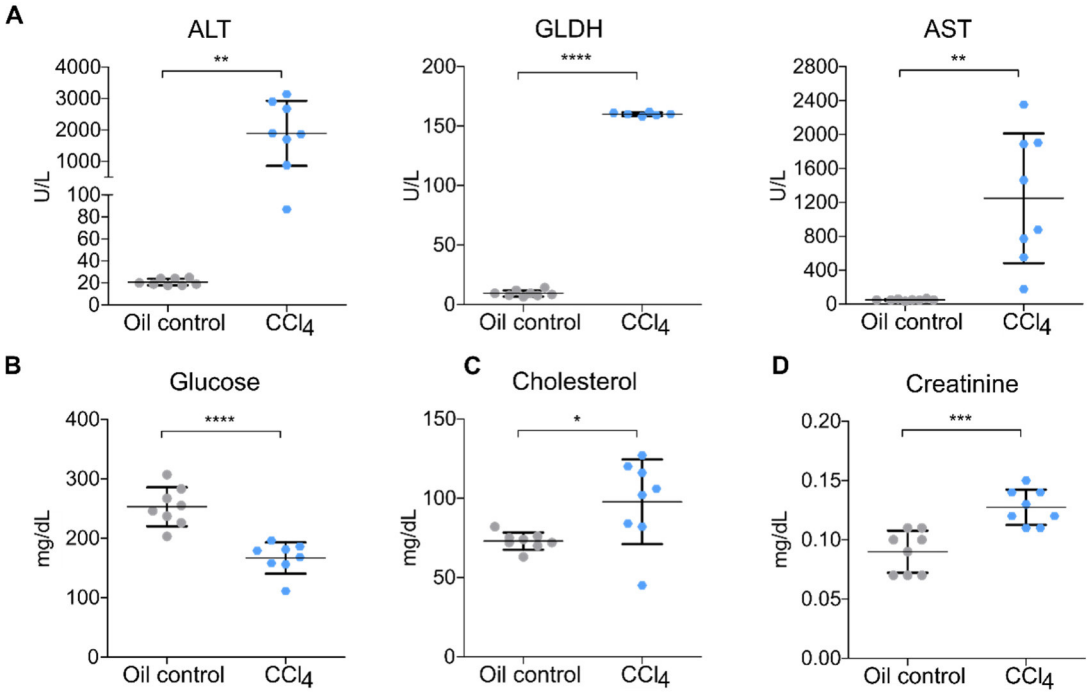

Figure 14. Changed plasma levels of mice in CCl_4 model.
Levels of **(A)** liver enzymes ALT, GLDH and AST and **(B)** glucose, **(C)** cholesterol and **(D)** creatinine in plasma of mice in CCl_4 liver fibrosis model. n = 8; mean ± SD; * p < 0.05, ** p < 0.01, *** p < 0.001, **** p < 0.0001.

4.1.1.2. Liver fibrosis development and vascular alterations in a chronic CCl_4 model

Activation of HSC results in production of ECM during liver fibrogenesis. Hence, activation of HSC in CCl_4 model was analyzed by RT-qPCR and immunofluorescence (IF) staining. All analyzed markers for activated HSCs (*Acta2*, *Col1a1*, *Col3a1*, *Desmin*, *Pdgfrb*) were increased on mRNA level in CCl_4 treated mice (Figure 15 A). Histolgical staining for H&E showed damage of peri-central hepatocytes and iniltration of immune cells (Figure 15 B). Moreover, histological staining of Picrosirius red (PSR) showed the development of bridging peri-central liver fibrosis in CCl_4 model (Figure 15 B, C). Concordantly, IF staining of peri-central activated HSC showed an increase of Desmin (Figure **15** B, C).

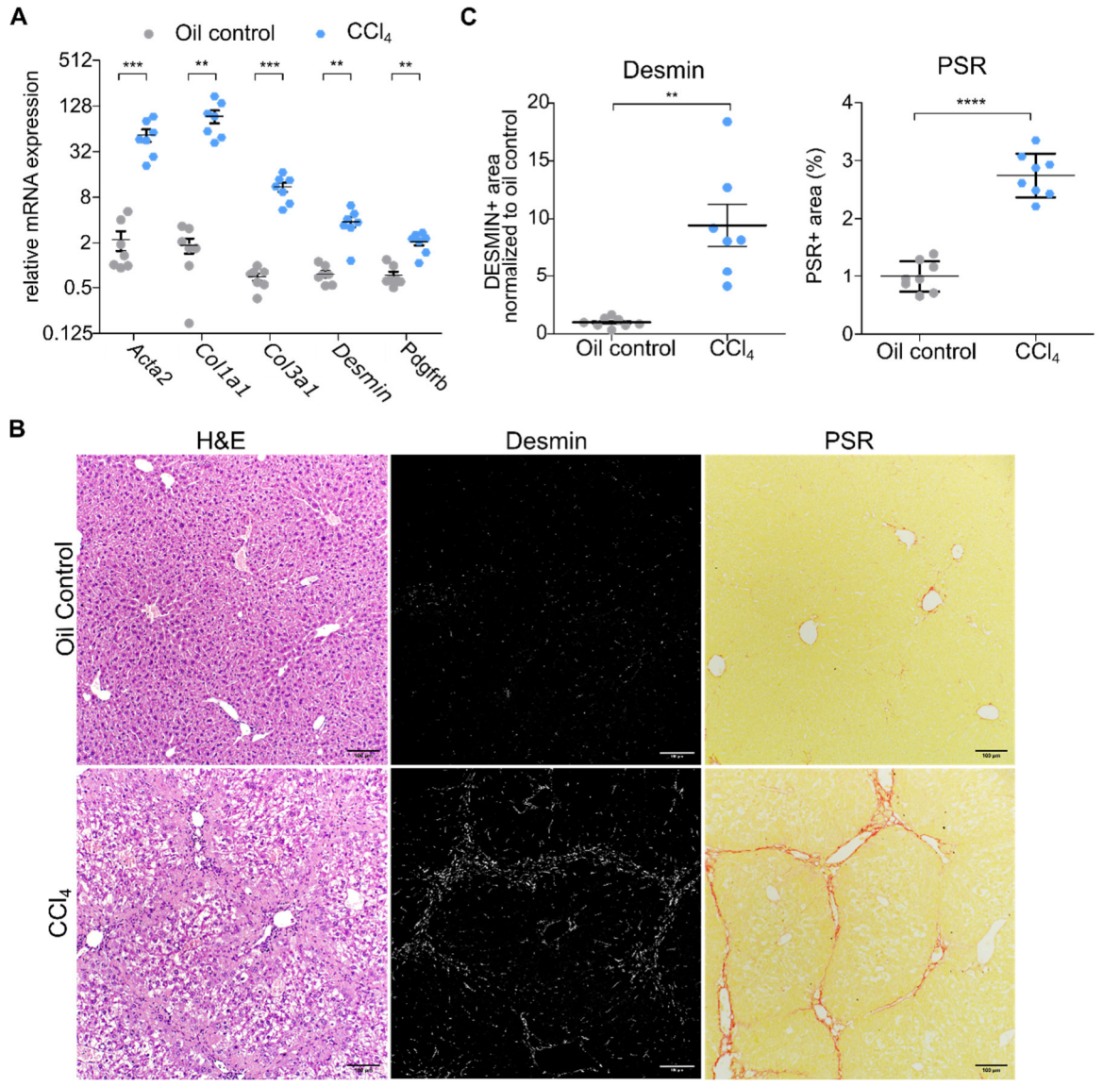

Figure 15. Development of bridging liver fibrosis in CCl_4 model.
(A) mRNA expression of activated hepatic stellate cell markers *Acta2, Col1a1, Col3a1, Desmin* and *Pdgfrb* in whole liver of CCl_4 model measured by RT-qPCR. **(B)** Histological staining of H&E and PSR and immunflouorescence staining of Desmin. Representative images from two independent experiments with eight biological replicates. Scale bar 100 µm. **(C)** Quantification of Desmin and PSR staining. n = 8; mean ± SD; ** $p < 0.01$, *** $p < 0.001$, **** $p < 0.0001$

Expression of different endothelial cell markers was assessed by IF staining. In CCl_4 treated mice endothelial zonation marker LYVE-1 was unchanged, whereas continuous EC marker Endomucin was increased (Figure 16 A, B). Additionally, expression of pan-endothelial cell marker Podocalycin was decreased (Figure 16 A, B).

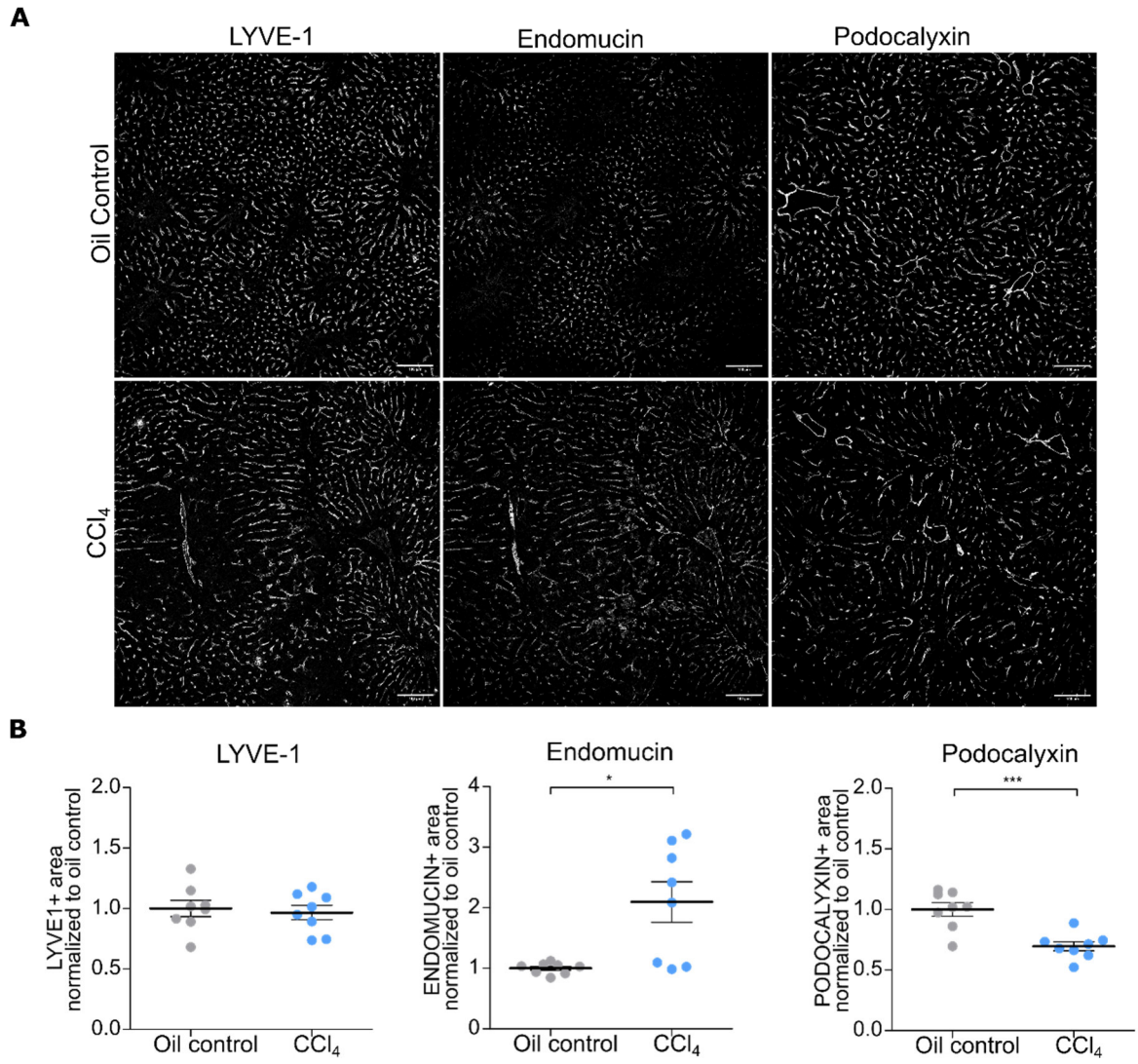

Figure 16. Expression of endothelial zonation and pan-endothelial markers in the CCl_4 model.
(A) Immunofluorescence staining of endothelial cell markers LYVE-1, Endomucin and Podocalyxin in CCl_4 model. Representative images from two independent experiments with eight biological replicates. Scale bar 100 µm **(B)** Quantification of immunofluorescence stainings of **(A)**. n = 8; mean ± SD; * $p < 0.05$, *** $p < 0.001$.

4.1.1.3. Expression of GATA4 in a chronic CCl4 model

To analyze the hepatic expression of GATA4 in the CCl_4 model, western blot and IF staining for GATA4 of CCl_4 treated and oil control mice were assessed. Hepatic GATA4 was slightly increased in CCl_4 mice as analyzed by western blotting (Figure 17 A, B).

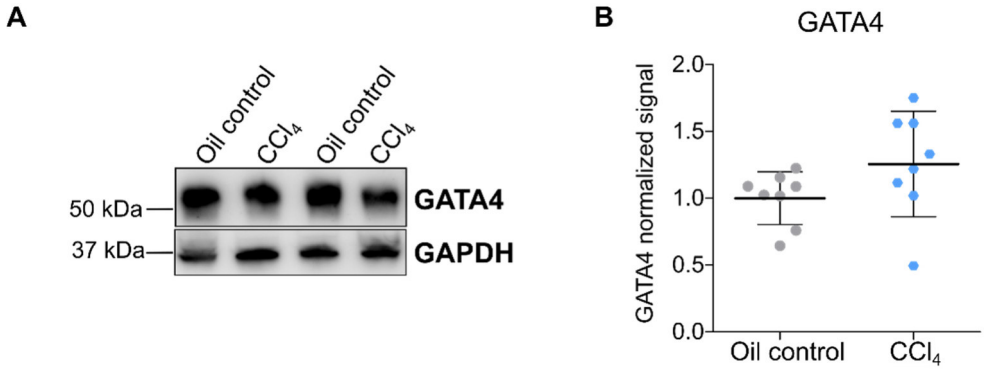

Figure 17. Hepatic GATA4 expression in CCl_4 treated mice.
(A) Expression of GATA4 in whole liver assessed by western blot analysis. Two representative samples from two independent experiments with eight biological replicates are shown. **(B)** Quantification of western blot of **(A)** using SPL technology. n = 8; mean ± SD.

Upon IF staining GATA4 expression was significantly increased (Figure 18 A, C). We wondered, which cell types are expressing GATA4 in CCl_4 model, thus co-staining of GATA4 with ERG or Desmin was performed. ERG is a nuclear marker for ECs and Desmin is a marker for HSCs. In general, CCl_4 livers displayed more ERG-positive ECs and higher colocalization of GATA4 and ERG compared to oil controls (Figure 18 A, C). Furthermore, most GATA4-positive cells mostly were surrounded by Desmin-positive filaments (Figure 18 B), which indicates that several activated HSCs are expressing GATA4 in CCl_4 treated mice.

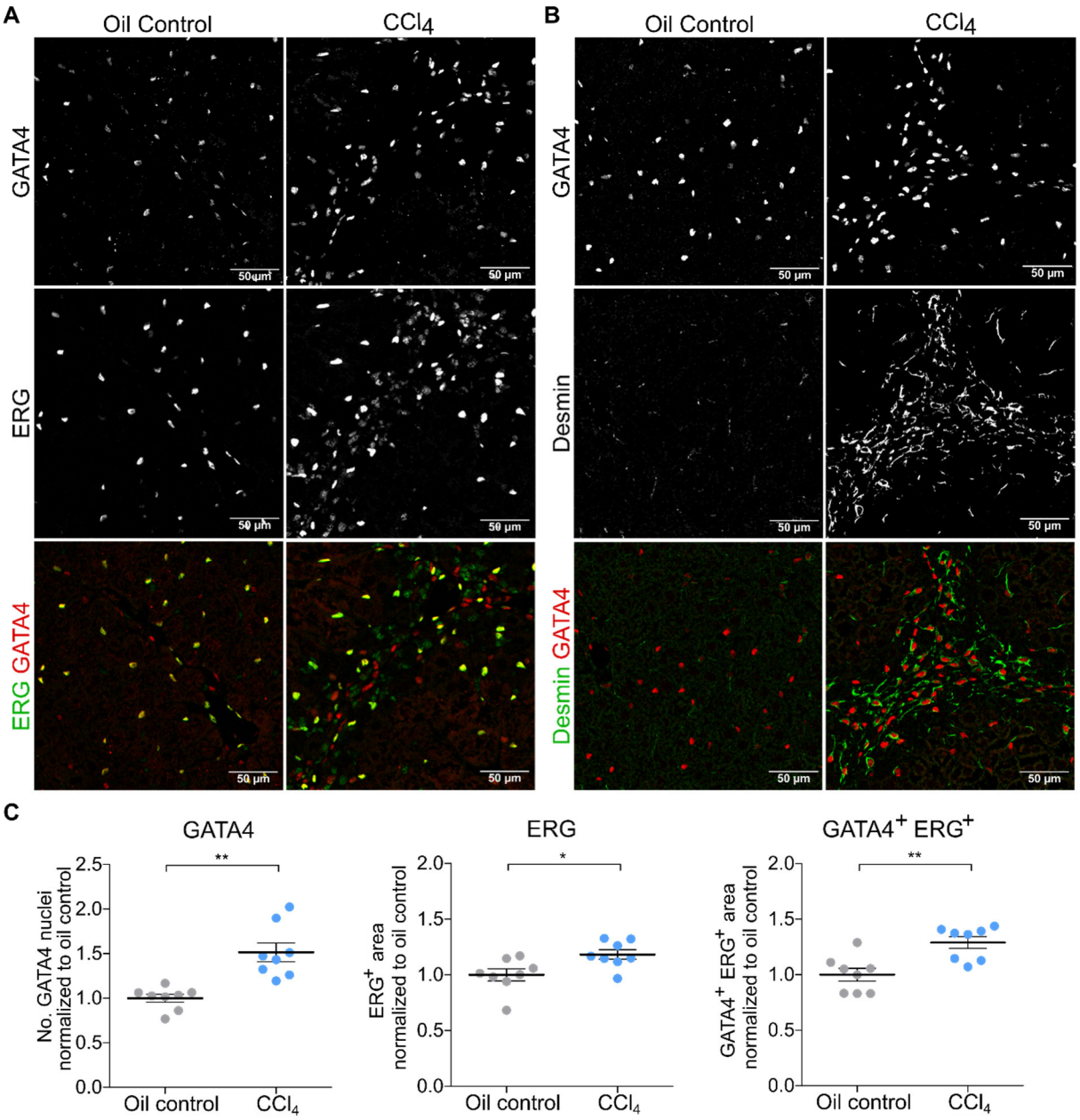

Figure 18. Expression pattern of GATA4 in livers of CCl_4 treated mice.
(A) Immunofluorescence co-staining of GATA4 with either ERG or Desmin. Representative images from two independent experiments with eight biological replicates. Scale bar 100 µm. **(D)** Quantification of Immunofluoresence staining of GATA4 and ERG as well the colocalization of both. n = 8; mean ± SD; * $p < 0.05$, ** $p < 0.01$.

Taken together, the data shows that chronic CCl_4 administration leads to hepatopathy and the development of a bridging liver fibrosis type with increased expression of hepatic GATA4 and induction of EC marker Endomucin, while sinusoidal EC marker LYVE-1 was unaltered.

4.1.2. Analysis of diet induced liver fibrosis NASH models

To identify a diet induced NASH-associated liver fibrosis model, which shows a relevant amount of perisinusoidal liver fibrosis, we decided to feed female B6N mice two different NASH diets for two different time periods, respectively.

4.1.2.1. Comparison of different NASH diets and feeding periods

B6N mice were fed either MCD diet for eight or ten weeks or CDAA diet for ten or twenty weeks (Figure 19 A). Each diet and time point led to the development of fatty liver, which was indicated by the pale surface color of the liver (Figure 19 B-D), and increased liver size in CDAA diet (Figure 19 C, D). Mice fed with MCD diet had smaller and lighter livers compared to standard diet fed mice (Figure 19 B, C, E), whereas mice fed with CDAA diet had bigger and heavier livers (Figure 19 C-E). But only in CDAA diet the liver-to-body-weight ratio was increased (Figure 19 F), as MCD mice lost weight upon feeding with MCD diet. However, there were no large differences between the different time points within the diets.

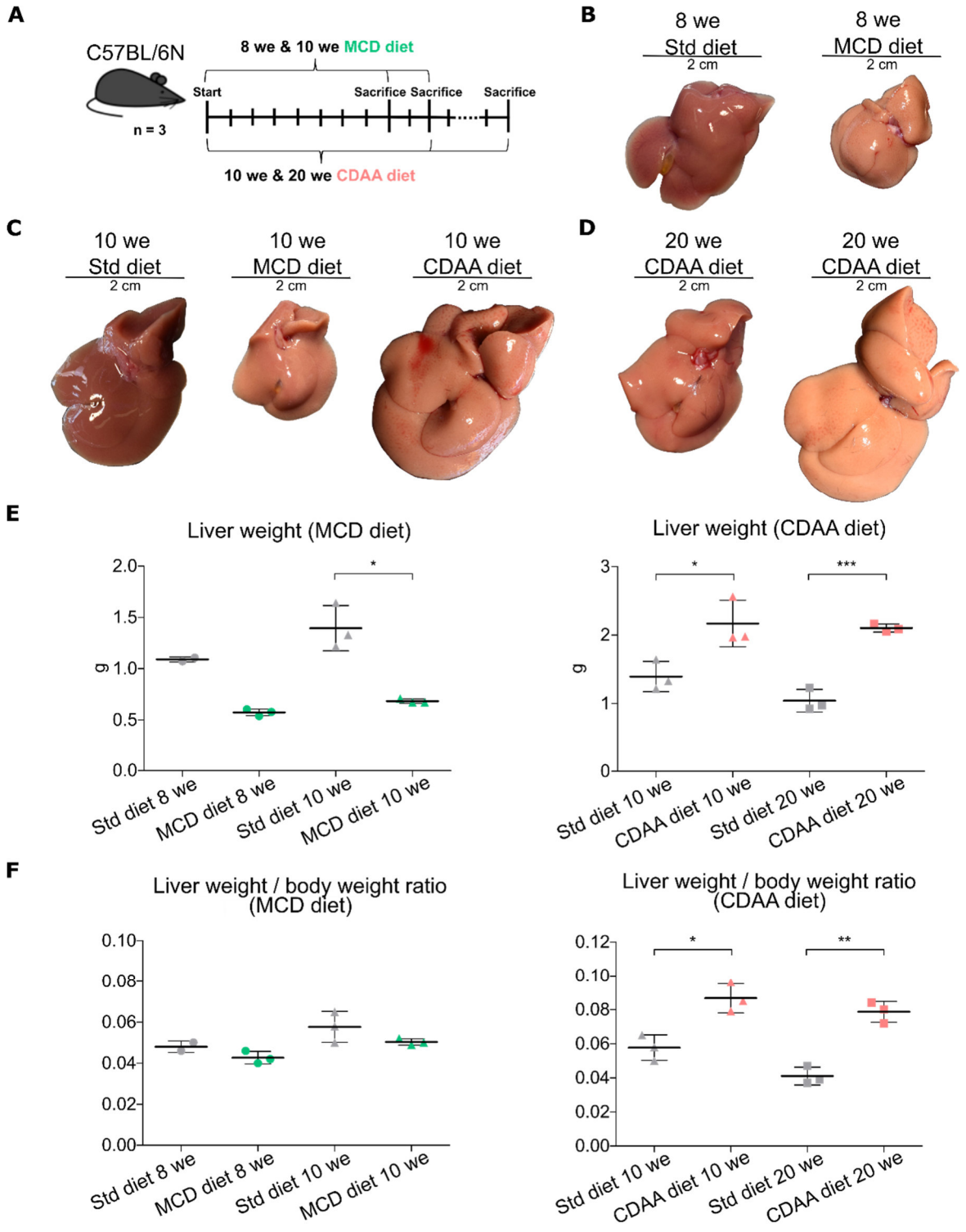

Figure 19. Establishment of MCD diet and CDAA diet induced liver fibrosis NASH models with different feeding periods.
(A) C57BL/6N female mice were fed either MCD diet for eight or ten weeks or CDAA diet for ten or twenty weeks. Control mice were fed standard diet for the different time points. Representative macroscopic pictures of livers after **(B)** 8 weeks (we) MCD or standard diet, **(C)** ten weeks MCD, CDAA or standard diet, **(D)** twenty weeks CDAA or standard diet. Scale bar 2 cm. **(E)** Liver weight and liver weight to body weight ration in MCD and CDAA models. n = 3; mean ± SD; * $p < 0.05$, ** $p < 0.01$, *** $p < 0.001$.

Results

Liver enzymes AST, GLDH and ALT in plasma of NASH model mice were increased in each diet type and feeding period (Figure 20 A-C). In comparison between MCD and CDAA diet, the levels in MCD were slightly higher, but did not reach statistical significance. Between eight and ten weeks MCD diet there was no difference in liver enzyme levels. Whereas after twenty weeks CDAA diet the levels were slightly lower compared to ten weeks CDAA diet.

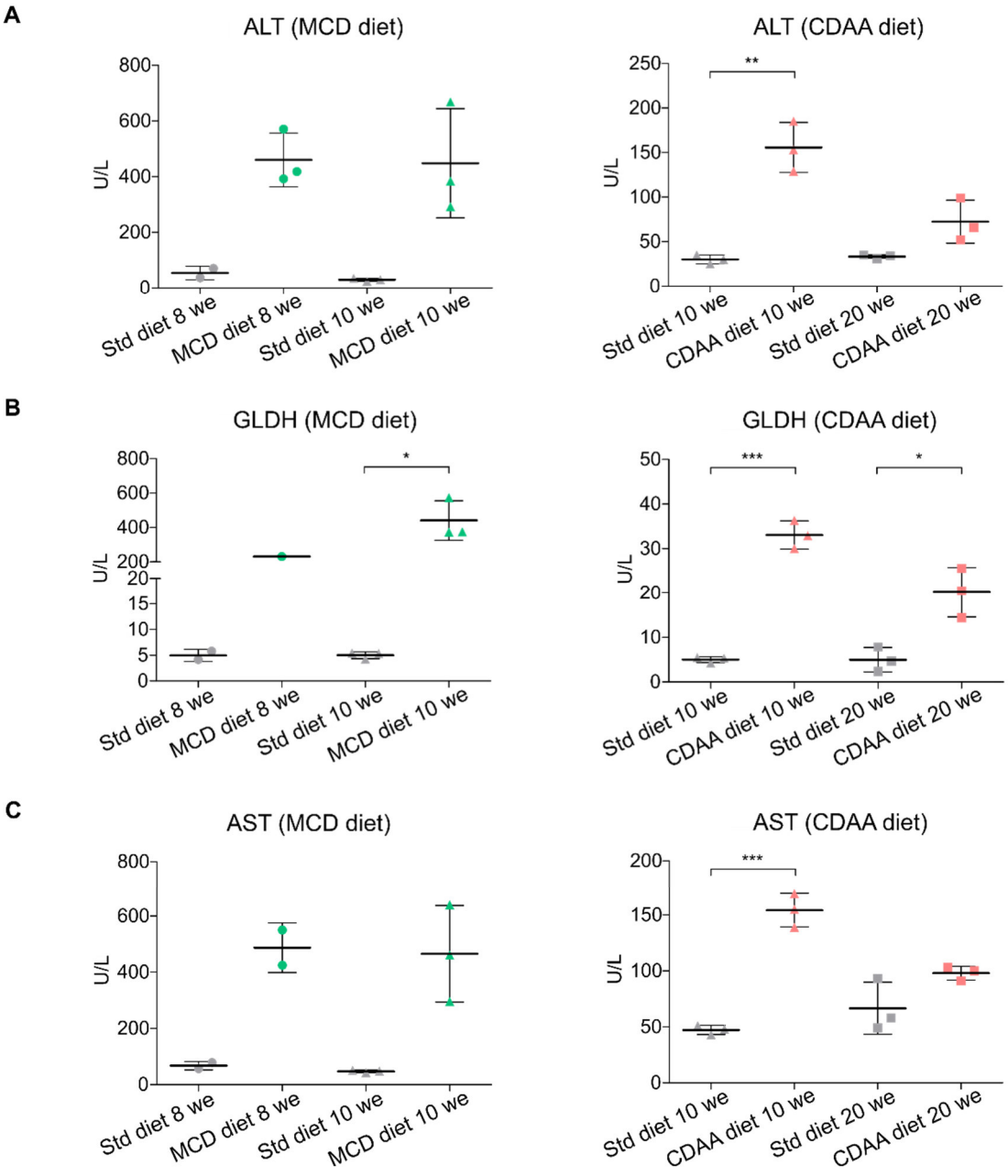

Figure 20. Liver enzyme levels in plasma of MCD and CDAA fed mice.
Plasma levels of **(A)** ALT, **(B)** GLDH and **(C)** AST in MCD of MCD and CDAA models. n = 3; mean ± SD; * $p < 0.05$, ** $p < 0.01$, *** $p < 0.001$.

Furthermore, MCD diet led to increased bilirubin levels in plasma but CDAA diet did not (Figure **21** A). These results indicate liver damage in all analyzed models. Whereas plasma levels of cholinesterase were increased only after ten weeks CDAA diet (Figure 21 B). Levels of urea were decreased in plasma of both diets and feeding periods (Figure 21 C).

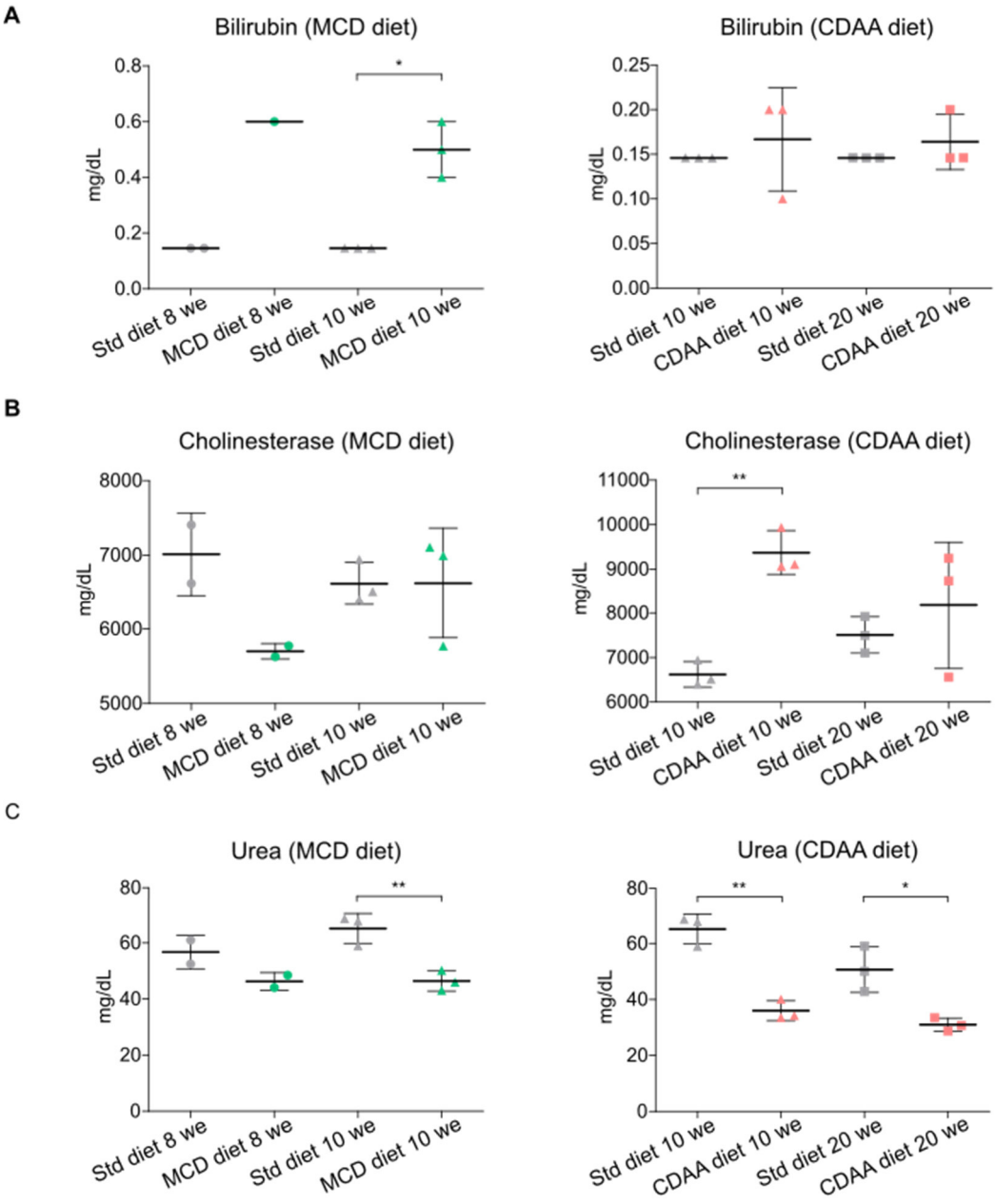

Figure 21. Plasma levels in MCD and CDAA fed mice.
Plasma levels of **(A)** bilirubin, **(B)** cholinesterase and **(C)** urea in MCD of MCD and CDAA models. n = 3; mean ± SD; * $p < 0.05$, ** $p < 0.01$.

NASH is characterized by steatosis (accumulation of lipid droplets), inflammation (infiltrating immune cells), and hepatocyte ballooning. Both diets and all feeding time periods led to the development of NASH seen in histological H&E staining (Figure 22 A, B). Furthermore, all conditions led to increased collagen deposition in PSR staining, indicating liver fibrosis (Figure **22** C, D), while MCD diet did not show statistical significance. In contrast to the CCl_4 model, the mice in the used NASH models developed perisinusoidal liver fibrosis type instead of bridging fibrosis type (Figure 22 A, B).

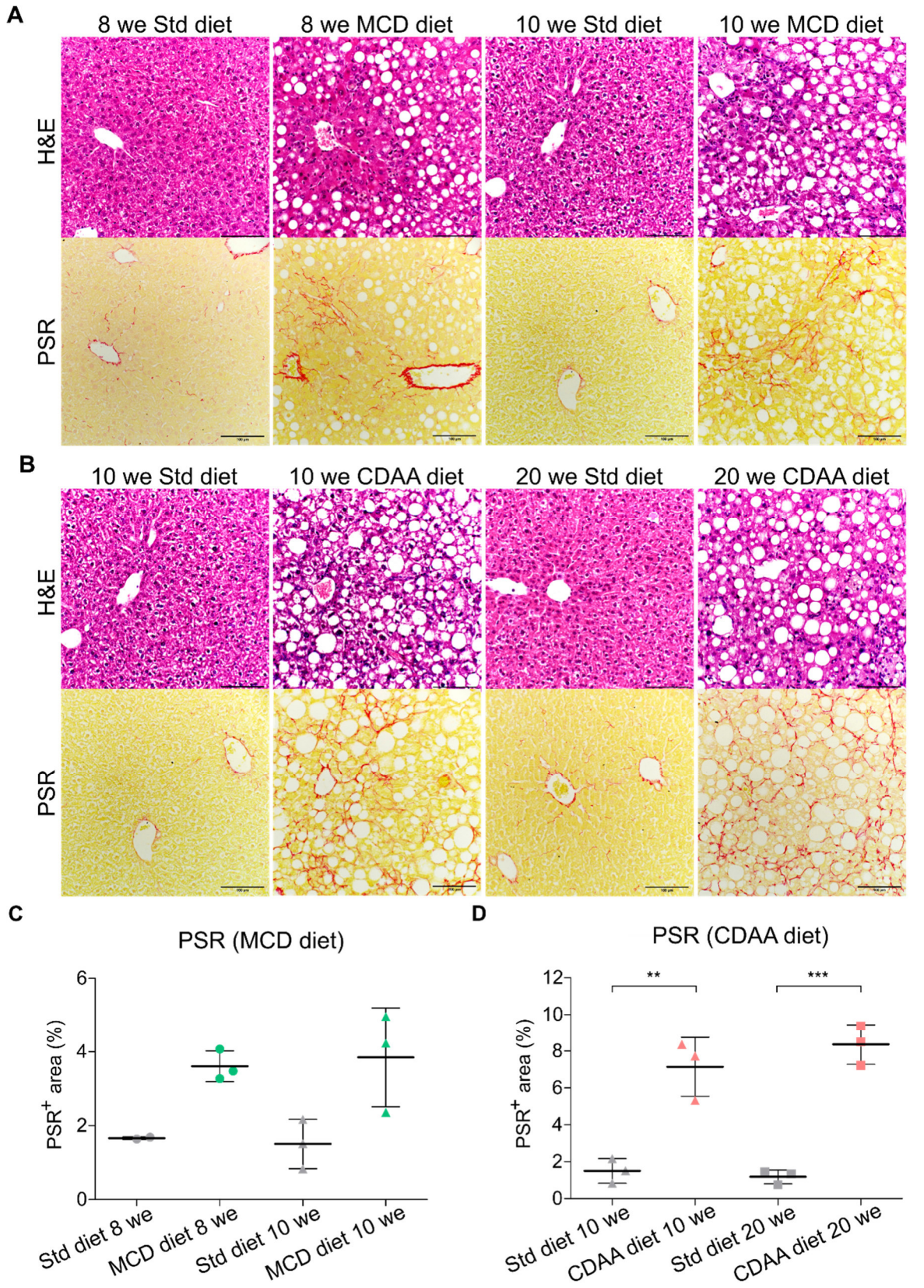

Figure 22. Development of perisinusoidal fibrosis in diet induced NASH models.
Histological H&E and PSR staining of **(A)** MCD diet and **(B)** CDAA diet model. Representative images from one experiment with three biological replicates. Scale bar 100 µm. Quantification of PSR staining in **(C)** MCD diet and **(D)** CDAA diet model. n = 3; mean ± SD; ** $p < 0.01$, *** $p < 0.001$.

Taken together, both diets and feeding periods led to the development of NASH-associated liver fibrosis. Furthermore, this data indicates that ten weeks of feeding either MCD or CDAA diet are sufficient to investigate NASH-associated perisinusoidal liver fibrosis. Hence, for the following experiments MCD and CDAA diet was fed for ten weeks.

4.1.2.2. Establishment of ten weeks MCD diet and CDAA diet

After feeding ten weeks either MCD diet or CDAA diet, female B6N mice (Figure 23 A) developed a fatty liver indicated by pale color of the liver and increased liver size in CDAA diet (Figure 23 B). As seen before (Figure 23 B, E), livers of MCD fed mice were smaller and had a reduced liver at reduced body weight, whereas livers of CDAA fed mice were bigger and heavier by unchanged body weight (Figure 23 B, C).

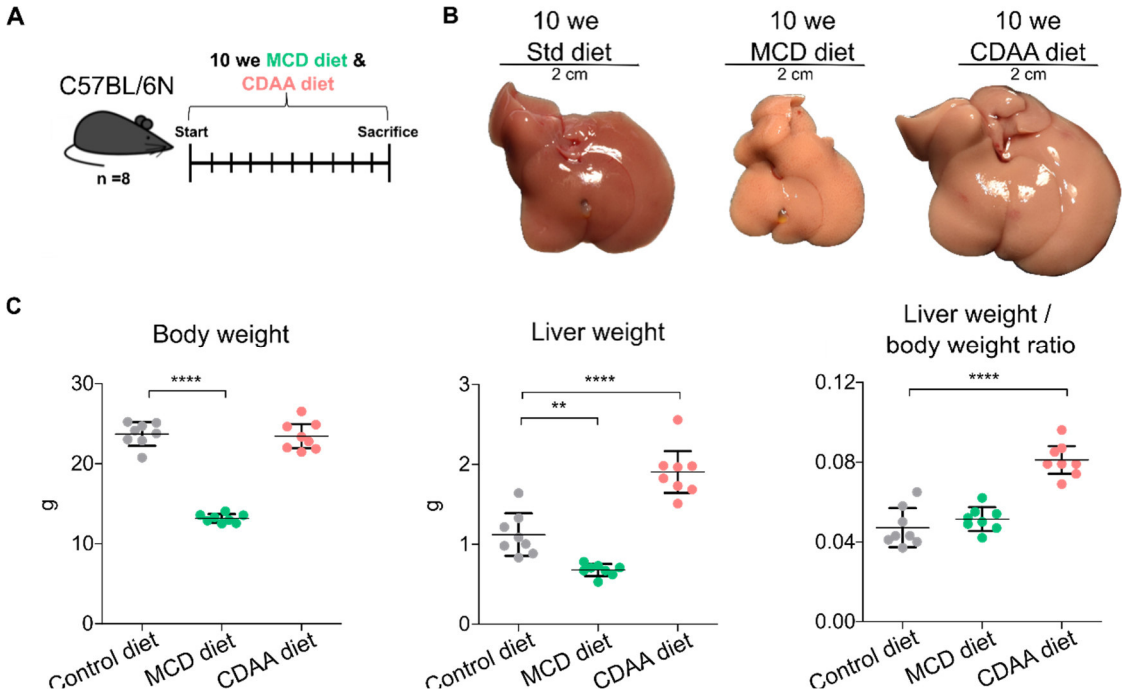

Figure 23. Comparison of MCD diet and CDAA diet induced liver fibrosis NASH models after ten weeks feeding.
(A) C57BL/6N female mice were fed either MCD diet or CDAA diet for ten weeks. Control mice were fed standard diet for ten weeks. **(B)** Representative macroscopic pictures of livers after ten weeks of feeding standard diet, MCD diet or CDAA diet. Scale bar 2 cm. **(C)** Body weight, liver weight and liver weight to body weight ratio in NASH model mice. n = 8; mean ± SD; ** $p < 0.01$, **** $p < 0.0001$

Both NASH models led to increased levels of liver enzymes AST, GLDH and ALT in plasma (Figure 24 A). In MCD diet fed mice plasma levels of glucose (Figure 24 B), triglyceride (Figure 24 C) and cholesterol (Figure 24 D) were significant decreased. However, in CDAA diet fed mice level of urea was decreased (Figure 24 E), whereas level of cholinesterase (Figure 24 F) was increased in plasma.

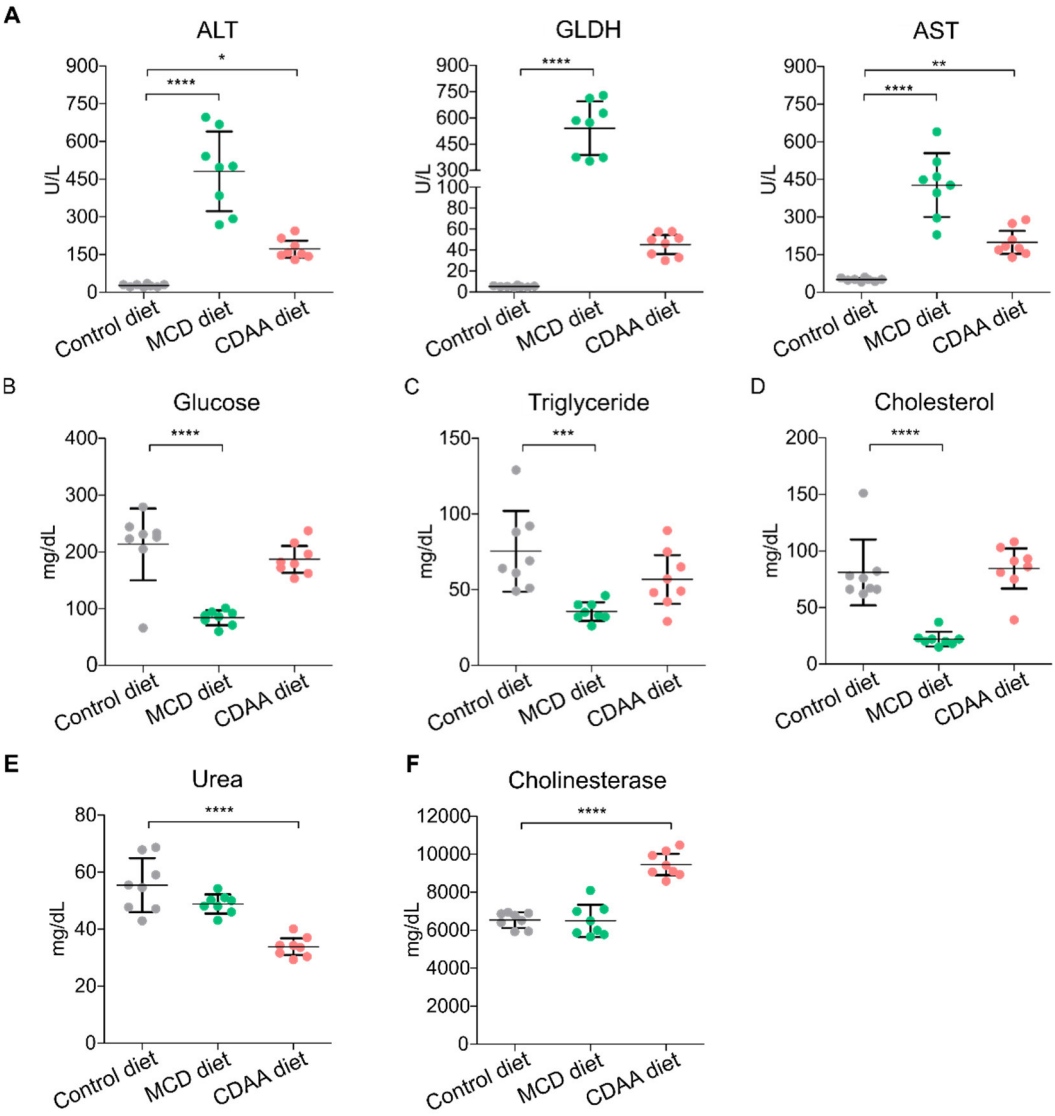

Figure 24. Plasma levels after ten weeks MCD and CDAA diet.
Levels of **(A)** liver enzymes ALT, GLDH and AST and **(B)** glucose, **(C)** triglyceride, **(D)** cholesterol, **(E)** urea and **(F)** cholinesterase in plasma of mice in NASH model. n = 8; mean ± SD; * $p < 0.05$, ** $p < 0.01$, *** $p < 0.001$, **** $p < 0.0001$.

4.1.2.3. Liver fibrosis development in MCD and CDAA diet fed mice

Activation of HSCs by increased expression of *Acta2*, *Col1a1*, *Col3a1*, *Desmin* and *Pdgfrb* was seen in both NASH models (Figure 25 A). This result was confirmed for Desmin on protein level in an IF staining (Figure 25 B). In histological H&E staining livers of MCD and CDAA diet fed mice showed steatosis, inflammation and hepatocyte ballooning (Figure 25 B). Furthermore, in both diets a perisinusoidal liver fibrosis was developed. Fibrosis was more severe in CDAA diet than in MCD diet (Figure 25 B, C) and further supported by the fact that MCD mice lose a lot of weight, which is contrary to human NASH. Therefore, the following experiments and analysis were only carried out with CDAA diet.

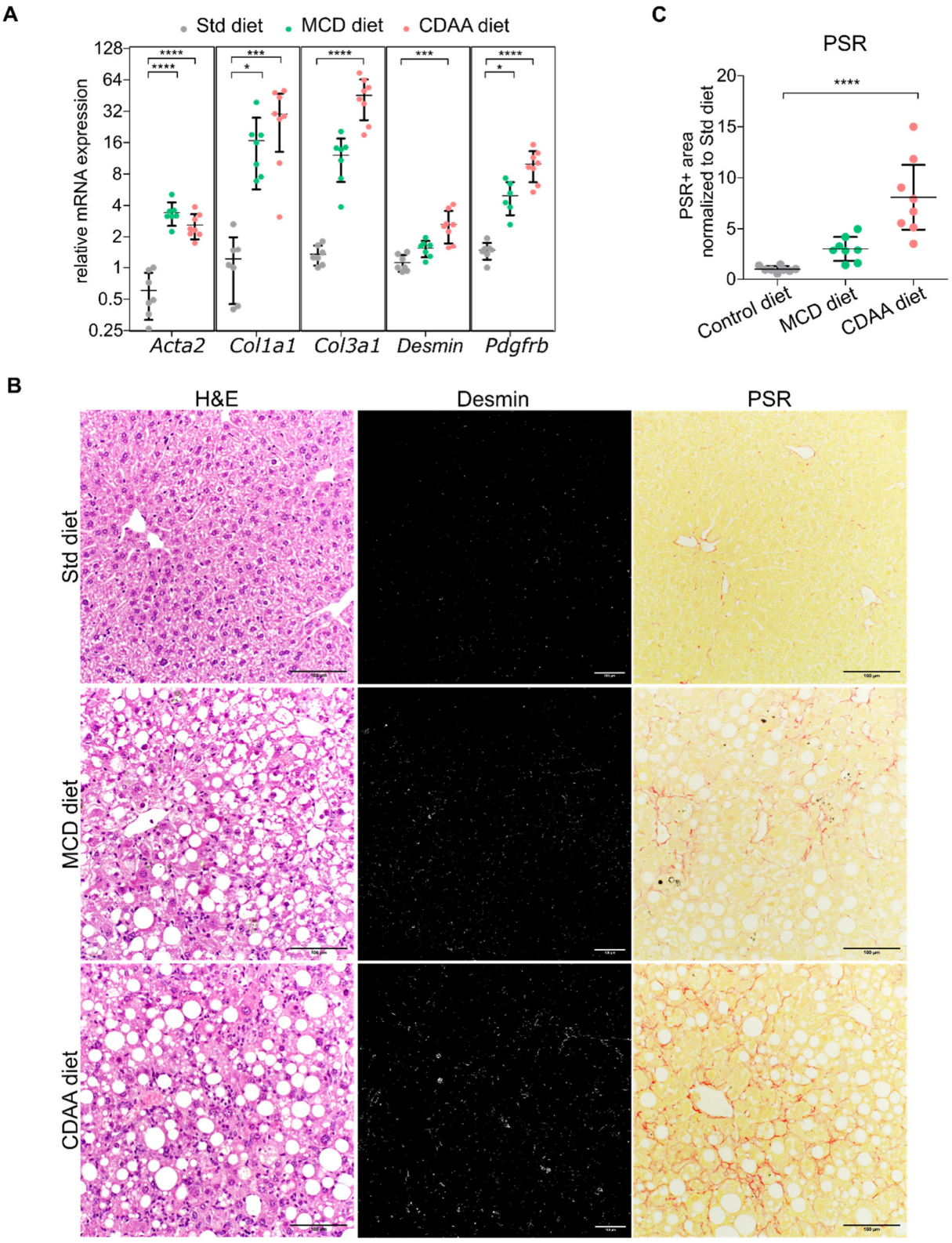

Figure 25. Development of perisinusoidal fibrosis in NASH models.
(A) mRNA expression of hepatic stellate cell markers *Acta2, Col1a1, Col3a1, Desmin* and *Pdgfrb* in whole liver in NASH model measured by RT-qPCR. **(B)** Histological staining of H&E and PSR and immunflouorescence staining of Desmin. Representative images from two independent experiments with eight biological replicates. Scale bar 100 µm. **(C)** Quantification of PSR staining. n = 8; mean ± SD; * $p < 0.05$, *** $p < 0.001$, **** $p < 0.0001$.

Investigations of EC marker expression in CDAA diet displayed a downregulation of LSEC endothelial zonation marker LYVE-1 and pan-endothelial cell marker Podocalyxin in comparison to standard diet (Figure 26 A, B). Expression of continuous EC marker Endomucin was heterogeneous with a tendency towards increased expression (Figure 26 A, B).

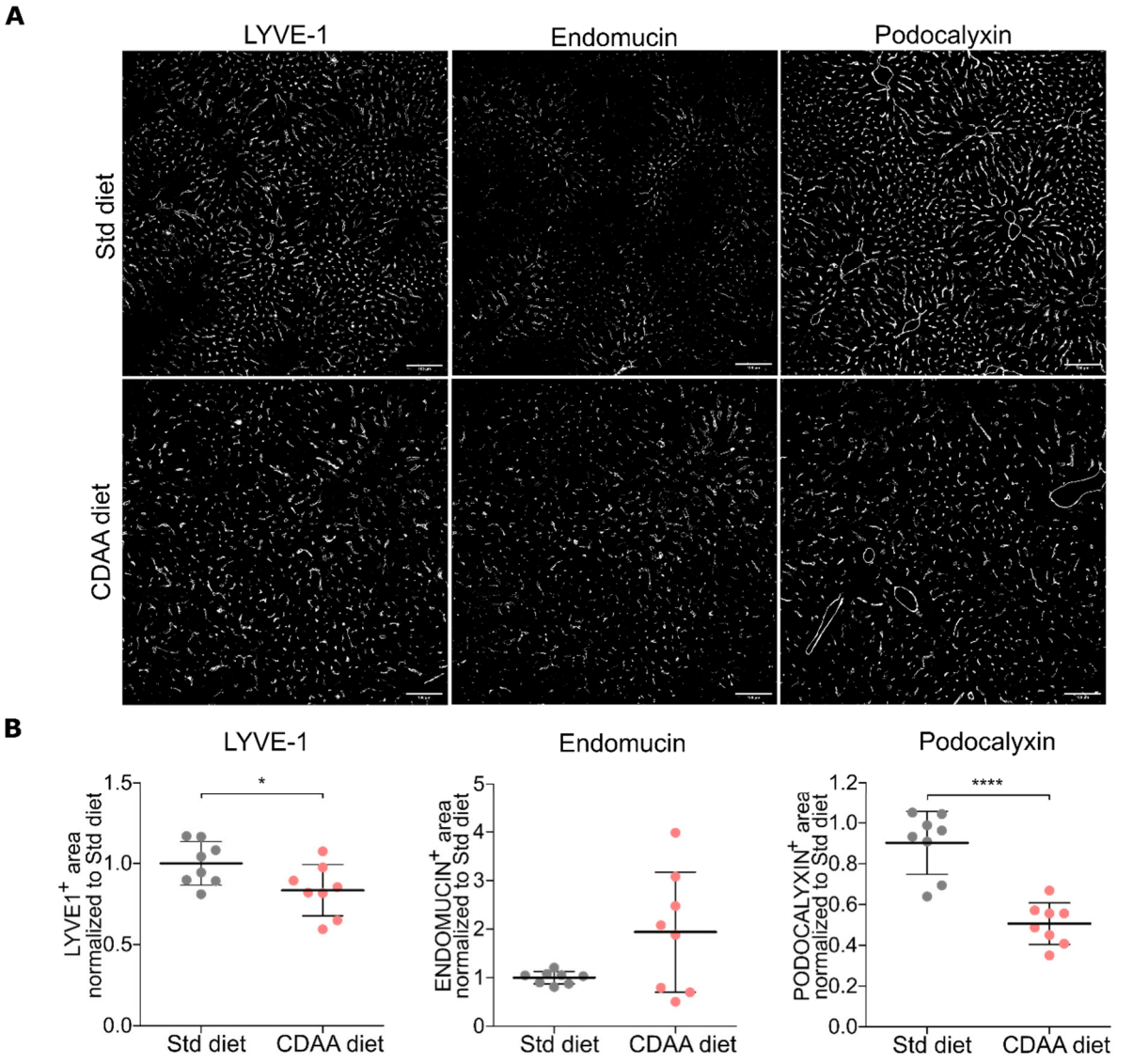

Figure 26. Expression of endothelial zonation and pan-endothelial markers in CDAA fed mice.
(A) Immunofluorescence staining of endothelial cell markers LYVE-1, Endomucin and Podocalyxin in NASH model. Representative images from two independent experiments with eight biological replicates. Scale bar 100 µm **(B)** Quantification of immunofluorescence stainings in **(A)**. n = 8; mean ± SD; * $p < 0.05$, **** $p < 0.0001$.

4.1.2.4. Expression of GATA4 in CDAA diet NASH model

Analysis of GATA4 expression revealed a downregulation of GATA4 in total liver lysates in CDAA diet fed mice (Figure 27 A, B). To analyze if LSEC downregulate *Gata4* upon CDAA diet, LSEC were isolated from CDAA diet and standard diet fed mice. mRNA expression analysis showed a decrease of *Gata4* expression in CDAA mLSEC (Figure 27 C).

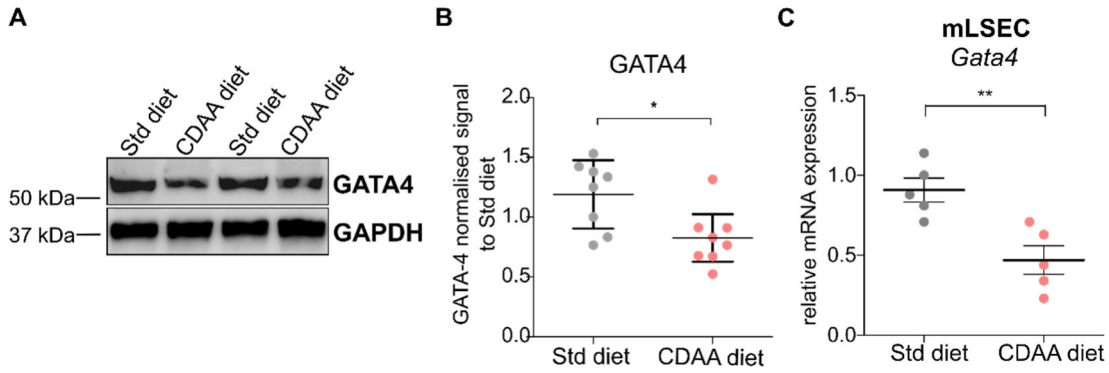

Figure 27. Expression of LSEC master regulator Gata4 in total liver and hepatic endothelial cells of CDAA fed mice.
(A) Expression of GATA4 in whole liver assessed by western blot analysis. Two representative samples from two independent experiments with eight biological replicates are shown. **(B)** Quantification of Western blot of **(A)** using SPL technology; n = 8 **(C)**. mRNA expression of *Gata4* in isolated mLSEC of CDAA fed mice assessed by RT-qPCR; n = 5; mean ± SD; * $p < 0.05$, ** $p < 0.01$. Results for **(C)** are taken from Winkler *et al. [95]* (CC BY-NC-ND 4.0) https://creativecommons.org/licenses/by-nc-nd/4.0/

Altogether, these data indicate that during NASH-associated perisinusoidal liver fibrosis endothelial *Gata4* is downregulated, which corresponds to the findings of genetic Gata4-deficiency in LSEC (Gata4$^{LSEC\text{-}KO}$ mice) that leads to the development of perisinusoidal liver fibrosis and moderate hepatopathy.

4.1.2.5. Transcriptomic analysis of CDAA LSEC

To get more insights into the molecular alterations in LSEC of CDAA-fed mice, microarray analysis of isolated LSEC from CDAA-fed and control mice were performed. Upon microarray analysis, 3890 genes were significantly downregulated in CDAA mLSEC compared to controls. Using established gene sets for sinusoidal endothelial versus continuous EC differentiation [117, 229, 234] downregulation of LSEC-specific genes in CDAA mLSEC were found (Figure **28** A-C). Comparison of significantly dysregulated genes in CDAA mLSEC with microarray data from Gata4-deficient LSEC (Gata4$^{LSEC\text{-}KO}$) revealed a notable overlap of up- and downregulated genes (Figure 28 D) [95].

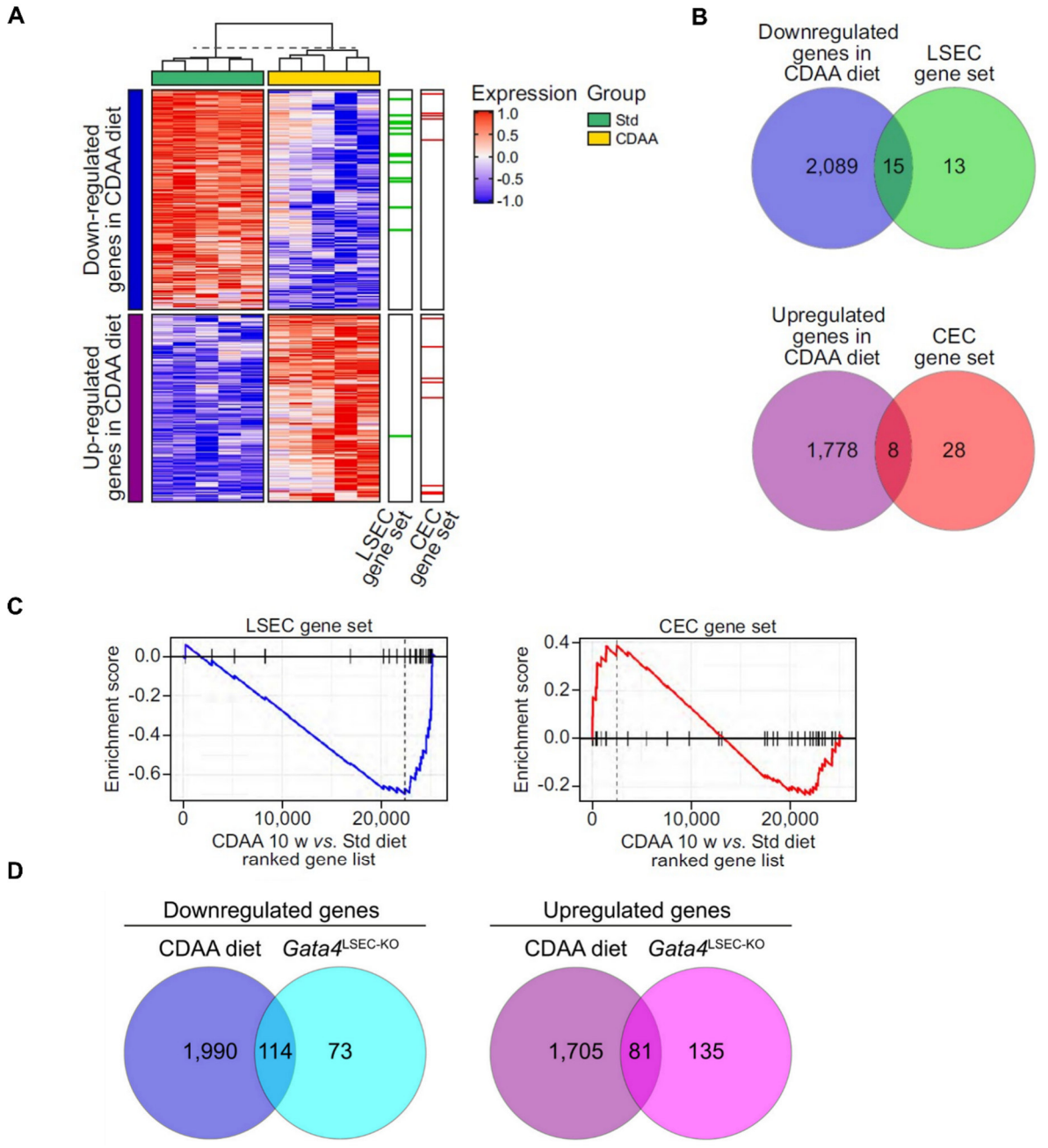

Figure 28. Transcriptional profile of isolated mLSEC in CDAA model and comparison with mLSEC from Gata4$^{LSEC-KO}$ mice.
After isolation of mLSEC of CDAA diet fed mice and standard diet fed control mice, microarray analysis was performed. **(A)** Heat map and **(B)** Venn diagram of significant dysregulated genes (Padj < 0.05). LSEC (p = 0.0015) and CEC (p = 0.2787) gene sets are annotated. **(C)** Enrichment plot of LSEC-associated (p = 0.0019, NES = −2.11) and CEC-associated (p = 0.15, NES = 1.27) genes. **(D)** Venn diagrams showing the overlap between significant dysregulated genes in mLSEC of Gata4$^{LSEC-KO}$ and CDAA diet. n = 5. Figure and labelling are adopted from *Winkler et al. [95]* (CC BY-NC-ND 4.0) https://creativecommons.org/licenses/by-nc-nd/4.0/

We were wondering, if GATA4 dependent genes in CDAA mLSEC were altered. Hence, a GATA4 gene set was defined. For that, 73 genes, which are significantly downregulated in Gata4$^{LSEC-KO}$ LSEC and have two or more binding sites for GATA4 in one or two published ChIP-seq data sets for GATA4 of whole liver from ENCODE (ENCSR194GNY) and GEO

(GSM1194141), were defined as endothelial GATA4 gene set (Figure 29 A). Two thirds of endothelial GATA4 gene set genes were downregulated in CDAA mLSEC (Figure 29 B). GSEA analysis further confirmed this finding, showing that the GATA4 gene set was enriched in LSEC of standard diet fed control versus CDAA mice (Figure 29 C).

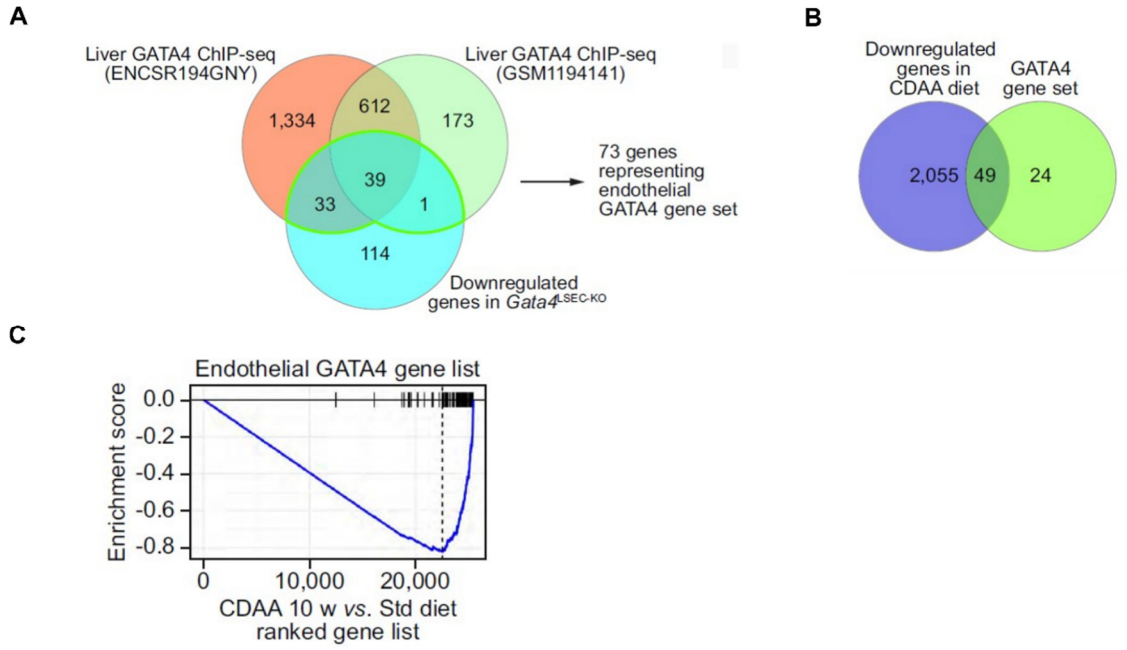

Figure 29. Reduction of GATA4 dependent genes in the CDAA model of liver fibrosis.
(A) Definition of the endothelial Gata4-gene-set. **(B)** Venn diagram showing the overlap of downregulated genes upon CDAA diet and endothelial Gata4-gene-set. **(C)** Enrichment plot of endothelial Gata4-gene-set (p = 0.0018, NES = −3.08) in CDAA mLSEC. Figure and labelling are adopted from Winkler *et al.* (CC BY-NC-ND 4.0) *[95]* https://creativecommons.org/licenses/by-nc-nd/4.0/

Taken together, loss of endothelial GATA4 seems to be an important factor during CDAA-associated liver fibrosis.

4.1.3. Application of CDAA NASH model on Gata4$^{LSEC-KO}$ mice

As downregulation of GATA4 during NASH seems to be associated with the formation of perisinusoidal liver fibrosis, we speculated that complete genetic deletion of *Gata4* in LSEC aggravates the formation of liver fibrosis in a CDAA model. Therefore, Gata4$^{LSEC-KO}$ mice and control siblings were fed with CDAA diet for ten weeks (Figure 30 A). Livers of sibling controls fed with CDAA diet were significant bigger and heavier with same body weight throughout all groups (Figure 30 B, C). Therefore, liver-to-body-weight ratio was significantly increased in CDAA fed control mice (Figure 30 C). Livers of Gata4$^{LSEC-KO}$ mice stayed the same size and weight upon CDAA diet (Figure 30 B, D).

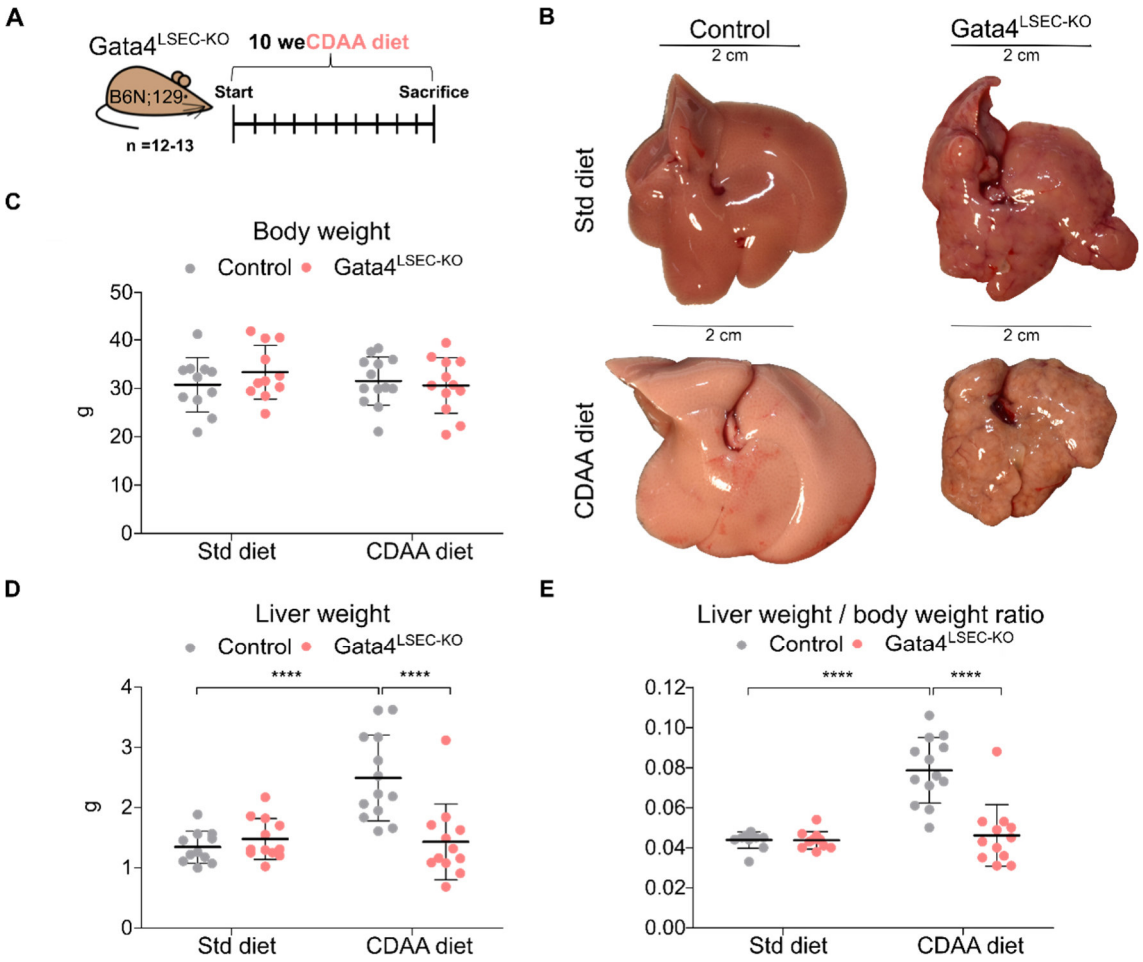

Figure 30. Impact of CDAA diet in Gata4$^{LSEC-KO}$ mice.
(A) Female Gata4$^{LSEC-KO}$ mice and sibling controls were fed CDAA diet and standard diet for ten weeks. **(B)** Representative macroscopic pictures and **(C)** body weight, liver weight and liver weight to body weight ratio of Gata4$^{LSEC-KO}$ and control mice fed with either CDAA diet or standard diet. Scale bar 2 cm. n = 12-13; mean ± SD; **** $p < 0.0001$.

Plasma levels of AST, GLDH, ALT and cholinesterase were increased in Gata4$^{LSEC-KO}$ mice and controls fed with CDAA diet (Figure 31 A, B, C, F). Moreover, levels of AST and bilirubin were increased in CDAA diet fed Gata4$^{LSEC-KO}$ mice compared to CDAA diet fed controls (Figure 31 A, D). In CDAA diet fed Gata4$^{LSEC-KO}$ mice glucose levels were decreased compared to all other groups (Figure 31 E).

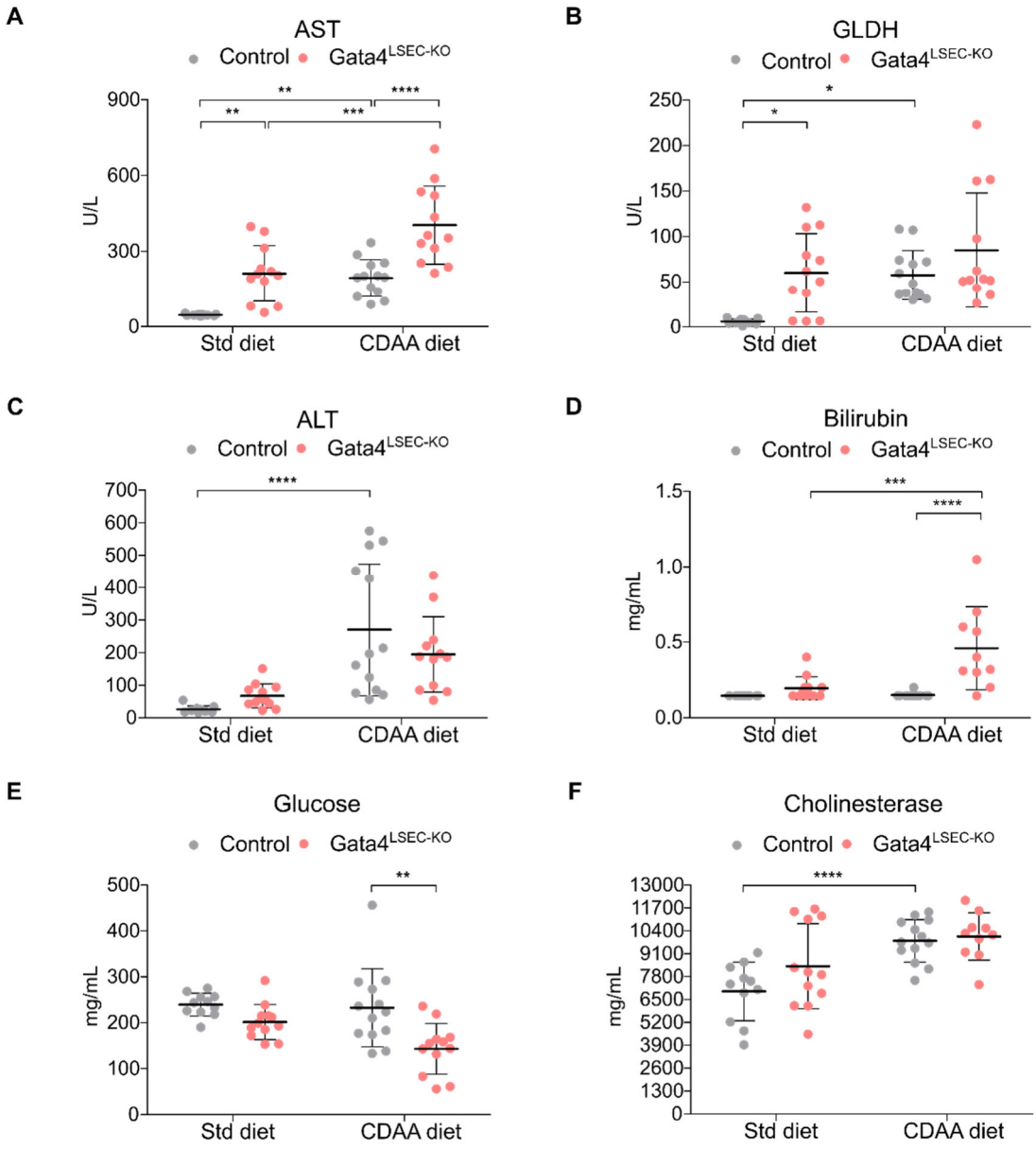

Figure 31. Plasma indices of Gata4$^{LSEC-KO}$ mice fed a CDAA diet.
Levels of liver enzymes **(A-C)** AST, GLDH, ALT and **(D)** bilirubin, **(E)** glucose and **(F)** cholinesterase in plasma of Gata4$^{LSEC-KO}$ and controls after ten weeks CDAA diet or standard diet. n = 12-13; mean ± SD; * < 0.05, ** p < 0.01, *** p < 0.001, **** p < 0.0001.

Histological H&E staining of CDAA model on Gata4$^{LSEC-KO}$ mice revealed all signs of NASH in CDAA fed Gata4$^{LSEC-KO}$ mice and controls (Figure 32 A). However, CDAA diet led to a reduced lipid accumulation in Gata4$^{LSEC-KO}$ livers compared to controls (Figure 32 B), which could be explain the reduced liver weight and size of CDAA fed Gata4$^{LSEC-KO}$ mice (Figure 30 B, C). All other measured plasma levels were not altered (not shown).

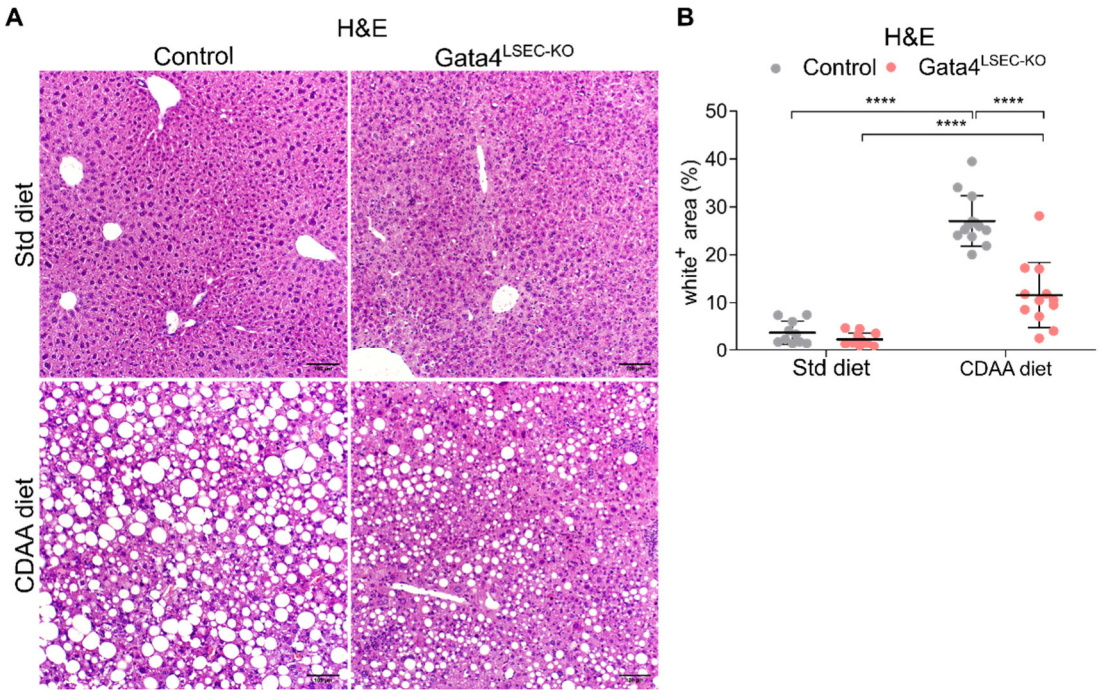

Figure 32. Reduced fat accumulation in CDAA fed Gata4$^{LSEC-KO}$ mice.
(A) Histological H&E staining of CDAA fed or standard fed Gata4$^{LSEC-KO}$ and controls. Representative images from two independent experiments with twelve - thirteen biological replicates. Scale bar 100 µm. **(B)** Quantification of white area in H&E staining of **(A)**. n = 12-13; mean ± SD; **** $p < 0.0001$.

Interestingly, CDAA diet led to an increased degree of perisinusoidal liver fibrosis in Gata4$^{LSEC-KO}$ mice compared to CDAA fed controls and Gata4$^{LSEC-KO}$ mice fed with standard diet (Figure 33 A, B).

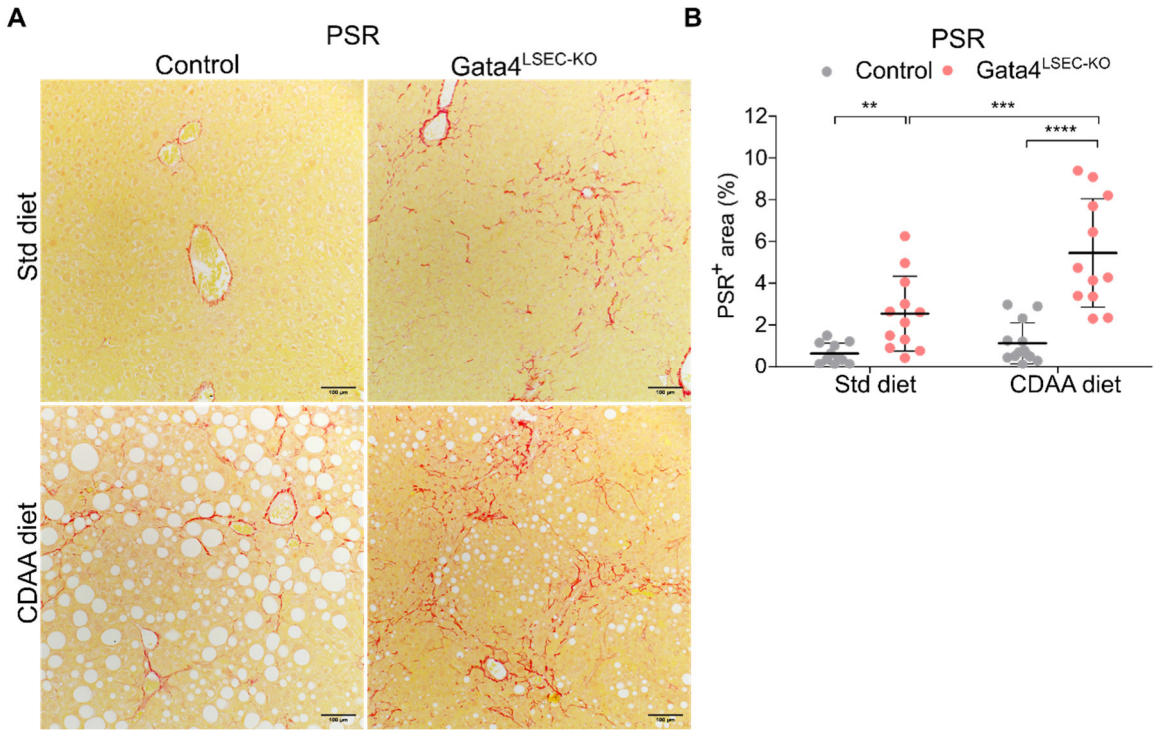

Figure 33. Increased fibrosis in CDAA fed Gata4$^{LSEC-KO}$ mice.
(A) Histological PSR staining of CDAA fed or standard fed Gata4$^{LSEC-KO}$ and controls. Representative images from two independent experiments with twelve - thirteen biological replicates. Scale bar 100 µm. **(B)** Quantification of PSR staining of **(A)**. n = 12-13; mean ± SD; ** $p < 0.01$, *** $p < 0.001$, **** $p < 0.0001$.

Analysis of HSC activation revealed increased activation of HSC in CDAA fed mice and controls by increased expression of *Acta2* (Figure 34 A), *Col1a1* (Figure 34 B), *Col3a1* (Figure 34 C), *Desmin* (Figure 34 D) and *Pdgfrb* (Figure 34 E) compared to standard diet fed mice. However, there was no difference between standard fed and CDAA diet fed Gata4$^{LSEC-KO}$ mice (Figure 34 A-E).

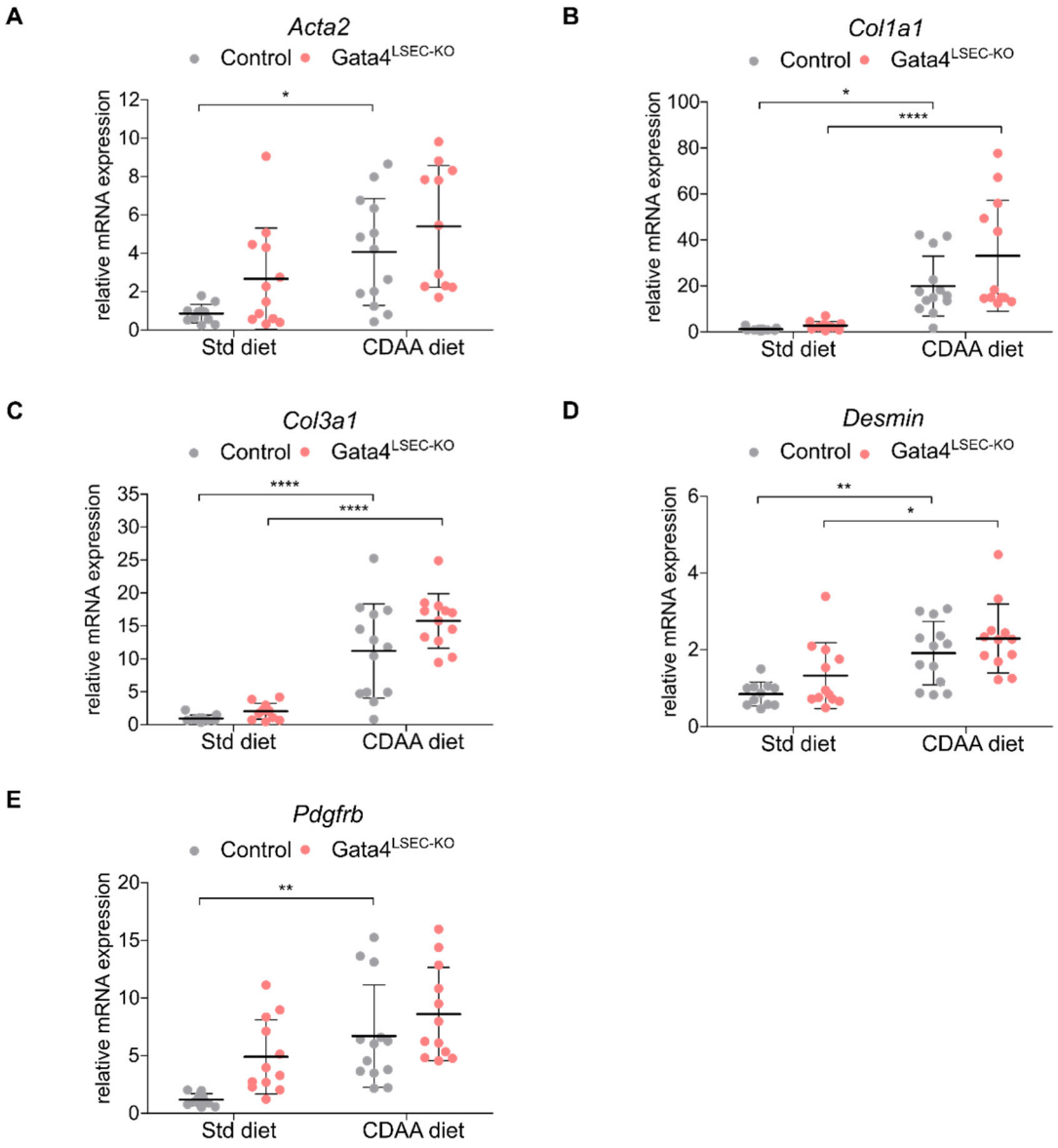

Figure 34. Increased expression of fibrosis markers in CDAA fed Gata4$^{LSEC-KO}$.
mRNA expression of hepatic stellate cell genes **(A)** *Acta2*, **(B)** *Col1a1*, **(C)** *Col3a1*, **(D)** *Desmin*, **(E)** *Pdgfrb* in Gata4$^{LSEC-KO}$ and controls fed with CDAA diet or standard diet. n = 12-13; mean ± SD; * $p < 0.05$, ** $p < 0.01$, **** $p < 0.0001$.

Taken together CDAA diet in Gata4$^{LSEC-KO}$ mice led to an increased hepatopathy accompanied by reduced fat accumulation in the liver and increased liver fibrosis development.

4.2. Generation and characterization of a LSEC-specific Gata4 knockin mouse

Deficiency of liver endothelial GATA4 leads to the development of perisinusoidal liver fibrosis in a genetical mouse model [95]. Furthermore, endothelial GATA4 itself (Figure 27 C) and GATA4 dependent genes were reduced in a CDAA diet induced NASH model (Figure 29 B, C). Therefore, we generated a LSEC-specific Gata4 knockin mouse to maintain *Gata4* expression during liver fibrosis models to prevent or attenuate liver fibrosis development.

4.2.1. Generation and characterization of LSEC-specific Gata4 knockin mouse

For generation of LSEC-specific Rosa26-Gata4 knockin mouse ($Gata4^{LSEC\text{-}KI}$), first the neomycin cassette was deleted by crossing ROSA26STGata4-neo mice with Flip-deleter mice. The resulting ROSA26STGata4 mouse was crossed with Clec4g-iCre driver mice to obtain $Gata4^{LSEC\text{-}KI}$ mice, that show LSEC-specific *Gata4* expression (Figure 35 A). First expression of reporter tdTomato was analyzed in the liver of $Gata4^{LSEC\text{-}KI}$ mouse and control siblings. A co-staining of CD31 and tdTomato confirmed expression of the tdTomato reporter in CD31-positive endothelial cells (Figure 35 B) in livers of $Gata4^{LSEC\text{-}KI}$ mice. However, total liver GATA4 expression analyzed by western blotting did not show increased GATA4 levels in $Gata4^{LSEC\text{-}KI}$ mice compared to sibling controls (Figure 35 C).

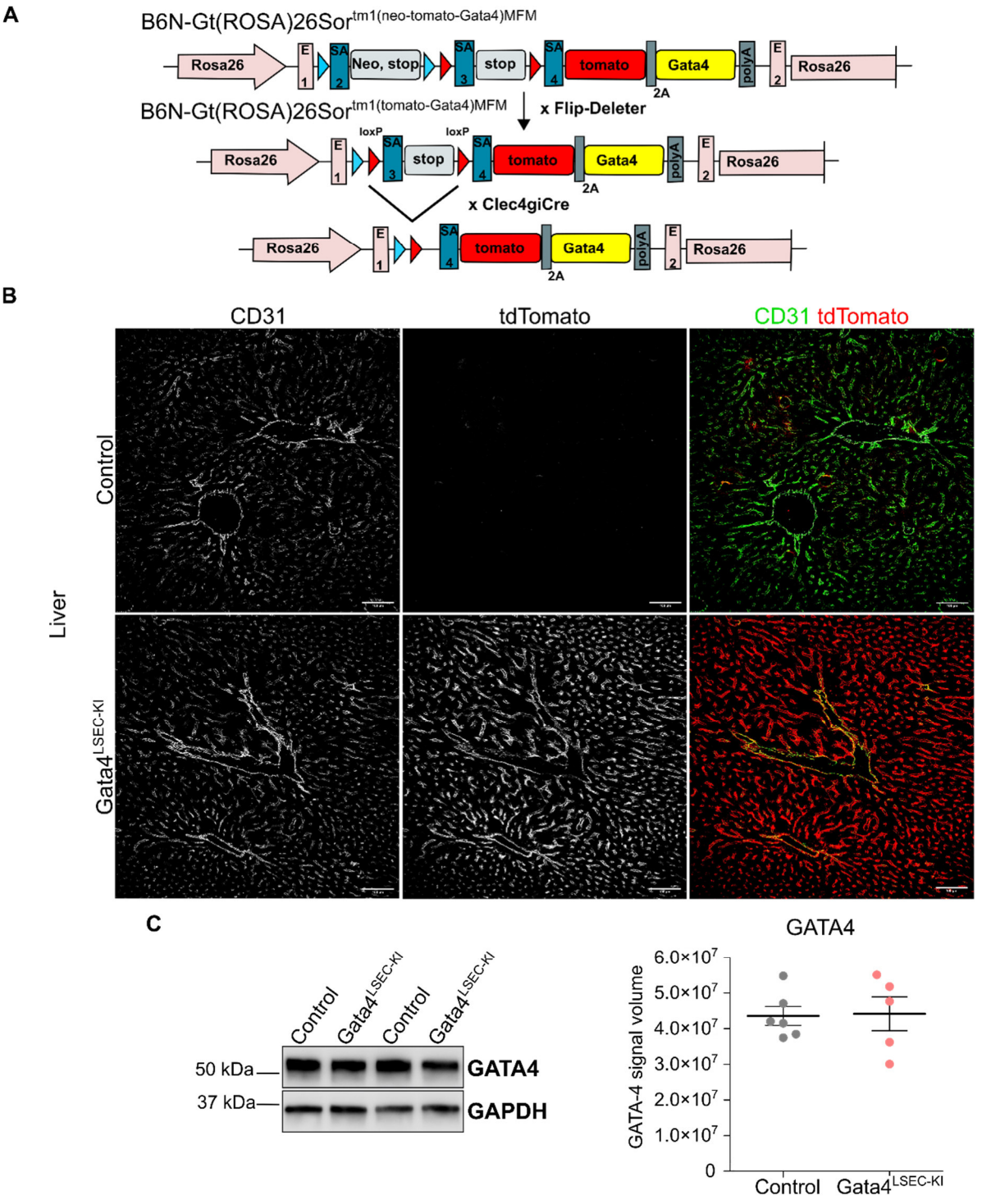

Figure 35. Hepatic expression of tdTomato and GATA4 in Gata4$^{LSEC-KI}$ mouse.
(A) Schematic overview to generate Gata4$^{LSEC-KI}$ mouse. To delete neomycin resistance gene from the gene locus the ROSA26STGata4-neo mouse is crossed with a Flip-deleter mouse. After mating ROSA26STGata4 mouse with Clec4g-iCre to generate Gata4$^{LSEC-KI}$ mouse *Gata4* is overexpressed LSEC-specific. **(B)** Immunofluorescence co-staining of CD31 and tdTomato in liver. **(C)** GATA4 expression quantified with SPL technology of Gata4$^{LSEC-KI}$ livers. Representative images from one experiment with five to six biological replicates. Scale bar 100 µm. n = 5-6; mean ± SD.

In addition to liver endothelial cells, there is Cre-activity in Clec4g-iCre mice in a subset of heart EC and in sinusoidal EC of the lymph node [229]. A co-staining of CD31 and tdTomato demonstrated expression of tdTomato in CD31-positive endothelial cells in lymph node (Figure 36 A) and heart (Figure 36 B) of Gata4$^{LSEC-KI}$ mice.

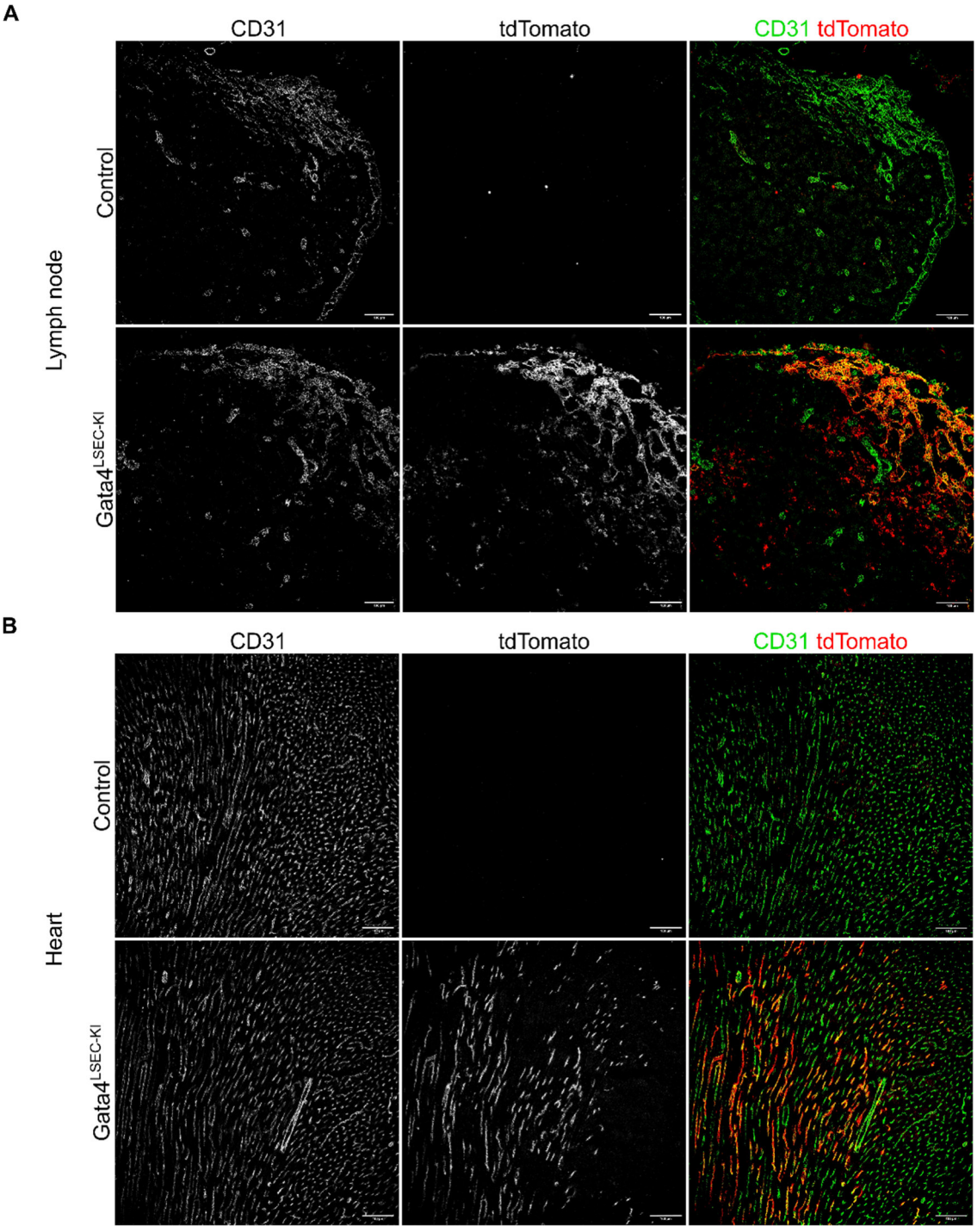

Figure 36. Expression of tdTomato and GATA4 in heart and lymph node of Gata4$^{LSEC-KI}$ mouse. Immunofluorescence co-staining of CD31 and tdTomato in **(A)** lymph node **(B)** and heart of Gata4$^{LSEC-KI}$ mouse and control siblings. Representative images from one experiment with five to six biological replicates. Scale bar 100 µm. n = 5-6; mean ± SD.

After validation of reporter expression in EC of the liver in Gata4$^{LSEC-KI}$ mouse, a basal characterization of the mouse line was conducted. Three-month-old Gata4$^{LSEC-KI}$ mice showed no difference in body weight, liver weight, liver size and liver-to-body-weight ratio compared to sibling controls (Figure 37 A-D). Moreover, levels of liver enzymes ALT, GLDH and AST were unchanged in the plasma of Gata4$^{LSEC-KI}$ mice (Figure 37 E-G).

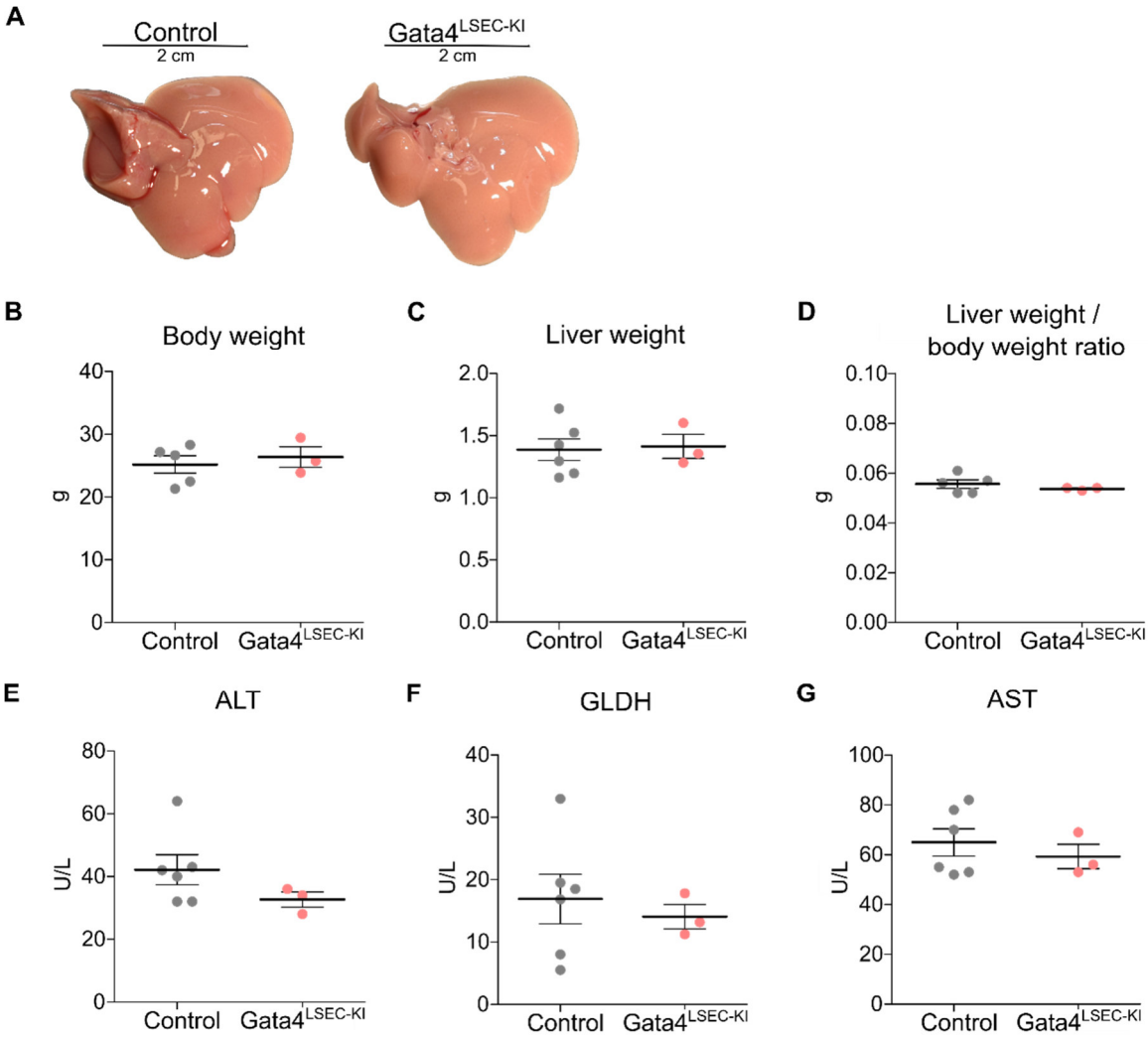

Figure 37. Characterization of Gata$^{4LSEC-KI}$ mouse.
(A) Representative macroscopic picture, **(B)** body weight, **(C)** liver weight, **(D)** liver weight to body weight ratio and plasma levels of liver enzymes **(E)** ALT, **(F)** GLDH, **(G)** AST in Gata4$^{LSEC-KI}$ mouse. n = 3-5; mean ± SD.

Routine H&E and PSR staining of the liver showed no abnormalities and no differences compared to controls (Figure 38).

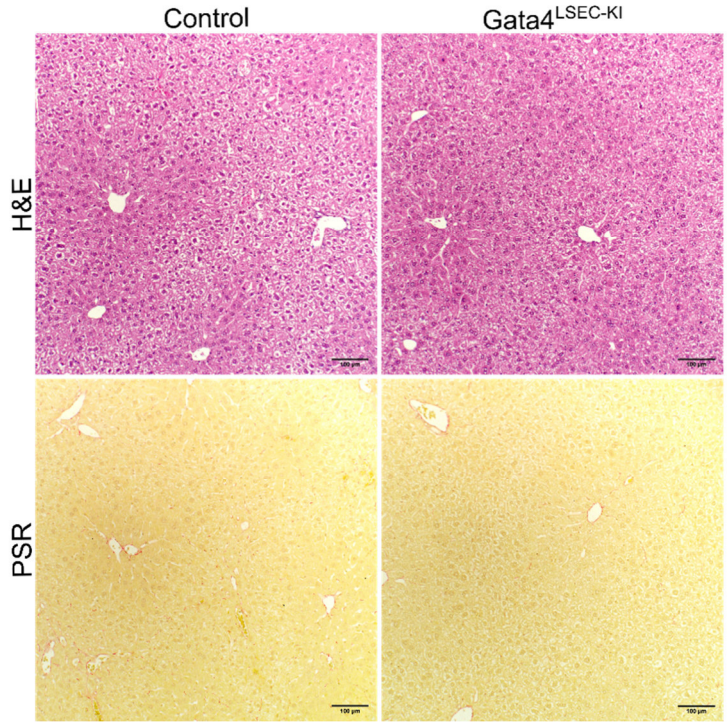

Figure 38. Histological stainings and hepatic GATA4 expression in Gata4$^{LSEC-KI}$ mouse.
Histological H&E and PSR staining and of Gata4$^{LSEC-KI}$ livers. Representative images from one experiment with five to six biological replicates. Scale bar 100 µm. n = 5-6; mean ± SD.

Taken together, reporter tdTomato is expressed in CD31-positive endothelial cells of the liver in Gata4$^{LSEC-KI}$ mice, but there is no difference between Gata4$^{LSEC-KI}$ mouse and control siblings in basal characterization.

4.2.2. Application of CDAA diet induced NASH model on Gata4 knockin mouse

In CDAA diet induced NASH, hepatic endothelial GATA4 itself (Figure 27 C) and its function is reduced (Figure 29 C). To maintain GATA4 expression and to potentially alleviate or prevent formation of perisinusoidal fibrosis in a NASH model, Gata4$^{LSEC-KI}$ mice were used in a CDAA model. After ten weeks of feeding a CDAA diet, Gata4$^{LSEC-KI}$ mice showed no difference in liver size (Figure 39 A), body weight (Figure 39 B), liver weight (Figure 39 C) and liver-to-body-weight ratio (Figure 39 D) compared to CDAA fed control siblings (Figure 39 A-D).

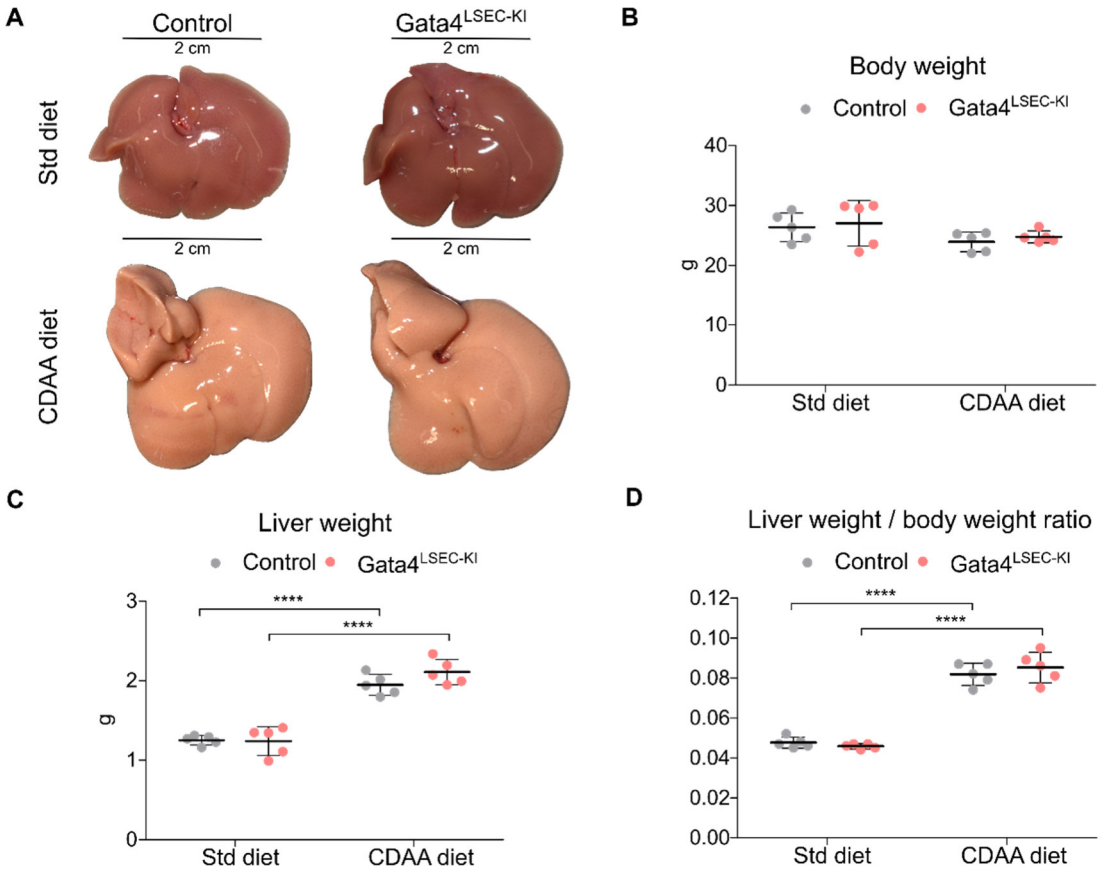

Figure 39. Impact of CDAA diet on Gata4$^{LSEC-KI}$ mouse.
(A) Representative macroscopic picture of livers and **(B)** body weight, **(C)** liver weight and **(D)** liver weight to body weight ratio of Gata4$^{LSEC-KI}$ mice and sibling controls fed ten weeks with CDAA or standard diet. Scale bar 2 cm. n = 5; mean ± SD; **** $p < 0.0001$.

Furthermore, plasma levels of liver enzymes ALT (Figure 40 A), GLDH (Figure 40 B) and AST (Figure 40 C) and levels of cholinesterase (Figure 40 D) were higher in CDAA fed Gata4$^{LSEC-KI}$ mice and controls. However, there was no difference between the different genotypes (Figure **40** A-D).

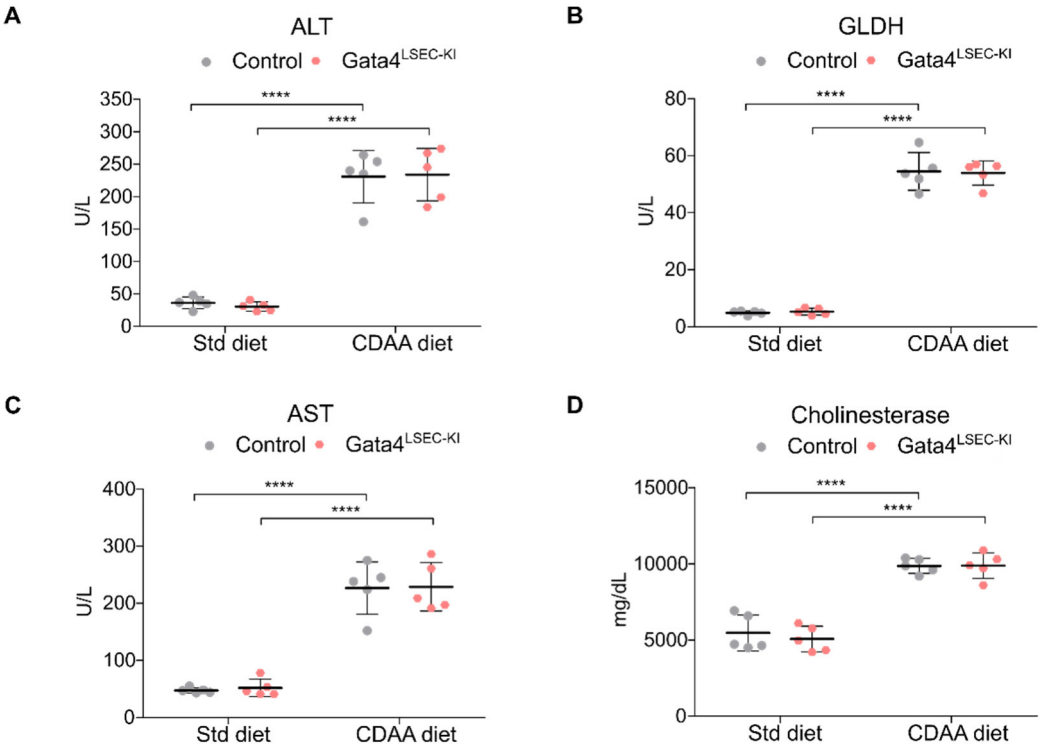

Figure 40. Plasma levels in Gata4$^{LSEC-KI}$ mice upon CDAA model.
Levels of **(A)** ALT, **(B)** GLDH, **(C)** AST and **(D)** cholinesterase in plasma of Gata4^{LSE-KI} mice and controls fed with CDAA or standard diet. n = 5; mean ± SD; **** $p < 0.0001$.

Moreover, CDAA fed Gata4$^{LSEC-KI}$ mice did not show a decrease in fibrosis development upon PSR staining of the liver compared to controls (Figure 41 A, B).

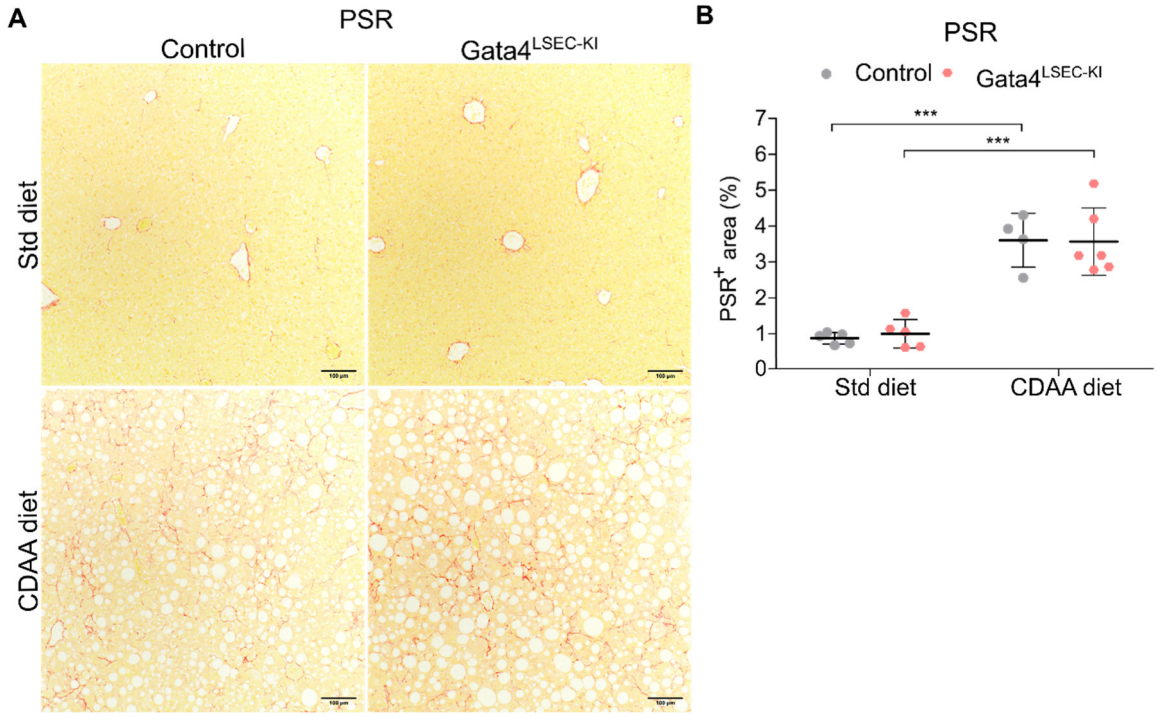

Figure 41. Development of fibrosis in Gata4$^{LSEC-KI}$ mouse in CDAA model.
(A) Histological picture and **(B)** quantification of PSR staining in Gata4^{LSE-KI} mice and controls fed with CDAA or standard diet. Representative images from one experiment with five biological replicates. Scale bar 100 µm. n = 5; mean ± SD; *** p < 0.001.

4.2.3. Generation and characterization of Gata4 rescue mice (Gata4$^{LSEC-KO}$ x Gata4$^{LSEC-KI}$) for functional verification of Gata4$^{LSEC-KI}$ mice

As CDAA-fed Gata4$^{LSEC-KI}$ mice did not show a decrease in fibrosis development, we started another strategy to validate the functionality of *Gata4*-overexpression in Gata4$^{LSEC-KI}$. We used the Gata4$^{LSEC-KO}$ mouse line with LSEC-specific Gata4-deficiency which was demonstrated to develop a perisinusoidal liver fibrosis [95]. For a proof of principle and to verify the functionality of Gata4$^{LSEC-KI}$ mouse, a genetical Gata4 rescue mouse (Gata4$^{LSEC-KO}$ x Gata4$^{LSEC-KI}$) was generated. Therefore, ROSA26STGata4 mice were first crossed with Gata4 homozygous floxed (Gata4$^{fl/fl}$) mice. To generate Gata4 rescue mouse, the resulting ROSA26STGata4$^{fl/fl;}$ Gata4$^{fl/fl}$ mice were crossed with Clec4g-iCre$^{tg/wt}$; Gata4$^{fl/fl}$ mice (Figure 42 A). As Gata4$^{LSEC-KO}$ mice have a reduced liver-to-body-weight ratio and develop a perisinusoidal liver fibrosis [95], Gata4 rescue mice were analyzed for these two parameters. Nine and twelve weeks old Gata4 rescue mice were analyzed and Gata4$^{LSEC-KO}$ mice in the same age served as controls. Macroscopically the livers of Gata4$^{LSEC-KO}$ mice and Gata4 rescue mice showed signs of liver fibrosis (Figure 42 B) and there was no difference in liver-weight-to-body weight ratio in both ages and genotypes (Figure 42 C).

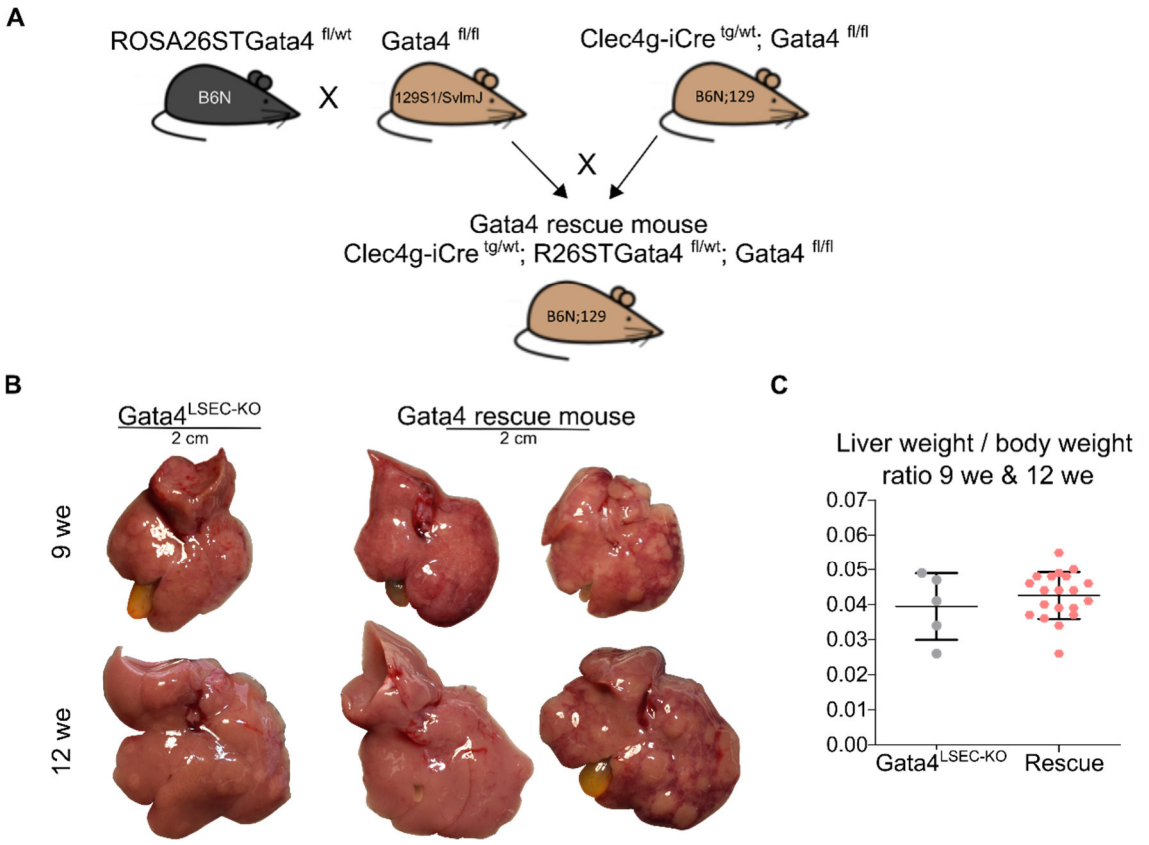

Figure 42. Generation of Gata4 rescue mouse.
(A) Mating scheme to generate Gata4 rescue mouse. **(B)** Representative macroscopic picture of livers and **(C)** liver weight to body weight ratio of Gata4 rescue mouse and Gata4$^{LSEC-KO}$ mice with nine and twelve weeks of age. Gata4$^{LSEC-KO}$: n = 5, Gata4 rescue mouse: n = 19; mean ± SD.

Furthermore, there amount of liver fibrosis in the Gata4 rescue mouse comparable to the controls (Figure 43 A, B).

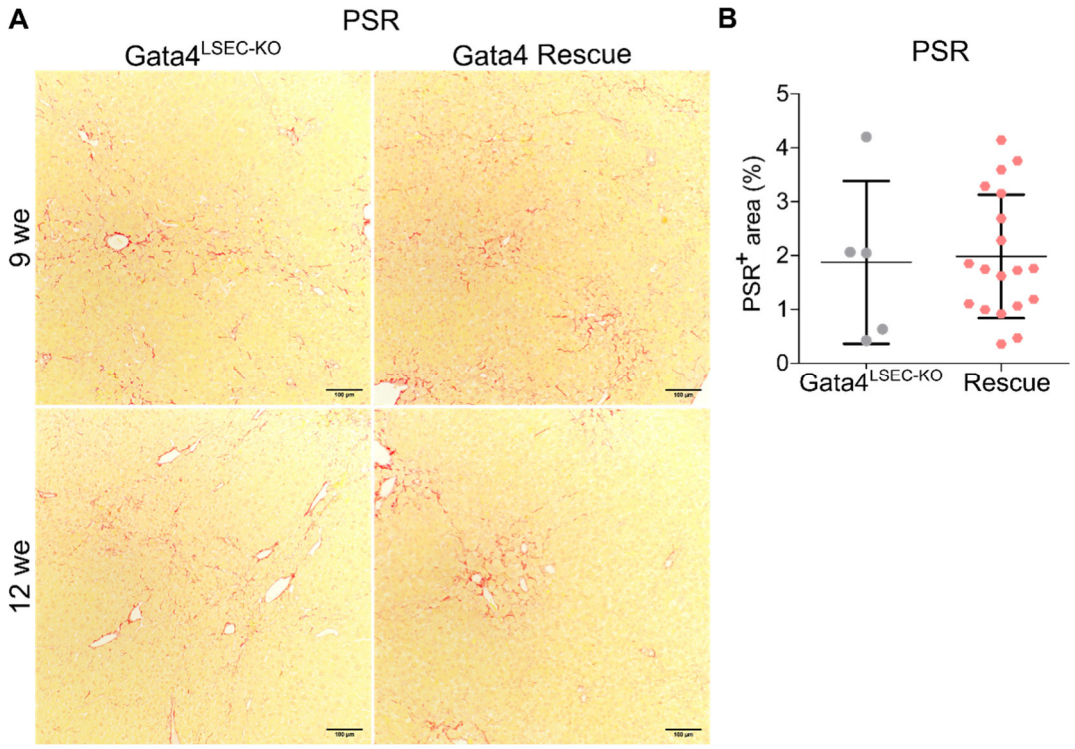

Figure 43. Development of fibrosis in Gata4 rescue mouse.
(A) Histological picture and **(B)** quantification of PSR staining of livers of Gata4 rescue mouse and Gata4$^{LSEC-KO}$ mice with nine and twelve weeks of age. Scale bar 100 µm. Gata4$^{LSEC-KO}$: n = 5, Gata4 rescue mouse: n = 19; mean ± SD.

Taken together, the Gata4 rescue mouse did not show a rescue of the phenotype seen in Gata4$^{LSEC-KO}$ mice, indicating insufficient *Gata4* overexpression.

4.2.4. Analysis of Gata4 overexpression efficiency in the Gata4 knockin mouse

Analysis of reporter expression in Gata4$^{LSEC-KI}$ mouse showed expression of tdTomato in hepatic CD31-positive EC cells (Figure 35 B). However, genetical Gata4 rescue mouse was not able to rescue the phenotype of Gata4$^{LSEC-KO}$ mouse (Figure 42 C; Figure 43 A). Therefore, LSEC from Gata4$^{LSEC-KI}$ mice were isolated and analyzed for *Gata4* expression. On the one hand, freshly isolated LSEC were used for RNA sequencing analyses. On the other hand, LSEC were cultivated for 48 h and 168 h to conduct RT-qPCR analysis of *Gata4* and Gata4 target genes (Figure 44 A). Correlation analysis of RNA sequencing data showed a tight correlation between Gata4$^{LSEC-KI}$ mice and sibling control data set. The correlation was between 0.96 and 1, therefore no big difference in expression profile between the two groups was excepted (Figure 44 B). A GSEA analysis of MSigDB Hallmark Gene Sets was conducted and showed that some pathways were significant different between the data sets. Pathway alterations in Gata4$^{LSEC-KI}$ mice compared to controls were associated with proliferation

(mitotic spindle and G2M checkpoint), oxygen radicals (reactive oxygen species), cellular respiration (oxidative phosphorylation), transcription (E2F targets) and TGFβ signaling (Figure **44** C). On single gene level there were just seven genes, that were above the p-value ($p > 0.05$) and log2 fold change value cutoff (Figure 44 D; Table 9) in $Gata4^{LSEC\text{-}KI}$ mice compared to controls. Using the endothelial Gata4 gene set (Figure 29 A) showed that the genes of the gene set are heterogeneous expressed across the two genotypes, indicating that GATA4 dependent genes were not significantly affected in $Gata4^{LSEC\text{-}KI}$ mice (Figure 44 E). Furthermore, none of the seven genes significantly dysregulated in $Gata4^{LSEC\text{-}KI}$ mice were included in the endothelial Gata4 gene set. The three highest increased genes Trappc5, Cd209a (Clec4l) and Fcer2a (Clec4j) are located on the Clec4g-iCre transgene of $Gata4^{LSEC\text{-}KI}$ mice.

These data indicate that in $Gata4^{LSEC\text{-}KI}$ mice there is no sufficient induction of GATA4 and of GATA4 dependent genes.

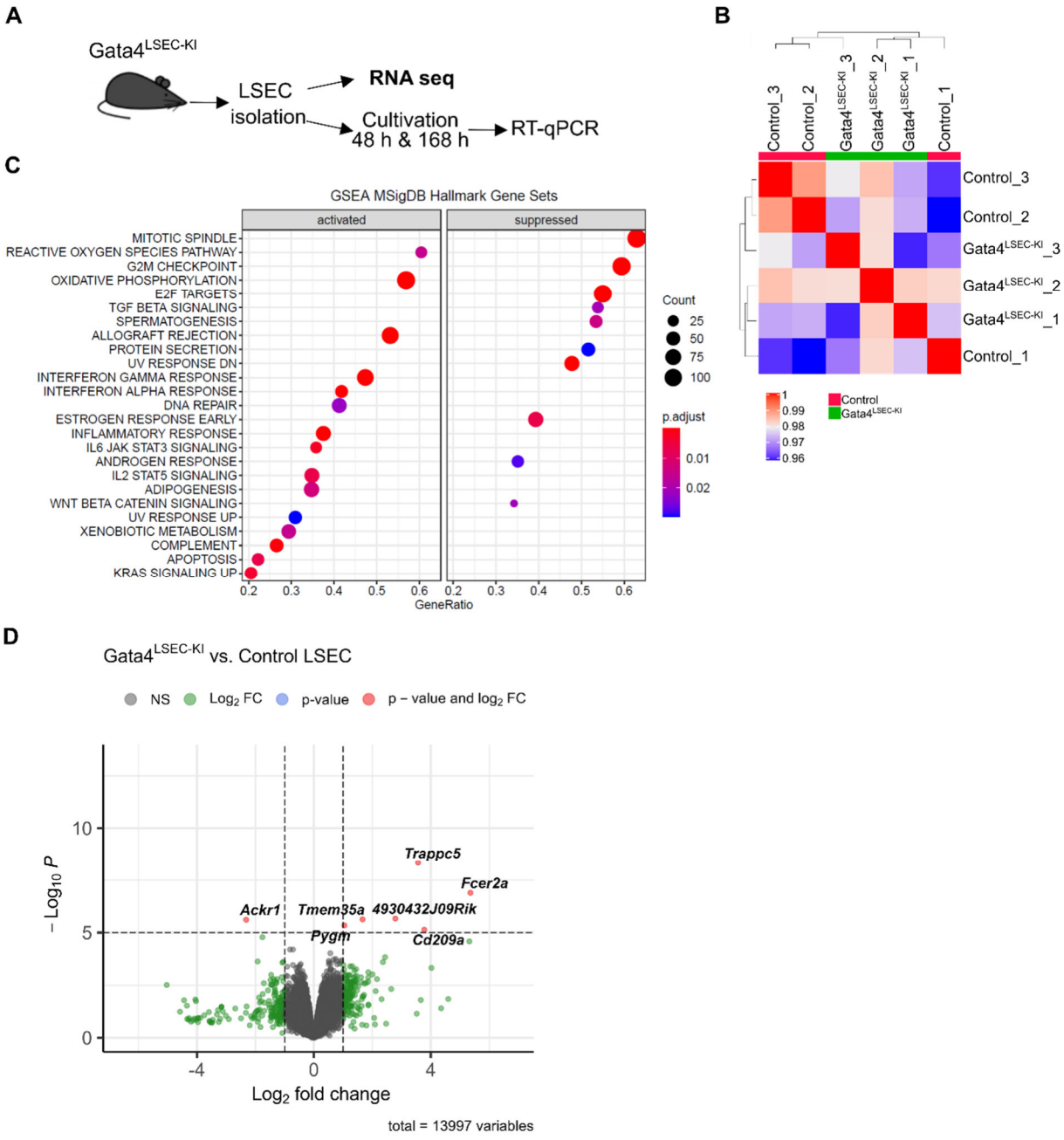

Figure 44. Transcriptomic profile of mLSEC of Gata4$^{LSEC-KI}$ mouse.
(A) After isolation of primary mLSEC from Gata4$^{LSEC-KI}$ mouse, a RNA-seq analysis were performed. **(B)** Correlation heatmap, **(C)** GSEA Hallmark Gene Sets Analysis, **(D)** Volcanoplot and **(E)** Heatmap of endothelial Gata4 gene set of RNA-seq data of Gata4$^{LSEC-KI}$ and control siblings. n = 3.

Table 9. Significant regulated genes in Gata4$^{LSEC-KI}$ mLSEC.
After isolation of primary mLSEC from Gata4$^{LSEC-KI}$ mouse, a RNA-seq analysis were performed. Fold change of Gata4$^{LSEC-KI}$ vs. control siblings were calculated.

Gene Symbol	Gene name	Adjusted p-value	Fold change
Ackr1	atypical chemokine receptor 1 (Duffy blood group)	0,006854	0,20
Pygm	muscle glycogen phosphorylase	0,010632	2,06
Tmem35a	transmembrane protein 35A	0,006854	3,17
4930432J09Rik	RIKEN cDNA 4930432J09 gene	0,006854	6,90
Trappc5	trafficking protein particle complex 5	0,000066	11,83
Cd209a	CD209a antigen	0,014520	13,69
Fcer2a	Fc receptor, IgE, low affinity II, alpha polypeptide	0,000898	40,91

Taken together, Gata4$^{LSEC-KI}$ mice displayed some minor transcriptomic alterations, but no increased expression of *Gata4* or GATA4 dependent genes.

Previous work by our group could demonstrate, that *Gata4* expression is reduced in rat LSEC upon cultivation for 42 h [234]. Based on these findings, I isolated LSEC of Gata4$^{LSEC-KI}$ mice and control siblings and cultivated them for 48 h and 168 h followed by RNA expression analysis (Figure 45 A). After cultivation for 168 h LSEC from Gata4$^{LSEC-KI}$ mice expressed reporter tdTomato but did not show phenotypic differences compared to LSEC from control siblings (Figure 45 B). Expression analysis by RT-qPCR showed increased expression of *tdTomato* and transgene *Gata4* in Gata4$^{LSEC-KI}$ mice compared to control mice with no difference between cultivation times (Figure 45 C, D). In contrast, expression of endogenous *Gata4* and Gata4 target genes *Bmp2* and *Wnt2* were unchanged in Gata4$^{LSEC-KI}$ mice compared to controls (Figure 45 E-G). *Bmp2* was reduced after 168 h cultivation compared to 48 h, independent of the genotype (Figure 45 F).

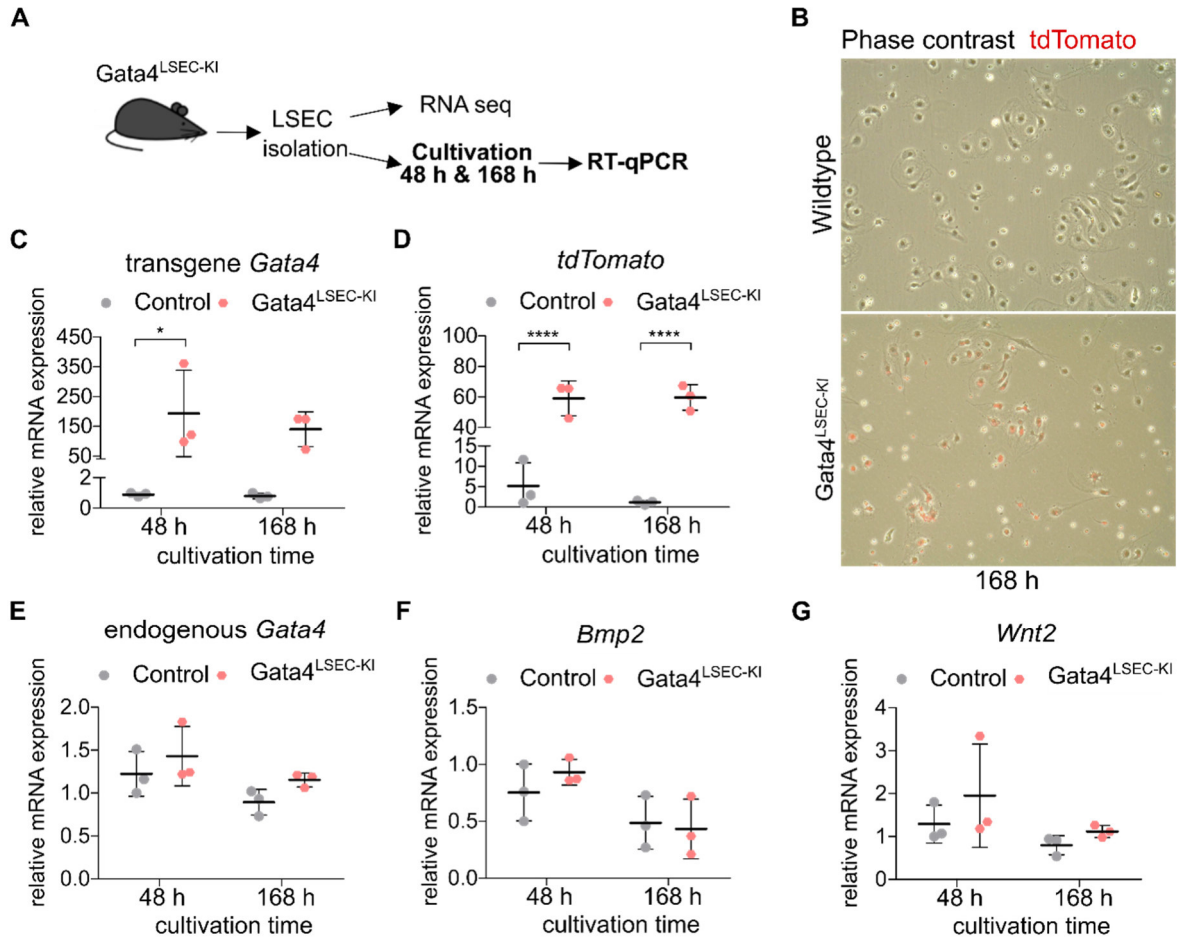

Figure 45. Analysis of transgenic Gata4 expression in mLSEC of Gata4$^{LSEC-KI}$.
(A) After isolation of primary mLSEC from Gata4$^{LSEC-KI}$ mouse and cultivation for 48 and 168 hours, mRNA expression analysis measured by RT-qPCR was performed. **(B)** Representative picture of brightfield and tdTomato expression of mLSEC after 168 hours cultivation. mRNA expression of **(C)** transgene *Gata4*, **(D)** *tdTomato*, **(E)** endogenous *Gata4*, **(F)** *Bmp2* and **(G)** *Wnt2* of Gata4$^{LSEC-KI}$ and control mLSEC after 48- and 168-hours cultivation. n = 3; mean ± SD; **** p < 0.001.

Altogether, *tdTomato* and transgene *Gata4* are expressed on RNA level, but no functional transgene GATA4 protein is expressed in Gata4$^{LSEC-KI}$ mice. Together with the RNA sequencing data these data indicate that Gata4$^{LSEC-KI}$ mice generated by us are insufficient for LSEC-specific *Gata4* overexpression *in vivo*.

4.3. Generation and analysis of LSEC-targeting Gata4 overexpressing lentivirus

Endothelial GATA4 expression seems to be essential for sinusoidal EC differentiation and liver homeostasis as loss of GATA4 in LSEC leads to development of liver fibrosis [95, 117] (Figure **27** C). Consequently, an overexpression of GATA4 in LSEC could be preventive for the development of liver fibrosis. To this end, a specific LSEC-targeting lentivirus with an overexpression of GATA4 was generated.

4.3.1. Functional testing of synthetic Gata4 (in LV-EF1α-ADR3-IRP)

For LSEC-targeting lentivirus a synthetic murine *Gata4* with a V5-tag had to be synthesized (Figure 7). For functional testing of synthetic Gata4-V5, it was cloned into LV-ADR3 empty vector (Figure 10). After transduction of bEnd.3 and HUVEC cells with LV-ADR3-Gata4-V5, both cell lines expressed GATA4-V5 on protein level compared to empty vector control (Figure **46** A). In HUVEC cells, transduction with LV-ADR3-Gata4-V5 leads to the induction of GATA4 target gene *Bmp2* (Figure 46 B). These results verified the functionality of synthetic Gata4-V5, so that it was cloned into the target lentiviral vector to generate LSEC-targeting LV-CD31-Gata4-V5 (Figure 11).

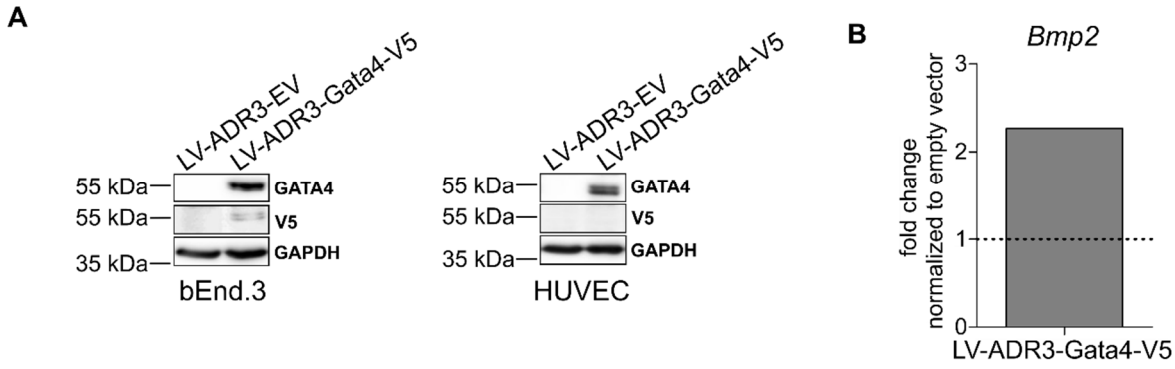

Figure 46. Validation of transduction of HUVEC and bEnd.3 cells with LV-ADR3-Gata-V5.
After generation of lentivirus LV-ADR3-Gata4-V5, HUVEC and bEnd.3 cells were transduced. **(A)** Expression of GATA4 and V5 on protein level in both cell types measured by western blot (n = 3) and **(B)** expression of Gata4 target gene Bmp2 on mRNA level measured by RT-qPCR in HUVEC was assessed.

4.3.2. Generation and functional analysis of LSEC-targeting Gata4 lentivirus LV-CD31-Gata-V5

After high titer production of LV-CD31-Gata4-V5, bEnd.3 cells were transduced with different concentrations (untransduced, 1:1600, 1:400 and 1:00) of the lentivirus and analyzed by RT-qPCR and western blot. Expression of synthetic *Gata4* increased with increasing concentrations of the lentivirus (Figure 47 A). Expression of endogenous *Gata4* is only increased with the highest lentivirus concentration (Figure 47 B). Furthermore, analyses of *Gata4* target gene expression showed only an induction of *Wnt2* with the highest lentivirus concentration (Figure 47 C, D). GATA4 expression on protein levels increased with higher concentrations of the lentivirus (Figure 47 E, F). These findings indicated that LV-CD31-Gata4-V5 seems to be functional to induce GATA4 expression and function in bEnd.3 cells.

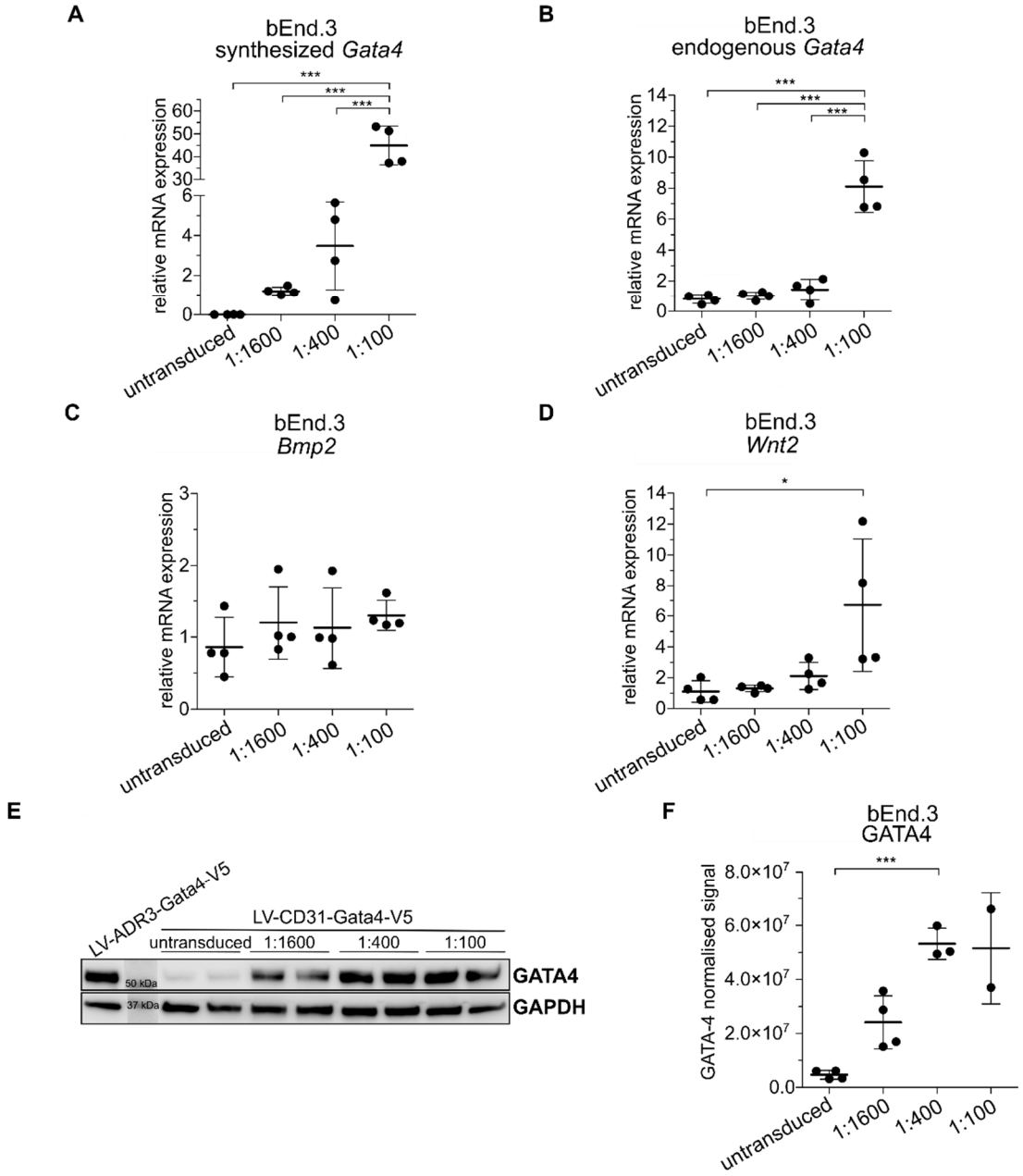

Figure 47. Validation of transduction of bEnd.3 cells with LV-CD31-Gata4-V5.
After generation of lentivirus LV-CD31-Gata4-V5, bEnd.3 cells were transduced with different concentrations (untransduced, 1:1600, 1:400, 1:100) of the lentivirus. mRNA expression of **(A)** synthesized *Gata4*, **(B)** endogenous *Gata4,* **(C)** *Bmp2* and **(D)** *Wnt2* measured by RT-qPCR and **(E)** expression of GATA4 measured by western blot and **(F)** quantified by SPL technology of transduced bEnd.3 cells with LV-CD31-Gata4-V5 was assessed. n = 4; mean ± SD; * $p < 0.05$, *** $p < 0.001$.

To test the functionality of the virus in the target cells, mLSEC were transduced. “Wildtype” mLSEC already express GATA4, so that there might be no additional effect seen after lentiviral transduction. Because of that, *Gata4* deficient LSEC were isolated from Gata4$^{LSEC\text{-}KO}$ mice and transduced with different concentrations of LV-CD31-Gata4-V5. Similar to bEnd.3 cells, expression of synthetic *Gata4* increased with higher lentivirus concentrations (Figure 48 A) in mLSEC. However, endogenous *Gata4* expression and GATA4 target gene expression of *Wnt2*

and *Bpm2* did not change after lentiviral transduction (Figure 48 B-D). Moreover, on protein level there was no difference in GATA4 expression after transduction (Figure 48 E, F).

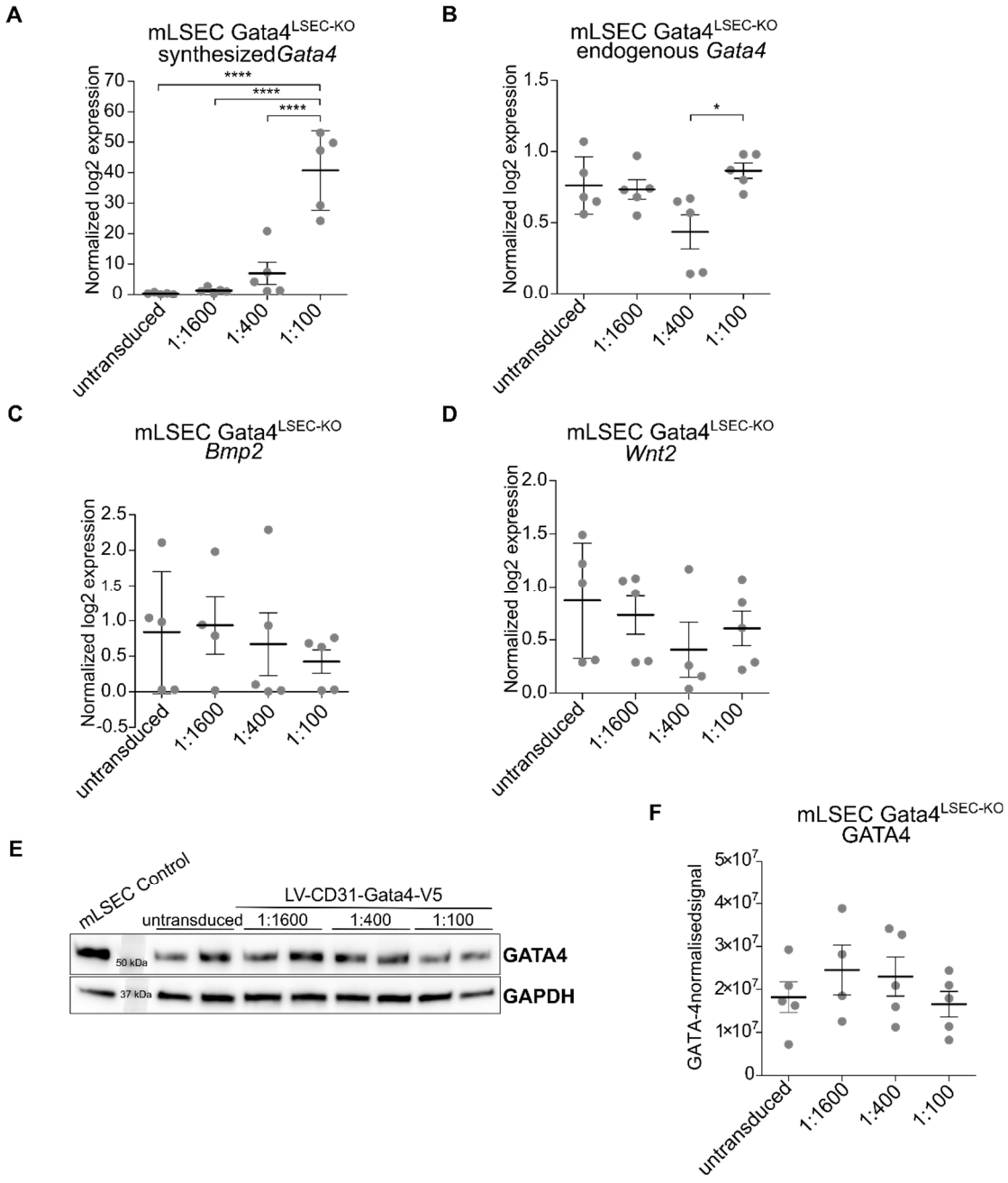

Figure 48. Validation of transduction of Gata4$^{LSEC-KO}$ mLSEC with LV-CD31-Gata4-V5.
After generation of lentivirus LV-CD31-Gata4-V5, isolated primary mLSEC from Gata4$^{LSEC-KO}$ and control siblings were transduced with different concentrations (untransduced, 1:1600, 1:400, 1:100) of the lentivirus. mRNA expression of **(A)** synthesized *Gata4*, **(B)** endogenous *Gata4*, **(C)** Bmp2 and **(D)** Wnt2 measured by RT-qPCR and **(E)** expression of GATA4 measured by western blot and **(F)** quantified by SPL technology of transduced mLSEC of Gata4$^{LSEC-KO}$ with LV-CD31-Gata4-V5 was assessed. n = 5; mean ± SD; * $p < 0.05$, **** $p < 0.0001$.

Taken together, LV-CD31-Gata4-V5 lentivirus is able to induce overexpression of GATA4 and its downstream target *Wnt2* in bEnd.3 cells but not in mLSEC *in vitro*.

5. Discussion

5.1. Gata4 expression in different liver fibrosis models with different fibrosis types

Recently, we identified transcription factor GATA4 as master regulator for specification of hepatic discontinuous sinusoidal endothelium during liver development [117]. Furthermore, we could show that loss of LSEC master regulator GATA4 leads to hepatopathy and development of perisinusoidal liver fibrosis [95]. In human NASH, the presence and degree of liver fibrosis in human NASH begins in pericentral regions causing perisinusoidal fibrosis. Perisinusoidal liver fibrosis can then spread to portal fibrosis with progression into bridging fibrosis, finally resulting in cirrhosis [143]. One aim of the study was to assess the expression and role of endothelial GATA4 in a chemical-based chronic CCl_4 liver fibrosis model leading to bridging fibrosis compared to a diet-based NASH mouse model leading to perisinusoidal liver fibrosis.

5.1.1. Gata4 expression in bridging fibrosis of toxic liver fibrosis model

For induction of toxic liver fibrosis, I used chronic CCl_4 liver fibrosis animal model. Mostly chronic CCl_4 liver fibrosis model is applied by two to three *i.p.* injections a week for four to six weeks with a dosage of 0.5 to 1 mL/kg body weight [205]. Established fibrosis with lower dosage is seen after two to four weeks and after six to eight weeks the mice develop severe fibrosis (cirrhosis). Moreover, it is known that different mouse strains have different susceptibility to CCl_4-mediated liver fibrosis. Among them C57BL/6N mice, which are used in this study, have an intermediate susceptibility to CCl_4-mediated liver fibrosis [235]. For this study, I decided to use the higher dosage of CCl_4 (1 mL/kg) and applied it for three weeks bi-weekly, which led to development of pericentral bridging fibrosis, without progression to cirrhosis. Activated HSC showed pericentral expression pattern, which was comparable to collagen deposition pattern seen in PSR staining, indicating activated HSC as a source for ECM producing cells in CCl_4 treated mice. In line with this, HSC are the major source of myofibroblasts in hepatocellular injuries, like CCl_4 induced toxic injury [149, 236]. Sinusoidal capillarization can lead to HSC activation and subsequent liver fibrogenesis. Capillarization of LSEC was demonstrated in CCl_4 treated mice [237]. During capillarization LSEC undergo transdifferentiation from sinusoidal to continuous EC differentiation with loss of fenestrations and the formation of a basement membrane [95]. Investigation of EC marker expression in CCl_4 treated mice in this study revealed increased expression of continuous EC marker

Endomucin but unchanged expression of LSEC marker LYVE-1. This data indicates a change of EC marker expression but no complete transdifferentiation of LSEC in CCl_4 treated mice in this study. However, expression analysis of further LSEC and continuous EC marker would more comprehensively demonstrate the degree of sinusoidal transdifferentiation in this model. Investigation of GATA4 expression in the used CCl_4 model revealed increased co-localization of ERG and GATA4, indicating increased expression of GATA4 in ERG-positive ECs, which is in line with incomplete sinusoidal transdifferentiation, that is only seen upon genetic Gata4-deficiency and obviously does not occur in CCl_4 fibrosis model in this study.

However, sinusoidal capillarization markers such CD34, CD31 and VWF were increased in a CCl_4 model with severe fibrosis [238]. Dufton *et al.* showed, that during chronic CCl_4 model ERG expression is lost. In their CCl_4 model they injected 1 mL/kg CCl4 *i.p.* bi-weekly for eight weeks leading to severe fibrosis [112]. In contrast, in this study the number of ERG-positive cells were unchanged in CCl_4 treated mice compared to oil controls. A possible explanation for this result can be, that ERG is lost later in liver fibrosis progression, because Dufton and colleagues administered CCl_4 for a longer time leading to a more progressive liver fibrosis compared to this study.

Several studies have shown that impaired regulation of transcription factors in LSEC could contribute to liver regeneration and liver fibrosis. During endothelial-to-mesenchymal transition (EndMT) endothelial cells downregulate endothelial markers and by upregulation of mesenchymal genes transforming to cells with the ability to migrate and produce ECM [239] which should contribute to liver fibrosis [240]. Transcription factor Twist-related protein 1 (TWIST1) was suggested as a master regulator for EndMT. It was shown that activation of TWIST1 contributes to EndMT and liver fibrosis. Dong and colleagues showed that chromatin remodeling protein Brahma related gene 1 (Brg1) activate TWIST1 in LSEC epigenetically which contributes to liver fibrosis [241]. Moreover, transcription factor MKL/megakaryoblastic leukemia 1 (MKL1) activates TWIST1 transcription in LSEC leading to EndMT and liver fibrosis [242]. In addition, downregulation of endothelial transcription factor ERG leads to EndMT and liver fibrogenesis [112]. Instead, LSEC-specific downregulation of transcription factor KLF2 reduces liver damage and increases hepatocyte proliferation in a chronic CCl_4 model without altering capillary density and liver fibrosis leading to liver regeneration [226]. However, we showed that application of our chronic CCl_4 model to LSEC-specific Gata4-deficient ($Gata4^{LSEC\text{-}KO}$) mice did not change hepatopathy or the extent of bridging liver fibrosis [95], indicating that endothelial *Gata4* plays no critical role in bridging liver fibrosis in chronic CCl_4 model. Moreover, there could be slight differences in the transcriptional regulation of mild

fibrosis like in our CCl_4 model compared to progressive fibrosis or cirrhosis with more and longer CCl_4 injections as shown by others.

GATA4 is a transcription factor mainly localized in the nucleus of the cells. In contrast Desmin is type III intermediate filament belonging to the cytoskeleton. Therefore, co-expression of GATA4 and Desmin is difficult to analyze in this data. However, several GATA4-positive nuclei seemed to be surrounded by Desmin-positive filaments, indicating increased expression of GATA4 in HSCs. Activated HSCs are the major producer of ECM in hepatocellular injuries like chronic CCl_4 model [243]. Analysis of the underlying molecular mechanisms revealed involvement of several transcription factors in activation of HSCs. Shi and colleagues showed that activating transcription factor 3 (ATF3) is overexpressed in activated HSC leading to expression of profibrotic genes in a chronic CCl_4 model. They revealed that the TGFβ/ATF3/lnc-SCARNA10 axis contributes to liver fibrosis [244]. Furthermore, another transcription factor activating transcription factor 6α is upregulated in activated HSCs and deletion of ATF6α is able to reduce liver fibrosis in a chronic CCl_4 model [245]. These data suggest a critical role of transcription factors in activated HSCs contributing to bridging liver fibrosis. However, not only one transcription factor but several are important for the quiescent state of HSC. Liu et al identified E26 transcription-specific transcription factors (ETS1/2), GATA4/6, interferon regulatory factors (IRF1/2) and ETS-target genes Neurofibromin 1 (NF1) and peroxisome proliferator-activated receptor–γ (PPARγ) as transcription factors or regulators involved in activation of HSC during liver fibrosis in mouse and human. However, GATA4/6 expression was associated with quiescent HSC, therefore interaction of several transcription factors is obviously involved in the activation of HSCs [246].

These results indicate that in toxic liver fibrosis GATA4 expression is not lost in LSEC, but rather mildly increased in endothelial cells and HSC. Interestingly, deletion of *Gata4* in LSEC did not alter the amount of bridging fibrosis [95], which excludes endothelial GATA4 as a driver of CCl4-mediated fibrosis. Thus, analyses of GATA4 expression in HSC would further elucidate the role of GATA4 in toxic bridging liver fibrosis.

5.1.2. Gata4 expression in perisinusoidal liver fibrosis of diet-induced NASH models

5.1.2.1. Establishment of diet-induced NASH model with perisinusoidal liver fibrosis

To analyze expression and role of GATA4 in perisinusoidal liver fibrosis associated with NASH, we wanted to find a diet-based liver fibrosis model which fits best for our purpose. Until now there is no diet-based model, which mimics human NASH in all features. Western diet and high fat diet mimic metabolic perturbations associated with mild human NASH, whereas MCD diet and CDAA diet are useful to induce severe liver damage and progressive fibrosis shortly [247]. Our primary goal was to analyze perisinusoidal fibrosis development in NASH models, why we decided to use MCD and CDAA diet. MCD diet induces steatohepatitis after only two weeks and liver fibrosis after eight to ten weeks [221, 248]. CDAA diet (plus moderate HFD and 0.2 % cholesterol) is able to induce steatohepatitis and fibrosis after eight to twelve weeks of feeding with progression of fibrosis with longer feeding periods [202]. Therefore, I decided to compare eight weeks with ten weeks feeding MCD diet and ten weeks with 20 weeks feeding CDAA diet. In this comparison the most critical parameter was the histopathological changes in the liver.

Both diets and both feeding periods respectively led to development of NASH (steatosis, inflammation, hepatocyte ballooning) with perisinusoidal liver fibrosis in different degrees. Taking feeding period and the degree of NASH and liver fibrosis in account, we decided to use the feeding period of ten weeks of both diets for analyses of diet-induced NASH model.

5.1.2.2. Comparison of MCD diet and CDAA diet for diet-induced NASH model with perisinusoidal liver fibrosis

As known from the literature, MCD diet led to significant weight loss, which is caused due to hypermetabolism [249] and lower caloric intake, however liver-to-body-weight ratio was unchanged compared to control diet. CDAA fed mice did not lose weight but had a higher liver-to-body-weight ratio. Both diets led to liver damage indicated by elevated liver enzyme levels in the plasma. Classical CDAA diet without added fat and cholesterol show higher ALT levels compared to CDAA diet [216]. Because of the use of modified CDAA plus diet the liver enzyme levels in this study were lower compared to MCD diet. Furthermore, decrease of glucose, triglyceride and cholesterol in the plasma of MCD fed mice, which is in contrast to human NASH, is always seen in MCD diet even at shorter feeding periods [216, 250]. CDAA diet was

able to overcome this decrease but neither show increase of the plasma levels. However, urea was decreased, and cholinesterase was increased in the plasma in CDAA diet. Urea is mostly synthesized in the liver and liver disease can lead to decreased urea synthesis and subsequent plasma levels [251]. Furthermore, decreased cholinesterase levels in plasma is seen in patients with liver dysfunction and cirrhosis [252]. However, cholinesterase levels are higher in patients with fatty liver [253] and in NASH patients with diabetes [254].

Activated HSCs were seen in both NASH diets, which was similar as in the CCl_4 model, although the fibrosis pattern in NASH versus toxic fibrosis is completely different. However, these results indicate activated HSC as a source of myofibroblast also in NASH-associated perisinusoidal liver fibrosis [149]. Activation of HSCs and deposition of collagen was higher in CDAA fed mice compared to MCD fed mice. Wei et al. compared MCD and CDAA diet with different levels of fat content. They showed that increase of fat content in MCD or CDAA diet increase liver fibrosis development. Moreover, degree of liver fibrosis increases in a dose-dependent manner to fat content (10 %, 45 %, 60 %) in CDAA diet [255]. In this study CDAA diet with moderate fat content of 31 % and additional 1 % cholesterol was used, which could be an explanation for the higher degree of liver fibrosis in CDAA diet.

Weight loss and decreased plasma levels of glucose, triglycerides and cholesterol, which was seen in MCD diet, is in contrast to human NASH [214]. As mentioned in the literature, CDAA diet is able to overcome these features, but it does not fully mimic the metabolic state in human NASH [202]. For this reason, CDAA diet was used as a diet-induced NASH model to analyze GATA4 expression in perisinusoidal liver fibrosis.

5.1.2.3. GATA4 expression in perisinusoidal fibrosis of CDAA diet-induced NASH model

Endothelial specific knockout of GATA4 in liver leads to sinusoidal capillarization and development of perisinusoidal liver fibrosis [95]. To investigate whether GATA4 is also downregulated in perisinusoidal liver fibrosis of CDAA-induced NASH and thus could play a role in NASH-associated fibrogenesis, I analyzed hepatic GATA4 expression in CDAA fed mice. GATA4 expression was downregulated on protein level in whole liver lysates. Delgado and colleagues used a G2-Cre driver mouse to delete GATA4 in septum transversum mesenchyme. The resulting Gata4 knockout mice were embryonic lethal around E13.5 and developed progressive liver fibrosis, indicating that mesenchymal GATA4 regulates HSC activation and inhibits liver fibrogenesis. Moreover, they showed that patients with advanced liver fibrosis and cirrhosis have decreased hepatic GATA4 expression. Using a G2-Cre reporter mouse expressing YFP they showed, that YFP is predominantly expressed in Desmin-

positive HSC, but a portion of CD31-positive EC as well expressed YPF, indicating that G2-Cre driver mouse only partly targets ECs [128]. However, we proposed, that GATA4 expression is downregulated in LSEC inducing liver fibrosis independent of GATA4 expression in HSC. To test this hypothesis, primary LSEC from CDAA fed mice were isolated. *Gata4* expression was decreased in isolated LSEC of CDAA mice compared to control mice. To exclude contamination with other cell types FACS analysis was performed. LSEC from CDAA fed mice had positivity for CD31 and/or Stabilin-2 of at least 88 % (not shown here but published in [95]). However, during LSEC isolation procedure after Nycodenz gradient the layer taken for LSEC enrichment using MACS is absent of HSC. Therefore, isolated mLSEC could rather be contaminated with macrophages (KC). GATA4 expression was reported in KC of fetal murine and human liver and in human postnatal livers [256]. In contrast, GATA4 expression in KC in the adult liver is not reported. Downregulation of endothelial *Gata4* led to transdifferentiation of LSEC to continuous EC resulting in sinusoidal capillarization [95]. Microarray analysis of CDAA mLSEC revealed downregulation of LSEC genes, which was further confirmed for LYVE-1 on protein level, indicating transdifferentiation of LSEC. GATA4 downregulation was accompanied by reduction of GATA4 dependent genes in CDAA mLSEC. These data indicate, that GATA4 expression is decreased in CDAA mLSEC during NASH-associated in perisinusoidal liver fibrosis. In line with this, it was shown that EC from cirrhotic patients, among them patients with NAFLD, display a loss of *Gata4* expression [95, 257].

CDAA diet resulted in a downregulation of endothelial *Gata4* but did not lead to a complete loss of GATA4. As downregulation of GATA4 during CDAA seems to contribute to formation of perisinusoidal liver fibrosis, we speculated that genetic deletion of Gata4 in LSEC aggravates the formation of liver fibrosis. Indeed, application of CDAA diet on $Gata4^{LSEC\text{-}KO}$ mouse aggravated hepatopathy and degree of perisinusoidal liver fibrosis. In contrast, application of chronic CCl_4 model on $Gata4^{LSEC\text{-}KO}$ mice did not aggravate hepatopathy and bridging liver fibrosis further indicating that endothelial GATA4 seems to be relevant to protect from NASH-associated perisinusoidal, but not from CCl_4- induced toxic liver fibrosis [95].

In $Gata4^{LSEC\text{-}KO}$ mice loss of GATA4 enable expression of transcription factor MYC by increased chromatin accessibility leading to *de novo* expression of profibrotic HSC activating cytokine PDGFB [95]. The underlying mechanism of GATA4-dependet liver fibrosis development in CDAA fed mice was not analyzed in this study. However, we showed that CDAA mLSEC have similar alterations in the transcriptomic profile compared to $Gata4^{LSEC\text{-}KO}$ mice including upregulation of *Pdgfb* and *Myc* in CDAA mLSEC, indicating a similar mechanism in CDAA fed mice as in $Gata4^{LSEC\text{-}KO}$ mice [95]. Moreover, additional angiocrine factors could play a role in CDAA-diet induced perisinusoidal liver fibrosis. Angiocrine factors like *Igfbp5*, *Mmp12* and

Bmp1 were upregulated in CDAA mLSEC and Gata4$^{LSEC-KO}$ [95] and are reported to be involved in liver fibrosis [258-260]. In contrast to *Gata4* loss, transcription factors *Gata6* and SRY-Box Transcription Factor 9 (*Sox9*) were enriched in CDAA mLSEC [95]. Both transcription factors were shown to be upregulated in activated HSCs and in human fibrotic liver tissues from different etiologies including NAFLD. Moreover, in comparison between mild and advanced NAFLD-associated fibrotic liver tissues both transcription factors were higher expressed in advanced compared to mild disease. However, the primary interest of He and colleagues was on HSCs which is why they only analyzed HSCs but no ECs in their study [261]. It is not known if *Gata4* is able to regulate expression of *Gata6* and *Sox9*, but involvement of different transcription factors in perisinusoidal liver fibrosis in CDAA-diet seems to be possible. Liu *et al.* revealed several transcription factors, including GATA4/6, crucial for the phenotype of HSCs, preventing activation of HSC [246]. Moreover, de Haan *et al.* identified transcription factors, including GATA4, involved in LSEC signature and regulation of the interaction of LSEC with virus. Additionally, genetic deletion of GTPase IMAP family member 5 (GIMAP5) led to sinusoidal capillarization of LSEC in mice and scRNA-seq data of $CD45^{-}CD31^{+}$ liver endothelial cells of Gimap-deficient mice placed GIMAP5 upstream of GATA4. Therefore, the authors suggest GIMAP5 as potential upstream regulator of GATA4 in regulating LSEC specification and homeostasis [262]. However, there must be other transcriptional regulators orchestrate the phenotype and function of LSEC [263].

Taken together, our data indicate that GATA4 in LSEC seems to play an important role in preventing development of diet-induced perisinusoidal liver fibrosis in NASH but not in toxic-induced bridging fibrosis.

5.3. Gata4$^{LSEC-KI}$ mouse for Gata4 overexpression in a diet-induced NASH model

In a genetic model and a CDAA-induced NASH model of perisinusoidal liver fibrosis endothelial GATA4 is reduced [95]. We therefore hypothesized, that endothelial GATA4 protects against perisinusoidal liver fibrosis. To maintain GATA4 expression during liver fibrosis, we generated in cooperation with the German Cancer Research Center (Division of Cellular Immunology, Prof. Dr. Hans-Reimer Rodewald and Transgenic Service, Frank van der Hoeven) a Gata4$^{LSEC-KI}$ mouse. A recombinant *Gata4* and *tdTomato* expression cassette were inserted into the R26-locus of C67BL/6N mice by homologous recombination. Mating of ROSA26 Stopflox-tdTomato-Gata4 with *Clec4g-iCre* driver mouse enable endothelial-specific *Gata4* expression

in Gata4$^{LSEC-KI}$ mice. In contrast to our hypothesis, Gata4$^{LSEC-KI}$ mice used in a CDAA diet displayed the same degree of liver damage and liver fibrosis compared to controls. This result indicated, that either endothelial GATA4 overexpression is not able to prevent perisinusoidal liver fibrosis in the CDAA model or that GATA4 in Gata4$^{LSEC-KI}$ mice is not functional.

5.3.1. Gata4$^{LSEC-KI}$ mice do not express functional GATA4 protein

Use of a genetic Gata4 rescue mouse (Gata4$^{LSEC-KO}$ x Gata4$^{LSEC-KI}$) was not able to rescue reduced liver-to-body-weight ratio and perisinusoidal liver fibrosis in Gata4$^{LSEC-KO}$ mice, indicating no functional GATA4 in Gata4$^{LSEC-KI}$ mouse. Furthermore, analysis of freshly isolated LSEC from Gata4$^{LSEC-KI}$ mice revealed no induction of GATA4 dependent genes. In genetically modified mice, gene silencing through epigenetic modifications, like DNA methylation of CpG islands at promotor region and histone modifications, can occur [264]. However, Kong and colleagues reported that Rosa26 locus protected exogeneous constructs against epigenetic silencing in pig [265]. Moreover, transgenic *Gata4* expression in cultivated LSEC of Gata4$^{LSEC-KI}$ mouse was present, but no induction of GATA4 target genes (*Bmp2* and *Wnt2*) was detected. This data indicated that transgenic *Gata4* of Gata4$^{LSEC-KI}$ mouse in LSEC is transcribed but not translated into a functional GATA4 protein. Expression analysis on protein level in whole liver of Gata4$^{LSEC-KI}$ mouse revealed no increased expression of GATA4, indicating no general translation of GATA4. To give a robust statement about translation of GATA4 in Gata4$^{LSEC-KI}$ mouse expression analysis in LSEC could be useful.

The expression cassette for generation of Gata4$^{LSEC-KI}$ mouse contained *tdTomato* and transgenic *Gata4* cDNA linked by a viral 2A peptide sequence enabling stoichiometric multi-protein expression of both proteins. During translation of this single open reading frame the ribosome ‘skips’ the synthesis of glycyl–prolyl peptide bond at the C-terminus of 2A leading to the release of the nascent protein from the ribosome. The ribosome continues translating the second protein [266, 267]. The C-terminus of the upstream protein contains extra amino acids of 2A and the N-terminus of the downstream protein contains an extra proline [268]. TdTomato expression was detected in CD31-postive cells of Clec4g expressing organs, indicating translation of the expression cassette was successful. However, no functional GATA4 protein was expressed. Some studies reported incomplete cleavage of the polyproteins linked by 2A peptides during translation resulting in a fusion protein of both proteins [269-271]. Incomplete cleavage could have led to a fusion protein of tdTomato and GATA4 preventing function of GATA4. Moreover, it was shown that 2A peptide-derived N-terminal proline added to the downstream protein after cleavage of 2A peptide can influence the protein stability and function within polycistronic constructs. N-terminal proline remnant of the 2A peptide increased protein

degradation of KLF4 impeding reprogramming function of the protein [272]. *Gata4* is the downstream protein in our construct, therefore proline residue of the 2A peptide at the N-terminus could influence the stability and function of GATA4 without effecting tdTomato protein.

Furthermore, the coding region of native *Gata4* mRNA, which was used for generation of Gata4$^{LSEC-KI}$ mouse, have a high GC content of an average around 70 % (calculated using [273]). Because of that, native cDNA sequence of *Gata4* cannot be amplified for use in Gata4$^{LSEC-KI}$ mouse. Therefore, codon optimization of coding region of *Gata4* cDNA was applied to ensure amplification. This adaptation could lead to rare codons in the transgenic *Gata4* cDNA leading to changed expression. It was reported that rare codons can influence the rate of translational elongation and co-translational protein folding [274]. Moreover, they can cause premature translation termination [275].

Taken together, transcription of transgenic *Gata4* was confirmed in LSEC of Gata4$^{LSEC-KI}$ mouse. However, translation of GATA4 itself or the function of GATA4 is affected, leading to no functional overexpression of GATA4 in Gata4$^{LSEC-KI}$ mouse. Therefore, we could not proof our hypothesis, that LSEC-specific GATA4 overexpression is able to diminish or prevent perisinusoidal liver fibrosis in CDAA-diet induced NASH model.

5.4. LV-CD31-Gata4-V5 lentivirus is not able to overexpress GATA4 in LSEC *in vitro*

We showed, that endothelial *Gata4* is decreased in perisinusoidal liver fibrosis in CDAA-induced NASH. Therefore, we hypothesized that LSEC-specific overexpression of *Gata4* could alleviate perisinusoidal liver fibrosis. For *Gata4* gene therapy I used a specific LSEC-targeting lentivirus. Murine CD31 promotor and miRNA-detargeting sequences targeting miRNA122 and miRNA142-3P were demonstrated to make the lentivirus LSEC-specific [226]. Testing the lentivirus *in vitro* prior to the use *in vivo*, revealed expression of synthetic *Gata4* in bEnd.3 cells. Furthermore, high levels of lentivirus induced GATA4 expression on protein level, which was able to induce Gata4 target gene expression of *Wnt2*. Moreover, high levels of lentivirus increased expression of endogenous *Gata4*. Whether expression of synthetic *Gata4* or of endogenous *Gata4* led to increased expression of *Wnt2* is not clear. For testing the lentivirus in LSEC I decided to isolate LSEC from Gata4-deficient (Gata4$^{LSEC-KO}$) mice because wildtype LSEC already express *Gata4* so that there might be no additional effect seen after lentiviral transduction. However, in mLSEC, for which the lentivirus should be specific, the lentivirus was

indeed able to increase synthetic *Gata4* expression but was not able to induce Gata4 target gene expression. Furthermore, there was no increase of GATA4 expression on protein level in transduced LSEC. These data indicated, that in bEnd.3 cells *Gata4* mRNA is translated into a functional protein and able to induce expression of Gata4 target genes, whereas in LSEC there is no translation of functional GATA4.

bEnd.3 cells were shown to express high levels of CD31 [276]. In turn, under physiological conditions LSEC do not express high levels of CD31 consistently, but increased expression is seen in dedifferentiated, defenestrated LSEC [277-279]. Gata4$^{LSEC-KO}$ mice display dedifferentiated LSEC and therefore should have increased CD31 expression [95]. Synthetic *Gata4* expression but no functional protein was seen Gata4$^{LSEC-KO}$ LSEC transduced with lentivirus. This indicate, that CD31 expression was high enough in dedifferentiated mLSEC to induce synthetic *Gata4* expression, but synthetic *Gata4* was not translated into a functional GATA4 protein.

Like for Gata4$^{LSEC-KI}$ mouse, *Gata4* cDNA used for lentivirus was codon optimized because of the high GC content. Abundance of tRNAs and presence of rare codons influence the decoding rate and the rate of translational elongation and co-translational protein folding [274]. Furthermore, tRNAs are expressed tissue- or cell type-specific and together with codon usage it can be important for tissue- and cell type–specific gene expression [280]. bEnd.3 cells are a brain endothelial cell line derived from BALB/c mice and LSEC used for lentiviral transduction are primary murine LSEC from Gata4$^{LSEC-KO}$ mice with a mixed C57BL/6N and 129/Sv background. Rare codons introduced into *Gata4* cDNA after codon optimization could therefore lead to different expression and translation of GATA4 in the different cell types used for *in vitro* analyses of the Gata4 lentivirus.

LV-pCD31Pr-KLF2-miT142+122-W vector, which we got from Prof. Buchholz (Paul-Ehrlich-Institut, Langen) was not analyzed *in vitro*. Manavski *et al.* showed that HUVECs transduced with LV-pCD31Pr-Luc-GFP-miT142+122-W were positive for GFP, but they did not analyze the lentiviral vector containing hKLF2 *in vitro*. However, expression of human *Klf2* was analyzed in isolated LSEC of KLF2 treated mice but they did not show expression of KLF2 protein in LSEC [226]. This data could suggest that overexpression of lentivirus-derived gene could function *in vivo*, even if the overexpression of the functional protein fails *in vitro*. To proof this hypothesis, *Gata4* overexpressing lentiviruses could be applied by tail vein injection into C57BL/6N wildtype mice to isolate LSEC followed by analysis of Gata4-V5 overexpression.

Moreover, as an alternative to lentiviral gene therapy there are non-viral techniques to target LSEC, which could be used for Gata4 therapy. Scavenging receptor Stabilin-2 is the main

receptor for hyaluronic acid and chondroitin sulfate [281]. Clearance of these molecules by LSEC can be used to target LSEC for gene therapy. Kren and colleagues generated hyaluronan (HA)-coated nanocapsules containing *Sleeping Beauty* transposase to target LSEC for gene therapy. They showed that injection of HA-coated nanocapsules, expressing the coagulation Factor VIII in *cis* with *Sleeping Beauty* transposase, via tail vein into knockout hemophilia A mice could correct their bleeding disorder by specifically targeting LSEC [282]. Another group developed chondroitin sulfate-functionalized nanoparticles for targeting LSEC. In colorectal liver metastasis miRNA-20a expression was repressed and LSEC-specific restoration of miRNA-20a using chondroitin sulfate-functionalized nanoparticles could decrease liver metastasis progression [283].

Taken together, I was not able to induce GATA4 overexpression in LSEC by using either a newly generated LSEC-specific Gata4-knockin mouse or by a LSEC-targeting lentivirus *in vitro*. Hence, follow up studies are of great importance and should include *in vivo* testing of lentiviral constructs or even non-viral techniques to specifically overexpress GATA4 in LSEC, as we could clearly demonstrate in this study that downregulation of GATA4 is an important factor in CDAA-associated perisinusoidal liver fibrosis.

References

[1] A. E. Read, "Clinical physiology of the liver," *Br J Anaesth,* vol. 44, no. 9, pp. 910-7, Sep 1972, doi: 10.1093/bja/44.9.910.

[2] E. Trefts, M. Gannon, and D. H. Wasserman, "The liver," *Curr Biol,* vol. 27, no. 21, pp. R1147-R1151, Nov 6 2017, doi: 10.1016/j.cub.2017.09.019.

[3] C. Couinaud, *Le foie; études anatomiques et chirurgicales.* Paris: Masson & Cie, 1957, p. 530.

[4] W. W. Lautt, in *Hepatic Circulation: Physiology and Pathophysiology*, (Colloquium Series on Integrated Systems Physiology: From Molecule to Function to Disease. San Rafael (CA), 2009.

[5] P. S. Koch, K. H. Lee, S. Goerdt, and H. G. Augustin, "Angiodiversity and organotypic functions of sinusoidal endothelial cells," *Angiogenesis,* vol. 24, no. 2, pp. 289-310, May 2021, doi: 10.1007/s10456-021-09780-y.

[6] R. S. McCuskey, "Morphological mechanisms for regulating blood flow through hepatic sinusoids," *Liver,* vol. 20, no. 1, pp. 3-7, Feb 2000, doi: 10.1034/j.1600-0676.2000.020001003.x.

[7] R. S. McCuskey, "A dynamic and static study of hepatic arterioles and hepatic sphincters," *Am J Anat,* vol. 119, no. 3, pp. 455-77, Nov 1966, doi: 10.1002/aja.1001190307.

[8] M. A. Turner and A. S. Fulcher, "The cystic duct: normal anatomy and disease processes," *Radiographics,* vol. 21, no. 1, pp. 3-22; questionnaire 288-94, Jan-Feb 2001, doi: 10.1148/radiographics.21.1.g01ja093.

[9] C. Lau *et al.*, "The Voronoi theory of the normal liver lobular architecture and its applicability in hepatic zonation," *Sci Rep,* vol. 11, no. 1, p. 9343, Apr 29 2021, doi: 10.1038/s41598-021-88699-2.

[10] F. Kiernan, "The anatomy and physiology of the liver," *Philos. Trans. R Soc. Lond,* vol. 123, pp. 711-770, 1833.

[11] F. Mall, "A study of the structural unit of the liver," *Am. J. Anat.,* vol. 5, pp. 227-308, 1906.

[12] A. M. Rappaport, Z. J. Borowy, W. M. Lougheed, and W. N. Lotto, "Subdivision of hexagonal liver lobules into a structural and functional unit; role in hepatic physiology and pathology," *Anat Rec,* vol. 119, no. 1, pp. 11-33, May 1954, doi: 10.1002/ar.1091190103.

[13] K. Jungermann and N. Katz, "Functional specialization of different hepatocyte populations," *Physiol Rev,* vol. 69, no. 3, pp. 708-64, Jul 1989, doi: 10.1152/physrev.1989.69.3.708.

[14] V. Racanelli and B. Rehermann, "The liver as an immunological organ," *Hepatology,* vol. 43, no. 2 Suppl 1, pp. S54-62, Feb 2006, doi: 10.1002/hep.21060.

[15] B. Z. Stanger, "Cellular homeostasis and repair in the mammalian liver," *Annu Rev Physiol,* vol. 77, pp. 179-200, 2015, doi: 10.1146/annurev-physiol-021113-170255.

[16] R. Manco and S. Itzkovitz, "Liver zonation," *J Hepatol,* vol. 74, no. 2, pp. 466-468, Feb 2021, doi: 10.1016/j.jhep.2020.09.003.

References

[17] J. Yang *et al.*, "beta-catenin signaling in murine liver zonation and regeneration: a Wnt-Wnt situation!," *Hepatology,* vol. 60, no. 3, pp. 964-76, Sep 2014, doi: 10.1002/hep.27082.

[18] K. Jungermann and T. Kietzmann, "Oxygen: modulator of metabolic zonation and disease of the liver," *Hepatology,* vol. 31, no. 2, pp. 255-60, Feb 2000, doi: 10.1002/hep.510310201.

[19] S. Benhamouche *et al.*, "Apc tumor suppressor gene is the "zonation-keeper" of mouse liver," *Dev Cell,* vol. 10, no. 6, pp. 759-70, Jun 2006, doi: 10.1016/j.devcel.2006.03.015.

[20] A. T. Nguyen-Lefebvre and A. Horuzsko, "Kupffer Cell Metabolism and Function," *J Enzymol Metab,* vol. 1, no. 1, 2015. [Online]. Available: https://www.ncbi.nlm.nih.gov/pubmed/26937490.

[21] M. W. Haaker, A. B. Vaandrager, and J. B. Helms, "Retinoids in health and disease: A role for hepatic stellate cells in affecting retinoid levels," *Biochim Biophys Acta Mol Cell Biol Lipids,* vol. 1865, no. 6, p. 158674, Jun 2020, doi: 10.1016/j.bbalip.2020.158674.

[22] J. F. Fitzgerald, A. Angelides, and R. Wyllie, "The hepatitis spectrum," *Curr Probl Pediatr,* vol. 11, no. 11, pp. 1-51, Sep 1981, doi: 10.1016/0045-9380(81)90027-x.

[23] M. J. Alter, E. E. Mast, L. A. Moyer, and H. S. Margolis, "Hepatitis C," *Infect Dis Clin North Am,* vol. 12, no. 1, pp. 13-26, Mar 1998, doi: 10.1016/s0891-5520(05)70405-0.

[24] M. Blachier, H. Leleu, M. Peck-Radosavljevic, D. C. Valla, and F. Roudot-Thoraval, "The burden of liver disease in Europe: a review of available epidemiological data," *J Hepatol,* vol. 58, no. 3, pp. 593-608, Mar 2013, doi: 10.1016/j.jhep.2012.12.005.

[25] M. R. Teli, C. P. Day, A. D. Burt, M. K. Bennett, and O. F. James, "Determinants of progression to cirrhosis or fibrosis in pure alcoholic fatty liver," *Lancet,* vol. 346, no. 8981, pp. 987-90, Oct 14 1995, doi: 10.1016/s0140-6736(95)91685-7.

[26] J. Xiao *et al.*, "Global liver disease burdens and research trends: Analysis from a Chinese perspective," *J Hepatol,* vol. 71, no. 1, pp. 212-221, Jul 2019, doi: 10.1016/j.jhep.2019.03.004.

[27] J. Ludwig, T. R. Viggiano, D. B. McGill, and B. J. Oh, "Nonalcoholic steatohepatitis: Mayo Clinic experiences with a hitherto unnamed disease," *Mayo Clin Proc,* vol. 55, no. 7, pp. 434-8, Jul 1980. [Online]. Available: https://www.ncbi.nlm.nih.gov/pubmed/7382552.

[28] E. J. Williams and J. P. Iredale, "Liver cirrhosis," *Postgrad Med J,* vol. 74, no. 870, pp. 193-202, Apr 1998, doi: 10.1136/pgmj.74.870.193.

[29] M. Colombo, "Hepatocellular carcinoma," *J Hepatol,* vol. 15, no. 1-2, pp. 225-36, May 1992, doi: 10.1016/0168-8278(92)90041-m.

[30] R. F. Meirelles Junior *et al.*, "Liver transplantation: history, outcomes and perspectives," *Einstein (Sao Paulo),* vol. 13, no. 1, pp. 149-52, Jan-Mar 2015, doi: 10.1590/S1679-45082015RW3164.

[31] K. K. Sorensen, J. Simon-Santamaria, R. S. McCuskey, and B. Smedsrod, "Liver Sinusoidal Endothelial Cells," *Compr Physiol,* vol. 5, no. 4, pp. 1751-74, Sep 20 2015, doi: 10.1002/cphy.c140078.

[32] E. Wisse, R. B. De Zanger, K. Charels, P. Van Der Smissen, and R. S. McCuskey, "The liver sieve: considerations concerning the structure and function of endothelial fenestrae, the sinusoidal wall and the space of Disse," *Hepatology,* vol. 5, no. 4, pp. 683-92, Jul-Aug 1985, doi: 10.1002/hep.1840050427.

[33] E. Wisse, "An electron microscopic study of the fenestrated endothelial lining of rat liver sinusoids," *J Ultrastruct Res,* vol. 31, no. 1, pp. 125-50, Apr 1970, doi: 10.1016/s0022-5320(70)90150-4.

[34] E. Wisse *et al.*, "Structure and function of sinusoidal lining cells in the liver," *Toxicol Pathol,* vol. 24, no. 1, pp. 100-11, Jan-Feb 1996, doi: 10.1177/019262339602400114.

[35] R. Fraser, W. A. Day, and N. S. Fernando, "The liver sinusoidal cells. Their role in disorders of the liver, lipoprotein metabolism and atherogenesis," *Pathology,* vol. 18, no. 1, pp. 5-11, Jan 1986, doi: 10.3109/00313028609090821.

[36] F. Vidal-Vanaclocha and E. Barbera-Guillem, "Fenestration patterns in endothelial cells of rat liver sinusoids," *J Ultrastruct Res,* vol. 90, no. 2, pp. 115-23, Feb 1985, doi: 10.1016/0889-1605(85)90102-8.

[37] D. G. Le Couteur, R. Fraser, V. C. Cogger, and A. J. McLean, "Hepatic pseudocapillarisation and atherosclerosis in ageing," *Lancet,* vol. 359, no. 9317, pp. 1612-5, May 4 2002, doi: 10.1016/S0140-6736(02)08524-0.

[38] E. Wisse, J. H. Van Dierendonck, R. De Zanger, R. Fraser, and R. S. McCuskey, "On the role of the liver endothelial filter in the transport of particulate fat (chylomicrons and their remnants) to parenchymal cells and the influence of certain hormones on the endothelial fenestrae," *Communications of Liver Cells,* p. 5, 1980.

[39] W. Nopanitaya, J. C. Lamb, J. W. Grisham, and J. L. Carson, "Effect of hepatic venous outflow obstruction on pores and fenestration in sinusoidal endothelium," *Br J Exp Pathol,* vol. 57, no. 5, pp. 604-9, Oct 1976. [Online]. Available: https://www.ncbi.nlm.nih.gov/pubmed/999794.

[40] R. Fraser, L. M. Bowler, and E. Wisse, "Agents related to fibrosis, such as alcohol and carbon tetrachloride, acutely effect endothelial fenestrae which cause fatty liver," *Connective Tissue of the Normal and Fibrotic Human Liver,* p. 2, 1982.

[41] R. F. McGuire, D. M. Bissell, J. Boyles, and F. J. Roll, "Role of extracellular matrix in regulating fenestrations of sinusoidal endothelial cells isolated from normal rat liver," *Hepatology,* vol. 15, no. 6, pp. 989-97, Jun 1992, doi: 10.1002/hep.1840150603.

[42] F. Braet and E. Wisse, "Structural and functional aspects of liver sinusoidal endothelial cell fenestrae: a review," *Comp Hepatol,* vol. 1, no. 1, p. 1, Aug 23 2002, doi: 10.1186/1476-5926-1-1.

[43] T. Madarame *et al.*, "Relationship between endothelial structure and capillarization in fatty liver," *Cells of the Hepatic Sinusoid* p. 2, 1993.

[44] N. Tsukada *et al.*, "Alterations of the hepatic sinusoidal endothelial fenestrae in response to vasoactive substances in the rat liver -in vivo and in vitro studies," *Cells of the Hepatic Sinusoid 1,* p. 2, 1986.

[45] R. Fraser, L. M. Bowler, W. A. Day, B. Dobbs, H. D. Johnson, and D. Lee, "High perfusion pressure damages the sieving ability of sinusoidal endothelium in rat livers," *Br J Exp Pathol,* vol. 61, no. 2, pp. 222-8, Apr 1980. [Online]. Available: https://www.ncbi.nlm.nih.gov/pubmed/7426378.

[46] U. Brauneis, Z. Gatmaitan, and I. M. Arias, "Serotonin stimulates a Ca2+ permeant nonspecific cation channel in hepatic endothelial cells," *Biochem Biophys Res Commun,* vol. 186, no. 3, pp. 1560-6, Aug 14 1992, doi: 10.1016/s0006-291x(05)81585-2.

[47] B. Le Bail, P. Bioulac-Sage, R. Senuita, A. Quinton, J. Saric, and C. Balabaud, "Fine structure of hepatic sinusoids and sinusoidal cells in disease," *J Electron Microsc Tech,* vol. 14, no. 3, pp. 257-82, Mar 1990, doi: 10.1002/jemt.1060140307.

[48] C. Geraud *et al.*, "Unique cell type-specific junctional complexes in vascular endothelium of human and rat liver sinusoids," *PLoS One,* vol. 7, no. 4, p. e34206, 2012, doi: 10.1371/journal.pone.0034206.

[49] B. Smedsrod, "Clearance function of scavenger endothelial cells," *Comp Hepatol,* vol. 3 Suppl 1, p. S22, Jan 14 2004, doi: 10.1186/1476-5926-2-S1-S22.

[50] B. Smedsrod, H. Pertoft, S. Eriksson, J. R. Fraser, and T. C. Laurent, "Studies in vitro on the uptake and degradation of sodium hyaluronate in rat liver endothelial cells," *Biochem J,* vol. 223, no. 3, pp. 617-26, Nov 1 1984, doi: 10.1042/bj2230617.

[51] B. Smedsrod, H. Pertoft, S. Gustafson, and T. C. Laurent, "Scavenger functions of the liver endothelial cell," *Biochem J,* vol. 266, no. 2, pp. 313-27, Mar 1 1990, doi: 10.1042/bj2660313.

[52] J. Melkko, T. Hellevik, L. Risteli, J. Risteli, and B. Smedsrod, "Clearance of NH2-terminal propeptides of types I and III procollagen is a physiological function of the scavenger receptor in liver endothelial cells," *J Exp Med,* vol. 179, no. 2, pp. 405-12, Feb 1 1994, doi: 10.1084/jem.179.2.405.

[53] O. Politz *et al.*, "Stabilin-1 and -2 constitute a novel family of fasciclin-like hyaluronan receptor homologues," *Biochem J,* vol. 362, no. Pt 1, pp. 155-64, Feb 15 2002, doi: 10.1042/0264-6021:3620155.

[54] B. Smedsrod, J. Melkko, N. Araki, H. Sano, and S. Horiuchi, "Advanced glycation end products are eliminated by scavenger-receptor-mediated endocytosis in hepatic sinusoidal Kupffer and endothelial cells," *Biochem J,* vol. 322 (Pt 2), pp. 567-73, Mar 1 1997, doi: 10.1042/bj3220567.

[55] R. Li *et al.*, "Role of liver sinusoidal endothelial cells and stabilins in elimination of oxidized low-density lipoproteins," *Am J Physiol Gastrointest Liver Physiol,* vol. 300, no. 1, pp. G71-81, Jan 2011, doi: 10.1152/ajpgi.00215.2010.

[56] S. Magnusson and T. Berg, "Extremely rapid endocytosis mediated by the mannose receptor of sinusoidal endothelial rat liver cells," *Biochem J,* vol. 257, no. 3, pp. 651-6, Feb 1 1989, doi: 10.1042/bj2570651.

[57] D. P. Praaning-van Dalen, A. M. de Leeuw, A. Brouwer, and D. L. Knook, "Rat liver endothelial cells have a greater capacity than Kupffer cells to endocytose N-acetylglucosamine- and mannose-terminated glycoproteins," *Hepatology,* vol. 7, pp. 672-679, 1987.

[58] I. Malovic *et al.*, "The mannose receptor on murine liver sinusoidal endothelial cells is the main denatured collagen clearance receptor," *Hepatology,* vol. 45, no. 6, pp. 1454-61, Jun 2007, doi: 10.1002/hep.21639.

[59] B. Smedsrod, S. Johansson, and H. Pertoft, "Studies in vivo and in vitro on the uptake and degradation of soluble collagen alpha 1(I) chains in rat liver endothelial and Kupffer cells," *Biochem J,* vol. 228, no. 2, pp. 415-24, Jun 1 1985, doi: 10.1042/bj2280415.

[60] S. A. Mousavi, M. Sporstol, C. Fladeby, R. Kjeken, N. Barois, and T. Berg, "Receptor-mediated endocytosis of immune complexes in rat liver sinusoidal endothelial cells is mediated by FcgammaRIIb2," *Hepatology,* vol. 46, no. 3, pp. 871-84, Sep 2007, doi: 10.1002/hep.21748.

[61] T. Skogh, R. Blomhoff, W. Eskild, and T. Berg, "Hepatic uptake of circulating IgG immune complexes," *Immunology,* vol. 55, no. 4, pp. 585-94, Aug 1985. [Online]. Available: https://www.ncbi.nlm.nih.gov/pubmed/4018843.

[62] C. Mouta Carreira *et al.*, "LYVE-1 is not restricted to the lymph vessels: Expression in normal liver blood sinusoids and down-regulation in human liver cancer and cirrhosis," *Cancer Res,* vol. 61, pp. 8079-8084, 2001.

[63] C. I. Oie *et al.*, "Rat liver sinusoidal endothelial cells (LSECs) express functional low density lipoprotein receptor-related protein-1 (LRP-1)," *J Hepatol,* vol. 55, no. 6, pp. 1346-52, Dec 2011, doi: 10.1016/j.jhep.2011.03.013.

[64] S. Pohlmann *et al.*, "DC-SIGNR, a DC-SIGN homologue expressed in endothelial cells, binds to human and simian immunodeficiency viruses and activates infection in trans," *Proc Natl Acad Sci U S A,* vol. 98, no. 5, pp. 2670-5, Feb 27 2001, doi: 10.1073/pnas.051631398.

[65] A. L. Wilkinson, M. Qurashi, and S. Shetty, "The Role of Sinusoidal Endothelial Cells in the Axis of Inflammation and Cancer Within the Liver," *Front Physiol,* vol. 11, p. 990, 2020, doi: 10.3389/fphys.2020.00990.

[66] S. Faure-Dupuy *et al.*, "Characterization of Pattern Recognition Receptor Expression and Functionality in Liver Primary Cells and Derived Cell Lines," *J Innate Immun,* vol. 10, no. 4, pp. 339-348, 2018, doi: 10.1159/000489966.

[67] T. Kawai and S. Akira, "The role of pattern-recognition receptors in innate immunity: update on Toll-like receptors," *Nat Immunol,* vol. 11, no. 5, pp. 373-84, May 2010, doi: 10.1038/ni.1863.

[68] T. Hayashi *et al.*, "Lipopolysaccharide-induced decreased protein S expression in liver cells is mediated by MEK/ERK signaling and NFkappaB activation: involvement of membrane-bound CD14 and toll-like receptor-4," *J Thromb Haemost,* vol. 4, no. 8, pp. 1763-73, Aug 2006, doi: 10.1111/j.1538-7836.2006.02042.x.

[69] A. Warren, D. G. Le Couteur, R. Fraser, D. G. Bowen, G. W. McCaughan, and P. Bertolino, "T lymphocytes interact with hepatocytes through fenestrations in murine liver sinusoidal endothelial cells," *Hepatology,* vol. 44, no. 5, pp. 1182-90, Nov 2006, doi: 10.1002/hep.21378.

[70] L. Diehl, A. Schurich, R. Grochtmann, S. Hegenbarth, L. Chen, and P. A. Knolle, "Tolerogenic maturation of liver sinusoidal endothelial cells promotes B7-homolog 1-dependent CD8+ T cell tolerance," *Hepatology,* vol. 47, no. 1, pp. 296-305, Jan 2008, doi: 10.1002/hep.21965.

[71] A. Limmer *et al.*, "Cross-presentation of oral antigens by liver sinusoidal endothelial cells leads to CD8 T cell tolerance," *Eur J Immunol,* vol. 35, no. 10, pp. 2970-81, Oct 2005, doi: 10.1002/eji.200526034.

[72] P. A. Knolle *et al.*, "IL-10 down-regulates T cell activation by antigen-presenting liver sinusoidal endothelial cells through decreased antigen uptake via the mannose receptor and lowered surface expression of accessory molecules," *Clin Exp Immunol,* vol. 114, no. 3, pp. 427-33, Dec 1998, doi: 10.1046/j.1365-2249.1998.00713.x.

[73] P. F. Lalor, P. Shields, A. Grant, and D. H. Adams, "Recruitment of lymphocytes to the human liver," *Immunol Cell Biol,* vol. 80, no. 1, pp. 52-64, Feb 2002, doi: 10.1046/j.1440-1711.2002.01062.x.

[74] S. Shetty *et al.*, "Common lymphatic endothelial and vascular endothelial receptor-1 mediates the transmigration of regulatory T cells across human hepatic sinusoidal endothelium," *J Immunol,* vol. 186, no. 7, pp. 4147-55, Apr 1 2011, doi: 10.4049/jimmunol.1002961.

[75] D. A. Patten *et al.*, "SCARF-1 promotes adhesion of CD4(+) T cells to human hepatic sinusoidal endothelium under conditions of shear stress," *Sci Rep,* vol. 7, no. 1, p. 17600, Dec 14 2017, doi: 10.1038/s41598-017-17928-4.

[76] T. Sato *et al.*, "Role for CXCR6 in recruitment of activated CD8+ lymphocytes to inflamed liver," *J Immunol,* vol. 174, no. 1, pp. 277-83, Jan 1 2005, doi: 10.4049/jimmunol.174.1.277.

[77] F. Geissmann *et al.*, "Intravascular immune surveillance by CXCR6+ NKT cells patrolling liver sinusoids," *PLoS Biol,* vol. 3, no. 4, p. e113, Apr 2005, doi: 10.1371/journal.pbio.0030113.

[78] K. Elvevold, B. Smedsrod, and I. Martinez, "The liver sinusoidal endothelial cell: a cell type of controversial and confusing identity," *Am J Physiol Gastrointest Liver Physiol,* vol. 294, no. 2, pp. G391-400, Feb 2008, doi: 10.1152/ajpgi.00167.2007.

[79] D. G. Le Couteur *et al.*, "Old age and the hepatic sinusoid," *Anat Rec (Hoboken),* vol. 291, no. 6, pp. 672-83, Jun 2008, doi: 10.1002/ar.20661.

[80] A. Couvelard, J. Y. Scoazec, and G. Feldmann, "Expression of cell-cell and cell-matrix adhesion proteins by sinusoidal endothelial cells in the normal and cirrhotic human liver," *Am J Pathol,* vol. 143, no. 3, pp. 738-52, Sep 1993. [Online]. Available: https://www.ncbi.nlm.nih.gov/pubmed/8362973.

[81] M. Falkowski, K. Schledzewski, B. Hansen, and S. Goerdt, "Expression of stabilin-2, a novel fasciclin-like hyaluronan receptor protein, in murine sinusoidal endothelia, avascular tissues, and at solid/liquid interfaces," *Histochem Cell Biol,* vol. 120, no. 5, pp. 361-9, Nov 2003, doi: 10.1007/s00418-003-0585-5.

[82] L. P. Ganesan *et al.*, "FcgammaRIIb on liver sinusoidal endothelium clears small immune complexes," *J Immunol,* vol. 189, no. 10, pp. 4981-8, Nov 15 2012, doi: 10.4049/jimmunol.1202017.

[83] K. Elvevold, J. Simon-Santamaria, H. Hasvold, P. McCourt, B. Smedsrod, and K. K. Sorensen, "Liver sinusoidal endothelial cells depend on mannose receptor-mediated recruitment of lysosomal enzymes for normal degradation capacity," *Hepatology,* vol. 48, no. 6, pp. 2007-15, Dec 2008, doi: 10.1002/hep.22527.

[84] B. S. Ding *et al.*, "Inductive angiocrine signals from sinusoidal endothelium are required for liver regeneration," *Nature,* vol. 468, no. 7321, pp. 310-5, Nov 11 2010, doi: 10.1038/nature09493.

[85] C. D. Schmid *et al.*, "GPR182 is a novel marker for sinusoidal endothelial differentiation with distinct GPCR signaling activity in vitro," *Biochem Biophys Res Commun,* vol. 497, no. 1, pp. 32-38, Feb 26 2018, doi: 10.1016/j.bbrc.2018.01.185.

[86] S. Rafii, J. M. Butler, and B. S. Ding, "Angiocrine functions of organ-specific endothelial cells," *Nature,* vol. 529, no. 7586, pp. 316-25, Jan 21 2016, doi: 10.1038/nature17040.

[87] T. Leibing *et al.*, "Angiocrine Wnt signaling controls liver growth and metabolic maturation in mice," *Hepatology,* vol. 68, no. 2, pp. 707-722, Aug 2018, doi: 10.1002/hep.29613.

[88] S. Canali *et al.*, "Endothelial cells produce bone morphogenetic protein 6 required for iron homeostasis in mice," *Blood,* vol. 129, no. 4, pp. 405-414, Jan 26 2017, doi: 10.1182/blood-2016-06-721571.

[89] P. S. Koch *et al.*, "Angiocrine Bmp2 signaling in murine liver controls normal iron homeostasis," *Blood,* vol. 129, no. 4, pp. 415-419, Jan 26 2017, doi: 10.1182/blood-2016-07-729822.

[90] J. Hu *et al.*, "Endothelial cell-derived angiopoietin-2 controls liver regeneration as a spatiotemporal rheostat," *Science,* vol. 343, no. 6169, pp. 416-9, Jan 24 2014, doi: 10.1126/science.1244880.

[91] B. S. Ding *et al.*, "Divergent angiocrine signals from vascular niche balance liver regeneration and fibrosis," *Nature,* vol. 505, no. 7481, pp. 97-102, Jan 2 2014, doi: 10.1038/nature12681.

[92] K. Shido, D. Chavez, Z. Cao, J. Ko, S. Rafii, and B. S. Ding, "Platelets prime hematopoietic and vascular niche to drive angiocrine-mediated liver regeneration," *Signal Transduct Target Ther,* vol. 2, 2017, doi: 10.1038/sigtrans.2016.44.

[93] L. Lorenz *et al.*, "Mechanosensing by beta1 integrin induces angiocrine signals for liver growth and survival," *Nature,* vol. 562, no. 7725, pp. 128-132, Oct 2018, doi: 10.1038/s41586-018-0522-3.

[94] F. Schaffner and H. Poper, "Capillarization of hepatic sinusoids in man," *Gastroenterology,* vol. 44, pp. 239-42, Mar 1963. [Online]. Available: https://www.ncbi.nlm.nih.gov/pubmed/13976646.

[95] M. Winkler *et al.*, "Endothelial GATA4 controls liver fibrosis and regeneration by preventing a pathogenic switch in angiocrine signaling," *J Hepatol,* Sep 8 2020, doi: 10.1016/j.jhep.2020.08.033.

[96] Y. Ito *et al.*, "Age-related changes in the hepatic microcirculation in mice," *Exp Gerontol,* vol. 42, no. 8, pp. 789-97, Aug 2007, doi: 10.1016/j.exger.2007.04.008.

[97] A. J. McLean *et al.*, "Age-related pseudocapillarization of the human liver," (in English), *Journal of Pathology,* vol. 200, no. 1, pp. 112-117, May 2003, doi: 10.1002/path.1328.

[98] L. E. C. DG *et al.*, "Age-related changes in the liver sinusoidal endothelium: a mechanism for dyslipidemia," *Ann N Y Acad Sci,* vol. 1114, pp. 79-87, Oct 2007, doi: 10.1196/annals.1396.003.

[99] T. Tsuchida and S. L. Friedman, "Mechanisms of hepatic stellate cell activation," *Nat Rev Gastroenterol Hepatol,* vol. 14, no. 7, pp. 397-411, Jul 2017, doi: 10.1038/nrgastro.2017.38.

[100] R. Sakata, T. Ueno, T. Nakamura, H. Ueno, and M. Sata, "Mechanical stretch induces TGF-beta synthesis in hepatic stellate cells," *Eur J Clin Invest,* vol. 34, no. 2, pp. 129-36, Feb 2004, doi: 10.1111/j.1365-2362.2004.01302.x.

[101] N. Kawada, T. A. Tran-Thi, H. Klein, and K. Decker, "The contraction of hepatic stellate (Ito) cells stimulated with vasoactive substances. Possible involvement of endothelin 1 and nitric oxide in the regulation of the sinusoidal tonus," *Eur J Biochem,* vol. 213, no. 2, pp. 815-23, Apr 15 1993, doi: 10.1111/j.1432-1033.1993.tb17824.x.

[102] D. Rockey, "The cellular pathogenesis of portal hypertension: stellate cell contractility, endothelin, and nitric oxide," *Hepatology,* vol. 25, no. 1, pp. 2-5, Jan 1997, doi: 10.1053/jhep.1997.v25.ajhep0250002.

[103] L. D. Deleve, X. Wang, and Y. Guo, "Sinusoidal endothelial cells prevent rat stellate cell activation and promote reversion to quiescence," *Hepatology,* vol. 48, no. 3, pp. 920-30, Sep 2008, doi: 10.1002/hep.22351.

[104] E. Lafoz, M. Ruart, A. Anton, A. Oncins, and V. Hernandez-Gea, "The Endothelium as a Driver of Liver Fibrosis and Regeneration," *Cells,* vol. 9, no. 4, Apr 10 2020, doi: 10.3390/cells9040929.

[105] L. D. DeLeve, X. Wang, L. Hu, M. K. McCuskey, and R. S. McCuskey, "Rat liver sinusoidal endothelial cell phenotype is maintained by paracrine and autocrine

regulation," *Am J Physiol Gastrointest Liver Physiol,* vol. 287, no. 4, pp. G757-63, Oct 2004, doi: 10.1152/ajpgi.00017.2004.

[106] V. Shah *et al.*, "Liver sinusoidal endothelial cells are responsible for nitric oxide modulation of resistance in the hepatic sinusoids," *J Clin Invest,* vol. 100, no. 11, pp. 2923-30, Dec 1 1997, doi: 10.1172/JCI119842.

[107] K. M. Parmar *et al.*, "Integration of flow-dependent endothelial phenotypes by Kruppel-like factor 2," *J Clin Invest,* vol. 116, no. 1, pp. 49-58, Jan 2006, doi: 10.1172/JCI24787.

[108] J. Gracia-Sancho, L. Russo, H. Garcia-Caldero, J. C. Garcia-Pagan, G. Garcia-Cardena, and J. Bosch, "Endothelial expression of transcription factor Kruppel-like factor 2 and its vasoprotective target genes in the normal and cirrhotic rat liver," *Gut,* vol. 60, no. 4, pp. 517-24, Apr 2011, doi: 10.1136/gut.2010.220913.

[109] J. L. Duan *et al.*, "Endothelial Notch activation reshapes the angiocrine of sinusoidal endothelia to aggravate liver fibrosis and blunt regeneration in mice," *Hepatology,* vol. 68, no. 2, pp. 677-690, Aug 2018, doi: 10.1002/hep.29834.

[110] L. Chen *et al.*, "Delta-like ligand 4/DLL4 regulates the capillarization of liver sinusoidal endothelial cell and liver fibrogenesis," *Biochim Biophys Acta Mol Cell Res,* vol. 1866, no. 10, pp. 1663-1675, Oct 2019, doi: 10.1016/j.bbamcr.2019.06.011.

[111] D. C. Rockey and J. J. Chung, "Reduced nitric oxide production by endothelial cells in cirrhotic rat liver: endothelial dysfunction in portal hypertension," *Gastroenterology,* vol. 114, no. 2, pp. 344-51, Feb 1998, doi: 10.1016/s0016-5085(98)70487-1.

[112] N. P. Dufton *et al.*, "Dynamic regulation of canonical TGFbeta signalling by endothelial transcription factor ERG protects from liver fibrogenesis," *Nat Commun,* vol. 8, no. 1, p. 895, Oct 12 2017, doi: 10.1038/s41467-017-01169-0.

[113] G. Xie *et al.*, "Hedgehog signalling regulates liver sinusoidal endothelial cell capillarisation," *Gut,* vol. 62, no. 2, pp. 299-309, Feb 2013, doi: 10.1136/gutjnl-2011-301494.

[114] R. P. Witek *et al.*, "Liver cell-derived microparticles activate hedgehog signaling and alter gene expression in hepatic endothelial cells," *Gastroenterology,* vol. 136, no. 1, pp. 320-330 e2, Jan 2009, doi: 10.1053/j.gastro.2008.09.066.

[115] Y. Xing, T. Zhao, X. Gao, and Y. Wu, "Liver X receptor alpha is essential for the capillarization of liver sinusoidal endothelial cells in liver injury," *Sci Rep,* vol. 6, p. 21309, Feb 18 2016, doi: 10.1038/srep21309.

[116] A. Desroches-Castan *et al.*, "Bone Morphogenetic Protein 9 Is a Paracrine Factor Controlling Liver Sinusoidal Endothelial Cell Fenestration and Protecting Against Hepatic Fibrosis," *Hepatology,* vol. 70, no. 4, pp. 1392-1408, Oct 2019, doi: 10.1002/hep.30655.

[117] C. Géraud *et al.*, "GATA4-dependent organ-specific endothelial differentiation controls liver development and embryonic hematopoiesis," in *J Clin Invest* vol. 127, 2017/02/22 ed, 2017, pp. 1099-1114.

[118] L. J. Ko and J. D. Engel, "DNA-binding specificities of the GATA transcription factor family," *Mol Cell Biol,* vol. 13, no. 7, pp. 4011-22, Jul 1993, doi: 10.1128/mcb.13.7.4011-4022.1993.

[119] S. F. Tsai, D. I. Martin, L. I. Zon, A. D. D'Andrea, G. G. Wong, and S. H. Orkin, "Cloning of cDNA for the major DNA-binding protein of the erythroid lineage through expression in mammalian cells," *Nature,* vol. 339, no. 6224, pp. 446-51, Jun 8 1989, doi: 10.1038/339446a0.

[120] M. Yamamoto, L. J. Ko, M. W. Leonard, H. Beug, S. H. Orkin, and J. D. Engel, "Activity and tissue-specific expression of the transcription factor NF-E1 multigene family," *Genes Dev,* vol. 4, no. 10, pp. 1650-62, Oct 1990, doi: 10.1101/gad.4.10.1650.

[121] T. Evans and G. Felsenfeld, "The erythroid-specific transcription factor Eryf1: a new finger protein," *Cell,* vol. 58, no. 5, pp. 877-85, Sep 8 1989, doi: 10.1016/0092-8674(89)90940-9.

[122] D. B. Wilson, D. M. Dorfman, and S. H. Orkin, "A nonerythroid GATA-binding protein is required for function of the human preproendothelin-1 promoter in endothelial cells," *Mol Cell Biol,* vol. 10, no. 9, pp. 4854-62, Sep 1990, doi: 10.1128/mcb.10.9.4854-4862.1990.

[123] C. Kelley, H. Blumberg, L. I. Zon, and T. Evans, "GATA-4 is a novel transcription factor expressed in endocardium of the developing heart," *Development,* vol. 118, no. 3, pp. 817-27, Jul 1993. [Online]. Available: https://www.ncbi.nlm.nih.gov/pubmed/8076520.

[124] A. C. Laverriere, C. MacNeill, C. Mueller, R. E. Poelmann, J. B. Burch, and T. Evans, "GATA-4/5/6, a subfamily of three transcription factors transcribed in developing heart and gut," *J Biol Chem,* vol. 269, no. 37, pp. 23177-84, Sep 16 1994. [Online]. Available: https://www.ncbi.nlm.nih.gov/pubmed/8083222.

[125] R. J. Arceci, A. A. King, M. C. Simon, S. H. Orkin, and D. B. Wilson, "Mouse GATA-4: a retinoic acid-inducible GATA-binding transcription factor expressed in endodermally derived tissues and heart," *Mol Cell Biol,* vol. 13, no. 4, pp. 2235-46, Apr 1993, doi: 10.1128/mcb.13.4.2235-2246.1993.

[126] J. D. Molkentin, Q. Lin, S. A. Duncan, and E. N. Olson, "Requirement of the transcription factor GATA4 for heart tube formation and ventral morphogenesis," *Genes Dev,* vol. 11, no. 8, pp. 1061-72, Apr 15 1997, doi: 10.1101/gad.11.8.1061.

[127] J. Rivera-Feliciano *et al.*, "Development of heart valves requires Gata4 expression in endothelial-derived cells," *Development,* vol. 133, no. 18, pp. 3607-18, Sep 2006, doi: 10.1242/dev.02519.

[128] I. Delgado *et al.*, "GATA4 loss in the septum transversum mesenchyme promotes liver fibrosis in mice," *Hepatology,* vol. 59, no. 6, pp. 2358-70, Jun 2014, doi: 10.1002/hep.27005.

[129] M. B. Hilscher *et al.*, "Mechanical Stretch Increases Expression of CXCL1 in Liver Sinusoidal Endothelial Cells to Recruit Neutrophils, Generate Sinusoidal Microthombi, and Promote Portal Hypertension," *Gastroenterology,* vol. 157, no. 1, pp. 193-209 e9, Jul 2019, doi: 10.1053/j.gastro.2019.03.013.

[130] B. L. Copple, S. Bai, L. D. Burgoon, and J. O. Moon, "Hypoxia-inducible factor-1alpha regulates the expression of genes in hypoxic hepatic stellate cells important for collagen deposition and angiogenesis," *Liver Int,* vol. 31, no. 2, pp. 230-44, Feb 2011, doi: 10.1111/j.1478-3231.2010.02347.x.

[131] C. Bocca, E. Novo, A. Miglietta, and M. Parola, "Angiogenesis and Fibrogenesis in Chronic Liver Diseases," *Cell Mol Gastroenterol Hepatol,* vol. 1, no. 5, pp. 477-488, Sep 2015, doi: 10.1016/j.jcmgh.2015.06.011.

[132] K. Neubauer, M. Kruger, F. Quondamatteo, T. Knittel, B. Saile, and G. Ramadori, "Transforming growth factor-beta1 stimulates the synthesis of basement membrane proteins laminin, collagen type IV and entactin in rat liver sinusoidal endothelial cells," *J Hepatol,* vol. 31, no. 4, pp. 692-702, Oct 1999, doi: 10.1016/s0168-8278(99)80350-x.

[133] Y. Sato *et al.*, "The mechanism for the activation of latent TGF-beta during co-culture of endothelial cells and smooth muscle cells: cell-type specific targeting of latent TGF-beta to smooth muscle cells," *J Cell Biol,* vol. 123, no. 5, pp. 1249-54, Dec 1993, doi: 10.1083/jcb.123.5.1249.

[134] R. Bataller and D. A. Brenner, "Liver fibrosis," *J Clin Invest,* vol. 115, no. 2, pp. 209-18, Feb 2005, doi: 10.1172/JCI24282.

[135] P. Ramachandran and J. P. Iredale, "Reversibility of liver fibrosis," *Ann Hepatol,* vol. 8, no. 4, pp. 283-91, Oct-Dec 2009. [Online]. Available: https://www.ncbi.nlm.nih.gov/pubmed/20009126.

[136] G. L. Davis, J. E. Albright, S. F. Cook, and D. M. Rosenberg, "Projecting future complications of chronic hepatitis C in the United States," *Liver Transpl,* vol. 9, no. 4, pp. 331-8, Apr 2003, doi: 10.1053/jlts.2003.50073.

[137] G. B. D. C. Collaborators, "The global, regional, and national burden of cirrhosis by cause in 195 countries and territories, 1990-2017: a systematic analysis for the Global Burden of Disease Study 2017," *Lancet Gastroenterol Hepatol,* vol. 5, no. 3, pp. 245-266, Mar 2020, doi: 10.1016/S2468-1253(19)30349-8.

[138] M. Rosselli, J. MacNaughtan, R. Jalan, and M. Pinzani, "Beyond scoring: a modern interpretation of disease progression in chronic liver disease," *Gut,* vol. 62, no. 9, pp. 1234-41, Sep 2013, doi: 10.1136/gutjnl-2012-302826.

[139] R. A. Standish, E. Cholongitas, A. Dhillon, A. K. Burroughs, and A. P. Dhillon, "An appraisal of the histopathological assessment of liver fibrosis," *Gut,* vol. 55, no. 4, pp. 569-78, Apr 2006, doi: 10.1136/gut.2005.084475.

[140] F. Imbert-Bismut *et al.*, "Biochemical markers of liver fibrosis in patients with hepatitis C virus infection: a prospective study," *Lancet,* vol. 357, no. 9262, pp. 1069-75, Apr 7 2001, doi: 10.1016/S0140-6736(00)04258-6.

[141] S. U. Kim *et al.*, "Non-invasive assessment of changes in liver fibrosis via liver stiffness measurement in patients with chronic hepatitis B: impact of antiviral treatment on fibrosis regression," *Hepatol Int,* vol. 4, no. 4, pp. 673-80, Aug 4 2010, doi: 10.1007/s12072-010-9201-7.

[142] M. Hirata, S. M. Akbar, N. Horiike, and M. Onji, "Noninvasive diagnosis of the degree of hepatic fibrosis using ultrasonography in patients with chronic liver disease due to hepatitis C virus," *Eur J Clin Invest,* vol. 31, no. 6, pp. 528-35, Jun 2001, doi: 10.1046/j.1365-2362.2001.00840.x.

[143] E. M. Brunt, C. G. Janney, A. M. Di Bisceglie, B. A. Neuschwander-Tetri, and B. R. Bacon, "Nonalcoholic steatohepatitis: a proposal for grading and staging the histological lesions," *Am J Gastroenterol,* vol. 94, no. 9, pp. 2467-74, Sep 1999, doi: 10.1111/j.1572-0241.1999.01377.x.

[144] V. Hernandez-Gea and S. L. Friedman, "Pathogenesis of liver fibrosis," *Annu Rev Pathol,* vol. 6, pp. 425-56, 2011, doi: 10.1146/annurev-pathol-011110-130246.

[145] R. C. Lo and H. Kim, "Histopathological evaluation of liver fibrosis and cirrhosis regression," *Clin Mol Hepatol,* vol. 23, no. 4, pp. 302-307, Dec 2017, doi: 10.3350/cmh.2017.0078.

[146] T. Kisseleva, "The origin of fibrogenic myofibroblasts in fibrotic liver," *Hepatology,* vol. 65, no. 3, pp. 1039-1043, Mar 2017, doi: 10.1002/hep.28948.

[147] S. Lemoinne, A. Cadoret, H. El Mourabit, D. Thabut, and C. Housset, "Origins and functions of liver myofibroblasts," *Biochim Biophys Acta,* vol. 1832, no. 7, pp. 948-54, Jul 2013, doi: 10.1016/j.bbadis.2013.02.019.

[148] M. Parola and M. Pinzani, "Liver fibrosis: Pathophysiology, pathogenetic targets and clinical issues," *Mol Aspects Med,* vol. 65, pp. 37-55, Feb 2019, doi: 10.1016/j.mam.2018.09.002.

[149] K. Iwaisako *et al.*, "Origin of myofibroblasts in the fibrotic liver in mice," *Proc Natl Acad Sci U S A,* vol. 111, no. 32, pp. E3297-305, Aug 12 2014, doi: 10.1073/pnas.1400062111.

[150] M. M. Aydin and K. C. Akcali, "Liver fibrosis," *Turk J Gastroenterol,* vol. 29, no. 1, pp. 14-21, Jan 2018, doi: 10.5152/tjg.2018.17330.

[151] W. C. Zhou, Q. B. Zhang, and L. Qiao, "Pathogenesis of liver cirrhosis," *World J Gastroenterol,* vol. 20, no. 23, pp. 7312-24, Jun 21 2014, doi: 10.3748/wjg.v20.i23.7312.

[152] M. Miyao *et al.*, "Pivotal role of liver sinusoidal endothelial cells in NAFLD/NASH progression," *Lab Invest,* vol. 95, no. 10, pp. 1130-44, Oct 2015, doi: 10.1038/labinvest.2015.95.

[153] L. D. DeLeve, "Liver sinusoidal endothelial cells in hepatic fibrosis," *Hepatology,* vol. 61, no. 5, pp. 1740-6, May 2015, doi: 10.1002/hep.27376.

[154] A. Hammoutene and P. E. Rautou, "Role of liver sinusoidal endothelial cells in non-alcoholic fatty liver disease," *J Hepatol,* vol. 70, no. 6, pp. 1278-1291, Jun 2019, doi: 10.1016/j.jhep.2019.02.012.

[155] J. Poisson *et al.*, "Liver sinusoidal endothelial cells: Physiology and role in liver diseases," *J Hepatol,* vol. 66, no. 1, pp. 212-227, Jan 2017, doi: 10.1016/j.jhep.2016.07.009.

[156] G. Marrone *et al.*, "KLF2 exerts antifibrotic and vasoprotective effects in cirrhotic rat livers: behind the molecular mechanisms of statins," *Gut,* vol. 64, no. 9, pp. 1434-43, Sep 2015, doi: 10.1136/gutjnl-2014-308338.

[157] B. S. Ding *et al.*, "HDL activation of endothelial sphingosine-1-phosphate receptor-1 (S1P1) promotes regeneration and suppresses fibrosis in the liver," *JCI Insight,* vol. 1, no. 21, p. e87058, Dec 22 2016, doi: 10.1172/jci.insight.87058.

[158] L. Wong, G. Yamasaki, R. J. Johnson, and S. L. Friedman, "Induction of beta-platelet-derived growth factor receptor in rat hepatic lipocytes during cellular activation in vivo and in culture," *J Clin Invest,* vol. 94, no. 4, pp. 1563-9, Oct 1994, doi: 10.1172/JCI117497.

[159] W. R. Jarnagin, D. C. Rockey, V. E. Koteliansky, S. S. Wang, and D. M. Bissell, "Expression of variant fibronectins in wound healing: cellular source and biological activity of the EIIIA segment in rat hepatic fibrogenesis," *J Cell Biol,* vol. 127, no. 6 Pt 2, pp. 2037-48, Dec 1994, doi: 10.1083/jcb.127.6.2037.

[160] G. Xie *et al.*, "Role of differentiation of liver sinusoidal endothelial cells in progression and regression of hepatic fibrosis in rats," *Gastroenterology,* vol. 142, no. 4, pp. 918-927 e6, Apr 2012, doi: 10.1053/j.gastro.2011.12.017.

[161] G. Marrone, V. H. Shah, and J. Gracia-Sancho, "Sinusoidal communication in liver fibrosis and regeneration," (in English), *Journal of Hepatology,* vol. 65, no. 3, pp. 608-617, Sep 2016, doi: DOI 10.1016/j.jhep.2016.04.018.

[162] N. Chalasani *et al.*, "The diagnosis and management of nonalcoholic fatty liver disease: Practice guidance from the American Association for the Study of Liver Diseases," *Hepatology,* vol. 67, no. 1, pp. 328-357, Jan 2018, doi: 10.1002/hep.29367.

[163] F. Schaffner and H. Thaler, "Nonalcoholic fatty liver disease," *Prog Liver Dis,* vol. 8, pp. 283-98, 1986. [Online]. Available: https://www.ncbi.nlm.nih.gov/pubmed/3086934.

[164] A. Gastaldelli and K. Cusi, "From NASH to diabetes and from diabetes to NASH: Mechanisms and treatment options," *JHEP Rep,* vol. 1, no. 4, pp. 312-328, Oct 2019, doi: 10.1016/j.jhepr.2019.07.002.

[165] K. P. H. Sharp, M. Schultz, and K. J. Coppell, "Is non-alcoholic fatty liver disease a reflection of what we eat or simply how much we eat?," *JGH Open,* vol. 2, no. 2, pp. 59-74, Apr 2018, doi: 10.1002/jgh3.12040.

[166] Z. M. Younossi, A. B. Koenig, D. Abdelatif, Y. Fazel, L. Henry, and M. Wymer, "Global epidemiology of nonalcoholic fatty liver disease-Meta-analytic assessment of prevalence, incidence, and outcomes," *Hepatology,* vol. 64, no. 1, pp. 73-84, Jul 2016, doi: 10.1002/hep.28431.

[167] P. Angulo *et al.*, "Liver Fibrosis, but No Other Histologic Features, Is Associated With Long-term Outcomes of Patients With Nonalcoholic Fatty Liver Disease," *Gastroenterology,* vol. 149, no. 2, pp. 389-97 e10, Aug 2015, doi: 10.1053/j.gastro.2015.04.043.

[168] P. S. Dulai *et al.*, "Increased risk of mortality by fibrosis stage in nonalcoholic fatty liver disease: Systematic review and meta-analysis," *Hepatology,* vol. 65, no. 5, pp. 1557-1565, May 2017, doi: 10.1002/hep.29085.

[169] M. Ekstedt *et al.*, "Fibrosis stage is the strongest predictor for disease-specific mortality in NAFLD after up to 33 years of follow-up," *Hepatology,* vol. 61, no. 5, pp. 1547-54, May 2015, doi: 10.1002/hep.27368.

[170] H. Hagstrom *et al.*, "Fibrosis stage but not NASH predicts mortality and time to development of severe liver disease in biopsy-proven NAFLD," *J Hepatol,* vol. 67, no. 6, pp. 1265-1273, Dec 2017, doi: 10.1016/j.jhep.2017.07.027.

[171] E. Buzzetti, M. Pinzani, and E. A. Tsochatzis, "The multiple-hit pathogenesis of non-alcoholic fatty liver disease (NAFLD)," *Metabolism,* vol. 65, no. 8, pp. 1038-48, Aug 2016, doi: 10.1016/j.metabol.2015.12.012.

[172] I. Pierantonelli and G. Svegliati-Baroni, "Nonalcoholic Fatty Liver Disease: Basic Pathogenetic Mechanisms in the Progression From NAFLD to NASH," *Transplantation,* vol. 103, no. 1, pp. e1-e13, Jan 2019, doi: 10.1097/TP.0000000000002480.

[173] R. G. Gieling, A. D. Burt, and D. A. Mann, "Fibrosis and cirrhosis reversibility - molecular mechanisms," *Clin Liver Dis,* vol. 12, no. 4, pp. 915-37, xi, Nov 2008, doi: 10.1016/j.cld.2008.07.001.

[174] A. A. Sohrabpour, M. Mohamadnejad, and R. Malekzadeh, "Review article: the reversibility of cirrhosis," *Aliment Pharmacol Ther,* vol. 36, no. 9, pp. 824-32, Nov 2012, doi: 10.1111/apt.12044.

[175] N. Roehlen, E. Crouchet, and T. F. Baumert, "Liver Fibrosis: Mechanistic Concepts and Therapeutic Perspectives," *Cells,* vol. 9, no. 4, Apr 3 2020, doi: 10.3390/cells9040875.

[176] M. J. Arthur, "Reversibility of liver fibrosis and cirrhosis following treatment for hepatitis C," *Gastroenterology,* vol. 122, no. 5, pp. 1525-8, May 2002, doi: 10.1053/gast.2002.33367.

[177] O. Basar *et al.*, "Non-invasive tests in prediction of liver fibrosis in chronic hepatitis B and comparison with post-antiviral treatment results," *Clin Res Hepatol Gastroenterol,* vol. 37, no. 2, pp. 152-8, Apr 2013, doi: 10.1016/j.clinre.2012.07.003.

[178] J. B. Dixon, P. S. Bhathal, N. R. Hughes, and P. E. O'Brien, "Nonalcoholic fatty liver disease: Improvement in liver histological analysis with weight loss," *Hepatology,* vol. 39, no. 6, pp. 1647-54, Jun 2004, doi: 10.1002/hep.20251.

[179] A. Pares, J. Caballeria, M. Bruguera, M. Torres, and J. Rodes, "Histological course of alcoholic hepatitis. Influence of abstinence, sex and extent of hepatic damage," *J Hepatol,* vol. 2, no. 1, pp. 33-42, 1986, doi: 10.1016/s0168-8278(86)80006-x.

[180] N. Chainani-Wu, "Safety and anti-inflammatory activity of curcumin: a component of tumeric (Curcuma longa)," *J Altern Complement Med,* vol. 9, no. 1, pp. 161-8, Feb 2003, doi: 10.1089/107555303321223035.

[181] S. Clichici, D. Olteanu, A. L. Nagy, A. Oros, A. Filip, and P. A. Mircea, "Silymarin inhibits the progression of fibrosis in the early stages of liver injury in CCl(4)-treated rats," *J Med Food,* vol. 18, no. 3, pp. 290-8, Mar 2015, doi: 10.1089/jmf.2013.0179.

[182] S. L. Devi, P. Viswanathan, and C. V. Anuradha, "Regression of liver fibrosis by taurine in rats fed alcohol: effects on collagen accumulation, selected cytokines and stellate cell activation," *Eur J Pharmacol,* vol. 647, no. 1-3, pp. 161-70, Nov 25 2010, doi: 10.1016/j.ejphar.2010.08.011.

[183] M. Galicia-Moreno *et al.*, "N-acetylcysteine prevents carbon tetrachloride-induced liver cirrhosis: role of liver transforming growth factor-beta and oxidative stress," *Eur J Gastroenterol Hepatol,* vol. 21, no. 8, pp. 908-14, Aug 2009, doi: 10.1097/MEG.0b013e32831f1f3a.

[184] S. A. Harrison, S. Torgerson, P. Hayashi, J. Ward, and S. Schenker, "Vitamin E and vitamin C treatment improves fibrosis in patients with nonalcoholic steatohepatitis," *Am J Gastroenterol,* vol. 98, no. 11, pp. 2485-90, Nov 2003, doi: 10.1111/j.1572-0241.2003.08699.x.

[185] A. C. Pfalzer *et al.*, "S-adenosylmethionine mediates inhibition of inflammatory response and changes in DNA methylation in human macrophages," *Physiol Genomics,* vol. 46, no. 17, pp. 617-23, Sep 1 2014, doi: 10.1152/physiolgenomics.00056.2014.

[186] M. Zhang, G. Song, and G. Y. Minuk, "Effects of hepatic stimulator substance, herbal medicine, selenium/vitamin E, and ciprofloxacin on cirrhosis in the rat," *Gastroenterology,* vol. 110, no. 4, pp. 1150-5, Apr 1996, doi: 10.1053/gast.1996.v110.pm8613004.

[187] Z. X. Wang *et al.*, "The treatment of liver fibrosis induced by hepatocyte growth factor-directed, ultrasound-targeted microbubble destruction in rats," *Clin Imaging,* vol. 33, no. 6, pp. 454-61, Nov-Dec 2009, doi: 10.1016/j.clinimag.2009.07.001.

[188] E. Borkham-Kamphorst, D. Stoll, A. M. Gressner, and R. Weiskirchen, "Antisense strategy against PDGF B-chain proves effective in preventing experimental liver fibrogenesis," *Biochem Biophys Res Commun,* vol. 321, no. 2, pp. 413-23, Aug 20 2004, doi: 10.1016/j.bbrc.2004.06.153.

[189] Y. Y. Tao, Q. L. Wang, L. Shen, W. W. Fu, and C. H. Liu, "Salvianolic acid B inhibits hepatic stellate cell activation through transforming growth factor beta-1 signal transduction pathway in vivo and in vitro," *Exp Biol Med (Maywood),* vol. 238, no. 11, pp. 1284-96, Nov 1 2013, doi: 10.1177/1535370213498979.

[190] F. Oakley *et al.*, "Inhibition of inhibitor of kappaB kinases stimulates hepatic stellate cell apoptosis and accelerated recovery from rat liver fibrosis," *Gastroenterology,* vol. 128, no. 1, pp. 108-20, Jan 2005, doi: 10.1053/j.gastro.2004.10.003.

[191] B. Saile *et al.*, "IGF-I induces DNA synthesis and apoptosis in rat liver hepatic stellate cells (HSC) but DNA synthesis and proliferation in rat liver myofibroblasts (rMF)," *Lab Invest,* vol. 84, no. 8, pp. 1037-49, Aug 2004, doi: 10.1038/labinvest.3700116.

[192] B. Saile, C. Eisenbach, J. Dudas, H. El-Armouche, and G. Ramadori, "Interferon-gamma acts proapoptotic on hepatic stellate cells (HSC) and abrogates the antiapoptotic effect of interferon-alpha by an HSP70-dependant pathway," *Eur J Cell Biol,* vol. 83, no. 9, pp. 469-76, Sep 2004, doi: 10.1078/0171-9335-00409.

[193] K. O. Doh, H. K. Jung, I. J. Moon, H. G. Kang, J. H. Park, and J. G. Park, "Prevention of CCl4-induced liver cirrhosis by ribbon antisense to transforming growth factor-beta1," *Int J Mol Med,* vol. 21, no. 1, pp. 33-9, Jan 2008. [Online]. Available: https://www.ncbi.nlm.nih.gov/pubmed/18097613.

[194] Q. Lang *et al.*, "The antifibrotic effects of TGF-beta1 siRNA on hepatic fibrosis in rats," *Biochem Biophys Res Commun,* vol. 409, no. 3, pp. 448-53, Jun 10 2011, doi: 10.1016/j.bbrc.2011.05.023.

[195] G. Li *et al.*, "Inhibition of connective tissue growth factor by siRNA prevents liver fibrosis in rats," *J Gene Med,* vol. 8, no. 7, pp. 889-900, Jul 2006, doi: 10.1002/jgm.894.

[196] Q. H. Nie, C. L. Zhu, Y. F. Zhang, J. Yang, J. C. Zhang, and R. T. Gao, "Inhibitory effect of antisense oligonucleotide targeting TIMP-2 on immune-induced liver fibrosis," *Dig Dis Sci,* vol. 55, no. 5, pp. 1286-95, May 2010, doi: 10.1007/s10620-009-0858-5.

[197] J. I. Beier and C. J. McClain, "Mechanisms and cell signaling in alcoholic liver disease," *Biol Chem,* vol. 391, no. 11, pp. 1249-64, Nov 2010, doi: 10.1515/BC.2010.137.

[198] L. W. Weber, M. Boll, and A. Stampfl, "Hepatotoxicity and mechanism of action of haloalkanes: carbon tetrachloride as a toxicological model," *Crit Rev Toxicol,* vol. 33, no. 2, pp. 105-36, 2003, doi: 10.1080/713611034.

[199] T. Y. Low, C. K. Leow, M. Salto-Tellez, and M. C. Chung, "A proteomic analysis of thioacetamide-induced hepatotoxicity and cirrhosis in rat livers," *Proteomics,* vol. 4, no. 12, pp. 3960-74, Dec 2004, doi: 10.1002/pmic.200400852.

[200] G. P. Smith, *Animal models for the study of human disease*. China: Elsevier, 2013.

[201] Q. M. Anstee and R. D. Goldin, "Mouse models in non-alcoholic fatty liver disease and steatohepatitis research," *Int J Exp Pathol,* vol. 87, no. 1, pp. 1-16, Feb 2006, doi: 10.1111/j.0959-9673.2006.00465.x.

[202] G. Farrell *et al.*, "Mouse Models of Nonalcoholic Steatohepatitis: Toward Optimization of Their Relevance to Human Nonalcoholic Steatohepatitis," *Hepatology,* vol. 69, no. 5, pp. 2241-2257, May 2019, doi: 10.1002/hep.30333.

[203] H. Miyoshi, C. Rust, P. J. Roberts, L. J. Burgart, and G. J. Gores, "Hepatocyte apoptosis after bile duct ligation in the mouse involves Fas," *Gastroenterology,* vol. 117, no. 3, pp. 669-77, Sep 1999, doi: 10.1016/s0016-5085(99)70461-0.

[204] M. L. Chang, C. T. Yeh, P. Y. Chang, and J. C. Chen, "Comparison of murine cirrhosis models induced by hepatotoxin administration and common bile duct ligation," *World J Gastroenterol,* vol. 11, no. 27, pp. 4167-72, Jul 21 2005, doi: 10.3748/wjg.v11.i27.4167.

[205] S. C. Yanguas *et al.*, "Experimental models of liver fibrosis," *Arch Toxicol,* vol. 90, no. 5, pp. 1025-1048, May 2016, doi: 10.1007/s00204-015-1543-4.

[206] A. P. McCaffrey *et al.*, "Inhibition of hepatitis B virus in mice by RNA interference," *Nat Biotechnol,* vol. 21, no. 6, pp. 639-44, Jun 2003, doi: 10.1038/nbt824.

[207] A. W. Cheever, J. A. Lenzi, H. L. Lenzi, and Z. A. Andrade, "Experimental models of Schistosoma mansoni infection," *Mem Inst Oswaldo Cruz,* vol. 97, no. 7, pp. 917-40, Oct 2002, doi: 10.1590/s0074-02762002000700002.

[208] T. H. Mauad *et al.*, "Mice with homozygous disruption of the mdr2 P-glycoprotein gene. A novel animal model for studies of nonsuppurative inflammatory cholangitis and hepatocarcinogenesis," *Am J Pathol,* vol. 145, no. 5, pp. 1237-45, Nov 1994. [Online]. Available: https://www.ncbi.nlm.nih.gov/pubmed/7977654.

[209] T. Arsov *et al.*, "Adaptive failure to high-fat diet characterizes steatohepatitis in Alms1 mutant mice," *Biochem Biophys Res Commun,* vol. 342, no. 4, pp. 1152-9, Apr 21 2006, doi: 10.1016/j.bbrc.2006.02.032.

[210] C. Z. Larter *et al.*, "Dietary modification dampens liver inflammation and fibrosis in obesity-related fatty liver disease," *Obesity (Silver Spring),* vol. 21, no. 6, pp. 1189-99, Jun 2013, doi: 10.1002/oby.20123.

[211] C. Constandinou, N. Henderson, and J. P. Iredale, "Modeling liver fibrosis in rodents," *Methods Mol Med,* vol. 117, pp. 237-50, 2005, doi: 10.1385/1-59259-940-0:237.

[212] S. Basu, "Carbon tetrachloride-induced lipid peroxidation: eicosanoid formation and their regulation by antioxidant nutrients," *Toxicology,* vol. 189, no. 1-2, pp. 113-27, Jul 15 2003, doi: 10.1016/s0300-483x(03)00157-4.

[213] T. F. Slater, K. H. Cheeseman, and K. U. Ingold, "Carbon tetrachloride toxicity as a model for studying free-radical mediated liver injury," *Philos Trans R Soc Lond B Biol Sci,* vol. 311, no. 1152, pp. 633-45, Dec 17 1985, doi: 10.1098/rstb.1985.0169.

[214] S. H. Ibrahim, P. Hirsova, H. Malhi, and G. J. Gores, "Animal Models of Nonalcoholic Steatohepatitis: Eat, Delete, and Inflame," *Dig Dis Sci,* vol. 61, no. 5, pp. 1325-36, May 2016, doi: 10.1007/s10620-015-3977-1.

[215] J. E. Vance and D. E. Vance, "The Role of Phosphatidylcholine Biosynthesis in the Secretion of Lipoproteins from Hepatocytes," (in English), *Canadian Journal of Biochemistry and Cell Biology,* vol. 63, no. 8, pp. 870-881, 1985, doi: DOI 10.1139/o85-108.

[216] F. Zhong, X. Zhou, J. Xu, and L. Gao, "Rodent Models of Nonalcoholic Fatty Liver Disease," *Digestion,* vol. 101, no. 5, pp. 522-535, 2020, doi: 10.1159/000501851.

[217] C. Z. Larter, M. M. Yeh, J. Williams, K. S. Bell-Anderson, and G. C. Farrell, "MCD-induced steatohepatitis is associated with hepatic adiponectin resistance and adipogenic transformation of hepatocytes," *J Hepatol,* vol. 49, no. 3, pp. 407-16, Sep 2008, doi: 10.1016/j.jhep.2008.03.026.

[218] I. A. Leclercq, J. Field, A. Enriquez, G. C. Farrell, and G. R. Robertson, "Constitutive and inducible expression of hepatic CYP2E1 in leptin-deficient ob/ob mice," *Biochem Biophys Res Commun,* vol. 268, no. 2, pp. 337-44, Feb 16 2000, doi: 10.1006/bbrc.2000.2125.

[219] I. A. Leclercq, V. A. Lebrun, P. Starkel, and Y. J. Horsmans, "Intrahepatic insulin resistance in a murine model of steatohepatitis: effect of PPARgamma agonist pioglitazone," *Lab Invest,* vol. 87, no. 1, pp. 56-65, Jan 2007, doi: 10.1038/labinvest.3700489.

[220] M. E. Rinella and R. M. Green, "The methionine-choline deficient dietary model of steatohepatitis does not exhibit insulin resistance," *J Hepatol,* vol. 40, no. 1, pp. 47-51, Jan 2004, doi: 10.1016/j.jhep.2003.09.020.

[221] H. Itagaki, K. Shimizu, S. Morikawa, K. Ogawa, and T. Ezaki, "Morphological and functional characterization of non-alcoholic fatty liver disease induced by a methionine-

choline-deficient diet in C57BL/6 mice," *Int J Clin Exp Pathol,* vol. 6, no. 12, pp. 2683-96, 2013. [Online]. Available: https://www.ncbi.nlm.nih.gov/pubmed/24294355.

[222] D. Nakae *et al.*, "Comparative changes in the liver of female Fischer-344 rats after short-term feeding of a semipurified or a semisynthetic L-amino acid-defined choline-deficient diet," *Toxicol Pathol,* vol. 23, no. 5, pp. 583-90, Sep-Oct 1995, doi: 10.1177/019262339502300504.

[223] Y. Kodama *et al.*, "c-Jun N-terminal kinase-1 from hematopoietic cells mediates progression from hepatic steatosis to steatohepatitis and fibrosis in mice," *Gastroenterology,* vol. 137, no. 4, pp. 1467-1477 e5, Oct 2009, doi: 10.1053/j.gastro.2009.06.045.

[224] K. Miura *et al.*, "Toll-like receptor 9 promotes steatohepatitis by induction of interleukin-1beta in mice," *Gastroenterology,* vol. 139, no. 1, pp. 323-34 e7, Jul 2010, doi: 10.1053/j.gastro.2010.03.052.

[225] M. J. Wolf *et al.*, "Metabolic activation of intrahepatic CD8+ T cells and NKT cells causes nonalcoholic steatohepatitis and liver cancer via cross-talk with hepatocytes," *Cancer Cell,* vol. 26, no. 4, pp. 549-64, Oct 13 2014, doi: 10.1016/j.ccell.2014.09.003.

[226] Y. Manavski *et al.*, "Endothelial transcription factor KLF2 negatively regulates liver regeneration via induction of activin A," *Proc Natl Acad Sci U S A,* vol. 114, no. 15, pp. 3993-3998, Apr 11 2017, doi: 10.1073/pnas.1613392114.

[227] T. Dull *et al.*, "A third-generation lentivirus vector with a conditional packaging system," *J Virol,* vol. 72, no. 11, pp. 8463-71, Nov 1998, doi: 10.1128/JVI.72.11.8463-8471.1998.

[228] A. J. Watt, M. A. Battle, J. Li, and S. A. Duncan, "GATA4 is essential for formation of the proepicardium and regulates cardiogenesis," *Proc Natl Acad Sci U S A,* vol. 101, no. 34, pp. 12573-8, Aug 24 2004, doi: 10.1073/pnas.0400752101.

[229] S. A. Wohlfeil *et al.*, "Hepatic Endothelial Notch Activation Protects against Liver Metastasis by Regulating Endothelial-Tumor Cell Adhesion Independent of Angiocrine Signaling," *Cancer Res,* vol. 79, no. 3, pp. 598-610, Feb 1 2019, doi: 10.1158/0008-5472.CAN-18-1752.

[230] F. Faden, L. Eschen-Lippold, and N. Dissmeyer, "Normalized Quantitative Western Blotting Based on Standardized Fluorescent Labeling," *Methods Mol Biol,* vol. 1450, pp. 247-58, 2016, doi: 10.1007/978-1-4939-3759-2_20.

[231] J. Schindelin *et al.*, "Fiji: an open-source platform for biological-image analysis," *Nat Methods,* vol. 9, no. 7, pp. 676-82, Jun 28 2012, doi: 10.1038/nmeth.2019.

[232] C. T. Rueden *et al.*, "ImageJ2: ImageJ for the next generation of scientific image data," *BMC Bioinformatics,* vol. 18, no. 1, p. 529, Nov 29 2017, doi: 10.1186/s12859-017-1934-z.

[233] R Core Team. "R: A language and environment for statistical computing. R Foundation for Statistical Computing; Vienna, Austria." http://www.r-project.org/index.html (accessed 2021, 16th of December.

[234] C. Geraud *et al.*, "Liver sinusoidal endothelium: a microenvironment-dependent differentiation program in rat including the novel junctional protein liver endothelial differentiation-associated protein-1," *Hepatology,* vol. 52, no. 1, pp. 313-26, Jul 2010, doi: 10.1002/hep.23618.

[235] D. Scholten, J. Trebicka, C. Liedtke, and R. Weiskirchen, "The carbon tetrachloride model in mice," *Lab Anim,* vol. 49, no. 1 Suppl, pp. 4-11, Apr 2015, doi: 10.1177/0023677215571192.

[236] T. Kisseleva *et al.*, "Myofibroblasts revert to an inactive phenotype during regression of liver fibrosis," *Proc Natl Acad Sci U S A,* vol. 109, no. 24, pp. 9448-53, Jun 12 2012, doi: 10.1073/pnas.1201840109.

[237] L. J. Kong *et al.*, "Vatalanib, a tyrosine kinase inhibitor, decreases hepatic fibrosis and sinusoidal capillarization in CCl4-induced fibrotic mice," *Mol Med Rep,* vol. 15, no. 5, pp. 2604-2610, May 2017, doi: 10.3892/mmr.2017.6325.

[238] Y. Wu, Z. Li, A. Y. Xiu, D. X. Meng, S. N. Wang, and C. Q. Zhang, "Carvedilol attenuates carbon tetrachloride-induced liver fibrosis and hepatic sinusoidal capillarization in mice," *Drug Des Devel Ther,* vol. 13, pp. 2667-2676, 2019, doi: 10.2147/DDDT.S210797.

[239] F. Lin, N. Wang, and T. C. Zhang, "The role of endothelial-mesenchymal transition in development and pathological process," *IUBMB Life,* vol. 64, no. 9, pp. 717-23, Sep 2012, doi: 10.1002/iub.1059.

[240] J. Ribera *et al.*, "A small population of liver endothelial cells undergoes endothelial-to-mesenchymal transition in response to chronic liver injury," *Am J Physiol Gastrointest Liver Physiol,* vol. 313, no. 5, pp. G492-G504, Nov 1 2017, doi: 10.1152/ajpgi.00428.2016.

[241] W. Dong *et al.*, "Activation of TWIST Transcription by Chromatin Remodeling Protein BRG1 Contributes to Liver Fibrosis in Mice," *Front Cell Dev Biol,* vol. 8, p. 340, 2020, doi: 10.3389/fcell.2020.00340.

[242] Z. Li *et al.*, "MKL1 promotes endothelial-to-mesenchymal transition and liver fibrosis by activating TWIST1 transcription," *Cell Death Dis,* vol. 10, no. 12, p. 899, Nov 27 2019, doi: 10.1038/s41419-019-2101-4.

[243] R. G. Wells, "Cellular sources of extracellular matrix in hepatic fibrosis," *Clin Liver Dis,* vol. 12, no. 4, pp. 759-68, viii, Nov 2008, doi: 10.1016/j.cld.2008.07.008.

[244] Z. Shi *et al.*, "Transcriptional factor ATF3 promotes liver fibrosis via activating hepatic stellate cells," *Cell Death Dis,* vol. 11, no. 12, p. 1066, Dec 14 2020, doi: 10.1038/s41419-020-03271-6.

[245] F. Xue *et al.*, "Coordinated signaling of activating transcription factor 6alpha and inositol-requiring enzyme 1alpha regulates hepatic stellate cell-mediated fibrogenesis in mice," *Am J Physiol Gastrointest Liver Physiol,* vol. 320, no. 5, pp. G864-G879, May 1 2021, doi: 10.1152/ajpgi.00453.2020.

[246] X. Liu *et al.*, "Identification of Lineage-Specific Transcription Factors That Prevent Activation of Hepatic Stellate Cells and Promote Fibrosis Resolution," *Gastroenterology,* vol. 158, no. 6, pp. 1728-1744 e14, May 2020, doi: 10.1053/j.gastro.2020.01.027.

[247] M. V. Machado *et al.*, "Correction: Mouse Models of Diet-Induced Nonalcoholic Steatohepatitis Reproduce the Heterogeneity of the Human Disease," *PLoS One,* vol. 10, no. 6, p. e0132315, 2015, doi: 10.1371/journal.pone.0132315.

[248] K. Stephenson *et al.*, "Updates on Dietary Models of Nonalcoholic Fatty Liver Disease: Current Studies and Insights," *Gene Expr,* vol. 18, no. 1, pp. 5-17, Mar 21 2018, doi: 10.3727/105221617X15093707969658.

[249] G. Rizki *et al.*, "Mice fed a lipogenic methionine-choline-deficient diet develop hypermetabolism coincident with hepatic suppression of SCD-1," *J Lipid Res,* vol. 47, no. 10, pp. 2280-90, Oct 2006, doi: 10.1194/jlr.M600198-JLR200.

[250] S. A. Montandon, E. Somm, U. Loizides-Mangold, C. de Vito, C. Dibner, and F. R. Jornayvaz, "Multi-technique comparison of atherogenic and MCD NASH models

highlights changes in sphingolipid metabolism," *Sci Rep,* vol. 9, no. 1, p. 16810, Nov 14 2019, doi: 10.1038/s41598-019-53346-4.

[251] E. Mezey, "Liver disease and protein needs," *Annu Rev Nutr,* vol. 2, pp. 21-50, 1982, doi: 10.1146/annurev.nu.02.070182.000321.

[252] F. Meng, X. Yin, X. Ma, X. D. Guo, B. Jin, and H. Li, "Assessment of the value of serum cholinesterase as a liver function test for cirrhotic patients," *Biomed Rep,* vol. 1, no. 2, pp. 265-268, Mar 2013, doi: 10.3892/br.2013.60.

[253] F. Nomura *et al.*, "Serum cholinesterase in patients with fatty liver," *J Clin Gastroenterol,* vol. 8, no. 5, pp. 599-602, Oct 1986, doi: 10.1097/00004836-198610000-00025.

[254] O. O. Ogunkeye, E. K. Chuhwak, and A. A. Otokwula, "Serum cholinesterase activity in the diagnosis of nonalcoholic fatty liver disease in type 2 diabetic patients," *Pathophysiology,* vol. 17, no. 1, pp. 29-32, Feb 2010, doi: 10.1016/j.pathophys.2009.05.003.

[255] G. Wei *et al.*, "Comparison of murine steatohepatitis models identifies a dietary intervention with robust fibrosis, ductular reaction, and rapid progression to cirrhosis and cancer," *Am J Physiol Gastrointest Liver Physiol,* vol. 318, no. 1, pp. G174-G188, Jan 1 2020, doi: 10.1152/ajpgi.00041.2019.

[256] T. Soini *et al.*, "Transcription factor GATA-4 is abundantly expressed in childhood but not in adult liver tumors," *J Pediatr Gastroenterol Nutr,* vol. 54, no. 1, pp. 101-8, Jan 2012, doi: 10.1097/MPG.0b013e31822d52cf.

[257] P. Ramachandran *et al.*, "Resolving the fibrotic niche of human liver cirrhosis at single-cell level," *Nature,* vol. 575, no. 7783, pp. 512-518, Nov 2019, doi: 10.1038/s41586-019-1631-3.

[258] W. Boers, S. Aarrass, C. Linthorst, M. Pinzani, R. O. Elferink, and P. Bosma, "Transcriptional profiling reveals novel markers of liver fibrogenesis: gremlin and insulin-like growth factor-binding proteins," *J Biol Chem,* vol. 281, no. 24, pp. 16289-95, Jun 16 2006, doi: 10.1074/jbc.M600711200.

[259] L. Grgurevic *et al.*, "Systemic inhibition of BMP1-3 decreases progression of CCl4-induced liver fibrosis in rats," *Growth Factors,* vol. 35, no. 6, pp. 201-215, Dec 2017, doi: 10.1080/08977194.2018.1428966.

[260] A. Naim, Q. Pan, and M. S. Baig, "Matrix Metalloproteinases (MMPs) in Liver Diseases," *J Clin Exp Hepatol,* vol. 7, no. 4, pp. 367-372, Dec 2017, doi: 10.1016/j.jceh.2017.09.004.

[261] L. He, H. Yuan, J. Liang, J. Hong, and C. Qu, "Expression of hepatic stellate cell activation-related genes in HBV-, HCV-, and nonalcoholic fatty liver disease-associated fibrosis," *PLoS One,* vol. 15, no. 5, p. e0233702, 2020, doi: 10.1371/journal.pone.0233702.

[262] K. Drzewiecki *et al.*, "GIMAP5 maintains liver endothelial cell homeostasis and prevents portal hypertension," *J Exp Med,* vol. 218, no. 7, Jul 5 2021, doi: 10.1084/jem.20201745.

[263] W. de Haan *et al.*, "Unraveling the transcriptional determinants of liver sinusoidal endothelial cell specialization," *Am J Physiol Gastrointest Liver Physiol,* vol. 318, no. 4, pp. G803-G815, Apr 1 2020, doi: 10.1152/ajpgi.00215.2019.

[264] J. Davis, M. Maillet, J. M. Miano, and J. D. Molkentin, "Lost in transgenesis: a user's guide for genetically manipulating the mouse in cardiac research," *Circ Res,* vol. 111, no. 6, pp. 761-77, Aug 31 2012, doi: 10.1161/CIRCRESAHA.111.262717.

[265] Q. Kong *et al.*, "Rosa26 locus supports tissue-specific promoter driving transgene expression specifically in pig," *PLoS One,* vol. 9, no. 9, p. e107945, 2014, doi: 10.1371/journal.pone.0107945.

[266] M. D. Ryan, A. M. King, and G. P. Thomas, "Cleavage of foot-and-mouth disease virus polyprotein is mediated by residues located within a 19 amino acid sequence," *J Gen Virol,* vol. 72 (Pt 11), pp. 2727-32, Nov 1991, doi: 10.1099/0022-1317-72-11-2727.

[267] M. L. L. Donnelly *et al.*, "Analysis of the aphthovirus 2A/2B polyprotein 'cleavage' mechanism indicates not a proteolytic reaction, but a novel translational effect: a putative ribosomal 'skip'," *J Gen Virol,* vol. 82, no. Pt 5, pp. 1013-1025, May 2001, doi: 10.1099/0022-1317-82-5-1013.

[268] V. A. Doronina, C. Wu, P. de Felipe, M. S. Sachs, M. D. Ryan, and J. D. Brown, "Site-specific release of nascent chains from ribosomes at a sense codon," *Mol Cell Biol,* vol. 28, no. 13, pp. 4227-39, Jul 2008, doi: 10.1128/MCB.00421-08.

[269] P. de Felipe, G. A. Luke, J. D. Brown, and M. D. Ryan, "Inhibition of 2A-mediated 'cleavage' of certain artificial polyproteins bearing N-terminal signal sequences," *Biotechnol J,* vol. 5, no. 2, pp. 213-23, Feb 2010, doi: 10.1002/biot.200900134.

[270] J. H. Kim *et al.*, "High cleavage efficiency of a 2A peptide derived from porcine teschovirus-1 in human cell lines, zebrafish and mice," *PLoS One,* vol. 6, no. 4, p. e18556, 2011, doi: 10.1371/journal.pone.0018556.

[271] Z. Liu *et al.*, "Systematic comparison of 2A peptides for cloning multi-genes in a polycistronic vector," *Sci Rep,* vol. 7, no. 1, p. 2193, May 19 2017, doi: 10.1038/s41598-017-02460-2.

[272] A. Reinhardt, H. Kagawa, and K. Woltjen, "N-Terminal Amino Acids Determine KLF4 Protein Stability in 2A Peptide-Linked Polycistronic Reprogramming Constructs," *Stem Cell Reports,* vol. 14, no. 3, pp. 520-527, Mar 10 2020, doi: 10.1016/j.stemcr.2020.01.014.

[273] Biologics International Corp. "biologicscorp." https://www.biologicscorp.com/tools/GCContent/ (accessed December 13, 2021.

[274] C. H. Yu *et al.*, "Codon Usage Influences the Local Rate of Translation Elongation to Regulate Co-translational Protein Folding," *Mol Cell,* vol. 59, no. 5, pp. 744-54, Sep 3 2015, doi: 10.1016/j.molcel.2015.07.018.

[275] Q. Yang *et al.*, "eRF1 mediates codon usage effects on mRNA translation efficiency through premature termination at rare codons," *Nucleic Acids Res,* vol. 47, no. 17, pp. 9243-9258, Sep 26 2019, doi: 10.1093/nar/gkz710.

[276] N. Sheibani and W. A. Frazier, "Down-regulation of platelet endothelial cell adhesion molecule-1 results in thrombospondin-1 expression and concerted regulation of endothelial cell phenotype," *Mol Biol Cell,* vol. 9, no. 4, pp. 701-13, Apr 1998, doi: 10.1091/mbc.9.4.701.

[277] L. D. DeLeve, X. Wang, M. K. McCuskey, and R. S. McCuskey, "Rat liver endothelial cells isolated by anti-CD31 immunomagnetic separation lack fenestrae and sieve plates," *Am J Physiol Gastrointest Liver Physiol,* vol. 291, no. 6, pp. G1187-9, Dec 2006, doi: 10.1152/ajpgi.00229.2006.

[278] J. Y. Scoazec and G. Feldmann, "The cell adhesion molecules of hepatic sinusoidal endothelial cells," *J Hepatol,* vol. 20, no. 2, pp. 296-300, Feb 1994, doi: 10.1016/s0168-8278(05)80072-8.

[279] O. Strauss, A. Phillips, K. Ruggiero, A. Bartlett, and P. R. Dunbar, "Immunofluorescence identifies distinct subsets of endothelial cells in the human liver," *Sci Rep,* vol. 7, p. 44356, Mar 13 2017, doi: 10.1038/srep44356.

[280] Y. Liu, Q. Yang, and F. Zhao, "Synonymous but Not Silent: The Codon Usage Code for Gene Expression and Protein Folding," *Annu Rev Biochem,* vol. 90, pp. 375-401, Jun 20 2021, doi: 10.1146/annurev-biochem-071320-112701.

[281] M. S. Pandey, E. N. Harris, J. A. Weigel, and P. H. Weigel, "The cytoplasmic domain of the hyaluronan receptor for endocytosis (HARE) contains multiple endocytic motifs targeting coated pit-mediated internalization," *J Biol Chem,* vol. 283, no. 31, pp. 21453-61, Aug 1 2008, doi: 10.1074/jbc.M800886200.

[282] B. T. Kren *et al.*, "Nanocapsule-delivered Sleeping Beauty mediates therapeutic Factor VIII expression in liver sinusoidal endothelial cells of hemophilia A mice," *J Clin Invest,* vol. 119, no. 7, pp. 2086-99, Jul 2009, doi: 10.1172/JCI34332.

[283] J. Marquez *et al.*, "Targeting liver sinusoidal endothelial cells with miR-20a-loaded nanoparticles reduces murine colon cancer metastasis to the liver," *Int J Cancer,* vol. 143, no. 3, pp. 709-719, Aug 1 2018, doi: 10.1002/ijc.31343.

Acknowledgements

A big thank go first of all to my second supervisor Prof. Dr. Sergij Goerdt for giving me the opportunity to perform my doctoral thesis in the “AG Angiodiversität und Organfunktion” and for the supervision of my work, as well as the support over the entire time of my PhD.

Another grateful appreciation goes to PD Dr. med. Philipp Reiners-Koch for the great support and supervision during my PhD thesis in all respects and for the revision of this thesis.

Furthermore, I would like to express my gratitude thank to Prof. Dr. Viktor Umansky for being my first supervisor, for reviewing this thesis and for the support during the Thesis Advisory Committee (TAC) meetings.

I want to thank the additional members of my Thesis Defense Committee Prof. Dr. Dr. Georg Stoecklin for being the chairperson and Prof. Dr. Peter Angel for being examiner.

I would like to thank Prof. Dr. Steven Dooley for being part of my Thesis Advisory Committee and for the scientific input during the annual TAC meetings.

Without the funding of the Deutsche Forschungsgemeinschaft (DFG) this thesis would not be possible. In this respect I will thank the members of research training group (RTG) 2099 „Hallmarks of Skin Cancer“ and the Collaborative Research Center (CRC) 1366 “Vascular Control of Organ Function” for the lecture series, the courses, the student retreats, the summer schools and conferences to get scientific input and support for my thesis.

I would like to thank Prof. Dr. Christian Buchholz for provisioning of the lentiviral plasmid and together with Gundula Braun for the production of high titer lentiviral stocks.

I would like to thank Cathleen Fichtner, Camela Jost, Maria Muciek and Elisabeth Wuehl for conducting histopathological stainings, running the “Autotechnikon” and for plasma level measurements in the core facility of the ZMF of the UMM.

Another thanks go to the animal caretakers of the animal facility of the UMM in H111 and H21 for the care of the mice used in the experiments and for breeding.

I would like to thank the Affymetrix core facility of the UMM for conducting the microarrays. Especially I want to thank Dr. Carolina DeLaTorre for the measurements at the bioanalyzer und Dr. Carsten Sticht for preparing the bioinformatic data.

I want to thank Jochen Weber, Hiltrud Schönhaber, Dr. Kai Schledzewski and Stephanie Riester of “AG Angiodiversität und Organfunktion” for the technical support and general support for all concerns regarding the work in the lab. A special thank goes to

Dr. Kai Schledzewski for teaching me his broad knowledge about mouse breeding and mouse genetics and for the support with animal experiments.

My warmest thanks go to former and actual lab members of “AG Angiodiversität und Organfunktion” and “AG Sektion Klinische und Molekulare Dermatologie”. In scientific terms I want especially thank Dr. Manuel Winkler and Dr. Christian Schmid for the excellent scientific input, for helping to analyze the RNA-Seq data, for supporting to design the experiments and for always being supportive. I want to thank Céline Weller for teaching me how to do flow cytometer measurements and for the support during the data analysis. In personal way I want to thank the former and actual members of our “Mittagsrunde” Theresa Staniczek, Dr. Loreen Kloss, Jochen Weber, Céline Weller, Johannes Hoffmann and Bianca Dietsch for making the lunch the funniest time of the day and for creating such a nice working atmosphere. I want especially thank Theresa Staniczek for the nice and productive teamwork in the “Gata4 group” and for always being by my side during my PhD from the beginning on. Another big thanks go to Loreen Kloss, Céline Weller and Theresa Staniczek for the scientific and especially the personal support. You always had an open ear for me and made my PhD time memorable. Thank you for not only being colleagues but for becoming friends!

Last but not least my deepest thanks go to my family and Ingmar who always supported me and encouraged me. Thank you for always being there for me and believing in me. Mom and Dad, without you I wouldn't be where I am and who I am. Thank you for everything, I love you!

Appendix

List of Figures

List of Tables

List of Abbreviations

AEC	Dako 3-amino-9-ethylcarbazole
AFLD	alcoholic liver disease
ALK1	activin receptor-like kinase 1
ALT	alanine transaminase
ANGPT2	Angiopoiteine-2
ASH	alcoholic steatohepatitis
aSMA	α-smooth muscle actin
AST	aspartate transaminase
ATF3	Activating transcription factor 3
B6N	C57BL/6N
BMP2	Bone morphogenetic protein 2
BMP9	Bone Morphogenetic Protein-9
BSA	bovine serum albumin
CCl_4	carbon tetrachloride
CDAA	choline-deficient l-amino acid-defined
cDNA	complementary DNA
CLEC	C-type lectin
DNA	deoxyribonucleic acid
DAPI	4',6-Diamidino-2-phenylindol
DMEM	Dulbecco's Modified Eagle Medium
dNTP	deoxynucleotide
DTT	dithiothreitol
EC	endothelial cell
ECM	extracellular matrix
EDTA	ethylenediaminetetraacetic acid
MACS	magnetic-activated cell sorting

EMT	epithelial-to-mesenchymal transition
EndMT	endothelial-to-mesenchymal transition
eNOS	endothelial nitric oxide synthase
ERG	ETS-related gene
ES	embryonic stem
FBS	fetal bovine serum
Fcγ	Fc-gamma
FFA	free fatty acids
$Gata4^{LSEC\text{-}KI}$	Clec4g-iCre x R26STGata4; LSEC-specific Gata4 knockin mouse
$Gata4^{LSEC\text{-}KO}$	Clec4g-iCre x Gata4 floxed; LSEC-specific Gata4 knockout mouse
GBSS	Grey's balanced salt solution
GLDH	glutamate dehydrogenase
GSEA	gene set enrichment analysis
H&E	hematoxylin and eosin
HA	hyaluronan
HCC	hepatocellular carcinoma
HEPES	4-(2-hydroxyethyl)-1-piperazineethane-sulfonic acid
HFD	high fat diet
HGF	hepatocyte growth factor
Hh	Hedgehog
HIER	Heat Induced Epitope Retrieval
HRP	horseradish peroxidase
HSC	hepatic stellate cell
i.p.	intraperitoneally
ID1	inhibitor of DNA binding 1
IF	immunofluorescence staining
KC	kupffer cell

kDa	kilodalton
KLF2	Kruppel-like factor 2
LB	lysogeny broth
LSEC	liver sinusoidal endothelial cell
LXRα	Liver X receptor α
MCD	methionine and choline-deficient
mLSEC	primary murine liver sinusoidal endothelial cell
MSigDB	molecular signatures database
NAFLD	non-alcoholic liver disease
NASH	non-alcoholic steatohepatitis
NDS	normal donkey serum
NO	nitric oxide
NP-40	Nonident P40
PBS	phosphate-buffered saline
PCR	polymerase chain reaction
PFA	paraformaldehyde
pH	pondus hydrogenii
PHx	partial hepatectomy
PSR	picrosirius red
PVDF	low fluorescence polyvinylidene fluoride
qPCR	quantitative polymerase chain reaction
R26	Rosa26
RFP	red fluorescent protein
RIPA	radioimmunoprecipitation assay
RT	room temperature
RT-qPCR	quantitative real-time polymerase chain reaction
SD	standard deviation

SDS	sodium dodecyl sulfate
SDS-PAGE	sodium dodecyl sulfate-polyacrylamide gel electrophoresis
S.O.C	super optimal broth with catabolite repression
Sox9	SRY-Box transcription factor 9
SPL	Smart Protein Layers
Std	standard
TGF-β1	Transforming growth factor beta 1
TLR	Toll-like receptors
TWIST1	Twist-related protein 1
VEGFR2	Vascular endothelial growth factor receptor 2
VEGFR23	Vascular endothelial growth factor receptor 3
VLDL	very low-density lipoprotein
we	weeks
Wls	Wnt cargo receptor Evi/Wntless
WNT2	Wingless-type MMTV integration site family, member 2
ZMF	Zentrum für Medizinische Forschung